Templated Interlocked Host Structures for the Recognition and Sensing of Charged-Substrates

Richard C. Knighton

Pembroke College, University of Oxford



A thesis submitted for the degree of Doctor of Philosophy

Inorganic Chemistry Laboratory

University of Oxford

Michaelmas Term 2014

Templated Interlocked Host Structures for the Recognition and Sensing of Charged-Substrates

Richard C. Knighton, Pembroke College, University of Oxford

Abstract of thesis submitted for the degree of D.Phil, Michaelmas Term 2014

This thesis describes the synthesis of acyclic, macrocyclic and, in particular, interlocked anion and ion-pair receptors and sensors.

Chapter One will introduce the field of supramolecular chemistry with particular emphasis on areas which are pertinent to this thesis, including anion receptor design and templated synthesis of interlocked structures.

Chapter Two focuses on the synthesis of new heteroditopic macrocycles functionalised with both cation and anion recognition sites and their incorporation into interlocked architectures. The affinity for a range of anions and ion-pairs is explored *via* ^{1}H NMR and UV-visible spectroscopy as well as by X-ray crystallography.

Chapter Three details the incorporation of *d*- and *f*-metal luminescent reporter groups into an isophthalamide motif in order to construct acyclic, macrocyclic and [2]rotaxane receptors.

Chapter Four investigates the synthesis of complex higher-order interlocked structures through post-synthetic modification of lower-order interlocked structures.

Chapter FIVE explores the potential for fluorescent gold nanoparticle conjugates to act as luminescent and colourimetric sensors for chemical warfare agents (CWAs) by employing a fluorescent displacement assay technique.

Contents

Chapter 1: Introduction 1
1.1 Supramolecular Chemistry 1
1.2 Non-covalent Interactions 2
1.2.1 Electrostatic Interactions 2
1.2.2 Hydrogen-bonding 3
1.2.3 Halogen-Bonding 3
1.2.4 π-π Donor Acceptor, Cation-π and Anion-π Interactions 4
1.2.5 Solvatophobic Effects 6
1.3 Principles of Host-Guest Chemistry 6
1.3.1 Complementarity 6
1.3.2 Preorganisation, the Chelate Effect and the Macrocyclic Effect 8
1.4 Recognition and Sensing of Charged Substrates 10
1.4.1 Cation Recognition 11
1.4.2 Cation Sensing 14
1.4.3 Anion Recognition 15
1.4.3.1 Positively Charged Receptors 16
1.4.3.2 Neutral Anion Receptors 20
1.4.3.3 Lewis Acid and Metal-based Receptors 24
1.4.4 Anion Sensing 25
1.4.4.1 Luminescent Anion Sensors 25
1.4.4.2 Electrochemical Anion Sensors 31
1.4.5 Recognition and Sensing of Ion-Pairs 31
1.5 Mechanically Interlocked Structures 39
1.5.1 Synthetic Strategies 40
1.5.2 Templated Synthesis 41
1.5.2.1 Cation Templation 41
1.5.2.2 Neutral Templation 44
1.5.2.3 Anion Templation 45
1.5.3 Applications of Interlocked Structures 47
1.5.3.1 Molecular Machines and Switches 47
1.5.3.2 Biological Applications, Recognition and Sensing 49
1.6 Project Aims 52
1.7 References 53
Chapter 2: Interlocked Structures for Ion-pair Recognition 63
2.1 Introduction 63
2.1.1 Introduction to the Calix[4]arene and Calix[4]diquinone Motifs 63
2.1.2 Calixarene Receptors for Cations, Anions and Ion-pairs 66
2.1.3 Introduction to the pyridine *N*-oxide motif 68

2.1.4 Chapter Objectives 70
2.2 Ion-pair binding interlocked structures 71
2.2.1 Heteroditopic Calix[4]diquinone Macrocycle Synthesis 71
2.2.2 Preliminary Pseudorotaxane Study 75
2.2.3 Synthesis of the target heteroditopic [2]rotaxane 77
2.2.3.1 Axle precursor synthesis 77
2.2.3.1 [2]Rotaxane Synthesis and Characterisation 79
2.2.3.2 Molecular Motion Investigation 83
2.2.3.3 Anion and ion-pair recognition properties 85
2.2.3.4 Extraction Studies 90
2.2.4 Attempted synthesis of a pH-dependent rotaxane molecular shuttle 91
2.2.4.1 [2]Rotaxane Precursor Syntheses 92
2.2.4.2 Rotaxane Synthesis 93
2.2.4.3 Summary 97
2.2.5 Synthesis of Interlocked Structures Using Activated Esters 97
2.2.5.1 Introduction 97
2.2.5.2 Axle Precursor Synthesis 99
2.2.5.3 Attempted Activated Ester [2]rotaxane Synthesis 100
2.2.6 Attempted Activated Ester [2]catenane Synthesis 101
2.2.6.1 Catenane precursor synthesis 101
2.2.6.2 Activated ester [2]catenane synthesis and characterisation 105
2.2.6.3 Summary 112
2.2.7 Imidazolium-containing [2]rotaxane 112
2.2.7.1 Introduction 112
2.2.7.2 [2]Rotaxane Precursor Synthesis 113
2.2.7.3 [2]Rotaxane Synthesis 116
2.2.7.4 Summary 118
2.3 Conclusions 119
2.4 References 120

Chapter 3: Anion Templated Synthesis of Interlocked Structures Containing *d*- and *f*-Metal Reporter Groups 123
3.1: Introduction 123
3.1.1 Interlocked Sensors 124
3.1.2 Chapter Objectives 126
3.2 [2]Rotaxanes Containing Lanthanide Reporter Groups 127
3.2.1 Lanthanide Photophysics 128
3.2.2 Azide Functionalised [2]Rotaxane Synthesis 129
3.2.3 [2]Rotaxane Anion Recognition Properties 134
3.2.4 Lanthanide Appended Rotaxane Preparation *via* Post-synthetic Modification 136
3.2.5 Europium Cyclen Appended [2]Rotaxane Photophysical and Anion Sensing Properties 140
3.2.6 Summary 147
3.3 [2]Rotaxanes Containing Transition Metal Reporter Groups 148

3.3.1 Dipyridylbenzene Transition Metal Complexes....148
3.3.2 Isophthalamide Functionalised Dipyridylbenzene Ligand Synthesis....149
3.3.3 Acyclic and Macrocyclic Anion Receptor Synthesis....151
3.3.4 Acyclic and Macrocyclic Luminescent Anion Sensing....157
3.3.4.1 Acyclic and macrocyclic platinum (II) receptors....158
3.3.4.2 Acyclic and macrocyclic ruthenium (II) receptors....162
3.3.5 Preliminary [2]pseudorotaxane Studies....165
3.3.6 Rotaxane Synthesis....167
3.3.7 Ruthenium (II) Rotaxane Anion Binding and Luminescence Titrations....173
3.3.8 Summary....176
3.4 Conclusions....177
3.5 References....179
Chapter 4: Higher Order Interlocked Structures....181
4.1: Introduction to Higher Order Interlocked Assemblies....181
4.2: Higher Order Anion-Templated Interlocked Assemblies....183
4.3 Chapter Objectives....185
4.4 Alkyne [2]Rotaxane Synthesis....186
4.5 Triazole- and Triazolium-containing [3]Rotaxane Syntheses....191
4.5.1 Triazole [3]Rotaxane Formation By CuAAC Post-synthetic Modification....191
4.5.2 Triazolium [3]Rotaxane Synthesis....194
4.6 Attempted Synthesis of 'Rotaxane Stoppered' [4]Rotaxane....197
4.7 Summary....203
4.8 Conclusions....204
4.9 References....205
Chapter 5: Detection of Sulphur Mustard by Fluorescent Displacement Assay....207
5.1 Introduction....207
5.2 Chemical Warfare Agent Receptors and Sensors....208
5.2.1 Chemodosimeters....208
5.2.2 Supramolecular and Coordination Strategies....209
5.3 Chapter Objectives....210
5.4 Nanoparticle Ligand Synthesis....211
5.5 Nanoparticle Synthesis and Characterisation....215
5.5.1 Nanoparticle Synthesis....215
5.5.2 Nanoparticle Characterisation....216
5.6 Displacement Studies....219

5.6.1 ^{1}H NMR Displacement Study 219
5.6.2 UV/visible Absorption Studies 220
5.6.3 Luminescence Displacement Studies 222
5.7 Summary 227

5.8 Conclusions 228

5.9 References 229

Chapter 6: Experimental 231
6.1 General Information 231

6.1.1 Solvents and Reagents 231
6.1.2 Intrumentation 231
6.2 Synthetic Procedures 232

General Procedure for Anion Exchange 232
Chapter 2 Syntheses 233
Chapter 3 Syntheses 263
Chapter 4 Syntheses 283
Chapter 5 Syntheses 288
6.3 References 296

Chapter 7: Summary of Conclusions 297
Chapter 2 297
Chapter 3 297
Chapter 4 298
Chapter 5 298
Appendices 299
A.1 Crystal Structure Information 299

A.1.1 General Information 299
A.1.2 Crystal structure of calix[4]diquinone macrocycle 1 301
A.1.3 Crystal structure of calix[4]diquinone pyridinium macrocycle 35 · Cl 302
A.1.4 Crystal structure of [2]catenane 41 · NaCl[BAr$^{F}_{4}$] 303
A.1.5 Crystal structure of azide [2]rotaxane 54 · Cl 305
A.1.6 Crystal structure of dipyridylbenzene ligand 62 306
A.1.7 Crystal structure of ruthenium (II) acyclic receptor 70 · Cl 307
A.1.8 Crystal structure of *syn*-ruthenium (II) macrocyclic receptor 72 · PF_6 308
A.1.9 Crystal structure of *anti*-ruthenium (II) macrocyclic receptor 72 · PF_6 309
A.1.10 Crystal structure of alkyne [2]rotaxane 79 · Cl 310
A.1.11 Crystal structure of dansyl-amine 88 311
A.1.12 Crystal structure of naphthalimide-imidazole ligand 90 312
A.2 Anion Titration Protocol 313

A.3 Chapter 5 Experiments 314

A.3.1 Quantitative Titrations 314

A.3.2 Qualitative Control Experiments 314
A.3.3 ^{1}H NMR Experiments 316
A.4 References 317

Chapter 1: Introduction

1.1 Supramolecular Chemistry

The field of supramolecular chemistry is a well established, wide-ranging interdisciplinary area of research concerned with the fundamental understanding of non-covalent interactions between molecules in addition to its use in the construction of complex architectures. Many areas of supramolecular chemistry are inspired by examples in Nature, which perfectly utilise non-covalent interactions in many vital processes, including DNA transcription and translation and enzyme-substrate complex formation. Supramolecular chemistry can be divided into two related areas: host-guest chemistry and self-assembly.

Host-guest chemistry involves the binding of an analyte or guest by a larger host, utilising intermolecular forces between the two. This may be used to describe a natural receptor such as a protein or an abiotic synthetic receptor which has been designed and synthesised.

Self-assembly is the formation of complex architectures by smaller, simpler molecules, by virtue of the favourable non-covalent interactions between them which provides the thermodynamic driving force for assembly. An example of this is the formation of DNA by nucleotide base pairs (Figure **1.1**). The formation of base pairs is driven by specific hydrogen-bonding between complementary nucleotide bases while the origin of the helical structure is due to aromatic donor-acceptor interactions induced by the hydrophobic effect.

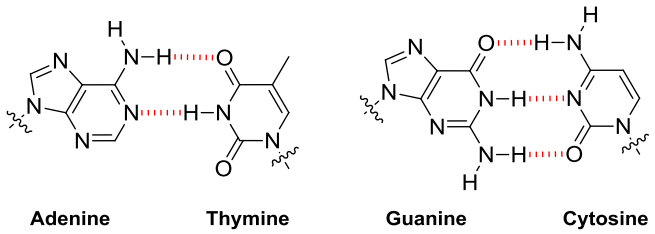

Figure 1.1: Hydrogen-bonded nucleotide base pairs which form the macromolecule DNA

1.2 Non-covalent Interactions

Supramolecular chemistry relies on non-covalent interactions for both host-guest chemistry and self-assembly. While individual non-covalent interactions are significantly weaker than covalent bonds (<50 kJ mol^{-1} in comparison with 300-500 kJ mol^{-1} for typical organic covalent bonds),[1] their strength can be enhanced by exploiting the cooperative synergistic effect of multiple interactions between two molecules.

1.2.1 Electrostatic Interactions

Electrostatic interactions describe all types of Coulombic attraction between opposing charges and can be divided into three main classes; ion-ion, ion-dipole and dipole-dipole (Figure **1.2**).

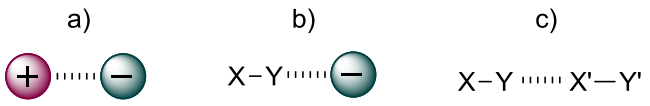

Figure 1.2: a) ion-ion b) ion-dipole and c) dipole-dipole interactions; X= electronegative atom or electron-withdrawing group; Y = electropositive atom

The ion-ion interaction is the strongest of the three classes and is purely electrostatic in nature; as a result they are largely non-directional and have no preference for orientation. In

contrast, ion-dipole and dipole-dipole interactions have directional preference due to the anisotropic distribution of charge of the dipole, although they are much weaker in comparison to ion-ion interactions.

In addition to these three main classes are dispersion forces which are the interactions between a permanent dipole and an induced dipole or two instantaneous induced dipoles. The interaction between the two is non-directional and typically very weak (<5 kJ mol^{-1}).

1.2.2 Hydrogen-bonding

Hydrogen-bonding is a specific type of ion-dipole or dipole-dipole interaction whereby a hydrogen atom is covalently linked to an electronegative atom or group and interacts with a negatively charged species, typically an anion or neighbouring dipole. As a result, hydrogen bonds are directional with a tendency to be linear, although they are also influenced by other factors such as the steric requirements of the system. The strength of hydrogen bonds is demonstrated in Nature by the sulphate and phosphate binding proteins, which employ a multiple hydrogen-bonded array to selectively bind these oxoanions in water.[2, 3]

1.2.3 Halogen-Bonding

Halogen-bonding is another example of a dipole-dipole or dipole-ion interaction which, although known to exist for quite some time, has only very recently been defined by IUPAC as, "*a net attractive interaction between an electrophilic region associated with a halogen atom in a molecular entity and a nucleophilic region in another, or the same, molecular entity.*"[4] This arises as a result of a halogen atom covalently bound to an electron

withdrawing atom or group which causes the electron density around the polarisable halogen atom to be anisotropic, with an area of electropositive charge (known as the σ-hole) located at the terminus of the halogen. Halogen bonds are of comparable strength to hydrogen bonds (10 kJ mol^{-1} to 200 kJ mol^{-1}) depending upon the halogen, the covalently bound electron withdrawing molecular entity and the nucleophile.[5, 6] Unlike hydrogen bonds however, halogen bonds exhibit a much stronger directional preference for the interaction to be linear due to the highly localised σ-hole (Figure **1.3**).[7]

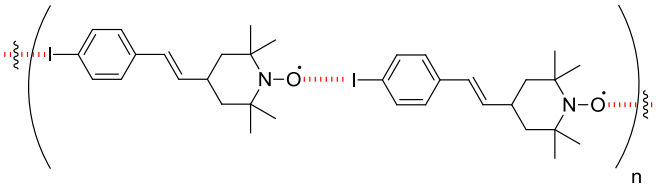

Figure 1.3: One-dimensional chain fragment of 4-(4-iodobenzylidene)-TEMPO halogen bonds

1.2.4 π-π Donor Acceptor, Cation-π and Anion-π Interactions

The most prevalent of the π-interactions are between conjugated systems and occur in a face-to-face or edge-to-edge fashion (Figure **1.4a** and **1.4b**). The magnitude and origin of these interactions is a contentious issue but there is significant evidence for favourable electrostatic and dispersive interactions,[8-10] which is enhanced by the presence of solvophobic contributions.[11]

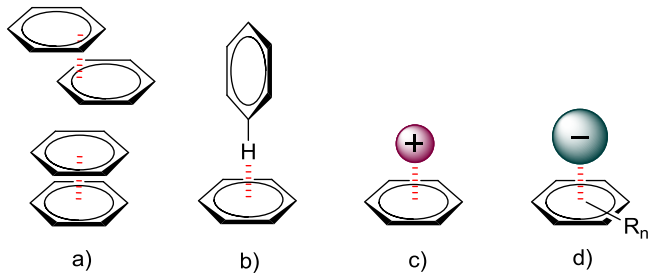

Fig. 1.4: Types of π-interactions a) face-to-face, stacked *(bottom)* and offset *(top)* b) Edge-to-face c) cation-π d) anion-π; R = electron withdrawing group

The strength of the electrostatic component of **π-π** donor-acceptor aromatic interactions can also be augmented by the use of electron-deficient and electron-rich aromatic species, particularly when introducing charge on one or more aromatic components. Cation-**π** and anion-**π** interactions are often employed in supramolecular chemistry with cation-**π** interactions more well-established, having been studied in the solid,[12] gas[13, 14] and solution states.[15] In recent years anion-**π** interactions have been studied more extensively and utilised in the design of synthetic receptors which exploit them in concert with other non-covalent interactions (Figure **1.5**).[16-18]

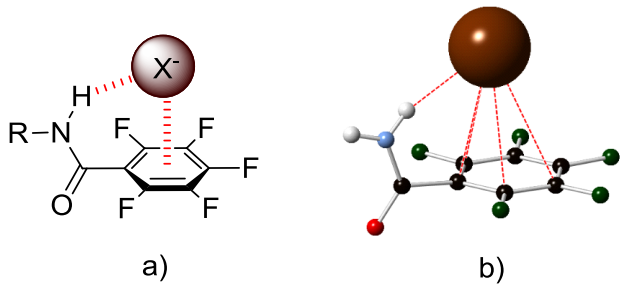

Figure 1.5: Interactions of anion with aromatic rings a) hydrogen-bond assisted anion-π receptor b) ball-and-stick crystal structure with bromide

1.2.5 Solvatophobic Effects

Although solvatophobic effects are strictly not classified as non-covalent interactions, their use is widely exploited in both biotic and abiotic receptors and can play a significant role in the design of synthetic receptors. The exclusion of polar ordered solvent molecules from a hydrophobic cavity results in an entropic gain by increasing disorder and in addition, gives rise to an enthalpic contribution by allowing solvent-solvent interactions to dominate. This effect is most pronounced in more polar solvents such as water and is referred to as the hydrophobic effect in this instance.

1.3 Principles of Host-Guest Chemistry

Charged species are ubiquitous in biological systems and this has been an inspirational driving force in supramolecular chemistry for the construction of abiotic receptors that are capable of complexing cationic and anionic guests. In this regard the core concepts of preorganisation, the chelate effect and the related macrocyclic effect are all important factors to consider when designing synthetic host-guest assemblies. This section gives a critique of these concepts in the design of abiotic host-guest systems.

1.3.1 Complementarity

The concept of complementarity is fundamental to host-guest receptor design. Consideration of the size and shape of the intended guest is key in ensuring that the host is complementary to the guest and is vital to achieving strong and selective binding. This is demonstrated by the binding of alkali-metal cations by crown ethers, first reported by Pedersen (Figure **1.6**).[19, 20] The synthetic receptors display different selectivities for alkali-metal ions dependent upon

the cation-cavity size match with 18-crown-6 forming the strongest complex with potassium and 21-crown-7, which has a larger cavity, binding caesium cations with the greater association constant.[21]

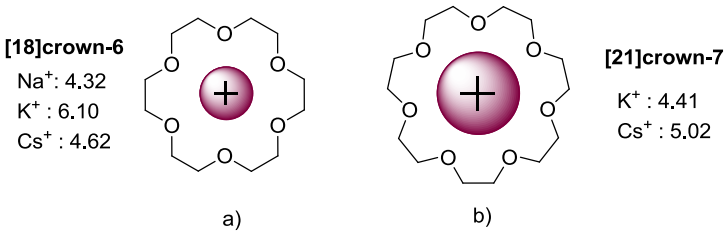

Figure 1.6: Alkali-metal cation binding with association constants ($\log K_a$) in methanol of a) 18-crown-6 and b) 21-crown-7

Most synthetic receptors take inspiration from examples found in Nature, specifically proteins which display high selectivity due to their high complementarity. Two main theories have emerged as a result of the study of host-guest chemistry of enzymes, the first being the lock and key model which has largely been superseded by the second, the induced-fit model. The lock and key model was first proposed by Emil Fischer in which the enzyme binding site acts as a 'lock' and the substrate the 'key'.[22,23] Only specific substrates are complementary to the enzyme binding site, a consequence of both their size and shape. The induced-fit model was proposed by Koshland in 1958[24] and builds on the previous theory by proposing that enzymes are not rigid but dynamic, and capable of adopting different conformations. Upon binding of the substrate the binding site of the enzyme undergoes subtle changes in conformation to accommodate the guest most efficiently.

1.3.2 Preorganisation, the Chelate Effect and the Macrocyclic Effect

The principle of preorganisation was defined by Cram as, "the more highly hosts and guests are organized for binding and low solvation prior to their complexation, the more stable will be their complexes."[25] This important point is emphasised by anion binding of the ubiquitous isophthalamide motif (Figure **1.7**). The unsubstituted isophthalamide receptor is less preorganised than the boron functionalised receptor which, through intramolecular oxygen-boron interactions, increases the preorganisation and hence the anion affinity of the host.[26]

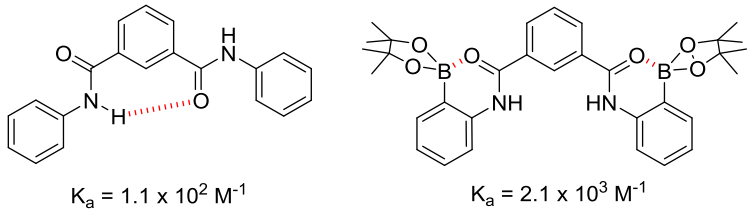

Figure 1.7: Increasing preorganisation a) unsubstituted isophthalamide receptor b) Smith's preorganised isophthalamide receptor; K_a values for acetate in $(CD_3)_2SO$

The principle of preorganisation manifests itself in the chelate effect and the macrocyclic effect, both of which increase the preorganisation of any given receptor. The chelate effect is the enhanced thermodynamic stability of metal complexes by chelating, multidentate ligands as compared to analogous complexes containing monodentate ligands. The effect is illustrated by the formation of nickel-amine complexes in water (Scheme **1.8**).

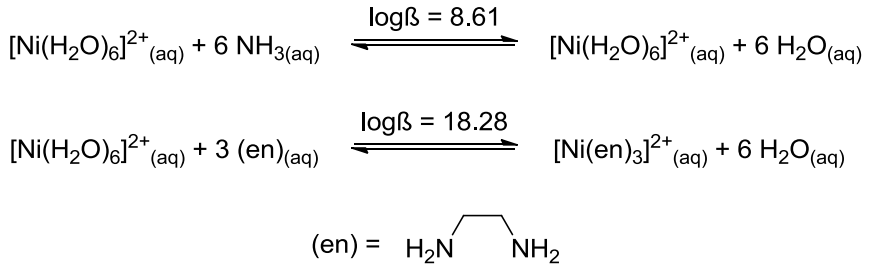

Scheme 1.8: The chelate effect demonstrated by the formation of nickel-amine complexes

The greater driving force for the formation of complexes containing chelating ligands is both entropic and enthalpic in origin.[27] The binding of a monodentate ligand is entropically neutral whereas upon coordination of a bidentate ligand such as ethylene diamine the entropy is increased due to the displacement of two water molecules. From an enthalpic viewpoint the coordination of two ammonia ligands has to overcome lone pair ligand-ligand repulsion whereas the enthalpic penalty has already been paid in the case of the ditopic amine during the synthesis of the ligand.

The macrocyclic effect is an extension of the chelate effect due to the prevalence of multiple chelating atoms in macrocyclic compounds. In addition, macrocycles are typically more rigid and fewer degrees of freedom are lost upon complexation which is entropically favourable. Macrocyclic hosts are typically less well solvated than their acyclic congeners which gives rise to a favourable enthalpic contribution when binding a guest species. The macrocyclic effect is nicely demonstrated by Flood's anion binding triazolophane; the macrocyclic compound binds chloride many orders of magnitude stronger than its acyclic analogue (Figure **1.9**).[28, 29]

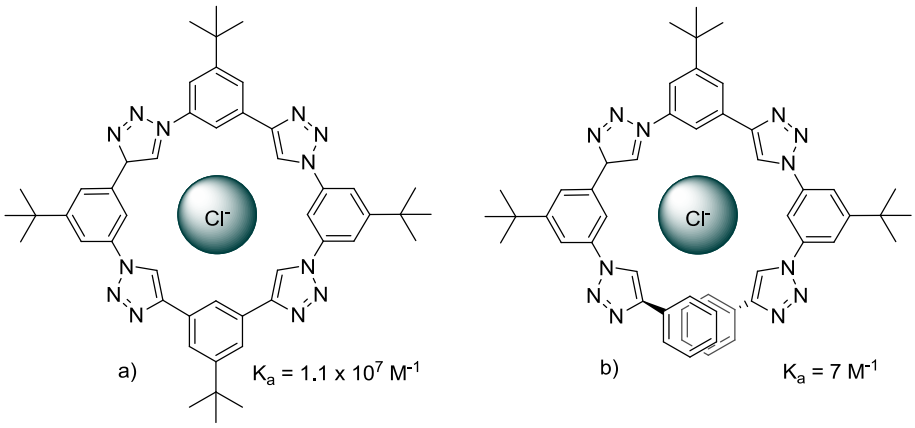

Figure 1.9: The macrocyclic effect a) Flood's macrocyclic triazole receptor b) acyclic analogue; anion binding titrations in CD_2Cl_2

1.4 Recognition and Sensing of Charged Substrates

The recognition of charged species is of paramount importance due to their prevalence in chemical, biological, environmental and industrial processes. As a consequence the presence of certain cations and anions can often have adverse effects on biological systems, for example lead and mercury are highly toxic to living organisms,[30-32] whereas eutrophication of lakes and rivers by overuse of nitrate and phosphate-based fertilisers leads to adverse affects on aquatic organisms.[33] Aside from their toxicity however, the recognition of charged species has important applications in the field of membrane transport research,[34] in the extraction of metal ions from mineral ores,[35,36] and in the field of medicine; magnetic resonance imaging (MRI) necessitates the *in vivo* use of paramagnetic gadolinium ion complexes.[37, 38]

In addition to the challenge of designing host systems to recognise charged species it is often desirable to sense their presence through the use of an integrated reporter group which typically exhibits an optical[39, 40] or electrochemical[41, 42] response upon complexation. This is

typically achieved by covalently incorporating a reporter group in proximity to the guest recognition site.

1.4.1 Cation Recognition

There are copious examples of cation receptors in biology such as the depsipeptide valinomycin, which is able to selectively bind and transport the potassium ion across membranes,[43] and more classical coordination complexes such as chlorophyll and haemoglobin which have provided inspiration in the field of synthetic cation hosts. The origins of the supramolecular chemistry approach to the design of synthetic receptors for the recognition of cations can be traced back to the seminal crown ether work by Pedersen (Section **1.3.1**).[20] Synthetic receptors have since turned to other non-covalent interactions such as cation-π[44-46] and ion-ion forces to construct selective cation hosts, particularly in concert with the more commonly used ion-dipole interaction.[47] While the pioneering work conducted on crown ethers established their interaction with alkali metal cations,[19, 20] accommodation of other cationic guests such as ammonium[48, 49] and guanidinium[50] has also been demonstrated. It has also been shown that selectivity for cations such as Hg^{2+} and Ag^{+} can be achieved by the use of softer donors such as thioethers and amines.[51]

The importance of the concepts of preorganisation and cooperativity are highlighted in the development of synthetic cation receptors (Figure **1.10**). Subtle variations to the classic crown ether structure by way of incorporation of a pendant ligating arm, known as a *lariat* crown ether, has been shown to increase the association constant of alkali-metal cations as well as displaying more favourable kinetics, which is crucial in the field of membrane transport research.[52] It was subsequently shown by Lehn in his work on macrobicyclic

cryptands, first reported in 1969,[53] that by increasing the number of ligating atoms the affinity for metal cations could be increased compared to the analogous macrocyclic complex. The increased association constant is a result of increased cooperativity and solvatophobic effects, although they typically exhibited slower kinetics due to the caged structure of the compounds.[54] The preorganisation of cation hosts was significantly enhanced through the use of *spherands*, cyclic compounds in which the macrocycle itself consists of only sp^2 hybridised atoms. These receptors, first synthesised by Cram,[55] are highly preorganised due to their rigid structure and, as a consequence, display much higher selectivities than the more compliant crown ethers and cryptands,[56] although their use is inhibited by their slow rates of association-dissociation with cations.

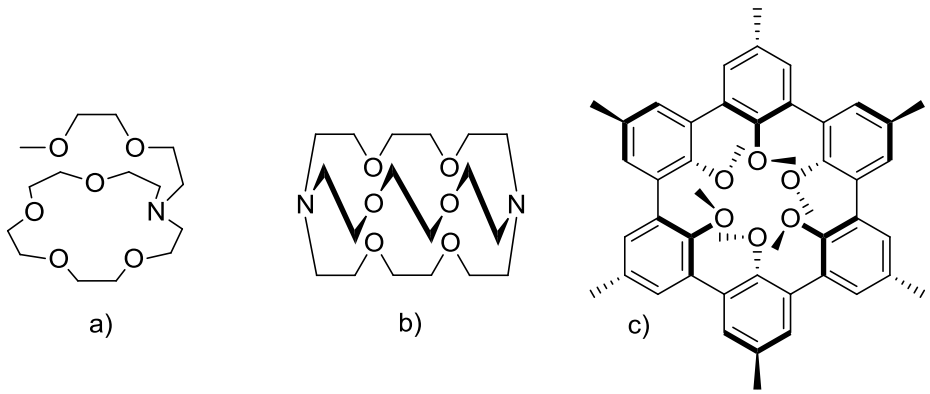

Figure 1.10: Cation receptors a) lariat aza-crown ether b) [2.2.2] cryptand c) spherand

Calixarenes are rigid aromatic frameworks, related to spherands but which contain a methylene linker bridging adjacent aryl groups. As a consequence calixarenes are less rigid than spherands but can exist in a range of confirmations (See Chapter **2** for more details). Calixarenes are capable of binding cationic species through the interaction of the phenolic oxygen atoms *via* ion-dipole interactions or by cation-π interactions.[57, 58] The donor atoms in

receptors incorporating this motif do not constitute part of the macrocycle itself but rather use the calixarene framework as a rigid scaffold and therefore enable a diverse variety of hosts to be constructed.[59, 60] Calixarenes have been functionalised with crown ether,[61] azacrown ether[62] and ester[63] motifs as well as the use of analogous thiacalixarenes[64] which can affect the affinity and selectivity for metal cations. The calixarene scaffold has been used to construct calix[4]tubes which exhibit a strong selectivity for potassium cations (Figure **1.11a**).[65, 66] Binding of potassium has been investigated by computer modelling and was shown to occur through the annulus of the calix[4]arene in a fashion analogous to a biological ion-channel.[67] Calixarenes, in common with crown ethers, can also be adapted to binding softer metal cations through the use of softer ligating groups (Figure **1.11b**). This thiacalixarene displays high selectivity for silver cations and exists in a 1,3-alternate cone conformation. This enables the cation to be bound through a combination of ion-dipole and cation-π interactions.[68]

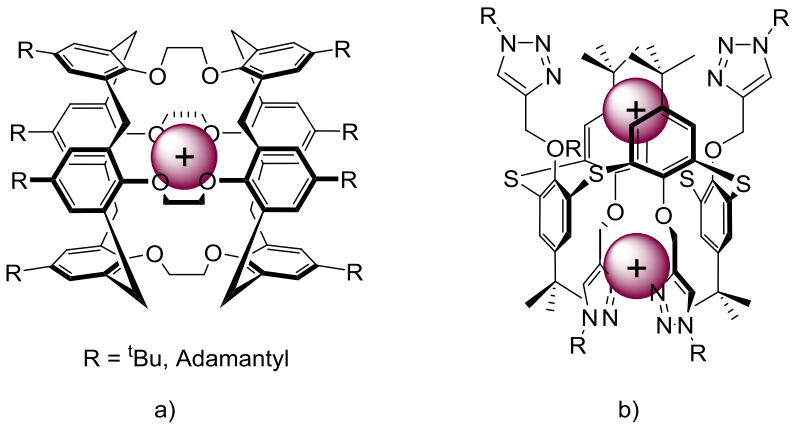

Figure 1.11: Calixarene cation receptors a) Calix[4]tube b) thiacalix[4]arene receptor

1.4.2 Cation Sensing

As mentioned previously, the cation binding event can be signalled through a macroscopic change. There are a plethora of cation sensors in the literature; through incorporation of an appropriate reporter group the binding of the cationic guest can be signalled *via* an optical or electrochemical response. Work by Gokel and co-workers has been reported which incorporates ferrocene into a cryptand backbone (Figure **1.12a**).[69] The close proximity of the reporter group gives rise to a redox couple at more positive potential in the presence of alkali-metal and silver cations due to the destabilisation of the oxidised ferrocenium ion. This is also elegantly illustrated by Martinez-Manez's fluorescent, squaraine based, Hg^{2+} sensor which is capable of signalling the presence of mercury ions at nanomolar concentrations in water (Figure **1.12b**).[51] By incorporating a ligating atom directly onto the fluorophore it is also possible to change the underlying photophysical processes which govern the degree of fluorescence; the naphthalene appended calix[4]arene (Figure **1.12c**) was shown to be selective for sodium ions in ethanol-water mixtures, the binding event being signalled by modulating the degree of photoinduced-electron-transfer (PET) within the fluorophore.[70]

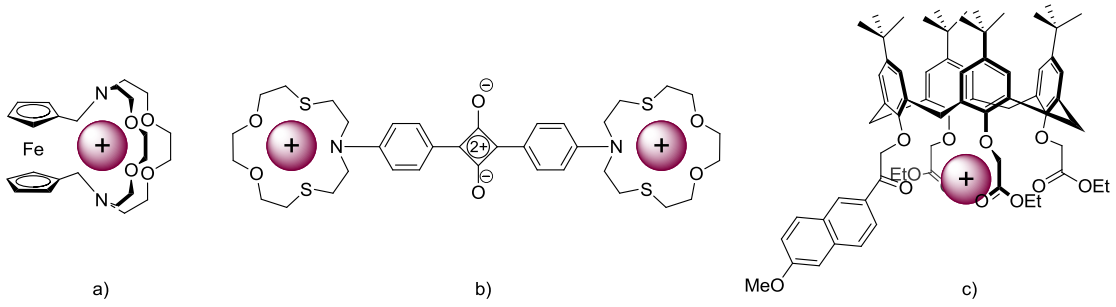

Figure 1.12: Cation sensors a) ferrocene cryptand b) squaraine Hg^{2+} sensor c) calixarene PET sensor

1.4.3 Anion Recognition

In common with cations, the regulation of anions in biological and environmental settings is of the utmost importance. This is emphasised by the fact that the majority of enzyme substrates and co-factors are anionic,[71] and the contribution of anions to pollution hazards such as the production of acid rain by nitrates and sulphates[72] and the threat posed by the release of the radioactive pertechnetate anion by the nuclear industry.[73] In addition, the misregulation of chloride has been linked to diseases such as cystic fibrosis[74] while it has been shown that the fluoride anion is crucial for healthy teeth and bones.[75, 76]

The area of anion recognition is relatively underdeveloped when compared to the field of cation recognition which is a result of several key factors. Anions are larger and are therefore less charge-dense than their isoelectronic cations and, in addition, display a range of geometries (Figure **1.13**). These lower symmetry geometries add to the difficulty of synthesising abiotic receptors in that a more complex three-dimensional cavity is required but do present an opportunity to distinguish by shape as well as size of the guest, a rarity in the cation coordination field.

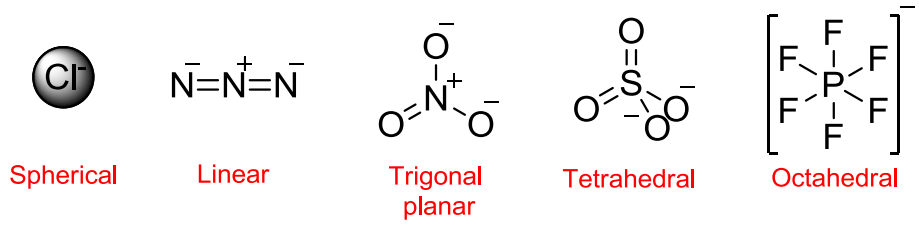

Figure 1.13: The range of geometries exhibited by anions

The affinity of a receptor for a given anion is affected by the identity of the solvent which interacts with both the free anion and receptor. The hydrogen-bond donating and accepting ability must be considered, since donors will interact strongly with the anion while acceptors

will typically interact strongly with the host. Solvents which have a strong donating and accepting capability, such as water and alcohols, are thus considered to be more competitive than solvents such as tetrahydrofuran which is a strong hydrogen-bond acceptor but only a weak donor. Furthermore, different anions are solvated to varying degrees which is related to the Hofmeister series of anion hydrophobicity.[33] As a consequence the larger hydrophobic iodide anion is less heavily solvated in polar protic solvents than smaller hydrophilic halides such as fluoride and chloride. An additional factor to consider is the pH dependence of anions where, in the case protonated receptors, anion complexation is restricted to a specific pH solvent-dependent window. Basic anions such as fluoride and acetate are also known to deprotonate acidic amide and urea based receptors in polar organic media.[77]

Taking inspiration from the numerous biotic receptors, considerable attention has been focused in the area of synthetic anion receptors in recent years. The design of such receptors typically relies on three different philosophies; firstly by incorporating positively charged moieties into the anion receptor to increase binding strength through electrostatics, secondly by use of ion-dipole interactions, for example through hydrogen- or halogen-bonding, and thirdly by using metal-anion interaction or Lewis acid coordination to effectively bind the anionic host.

1.4.3.1 Positively Charged Receptors

1.4.3.1.1 Protonated Amine Receptors

The first synthetic anion receptors, reported by Park and Simmons in 1968,[78, 79] were macrobicyclic hosts that incorporated protonated secondary ammonium groups within a cryptand-like structure. These hosts, named katapinands, recognised halide anions in

aqueous acidic media though a combination of electrostatic and hydrogen-bonding interactions.[78] The receptor, which displayed the greatest affinity for chloride, was shown by X-ray crystallography to bind the guest within the macrocyclic cavity (Figure **1.14**).[80] Although the receptor only displayed modest selectivity between the halides it established the field of synthetic anion receptors.

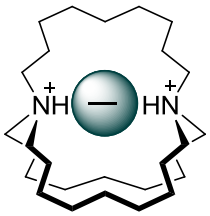

Figure 1.14: Park and Simmon's [9.9.9]katapinand

The cryptand-like structure of the katapinands led to a systematic study by Lehn in which a variety of macrobicyclic polyammonium hosts were synthesised. It was demonstrated that these hosts exhibited a strong relationship between selectivity and the size and shape of the macrobicyclic cavity. For example, a relatively small hexaprotonated host (Figure **1.15a**) displayed selectivity for fluoride ($\log K_{(aq)} = 10.55$ in aqueous media) while a larger receptor was found to be selective for the linear azide anion (Figure **1.15b**).[81, 82] Sessler has expanded this approach by using protonated forms of expanded porphyrins to bind fluoride.[83] More recently, it has been shown that protonated amine receptors can also be used to bind oxoanions including the biologically relevant ADP and ATP.[84-86]

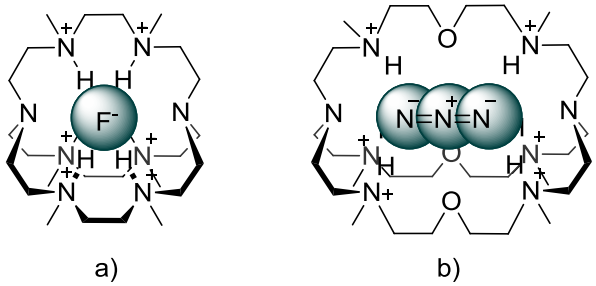

Figure 1.15: Macrobicyclic polyammonium receptors a) fluoride selective host d) azide selective host

1.4.3.1.2 Quaternary Ammonium Receptors

In order to circumvent the pH-dependent limitations of polyammonium based receptors, Schmidtchen synthesised caged-like host structures containing a tetrahedral array of quaternary ammonium groups. The absence of significant hydrogen bond donors means that these receptors rely almost entirely on electrostatic interactions. However, they were observed to bind halides in water within the central cavity (Figure **1.16**),[87, 88] and displayed size-discrimination between the halides by varying the length of the X linker and thereby altering the size of the cavity.

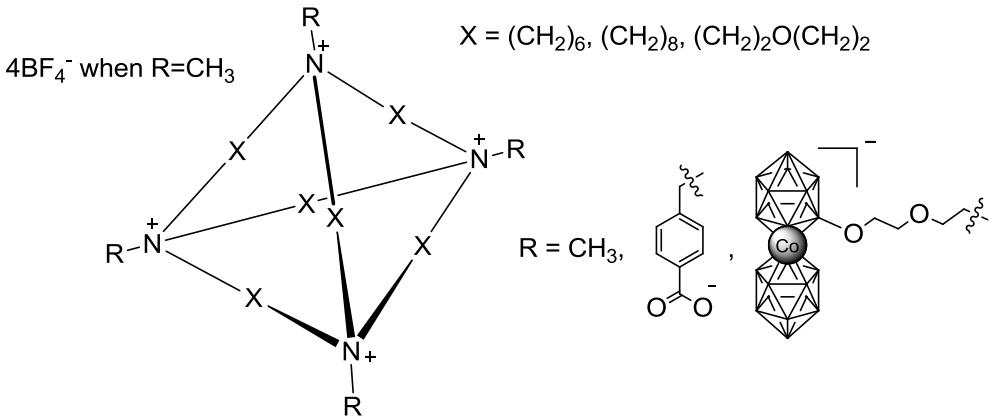

Figure 1.16: Schmidtchen's quaternary tetraammonium hosts

In subsequent work, using zwitterionic hosts that contain appended negatively charged groups such as carboxylate and a cobalt carborane, it was demonstrated that the binding of

the halide guest could be enhanced significantly as a consequence of negated competitive counteranion host interactions.[89, 90]

1.4.3.1.3 Guanidinium-based Receptors

Despite the high affinity for anions exhibited by Schmidtchen's cages, the non-directionality of electrostatic interactions in quaternary ammonium receptors mean they suffer from low selectivity compared to hydrogen-bond based hosts. This limitation is alleviated in guanidinium receptors which marry the strong electrostatic attraction of ammonium hosts with the directional requirement of hydrogen-bond based receptors. Although guanidinium cations are protonated, the basicity of the conjugate-base is significantly higher than amines and thus remain protonated over a larger pH window (pK_a = 13.5).[91] The planar, Y-shaped geometry of this motif, coupled with the positive charge is complementary to oxoanions such as carboxylates (Figure **1.17a**).[92]

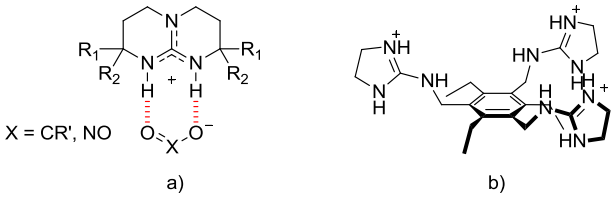

Figure 1.16: Guanidinium anion receptors a) oxoanions binding mode b) Anslyn's citrate receptor

This high degree of complementarity and selectivity is illustrated in Anslyn's tripodal citrate receptor (Figure **1.17b**). Citrate was found to have an association constant of 6.9 × 10^3 M^{-1} in water, whereas other simpler oxoanions were bound over an order of magnitude more weakly.[93]

1.4.3.1.4 Imidazolium and Triazolium Receptors

In recent years attention has been directed to cationic heteroaromatic species such as imidazolium and triazolium. Receptors of this type share the advantages of guanidinium receptors in that strong electrostatics are combined with directional C-H hydrogen-bonding. Since the first imidazolium-based anion receptors were reported in 1999 by Sato[94] and Alcalde (Figure **1.18a** and **1.18b**),[95] the area has flourished. This has been stimulated by the copper catalysed azide-alkyne cycloaddition (CuAAC) 'click' reaction which enables facile synthesis of 1,2,3-triazoles.[96] Recent work by Sessler and co-workers incorporates the triazolium motif into a tetracationic macrocycle (Figure **1.18c**).[97] The host was found to be selective for tetrahedral oxoanions, $K_a = 3.92 \times 10^5$ M^{-1} for HSO_4^- in $(CH_3)_2CO/H_2O$ (2:3) where halides, carboxylates and nitrate displayed no significant binding in this solvent system.

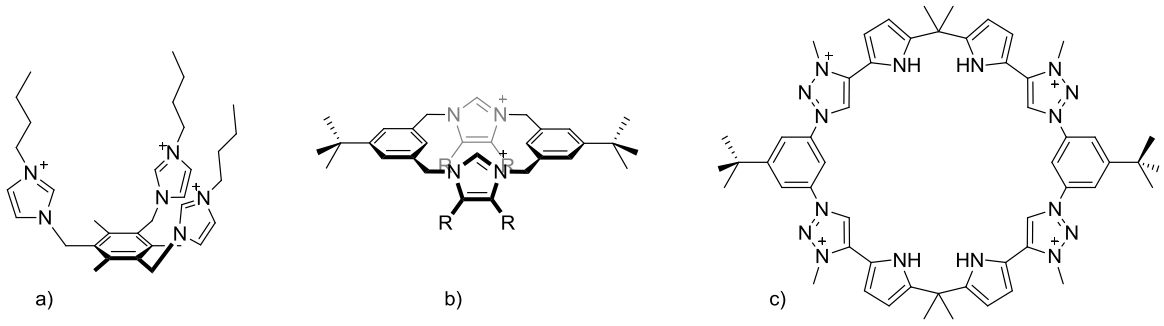

Figure 1.18: Imidazolium and triazolium-based anion receptors by a) Sato b) Alcalde c) Sessler

1.4.3.2 Neutral Anion Receptors

The vast majority of neutral anion receptors utilise ion-dipole interactions such as hydrogen- or halogen-bonding to recognise anions. The directional requirements of these interactions provide an opportunity to increase the selectivity of the hosts by designing three-dimensional cavities that are complementary to the geometry of the guest of interest. Research in this

area is dominated by hydrogen-bond based receptors but halogen-bonding receptors are becoming increasingly common in the literature.[98]

1.4.3.2.1 Amide- and Urea-based Receptors

The amide motif is a powerful tool in the supramolecular chemists arsenal in constructing synthetic anion hosts. Although the first amide-based anion receptor was reported in 1986 by Pascal (Figure **1.19a**),[99] research in this area was not fully appreciated until Crabtree reported the now ubiquitous isophthalamide motif in 1997 (Figure **1.19b**),[100] since then there has been a rapid expansion of interest.[101, 102] Due to the prevalence of amides in proteins and other biological molecules, neutral amide receptors typically look to Nature for inspiration. One notable example is Kubik's peptidic macrocycles which strongly bind iodide and sulphate in the highly competitive 4:1 D_2O/CD_3OD solvent mixture. The magnitude of the association is due to hydrogen-bonding which is augmented by favourable conformational and solvatophobic effects (Figure **1.19c**).[103, 104]

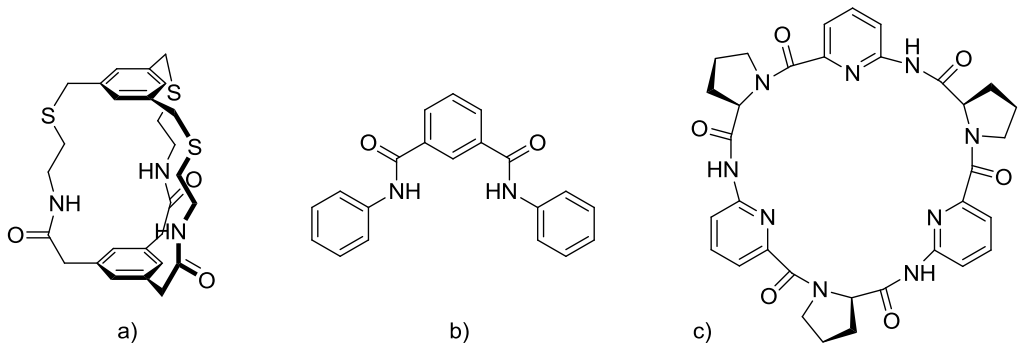

Figure 1.19: Amide receptors a) Pascal's cyclophane b) Crabtree's isophthalamide receptor c) Kubik's peptidic macrocycle

The urea and thiourea motifs are a specific type of hydrogen-bonding motif that have been exploited extensively in many abiotic anion receptors in part due to their facile synthesis and synergistic arrangement of hydrogen bonds.[105] This arrangement makes them particularly

potent chelators of oxoanions such as carboxylates and nitrates.[106] For example, Gale's acyclic diurea binds oxoanions up to three orders of magnitude more strongly than halides in DMSO/D_2O (99.5:0.5) due to the convergent arrangement of the two urea groups (Figure **1.20a**).[107] Gale and Davis have recently reported a simple aromatic thiourea compound which can function as an anion membrane transporting reagent (Figure **1.20b**) displaying a chloride efflux of 30% across a unilamellar POPC vesicle membrane at only 2 mol% loading.[108,109]

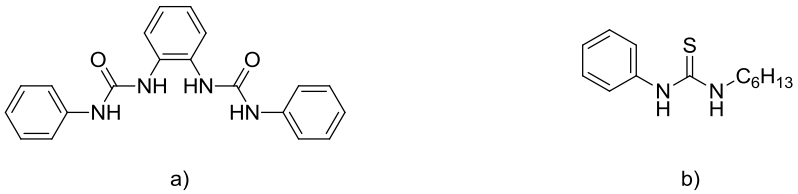

Figure 1.20: Urea and thiourea receptors a) Gale's convergent diurea b) Davis' thiourea membrane transport reagent

1.4.3.2.2 C-H Hydrogen-bonding Receptors

The hydrogen bond strength of C-H donors compared to analogous N-H and O-H donors is relatively weak. This is due to the lower electronegativity of carbon when compared to nitrogen and oxygen and hence a lower degree of polarisation across the X-H bond, although this can be augmented by positive charge as seen in imidazolium and triazolium based receptor systems (Section 1.4.3.1.4). As a consequence, neutral C-H donors have traditionally been overlooked as a motif to construct efficacious anion receptors. Theoretical calculations by Hay have shown, however, that C-H hydrogen-bonding can display significant, if not similar, bond strengths when compared to N-H and O-H donors depending upon the nature of the electron–withdrawing moiety to which it is linked.[110] The cumulative strength of

multiple C-H donors incorporated into a highly preorganised cyclic triazolophane receptor has been demonstrated by Flood and co-workers (Figure **1.21a**). The neutral macrocyclic triazole host exhibits strong binding of chloride in CH_2Cl_2 (K_a = 1.1 × 10^7 M^{-1}) through purely C-H hydrogen-bonding.[29] An acyclic receptor reported by Craig incorporating the triazole motif is capable of wrapping around a halide. This foldamer exhibited a large preference for smaller halides over iodide in acetone with K_a = 1.2 × 10^4 M^{-1} and K_a = 1.1 × 10^4 M^{-1} for chloride and bromide respectively (Figure **1.21b**).[111, 112]

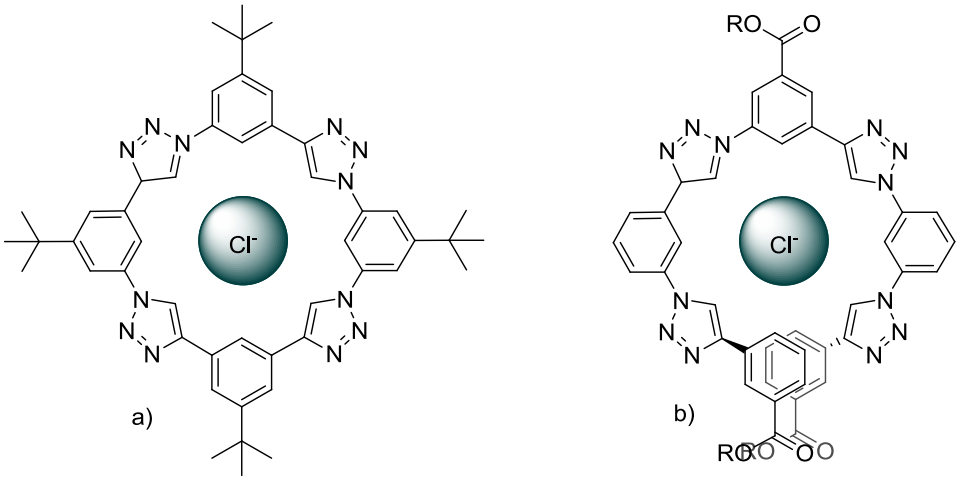

Figure 1.21: C-H hydrogen bond receptors by a) Flood b) Craig

1.4.3.2.3 Halogen-bonding Receptors

Halogen-bonding shares many similarities with ubiquitous hydrogen-bonding, although it has only relatively recently been exploited in the field of anion recognition. Although halogen-bonding interactions have been well documented in the solid state for some time, the first solution state all halogen bonding monotopic anion receptor was reported by Taylor and co-workers in 2010. The neutral tripodal receptor was found to be selective for chloride over bromide and iodide with an association constant of K_a = 1.9 × 10^4 M^{-1} in acetone (Figure

1.22a).[113] More recently, Resnati has shown that potent anion receptors can be constructed by using charge-assisted halogen-bonding. The imidazolium halogen-bonding anion receptor (Figure **1.22b**) was found to bind strongly the oxoanions acetate (K_a = 260 M^{-1}) and dihydrogenphosphate (K_a = 1100 M^{-1}) in DMSO.

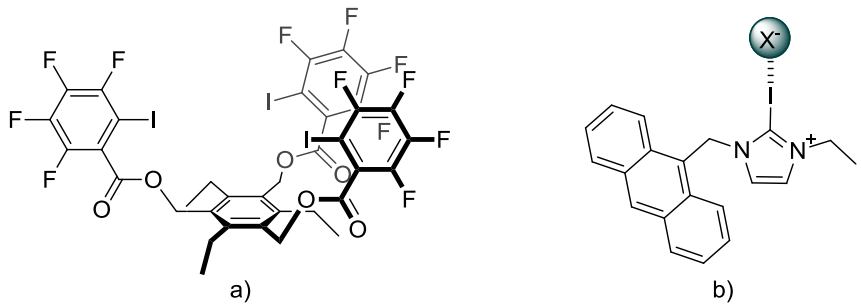

Figure 1.22: Halogen-bonding anion receptors by a) Taylor b) Resnati

1.4.3.3 Lewis Acid and Metal-based Receptors

Another class of receptors are Lewis acid based systems in which anion-binding is driven by the formation of a dative bond between the anion and the Lewis acid. A wide range of Lewis acids have been employed including those of boron,[114-117] tin,[118] transition metals[119-122] and even the actinides.[123, 124] These types of receptors often utilise multiple electrophilic centres to bind the anionic guest, such as Gabbai's boron-mercury based receptor (Figure **1.23**), which selectively complexes fluoride in tetrahydrofuran between the heteronuclear Lewis-acidic sites.[125]

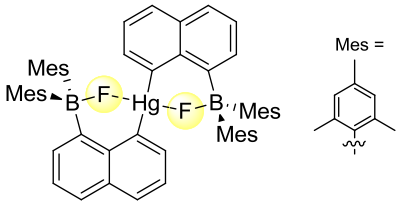

Figure 1.23: Gabbai's boron-mercury based fluoride receptor

1.4.4 Anion Sensing

In order to have practical application it is often desirable for an anion receptor to simultaneously bind and sense the guest substrate. This is typically achieved through the use of a covalently attached reporter group, although more advanced methods exist such as the use of chemodosimeters and displacement assay techniques. In a displacement assay the host molecule forms a complex with a signalling molecule or group. Upon addition of the appropriate analyte the substrate will preferentially bind to the receptor and thereby displace the signalling group from the binding site, giving rise to a macroscopic response. Chemodosimeters are sensors which are reactive to the target analyte; upon addition of the substrate the guest reacts with the host, inducing a change in the signal from the sensing unit. The area of luminescent sensing of anions is pertinent to the content of this thesis, with particular attention focused on the use of inorganic luminophores as the reporter group.

1.4.4.1 Luminescent Anion Sensors

Luminescent anion sensors typically produce a change in the emissive properties of the host molecule. This is observed as a change in wavelength, intensity or lifetime of the attached luminophore which signals the binding of the analyte. Luminescence can itself be split into two main categories; *fluorescence* and *phosphorescence*. These are differentiated by whether the relaxation of the photon to the ground state is an allowed or forbidden transition. Fluorescence is the emission from a singlet excited state to a singlet ground state and is thus an allowed transition, typically exhibited by simple organic dyes. Phosphorescence refers to the emission arising from a forbidden transition and as a result is generally much weaker

than fluorescence. These disallowed transitions are typical for metal-based systems such as transition metal and lanthanide complexes.

The advantages of luminescence spectroscopy over other sensing methods are two-fold. Firstly, the ability to observe emissive species at nanomolar concentrations is desirable as it permits the detection of very low concentrations of the analyte. Secondly, this method negates the use of expensive instrumentation as naked-eye detection is often possible for qualitative analysis, although quantitative data can be obtained with the use of spectrophotometers.

One of the seminal examples of a luminescent sensor for carboxylate anions was a zinc-anthracene based receptor reported by Fabbrizzi and co-workers (Figure **1.24**).[125]

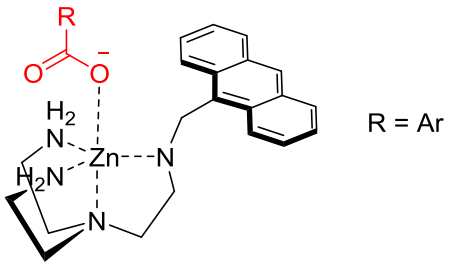

Figure 1.24: Fabbrizzi's zinc-based carboxylate anion sensor

In methanol the authors found that fluorescence quenching of the anthracene unit was observed with certain aromatic carboxylates which was ascribed to electron transfer from the anthracene to the anionic guest, facilitated by coordination. This method of anion-induced photo-electron-transfer has been widely exploited by many subsequent examples, for instance in Gunnlaugsson's series of naphthalimide thiourea receptors (Figure **1.25**).[126] These employ the same principles but negate the use of an aromatic guest. The naphthalimide receptors display an internal charge-transfer (ICT) band which was quenched upon the addition of

dihydrogenphosphate in DMSO. The ground state absorbance of the receptor upon addition of the guest displayed no change, indicating an electron-transfer mechanism.[127]

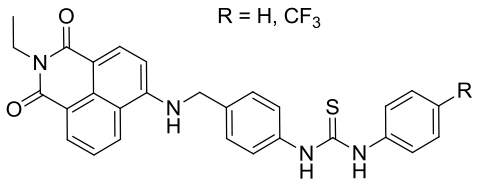

Figure 1.25: Gunnlaugsson's naphthalimide thiourea PET sensors

Despite the relatively facile synthesis of receptors incorporating simple organic dyes, much attention has been focused on the use of inorganic luminophores such as transition-metal and lanthanide reporter groups for sensing purposes. This is driven in part by the relevance of sensing to biological applications, to which inorganic complexes have distinct advantages over organic dyes. These include their high photostability and hence low toxicity, long lifetimes and emission in the optical window for optimum tissue penetration.

Transition-metal based receptors typically exhibit ^{3}MLCT luminescence. Well studied examples are derivatives of ruthenium (II) tris-bipyridyl systems which display long lifetimes,[128] meaning they are more susceptible to non-radiative decay than organic dyes. As a result anion complexation can result in rigidification of the system which decreases the vibronic and rotational relaxation of the excited state compared to the more flexible free host.[129] The rigidity effect is exploited by two examples by Beer and Pinet (Figure **1.26a** and **1.26b**).

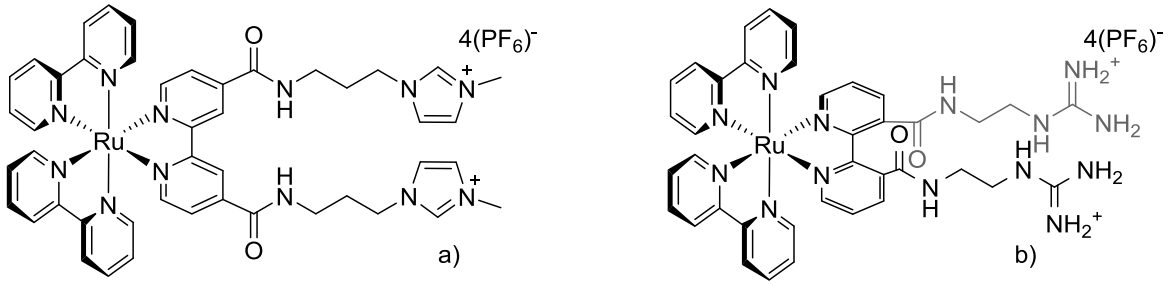

Figure 1.26: Ruthenium diimine sensors by a) Beer b) Pinet

Beer's receptor was found to display an increase in emission intensity upon addition of chloride, bromide and dihydrogenphosphate in MeCN/H_2O (9:1).[130] The guanidinium functionalised complex reported by Pinet also shows a four-fold increase in emission intensity in the presence of L-glutamate in acetonitrile solution.[131] Both examples report a slight hypsochromic shift due to the destabilisation of the ^{3}MLCT state induced by anion-binding.

A different approach reported by Williams married the unique properties of metal-based luminescence with that of already established sensing methods. By incorporating the pyridinium motif into an iridium (III) bis-terpyridine complex the authors reported the quenching of the emission by chloride anions in aqueous solution (Figure **1.27**).[132] This operates through the well-established charge-transfer quenching of quinolinium systems by chloride[133] but has advantages for *in vivo* use due to the long-lived phosphorescence.

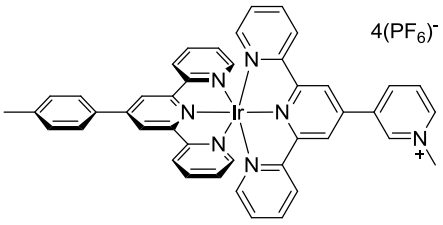

Figure 1.27: Iridium (III) bis-terpyridine chloride sensor

In addition to the use of transition metals, lanthanides have long proven to be effective molecular sensors,[134] particularly in a biological setting.[135] The high coordination number of

lanthanides results in the ligation of solvent molecules to otherwise unsaturated complexes. This propensity for ligation has led to the widely-exploited strategy of coordination of the anion to the metal centre in receptors of this type.[136] Parker and co-workers reported a europium complex capable of detecting citrate anions in aqueous media (Figure **1.28a**). Changes in the emission spectrum of the complex enabled ratiometric determination of citrate in the presence of other biologically relevant oxoanions.[137] Importantly, the change in the $\Delta J = 2$ transition supported the proposed binding at the lanthanide centre. Another example has shown strong selectivity for fluoride in aqueous buffered solution (Figure **1.28b**). A significant increase in the europium's luminescence spectrum was observed upon fluoride binding to the lanthanide metal centre as a consequence of the displacement of axially coordinated water from the metal's ninth coordination site. All other halides and oxoanions gave no change in the emission spectrum, presumably due to their inability to displace the europium coordinated water solvent molecule.

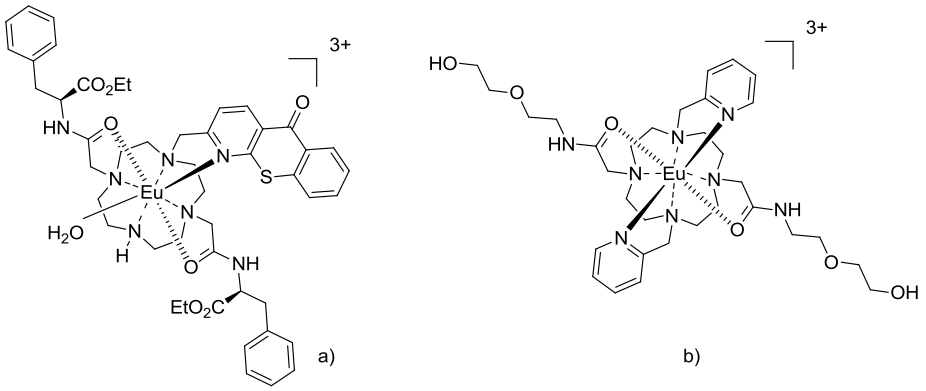

Figure 1.28: Lanthanide sensors for a) citrate b) fluoride

In addition to using covalently attached reporter groups to sense anionic species, the fluorescent displacement assay technique and chemodosimeter approaches have also afforded

highly selective probes for anions.[138, 139] The displacement assay technique has been exploited in a variety of sensors since the pioneering work by Anslyn and Fabbrizzi.[140-143] In this example a dimetallic zinc complex is capable of detecting the biologically relevant adenosine triphosphate (ATP) in buffered aqueous solution (Figure **1.29**). The anthracene fluorescence is quenched by the coordinated pyrocatechol violet (PV) but is recovered upon displacement of PV by ATP. Importantly, the probe can distinguish between ATP and other anions such as halides and adenosine diphosphate due to the large intermetallic distance.

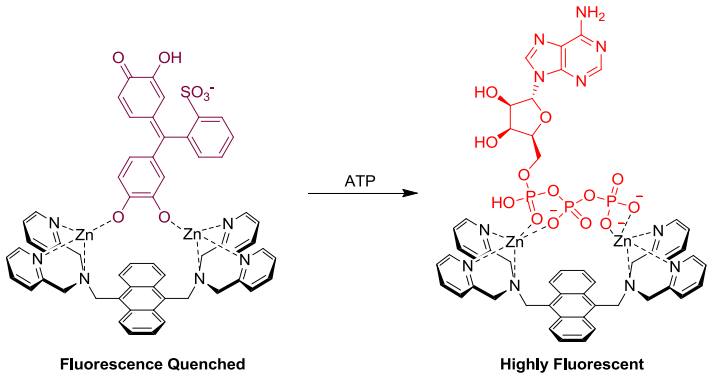

Figure 1.29: Displacement assay sensor for adenosine triphosphate

A cyanide sensor reported by Hong and co-workers utilises the chemodosimeter principle.[144] The nucleophilic anion undergoes addition to a non-fluorescent aromatic aldehyde in water to produce the cyanide adduct. Subsequent proton transfer resulted in a low-lying charge transfer state being formed which was highly fluorescent, signalling the presence of cyanide (Figure **1.30**). This approach can yield highly selective chemosensors but is inherently limited to reactive analytes.

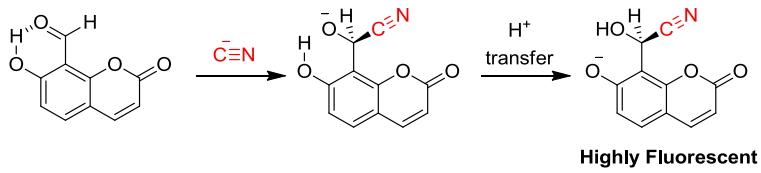

Figure 1.30: Chemodosimeter for cyanide anions

1.4.4.2 Electrochemical Anion Sensors

The electrochemical sensing of anions is achieved through incorporation of redox-active groups such as ferrocene or tetrathiafulvalene (TTF) into anion receptors. The binding of the anionic guest is signalled by a change in the redox couple of the reporter molecule and is usually as a result of the stabilisation of the oxidised or destabilisation of the reduced species due to electrostatic interactions between the host and the guest.[116] A classic example is a poly-azaferrocene macrocycle, which displayed a cathodic shift of 50 mV upon the addition of phosphate in aqueous media (Figure **1.31a**).[145] Aldridge and co-workers have reported a fluoride sensor incorporating the ferrocene motif (Figure **1.31b**). The redox couple in the presence of fluoride displayed a large 550 mV shift upon complexation in dichloromethane.[146] This is a result of the conversion of the conjugated 3-coordinate arylborane motif to a non-conjugated anionic 4-coordinate borate, which impacts on the redox couple potential of the ferrocene moiety.

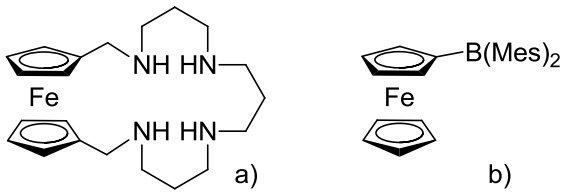

Figure 1.31: Electrochemical anion sensors for a) phosphate b) fluoride

1.4.5 Recognition and Sensing of Ion-Pairs

In comparison with the fields of cation and anion recognition, the simultaneous binding of both cationic and anionic ion-pair species is less well explored. Ion-pair recognition has advantages over monotopic complexation such as increased strengths of association and

greater selectivity, but also has application in the fields of membrane-transport research, salt solubilisation and extraction.[147, 148]

There are three main classes of ion-pair receptor, two of which are heteroditopic and the third being a *ditopic* cascade complex (Figure **1.32a**). Heteroditopic receptors can bind the ion-pair either as a contact ion-pair (Figure **1.32b**), which directly utilises the Coulombic attraction between the two charged species to aid binding, or as a solvent separated ion-pair (Figure **1.31c**).

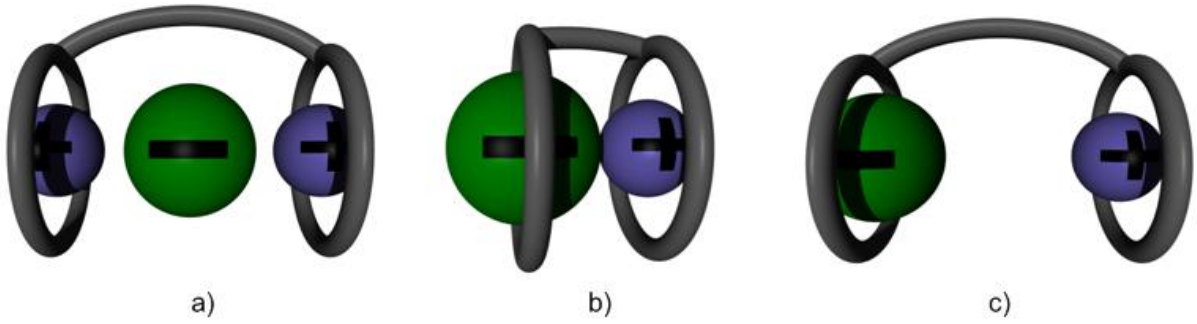

Figure 1.32: Ion-pair binding motifs a) cascade-complex b) contact c) separated

The equilibria of ion-pair receptors are more complex than simple monotopic hosts due to the number of species in solution which can associate (Figure **1.33**). These various equilibria have a profound effect on the strength of association of the ion-pair and also give rise to cooperativity effects.[149] Ion-pair complex formation with the host (K_2) competes with the conflicting processes of host-cation complexation (K_1), host-anion complexation (K_3) and ion-pair sequestration (K_{ip}). Competitive ion-pair sequestration is an important consideration, particularly in non-polar solvents where it leads to precipitation. If the cation and anion binding events act independently, then $K_2 = K_1 + K_3$ and ion-pair binding is non-cooperative. This is usually the case for heteroditopic systems containing rigid widely

separated cation and anion binding sites. Alternatively, the binding may be cooperative whereby the two charged substrates produce a stabilising interaction by virtue of favourable electrostatic or allosteric effects ($K_2 > K_1 + K_3$). Finally, the binding may be anti-cooperative ($K_2 < K_1 + K_3$), where the binding of a charged guest inhibits binding of the counter-ion, either via competing ion-pairing outside the receptor or by unfavourable host conformational effects. While negative cooperativity is generally not desired in ion-pair receptors it has application in the construction of molecular INHIBIT logic gates.[150]

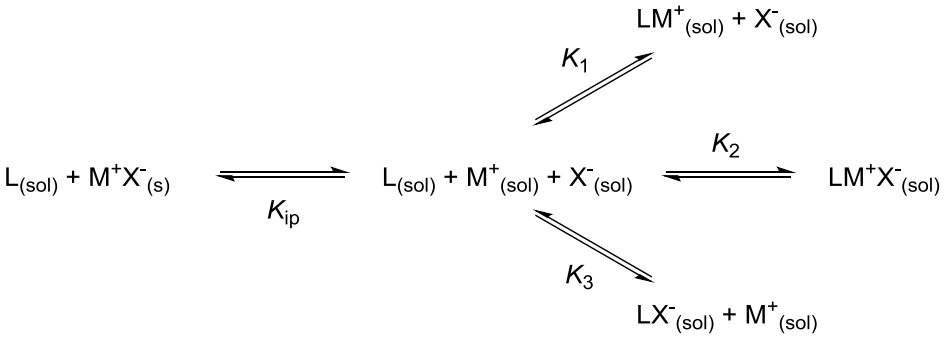

Figure 1.33: Simplified ion-pair binding equilibria

Ion-pair binding can be achieved by using a cascade-complex approach. The literature is dominated by examples wherein two or more metal cationic centres are bound within the receptor and are able to associate with an anionic guest species. This is attained through metal-anion coordination and coulombic interactions. The selectivity in these systems has been shown to depend not only on the size and shape of the receptor cavity but also on the interatomic distance between the two metal centres.[151, 152] One of the earliest examples is a dinuclear copper complex which is selective for linear azide and cyanate anions (Figure **1.34a**).[153] A related example, also selective for azide and the isostructural cyanate in aqueous solution, incorporates the fluorescent anthracene unit. Although the cage compound

complexes azide and cyanate, the binding event is only signalled for azide due to an efficient electron-transfer process to the anthracene moiety (Figure **1.34b**).[154] In a recent example by Lu, the zinc(II) cryptate has been shown to bind bicarbonate *via* fixation of carbon dioxide (Figure **1.34c**).[155, 156] Heterometallic cascade complexes are also known, one example having been reported by Shinkai in which iodide is complexed between a zinc porphyrin and a calix[4]arene lower rim bound sodium cation (Figure **1.34d**).[157] Interestingly, the binding affinity of iodide in $CHCl_3/CH_3CN$ (4:1) could be tuned by varying the identity of the alkali-metal cation.

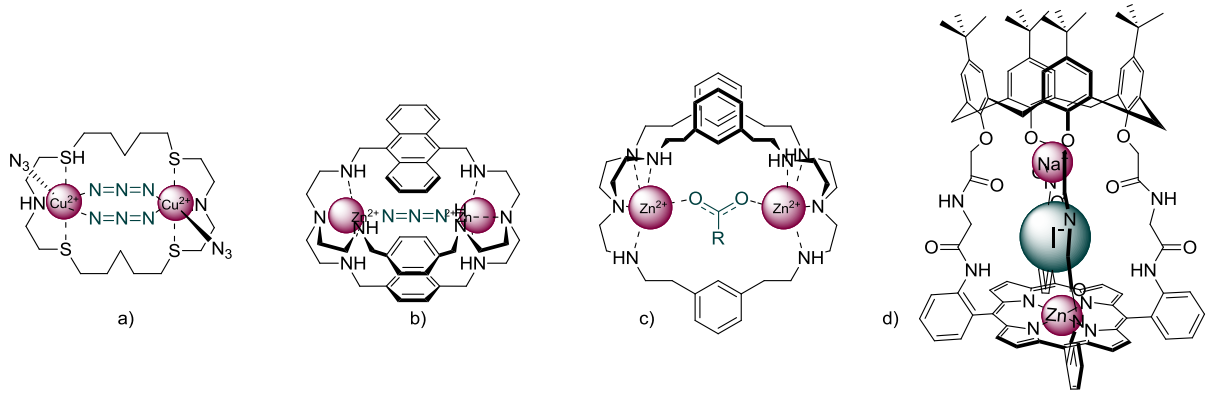

Figure 1.34: Transition metal cascade complexes by a) Lehn b) Fabbrizzi c) Lu d) Shinkai

Despite the prevalence of transition-metal cascade complexes in the literature there is a dearth of examples of two anion bound-cation cascade analogues. The first example of such a receptor was reported by Bowman-James, which shows encapsulation of a water molecule bridging two fluoride anionic centres *via* hydrogen-bonding (Figure **1.35a**).[158] While not a true cascade complex, it demonstrated the approach by which anion-based cascade complexes could be constructed. A recent example by Ballester and co-workers demonstrates the high degree of cooperativity observed in these types of receptors. The calix[4]pyrrole receptor bound an ion-pair quartet in a cascade and separated binding mode (Figure **1.35b**).

Isothermal titration calorimetry (ITC) measurements against a model compound determined the cooperativity factor to be in excess of 10^5 for tetrabutylammonium (TBA) cyanate and TBA chloride. This is due to the enforced close-contact of the three ions which associate inside the cavity. Importantly, when the larger methyltrioctylammonium cation was used no cooperativity was observed.[159]

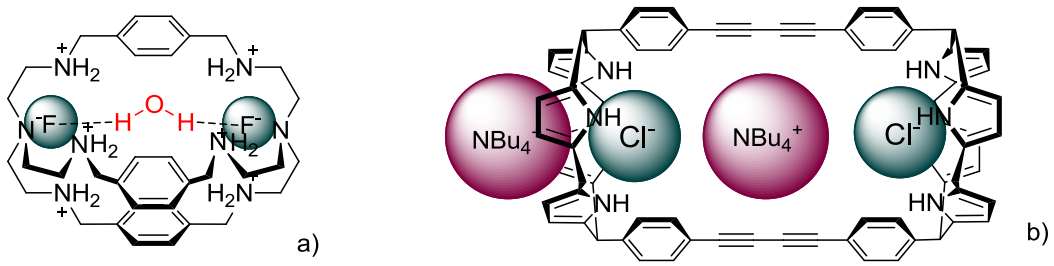

Figure 1.35: Anion cascade complexes by a) Bowman-James b) Ballester

Unlike cascade-complexes, separated ion-pair heteroditopic host systems do not exploit any direct electrostatic interaction between the constituent ions. In spite of this however, favourable through-space and through-bond electrostatic interactions, in combination with conformational effects, can lead to cooperative ion-pair binding behaviour. An early example was reported by Reinhoudt in 1996 which illustrates this principle (Figure **1.36**).[160] The calix[4]arene receptor in $CDCl_3$ displayed intramolecular hydrogen-bonding which competed with anion binding. However, upon addition of alkali-metal cations this intramolecular interaction was broken, thereby increasing the preorganisation of the host. As a consequence halide binding was significantly increased, with chloride displaying an association constant of $K_a > 1.0 \times 10^4\ M^{-1}$ in the presence of sodium whereas no binding was observed in the absence of the alkali-metal cation.

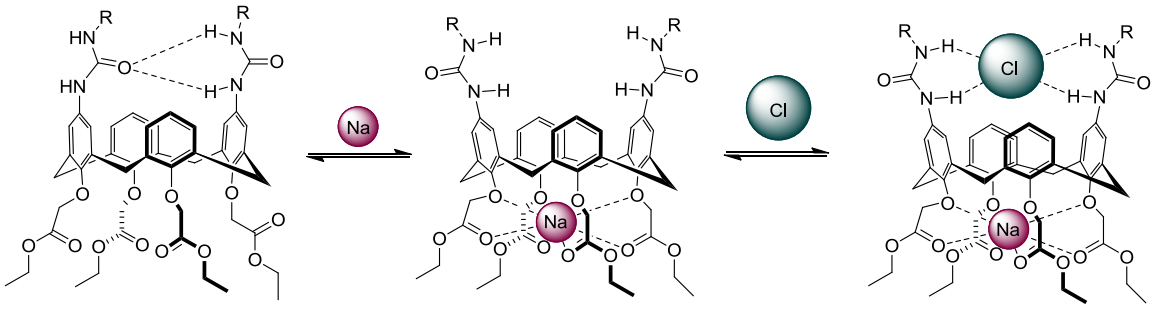

Figure 1.36: Reinhoudt's alkali-metal halide receptor

Other separated ion-pair receptors also employ similar principles whereby the binding of the first analyte preorganises the receptor for the binding of its charged congener and thus gives rise to positive cooperativity. The Lewis-acidic uranyl based receptor complexes potassium dihydrogenphosphate through bis-crown ether potassium cation sandwich complex formation preorganising the receptor's anion recognition site for binding (Figure **1.37a**).[161] This is also exploited in Kubo's urea receptor (Figure **1.37b**); prior addition of potassium ions induces a conformational change giving rise to a chelating urea binding cleft which significantly increases the affinity for phosphate anions.[162] In other work Kim demonstrated how allosteric effects could be employed to construct effective ion-pair sensors (Figure **1.37c**).[163] The calix[4]arene INHIBIT gate displayed maximum excimer emission upon potassium complexation due to efficient **π-π** stacking. Subsequent ligation of dihydrogenphosphate quenched the excimeric emission via PET due to the proximal anion.

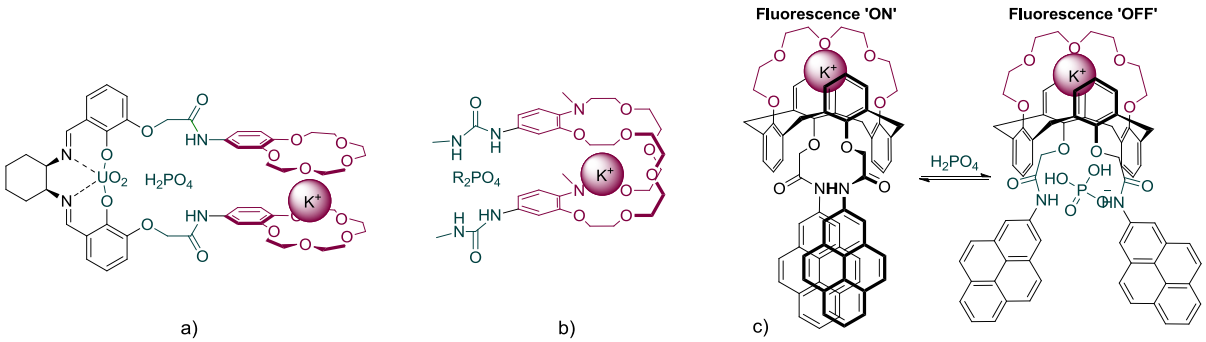

Figure 1.37: Separated ion-pair receptors a) uranyl salen system b) crown-urea c) calix[4]arene INHIBIT gate

Aside from conformational effects, separated ion pair receptors can be prepared which employ indirect interactions between the two constituent ions, such as a solvent bridge. This method not only provides additional stabilising interactions through solvent polarisation but also rigidifies the receptor which is advantageous for strong and selective binding. The sodium fluoride receptor reported by Jurkschat binds sodium fluoride ion-pairs as a contact ion-pair in acetonitrile but in methanol exhibits a bridged structure (Figure **1.38**).[164, 165]

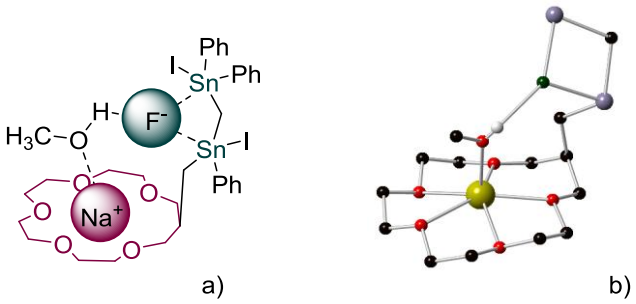

Figure 1.38: Solvent effects a) sodium fluoride receptor with methanol bridge b) crystal structure (ancillary tin ligands and non-hydrogen-bonded hydrogen omitted for clarity)[166]

In recent years Sessler has developed a new class of separated ion-pair receptors. These multi-topic systems have multiple recognition sites for a given targeted ion which enables metathesis of ions in solution.[167] In the example shown in Figure **1.39**, two cation binding sites exist with a strong affinity for potassium and moderate affinity for caesium. The receptor was found to extract caesium nitrate from water into nitrobenzene solution. Uniquely, the expulsion of caesium nitrate could be controlled via addition of potassium perchlorate due to the higher affinity of the host for potassium.[168] This metathesis approach represents a new class of ion-pair receptor with applications in membrane transport and salt solubilisation.

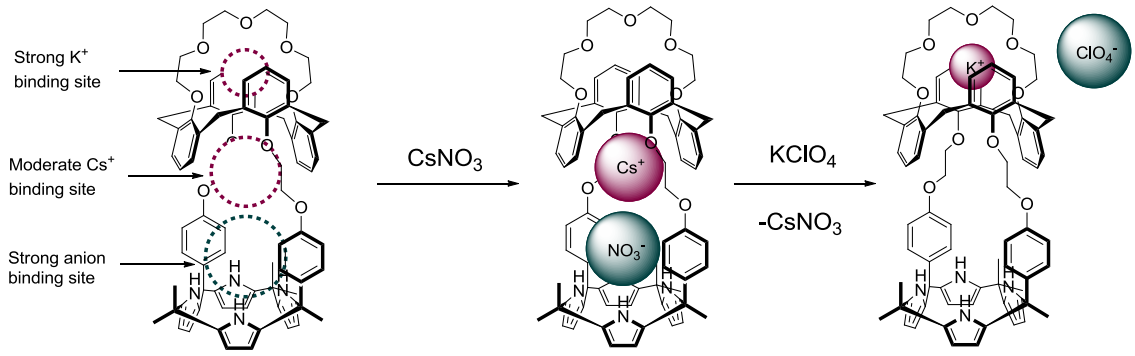

Figure 1.39: Sessler's multitopic caesium transporter

In spite of receiving less attention than separated systems, contact ion-pair receptors are an important area of research, not least for their ability to utilise the direct electrostatic attraction between the two ions. In an early example by Kilburn and co-workers, potassium salts of dicarboxylic acids were bound as a contact ion-pair within an isophthalamide macrocycle (Figure **1.40a**). Additionally the receptor acted as a phase-transfer reagent by extracting aqueous solutions of the salts into chloroform.[169] A related compound reported by Smith illustrates the profound effect coulombic interactions play in the binding affinity of such hosts (Figure **1.40b**). In $CDCl_3$/DMSO-d_6 (85:15) solution the receptor exhibited remarkable cooperativity, with the association of chloride increased over 300 times in the presence of potassium ions.[170] In recent work a receptor which is selective for alkylammonium fluoride ion pairs has been reported by Jabin (Figure **1.40c**).[171] The calix[6]cryptand discriminates between anionic guests based on size with, only fluoride bound in $CDCl_3$. This effectively 'turns on' the receptors ability to subsequently bind alkylammonium ions via electrostatic interactions.

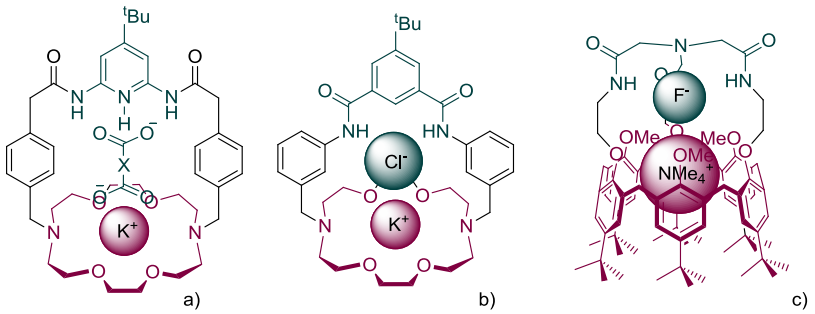

Figure 1.40: Contact ion pair receptors for a) carboxylates b) alkali halides c) alkylammonium fluoride

1.5 Mechanically Interlocked Structures

The area of mechanically interlocked structures is a specific area of research within supramolecular chemistry which has grown significantly in recent years.[172, 173] Rather than being concerned with covalently-bonded species this field is focused on species which are mechanically bonded.[174] The term *mechanically interlocked* describes two or more species which are interpenetrated and cannot be separated without the prior cleavage of a covalent bond. As a result mechanically interlocked structures are kinetically stable even though they are entropically disfavoured with respect to their constituent components.

The most prevalent interlocked structures are rotaxanes and catenanes, whose names are derived from the Latin for wheel and axle, 'rota and 'axis' and chain 'catena'. In analogy to a chain, catenanes consists of two or more interlinked rings (Figure **1.41b**) while a rotaxane comprises a macrocycle threaded over an axle which is terminated with 'stopper' groups that are larger than the annulus of the ring (Figure **1.41a**). The corresponding pseudorotaxane is one which contains no stoppers at the termini and is thus not mechanically interlocked but rather interpenetrated (Figure **1.41c**). The nomenclature of interlocked and interpenetrated

structures typically have a prefix [n] where n refers to the number of constituent parts which are mechanically bonded e.g. a [2]catenane.

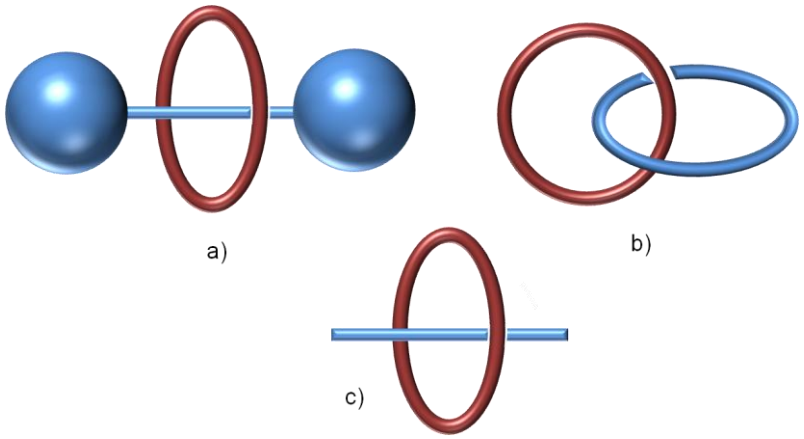

Figure 1.41: Schematic representations of a) [2]rotaxane b) [2]catenane c) [2]pseudorotaxane

1.5.1 Synthetic Strategies

There are a multitude of synthetic strategies by which interlocked structures can be synthesised, although most share the common approach of prior formation of an interpenetrated pseudorotaxane which is converted to the interlocked species *via* covalent bond formation. Catenanes can be synthesised by either 'clipping' a macrocycle precursor[175-177] (Figure **1.42a**) around a macrocycle or by 'double clipping' of two precursors (Figure **1.42b**).[178, 179] Rotaxanes can be constructed through a range of methodologies although formation *via* 'clipping'[180-182] (Figure **1.42c**) and 'stoppering'[183, 184] (Figure **1.42d**), whereby bulky groups are added to the termini of the pseudorotaxane thread, are most commonly employed. Additionally, in the case where the stoppers are of comparable size to the macrocyclic annulus 'slippage' (Figure **1.42e**) may be used to construct the interlocked molecule.[181, 185, 186] In this case the macrocycle is able to 'slip' over the stopper groups under certain conditions such as solvent effects[187] or elevated temperatures.[188]

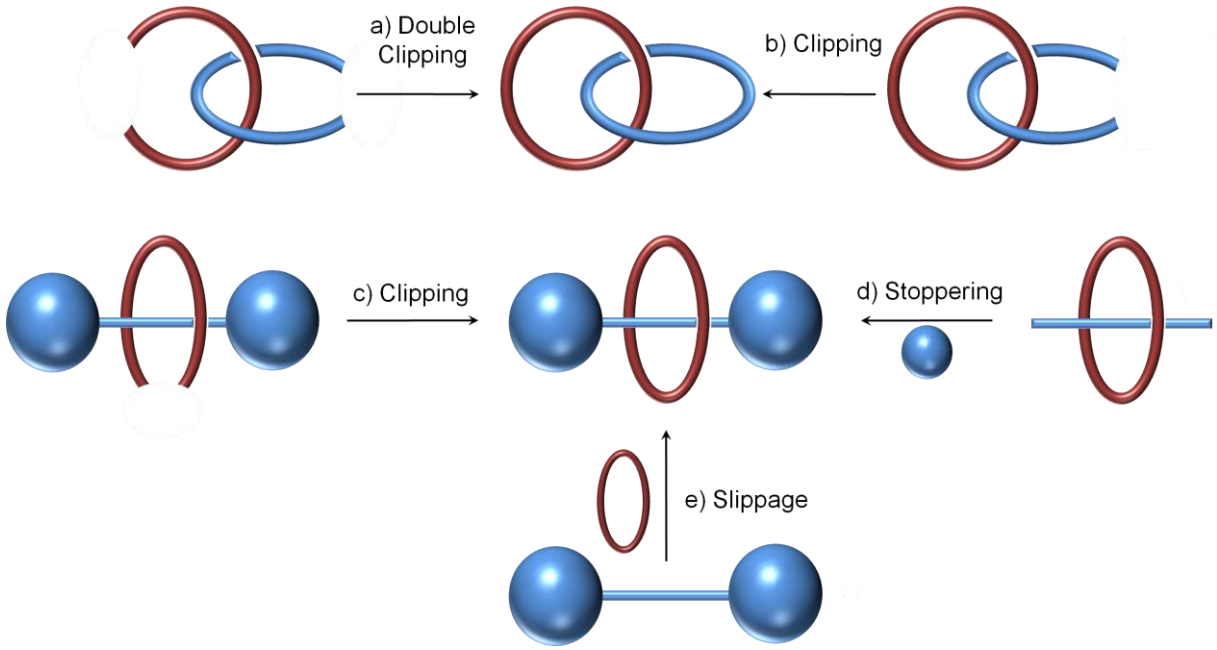

Figure 1.42: Synthetic strategies a) double clipping b) clipping c) clipping d) stoppering e) slippage

1.5.2 Templated Synthesis

In the earliest examples, interlocked structures were formed using a purely statistical approach. The first example by Wasserman in 1960 reported the synthesis of a [2]catenane which was isolated in less than 1% yield.[189, 190] A subsequent resin-supported rotaxane synthesis by Harrison improved yields to 6% through recycling of the axle component multiple times.[191] These limitations led to the use of an alternative *templated* strategy which facilitated self-assembly of the constituent components around the templating species to significantly increase the efficiency of the synthesis.

1.5.2.1 Cation Templation

The use of templation to facilitate the synthesis of interlocked structures was pioneered by Sauvage in the 1980s.[192] The tetrahedral preference of the copper (I) ion was exploited to form an orthogonal complex with two appropriately functionalised phenanthroline ligands

which, upon a 'double clipping' reaction, afforded a [2]catenane (Figure **1.43a**).[193] This metal template approach has since been used to synthesise ever more complex mechanically bonded systems.[183, 184] The advantages of utilising metal templates are many, including strong metal-ligand interactions and well-defined stereochemical preferences. This has been exploited by Leigh, who has demonstrated the viability of differing metal geometries including square-planar palladium (II) (Figure **1.43b**)[194] and linear gold (I) (Figure **1.43c**),[195] as well as a range of octahedral metals.[196, 197] Alkali-metal cations have also recently been used as templates for the construction of interlocked architectures. Chui has reported a sodium cation-templated catenane formed *via* reversible imine formation (Figure **1.43d**) and utilises the well known interaction of alkali-metal cations with polyether compounds.[198]

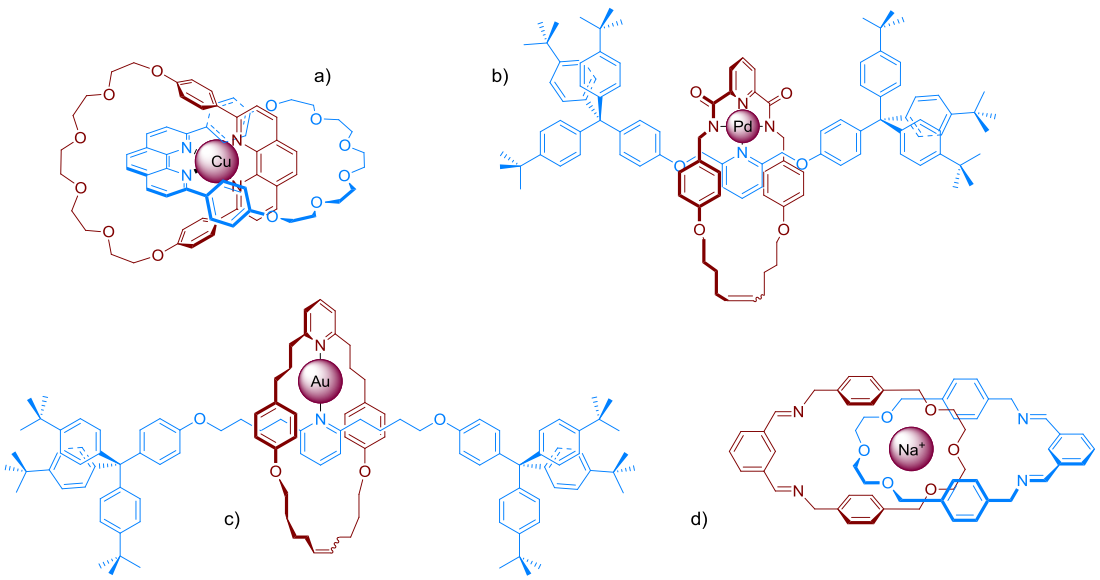

Figure 1.43: Metal templation by a) Sauvage b) and c) Leigh d) Chui

The role of the metal templates described thus far has been *passive*; in recent years Leigh has pioneered the use of *active templation* in which a catalytically-active metal is used as both the template and as the catalyst for the bond forming reaction.[199] These have largely focused on copper-mediated reactions such as the 'click' CuAAC[200, 201] and alkyne heterocoupling[201]

reactions, but more recently palladium catalysed methodologies have also been realised (Figure **1.44**). In this example palladium catalysis is used to couple two stoppered alkynes through the macrocyclic annulus to furnish the interlocked product.[202]

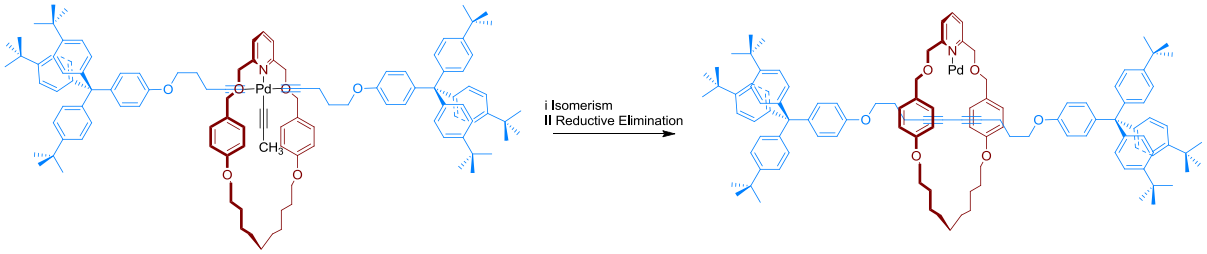

Figure 1.44: Leigh's Pd-catalysed rotaxane synthesis

The area of organic ammonium cation-templation is also a diverse area of research; in combination with polyether macrocycles it has been employed in innumerable examples in the literature for the formation of rotaxanes,[203, 204] catenanes[205](Figure **1.45a**) and molecular machines.[206, 207] Another example of organic cation-templation is the seminal work by Stoddart.[208] These charge-assisted donor-acceptor aromatic interactions occur between electron-poor 4,4'-bipyridinium macrocycles paired with electron-rich hydroquinone (Figure **1.45b**) or dihydroxynaphthalene groups and have been used to construct a variety of higher order architectures.[209, 210]

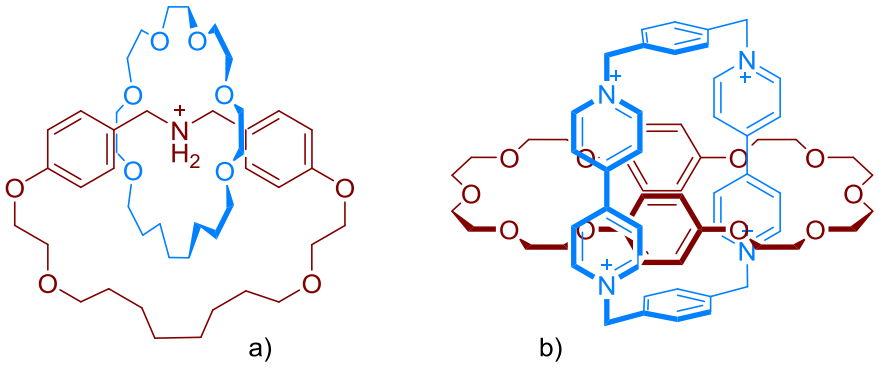

Figure 1.45: Organic cation templation a) ammonium b) bipyridinium

1.5.2.2 Neutral Templation

The presence of charged template species is not always necessary for the construction of interlocked architectures. In 1992 Hunter reported the synthesis of a rotaxane through the use of favourable hydrogen-bonding.[211] This serendipitous discovery arose from the reaction of isophthaloyl dichloride with a bis-amine which produced a [2]catenane with intramolecular hydrogen bonds between the isophthalamide components of the rings (Figure **1.46**). Similar hydrogen-bonded assemblies have been reported by Vögtle and Leigh which utilise interactions with amide-containing macrocycles.[212-214]

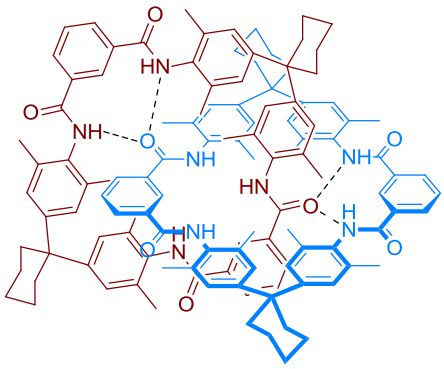

Figure 1.46: Hunter's hydrogen-bonded [2]catenane

Aside from hydrogen-bonding, aromatic donor-acceptor interactions have also been employed which take advantage of solvatophobic effects. This work was pioneered by Sanders using a dynamic combinatorial library approach to synthesise [2] and [3]catenanes. The low yield of the interlocked structures in water was augmented by increasing the ionic strength of the media and thereby enhancing the solvophobic effect (Figure **1.47**).[215-217]

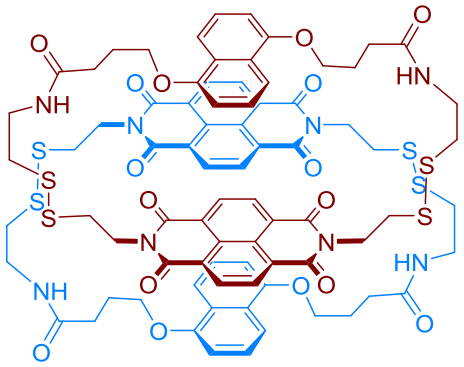

Figure 1.47: Sander's donor-acceptor [2]catenane

1.5.2.3 Anion Templation

Despite receiving less attention in comparison to cation templation, the use of anions as effective agents for the assembly of mechanically bonded structures has garnered much attention in recent years.[218] The first anion templated interlocked structure was described by Vögtle in 1999, which exploited the association of a phenoxide anion with an isophthalamide macrocycle (Figure **1.48a**). Reaction of the [2]pseudorotaxane with stopper functionalised benzyl bromide furnished the fully interlocked structure with a concomitant consumption of the anionic template.[219] Subsequent strategies have incorporated the anionic template into the resultant interlocked assembly.[220] These include recent examples by Smith, in which a zwitterionic squaraine dye is incorporated into the axle (Figure **1.48b**),[221] and by Flood who uses an organophosphate to assemble a [3]rotaxane (Figure **1.48c**).[222]

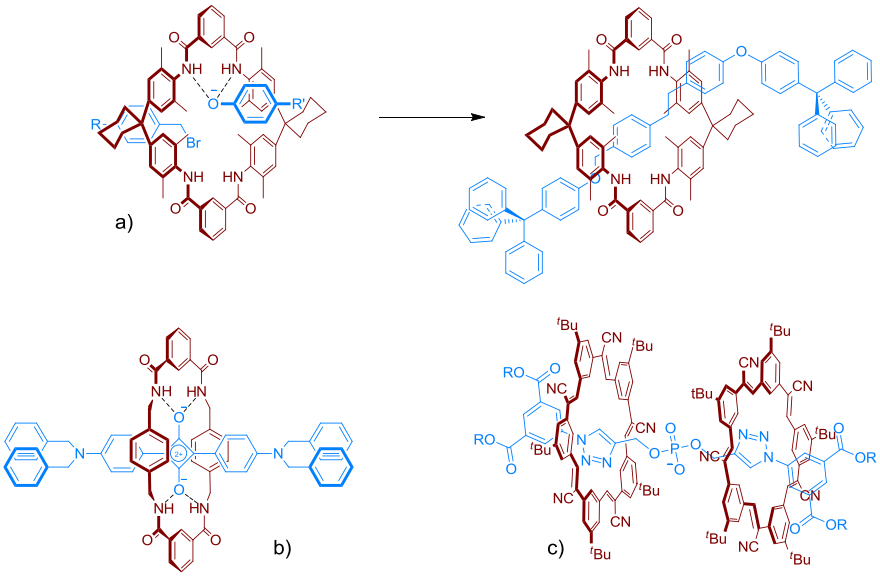

Figure 1.48: Anion-templated interlocked structures by a) Vögtle b) Smith c) Flood

Influenced by the pioneering work of Sauvage with tetrahedral copper (I) phenanthroline complexes, Beer envisioned a strategy using an array of amide hydrogen bond donors around a central anion to form an orthogonal complex (Figure **1.49a**). This approach relies on a pyridinium-3,5-bis-amide motif and an isophthalamide group forming a pseudo-tetrahedral complex around a chloride anion. This led to the synthesis of the first *discrete* anion-templated [2]rotaxane which used chloride to template the formation of the interlocked structure assisted by favourable hydrogen-bonding and aromatic donor-acceptor interactions between methyl pyridinium and hydroquinone groups (Figure **1.49b**).[223] Unlike the previous examples, this *discrete* anion templation approach allowed the removal of the anionic template to give a three-dimensional cavity suitable for recognition of negatively charged species. The size and shape of the resulting interlocked cavity imparts selectivity for chloride over larger, more basic oxoanions which are unable to penetrate the binding pocket. This approach has since been expanded to construct more complex interlocked anion hosts such as

a [3]rotaxane and a handcuff catenane,[224, 225] in addition to interlocked anion sensors[226, 227] and molecular machines.[228, 229]

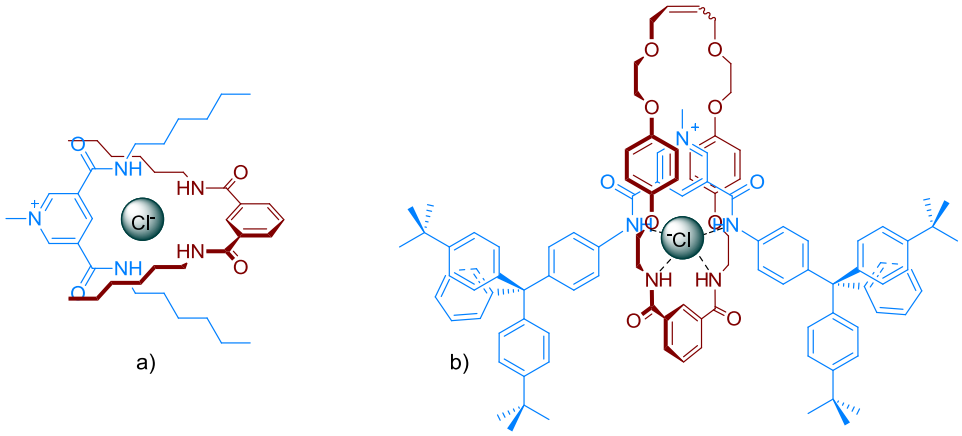

Figure 1.49: Discrete anion templation a) orthogonal complex b) chloride templated [2]rotaxane

1.5.3 Applications of Interlocked Structures

With the advent of efficient templating strategies for synthesising interlocked structures, recent research has focused on their potential nanotechnological applications in the fields of molecular machines, switches, sensing and medicinal chemistry.

1.5.3.1 Molecular Machines and Switches

The natural world is full of examples where molecular motion is used to perform a range of important biological functions e.g. protein transcription.[230, 231] Inspired by this, chemists have sought to synthesise interlocked systems which are capable of mimicking this motion. This is typically exhibited as molecular pirouetting in catenanes and as shuttling behaviour between two or more stations in rotaxanes. Interlocked structures are capable of switching co-conformations in response to external stimuli such as pH changes,[206, 207, 232] electrochemical[233] and photochemical[234, 235] stimulus or by the addition of charged substrates.[228, 236] The

molecular motion of janus rotaxane structures are particularly interesting as they mimic the motion exhibited by the sarcomeres of muscle tissue.[210] One example by Coutrot displays pH switchable behaviour. By incorporating positively charged ammonium and pyridinium stations within the axle it was demonstrated that extended or contracted co-conformations could be favoured upon the addition of acid or base (Figure **1.50**). Importantly this behaviour was entirely reversible and permitted many cycles between the two states.[237]

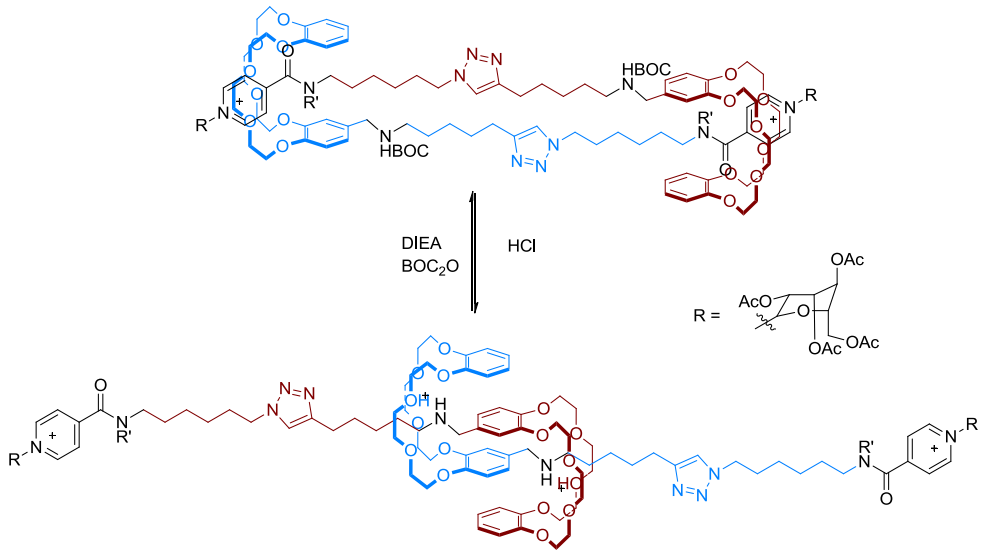

Figure 1.50: Molecular contraction and extension induced by pH induced protection-deprotection

The characteristics of molecular machines can also be influenced by solvent effects.[238] In 2013 Leigh reported the hydrogen-bonded molecular shuttle (Figure **1.51**). At room temperature an isophthalamide macrocycle was found to oscillate between two carbonyl stations on the axle of the [2]rotaxane. By using time-resolved vibrational spectroscopy the oscillation frequency was determined and it was found that in aqueous media the rate of shuttling was increased two-fold compared to when alcohols such as methanol or ethanol were used. They ascribed this to a 'lubricating' effect due to the hydrogen-bonded network of water that was not present in other media.[239]

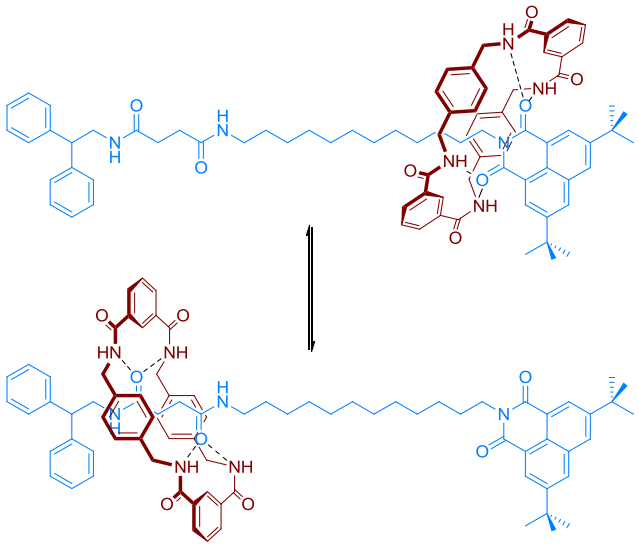

Figure 1.51: Leigh's hydrogen-bonded shuttle

1.5.3.2 Biological Applications, Recognition and Sensing

The recognition properties of interlocked structures have been explored in recent years. Removal of discrete templates furnishes a binding cavity that is capable of acting as an effective receptor for the templating species. For example, work by Beer has shown that the anion templation strategy affords interlocked hosts that are capable of strong and selective binding of spherical halide guests (See Section 1.5.2.3).[223] This has also been reported by Jeong who synthesised an indolocarbazole [2]catenane by anion templation (Figure **1.52**). This host shows a marked preference for chloride anions over more basic acetate and dihydrogenphosphate and, in addition, signals the binding event *via* modulation of the fluorescence of the indolocarbazole luminophore.

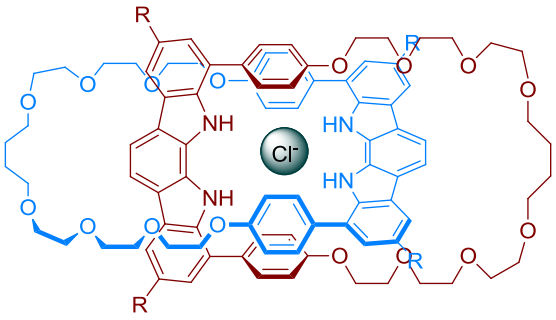

Figure 1.52: Jeong's indolocarbazole [2]catenane

The utility of interlocked structures to medical applications has also been demonstrated,[240] having been used in preventing signalling in cancer cells[241] and as cytotoxic agents.[242] The pioneering work by Smith has also shown their viability as chemosensors[243] and biosensors.[244] The encapsulation of squaraine dyes within macrocyclic compounds has allowed these metastable compounds to be used *in vivo* by preventing nucleophilic attack. Recent work has demonstrated their utility to bimodal sensing; through oxidation to form an endoperoxide the catenane is both fluorescent and chemiluminescent by virtue of the squaraine dye and a cycloreversion process (Figure **1.53**). The catenane was attached to a nanoparticle surface and was subsequently used to image *in vivo,* taking advantage of the differing tissue penetration of both forms of emission.[245]

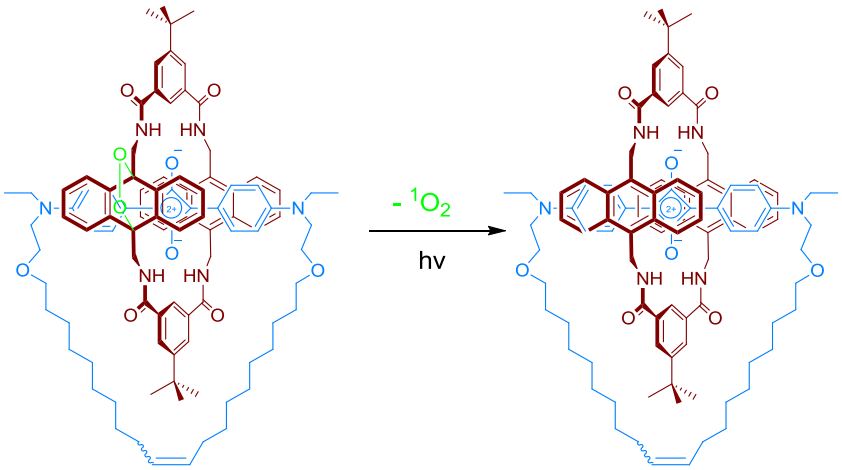

Figure 1.53: Cycloreversion process of Smith's bimodal imaging catenane

Finally, Leigh has reported a [2]rotaxane that is capable of synthesising a simple amino acid sequence (Figure **1.54**).[246] Addition of acid unmasks the amine functionalities and allows the reaction sequence to proceed, causing the macrocycle to translate along the axle of the rotaxane to each subsequent station. In analogy with mRNA, the axle of the rotaxane predetermines the order of reaction of the amino acids by virtue of the rigid axle which prevents 'translation' of the amino acids in the wrong sequence. This approach, while synthetically onerous, demonstrates proof of principle of automated protein synthesis and could be applied to synthesise peptides of almost any length.

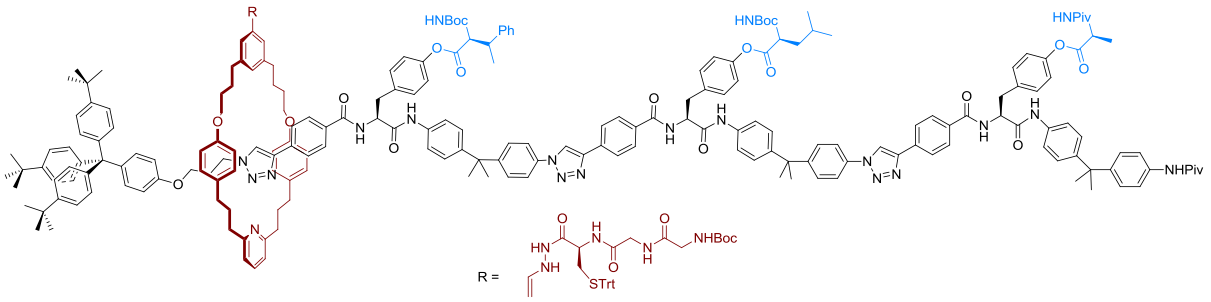

Figure 1.54: Leigh's synthetic amino acid synthesising [2]rotaxane

1.6 Project Aims

The aim of this project is to synthesise novel macrocyclic and interlocked structures *via* strategic templation by both anions and cations. The resultant host systems are functionalised with appropriate anion and cation recognition sites for the binding and sensing of anions and ion-pairs.

Chapter Two focuses on the synthesis of new heteroditopic macrocycles functionalised with both cation and anion recognition sites and their incorporation into interlocked architectures. The affinity for a range of anions and ion-pairs is explored *via* ^{1}H NMR and UV-visible spectroscopy as well as by elucidation of the ion-pair binding mode in the solid state by single crystal X-ray crystallography.

Chapter Three details the incorporation of *d*- and *f*-metal luminescent reporter groups into an isophthalamide motif in order to construct acyclic, macrocyclic and [2]rotaxane receptors. The first part of this chapter describes the use of transition metal complexes of dipyridylbenzene to bind and sense anions *via* luminescence spectroscopy. The second part concerns the integration of lanthanide DOTA complexes into [2]rotaxane host systems through the use of a post-synthetic 'click' modification method to construct the first lanthanide containing rotaxane and photophysical property investigations of the resultant anion host.

Chapter Four investigates the synthesis of complex higher-order interlocked structures through post-synthetic modification of lower-order interlocked structures.

Chapter FIVE explores the potential for fluorescent gold nanoparticle conjugates to act as luminescent and colorimetric sensors for chemical warfare agents (CWAs) by employing a fluorescent displacement assay technique.

1.7 References

1. J. W. Steed, D. R. Turner and K. J. Wallace, Core Concepts in Supramolecular Chemistry and Nanochemistry, John Wiley and Sons, Chichester, 2007.
2. J. W. Pflugrath and F. A. Quiocho, *Nature*, 1985, **314**, 257-260.
3. H. Luecke and F. A. Quiocho, *Nature*, 1990, **347**, 402-406.
4. P. Muller, *Pure Appl. Chem.*, 1994, **66**, 1077-1184.
5. P. Metrangolo, F. Meyer, T. Pilati, G. Resnati and G. Terraneo, *Angew. Chem.-Int. Edit.*, 2008, **47**, 6114-6127.
6. P. Metrangolo and G. Resnati, *Science*, 2008, **321**, 918-919.
7. F. Iwasaki, J. H. Yoshikawa, H. Yamamoto, K. Takada, E. Kan-nari, M. Yasui, T. Ishida and T. Nogami, *Acta Crystallogr. Sect. B-Struct. Sci.*, 1999, **55**, 1057-1067.
8. C. A. Hunter, K. R. Lawson, J. Perkins and C. J. Urch, *J. Chem. Soc.-Perkin Trans. 2*, 2001, 651-669.
9. S. L. Cockroft, C. A. Hunter, K. R. Lawson, J. Perkins and C. J. Urch, *J. Am. Chem. Soc.*, 2005, **127**, 8594-8595.
10. S. Grimme, *Angew. Chem.-Int. Edit.*, 2008, **47**, 3430-3434.
11. M. S. Cubberley and B. L. Iverson, *J. Am. Chem. Soc.*, 2001, **123**, 7560-7563.
12. K. Aoki, K. Murayama and H. Nishiyama, *J. Chem. Soc.-Chem. Commun.*, 1995, 2221-2222.
13. M. Meotner and C. A. Deakyne, *J. Am. Chem. Soc.*, 1985, **107**, 469-474.
14. C. A. Deakyne and M. Meotner, *J. Am. Chem. Soc.*, 1985, **107**, 474-479.
15. M. A. Petti, T. J. Shepodd, R. E. Barrans and D. A. Dougherty, *J. Am. Chem. Soc.*, 1988, **110**, 6825-6840.
16. B. L. Schottel, H. T. Chifotides and K. R. Dunbar, *Chem. Soc. Rev.*, 2008, **37**, 68-83.
17. M. Giese, M. Albrecht, C. Bohnen, T. Repenko, A. Valkonen and K. Rissanen, *Dalton Trans.*, 2014, **43**, 1873-1880.
18. M. Tapia-Juarez, J. B. Gonzalez-Campos, C. Contreras-Celedon, D. Corona, E. Cuevas-Yanez and L. Chacon-Garcia, *RSC Adv.*, 2014, **4**, 5660-5665.
19. C. J. Pedersen, *J. Am. Chem. Soc.*, 1967, **89**, 7017-7036.
20. C. J. Pedersen, *J. Am. Chem. Soc.*, 1967, **89**, 2495-2496.
21. Frensdor.Hk, *J. Am. Chem. Soc.*, 1971, **93**, 600-&.
22. E. Fischer, Ber. Dtsch. Chm. Grs. 1890, 23, 2611
23. E. Fischer, Ber. Dtsch. Chm. Gc.s. 1894. 27. 2985
24. D. E. Koshland, *Proceedings of the National Academy of Sciences of the United States of America*, 1958, **44**, 98-104.
25. D. J. Cram, *Angew. Chem.-Int. Edit. Engl.*, 1988, **27**, 1009-1020.

26. M. P. Hughes and B. D. Smith, *The Journal of Organic Chemistry*, 1997, **62**, 4492-4499.
27. A. E. Martell, R. D. Hancock and R. J. Motekaitis, *Coord. Chem. Rev.*, 1994, **133**, 39-65.
28. Y. L. Li and A. H. Flood, *J. Am. Chem. Soc.*, 2008, **130**, 12111-12122.
29. Y. J. Li and A. H. Flood, *Angew. Chem.-Int. Edit.*, 2008, **47**, 2649-2652.
30. M. F. Wolfe, S. Schwarzbach and R. A. Sulaiman, *Environ. Toxicol. Chem.*, 1998, **17**, 146-160.
31. A. Sanchez-Chardi, M. J. Lopez-Fuster and J. Nadal, *Environ. Pollut.*, 2007, **145**, 7-14.
32. H. N. Kim, W. X. Ren, J. S. Kim and J. Yoon, *Chem. Soc. Rev.*, 2012, **41**, 3210-3244.
33. P. D. Beer and P. A. Gale, *Angew. Chem.-Int. Edit.*, 2001, **40**, 486-516.
34. J. M. Boon and B. D. Smith, *Curr. Opin. Chem. Biol.*, 2002, **6**, 749-756.
35. S. K. Kim and J. L. Sessler, *Chem. Soc. Rev.*, 2010, **39**, 3784-3809.
36. B. D. Smith, Macrocyclic Chemistry: Current Trends and Future Perspectives, Springer, Dordrecht, 2005.
37. H. J. Weinmann, R. C. Brasch, W. R. Press and G. E. Wesbey, *Am. J. Roentgenol.*, 1984, **142**, 619-624.
38. W. P. Cacheris, S. C. Quay and S. M. Rocklage, *Magn. Reson. Imaging*, 1990, **8**, 467-481.
39. I. Oehme and O. S. Wolfbeis, *Mikrochim. Acta*, 1997, **126**, 177-192.
40. C. Suksai and T. Tuntulani, *Chem. Soc. Rev.*, 2003, **32**, 192-202.
41. D. Grieshaber, R. MacKenzie, J. Voros and E. Reimhult, *Sensors*, 2008, **8**, 1400-1458.
42. P. D. Beer, P. A. Gale and G. Z. Chen, *Coord. Chem. Rev.*, 1999, **185-6**, 3-36.
43. M. M. Shemyakin, N. A. Aldanova, E. I. Vinogradova and M. Y. Feigina, *Tetrahedron Letters*, 1963, **4**, 1921-1925.
44. R. Shukla, S. V. Lindeman and R. Rathore, *J. Am. Chem. Soc.*, 2006, **128**, 5328-5329.
45. N. S. Scrutton and A. R. C. Raine, *Biochem. J.*, 1996, **319**, 1-8.
46. M. M. Watt, M. S. Collins and D. W. Johnson, *Accounts Chem. Res.*, 2013, **46**, 955-966.
47. E. A. Meyer, R. K. Castellano and F. Diederich, *Angew. Chem.-Int. Edit.*, 2003, **42**, 1210-1250.
48. S. Kado and K. Kimura, *J. Am. Chem. Soc.*, 2003, **125**, 4560-4564.
49. R. C. Helgeson, J. M. Timko and D. J. Cram, *J. Am. Chem. Soc.*, 1973, **95**, 3023-3025.
50. E. P. Kyba, R. C. Helgeson, K. Madan, G. W. Gokel, T. L. Tarnowski, S. S. Moore and D. J. Cram, *J. Am. Chem. Soc.*, 1977, **99**, 2564-2571.
51. J. V. Ros-Lis, R. Martinez-Manez, K. Rurack, F. Sancenon, J. Soto and M. Spieles, *Inorganic Chemistry*, 2004, **43**, 5183-5185.
52. G. W. Gokel, *Chem. Soc. Rev.*, 1992, **21**, 39-47.
53. J. M. Lehn, *Angew. Chem.-Int. Edit.*, 1970, **9**, 175-&.

54. P. B. Smith, J. L. Dye, J. Cheney and J. M. Lehn, *J. Am. Chem. Soc.*, 1981, **103**, 6044-6048.
55. D. J. Cram, T. Kaneda, G. M. Lein and R. C. Helgeson, *J. Chem. Soc.-Chem. Commun.*, 1979, 948-950.
56. D. J. Cram and G. M. Lein, *J. Am. Chem. Soc.*, 1985, **107**, 3657-3668.
57. C. Gaeta, C. Talotta, F. Farina, F. A. Teixeira, P. M. Marcos, J. R. Ascenso and P. Neri, *J. Org. Chem.*, 2012, **77**, 10285-10293.
58. D. S. Guo, V. D. Uzunova, X. Su, Y. Liu and W. M. Nau, *Chemical Science*, 2011, **2**, 1722-1734.
59. D. Diamond and M. A. McKervey, *Chem. Soc. Rev.*, 1996, **25**, 15-&.
60. H. J. Kim, M. H. Lee, L. Mutihac, J. Vicens and J. S. Kim, *Chem. Soc. Rev.*, 2012, **41**, 1173-1190.
61. E. Ghidini, F. Ugozzoli, R. Ungaro, S. Harkema, A. Abuelfadl and D. N. Reinhoudt, *J. Am. Chem. Soc.*, 1990, **112**, 6979-6985.
62. J. S. Kim, K. H. Noh, S. H. Lee, S. K. Kim, S. K. Kim and J. Y. Yoon, *J. Org. Chem.*, 2003, **68**, 597-600.
63. T. Nabeshima, T. Saiki, J. Iwabuchi and S. Akine, *J. Am. Chem. Soc.*, 2005, **127**, 5507-5511.
64. N. Morohashi, N. Iki and S. Miyano, *J. Synth. Org. Chem. Jpn.*, 2002, **60**, 550-562.
65. P. Schmitt, P. D. Beer, M. G. B. Drew and P. D. Sheen, *Angewandte Chemie International Edition in English*, 1997, **36**, 1840-1842.
66. K. Puchnin, P. Zaikin, D. Cheshkov, I. Vatsouro and V. Kovalev, *Chemistry – A European Journal*, 2012, **18**, 10954-10968.
67. V. Felix, S. E. Matthews, P. D. Beer and M. G. B. Drew, *Phys. Chem. Chem. Phys.*, 2002, **4**, 3849-3858.
68. H. Zhao, J. Zhan, Z. Zou, F. Miao, H. Chen, L. Zhang, X. Cao, D. Tian and H. Li, *RSC Adv.*, 2013, **3**, 1029-1032.
69. J. C. Medina, T. T. Goodnow, M. T. Rojas, J. L. Atwood, B. C. Lynn, A. E. Kaifer and G. W. Gokel, *J. Am. Chem. Soc.*, 1992, **114**, 10583-10595.
70. I. Leray, J. P. Lefevre, J. F. Delouis, J. Delaire and B. Valeur, *Chem.-Eur. J.*, 2001, **7**, 4590-4598.
71. P. Chakrabarti, *J. Mol. Biol.*, 1993, **234**, 463-482.
72. S. G. Chang, D. Littlejohn and K. Y. Hu, *Science*, 1987, **237**, 756-758.
73. E. A. Katayev, G. V. Kolesnikov and J. L. Sessler, *Chem. Soc. Rev.*, 2009, **38**, 1572-1586.
74. S. M. Rowe, S. Miller and E. J. Sorscher, *N. Engl. J. Med.*, 2005, **352**, 1992-2001.
75. M. Cametti and K. Rissanen, *Chem. Commun.*, 2009, 2809-2829.
76. J. Aaseth, M. Shimshi, J. L. Gabrilove and G. S. Birketvedt, *J. Trace Elem. Exp. Med.*, 2004, **17**, 83-92.
77. C. Caltagirone, G. W. Bates, P. A. Gale and M. E. Light, *Chem. Commun.*, 2008, 61-63.
78. C. H. Park and H. E. Simmons, *J. Am. Chem. Soc.*, 1968, **90**, 2429-2431.
79. H. E. Simmons and C. H. Park, *J. Am. Chem. Soc.*, 1968, **90**, 2428-2429.

80. R. A. Bell, G. G. Christoph, F. R. Fronczek and R. E. Marsh, *Science*, 1975, **190**, 151-152.
81. B. Dietrich, J. M. Lehn, J. Guilhem and C. Pascard, *Tetrahedron Letters*, 1989, **30**, 4125-4128.
82. B. Dietrich, B. Dilworth, J. M. Lehn, J. P. Souchez, M. Cesario, J. Guilhem and C. Pascard, *Helv. Chim. Acta*, 1996, **79**, 569-587.
83. J. L. Sessler, M. J. Cyr, V. Lynch, E. McGhee and J. A. Ibers, *J. Am. Chem. Soc.*, 1990, **112**, 2810-2813.
84. C. Bazzicalupi, A. Bencini, C. Giorgi, B. Valtancoli, V. Lippolis and A. Perra, *Inorganic Chemistry*, 2011, **50**, 7202-7216.
85. A. Bencini, C. Coluccini, A. Garau, C. Giorgi, V. Lippolis, L. Messori, D. Pasini and S. Puccioni, *Chem. Commun.*, 2012, **48**, 10428-10430.
86. C. Bazzicalupi, A. Bencini, S. Puccioni, B. Valtancoli, P. Gratteri, A. Garau and V. Lippolis, *Chem. Commun.*, 2012, **48**, 139-141.
87. F. P. Schmidtchen, *Angew. Chem.-Int. Edit. Engl.*, 1977, **16**, 720-721.
88. F. P. Schmidtchen and G. Muller, *J. Chem. Soc.-Chem. Commun.*, 1984, 1115-1116.
89. K. Worm and F. P. Schmidtchen, *Angew. Chem.-Int. Edit. Engl.*, 1995, **34**, 65-66.
90. A. Ursu and F. P. Schmidtchen, *Angew. Chem.-Int. Edit.*, 2012, **51**, 242-246.
91. T. H. Wirth and N. Davidson, *J. Am. Chem. Soc.*, 1964, **86**, 4314-4318.
92. G. Muller, J. Riede and F. P. Schmidtchen, *Angew. Chem.-Int. Edit. Engl.*, 1988, **27**, 1516-1518.
93. A. Metzger, V. M. Lynch and E. V. Anslyn, *Angew. Chem.-Int. Edit. Engl.*, 1997, **36**, 862-865.
94. K. Sato, S. Arai and T. Yamagishi, *Tetrahedron Letters*, 1999, **40**, 5219-5222.
95. E. Alcalde, S. Ramos and L. Perez-Garcia, *Org. Lett.*, 1999, **1**, 1035-1038.
96. H. C. Kolb, M. G. Finn and K. B. Sharpless, *Angew. Chem.-Int. Edit.*, 2001, **40**, 2004-+.
97. J. Cai, B. P. Hay, N. J. Young, X. Yang and J. L. Sessler, *Chemical Science*, 2013, **4**, 1560-1567.
98. P. A. Gale, N. Busschaert, C. J. E. Haynes, L. E. Karagiannidis and I. L. Kirby, *Chem. Soc. Rev.*, 2014, **43**, 205-241.
99. R. A. Pascal, J. Spergel and D. Vanengen, *Tetrahedron Letters*, 1986, **27**, 4099-4102.
100. K. Kavallieratos, S. R. deGala, D. J. Austin and R. H. Crabtree, *J. Am. Chem. Soc.*, 1997, **119**, 2325-2326.
101. K. Kavallieratos, C. M. Bertao and R. H. Crabtree, *J. Org. Chem.*, 1999, **64**, 1675-1683.
102. P. A. Gale, *Accounts Chem. Res.*, 2006, **39**, 465-475.
103. S. Kubik, *Chem. Soc. Rev.*, 2010, **39**, 3648-3663.
104. S. Kubik and R. Goddard, *Proceedings of the National Academy of Sciences of the United States of America*, 2002, **99**, 5127-5132.
105. V. Amendola, L. Fabbrizzi and L. Mosca, *Chem. Soc. Rev.*, 2010, **39**, 3889-3915.
106. A. F. Li, J. H. Wang, F. Wang and Y. B. Jiang, *Chem. Soc. Rev.*, 2010, **39**, 3729-3745.
107. S. J. Brooks, P. A. Gale and M. E. Light, *Crystengcomm*, 2005, **7**, 586-591.

108. With respect to the lipid
109. M. Wenzel, M. E. Light, A. P. Davis and P. A. Gale, *Chem. Commun.*, 2011, **47**, 7641-7643.
110. V. S. Bryantsev and B. P. Hay, *Org. Lett.*, 2005, **7**, 5031-5034.
111. H. Juwarker, J. M. Lenhardt, D. M. Pham and S. L. Craig, *Angew. Chem.-Int. Edit.*, 2008, **47**, 3740-3743.
112. H. Juwarker, J. M. Lenhardt, J. C. Castillo, E. Zhao, S. Krishnamurthy, R. M. Jamiolkowski, K. H. Kim and S. L. Craig, *J. Org. Chem.*, 2009, **74**, 8924-8934.
113. M. G. Sarwar, B. Dragisic, S. Sagoo and M. S. Taylor, *Angew. Chem.-Int. Edit.*, 2010, **49**, 1674-1677.
114. T. W. Hudnall, C. W. Chiu and F. P. Gabbai, *Accounts Chem. Res.*, 2009, **42**, 388-397.
115. I. R. Morgan, A. E. J. Broomsgrove, P. Fitzpatrick, D. Vidovic, A. L. Thompson, I. A. Fallis and S. Aldridge, *Organometallics*, 2010, **29**, 4762-4765.
116. A. E. J. Broomsgrove, D. A. Addy, A. Di Paolo, I. R. Morgan, C. Bresner, V. Chislett, I. A. Fallis, A. L. Thompson, D. Vidovic and S. Aldridge, *Inorganic Chemistry*, 2010, **49**, 157-173.
117. C. R. Wade, A. E. J. Broomsgrove, S. Aldridge and F. P. Gabbai, *Chem. Rev.*, 2010, **110**, 3958-3984.
118. M. Newcomb, J. H. Horner and M. T. Blanda, *J. Am. Chem. Soc.*, 1987, **109**, 7878-7879.
119. X. Yang, C. B. Knobler and M. F. Hawthorne, *Angew. Chem.-Int. Edit. Engl.*, 1991, **30**, 1507-1508.
120. T. J. Wedge and M. F. Hawthorne, *Coord. Chem. Rev.*, 2003, **240**, 111-128.
121. J. V. Carolan, S. J. Butler and K. A. Jolliffe, *J. Org. Chem.*, 2009, **74**, 2992-2996.
122. A. V. Koulov, K. A. Stucker, C. Lakshmi, J. P. Robinson and B. D. Smith, *Cell Death Differ.*, 2003, **10**, 1357-1359.
123. D. M. Rudkevich, W. Stauthamer, W. Verboom, J. F. J. Engbersen, S. Harkema and D. N. Reinhoudt, *J. Am. Chem. Soc.*, 1992, **114**, 9671-9673.
124. D. M. Rudkevich, W. Verboom, Z. Brzozka, M. J. Palys, W. Stauthamer, G. J. Vanhummel, S. M. Franken, S. Harkema, J. F. J. Engbersen and D. N. Reinhoudt, *J. Am. Chem. Soc.*, 1994, **116**, 4341-4351.
125. G. DeSantis, L. Fabbrizzi, M. Licchelli, A. Poggi and A. Taglietti, *Angew. Chem.-Int. Edit. Engl.*, 1996, **35**, 202-204.
126. T. Gunnlaugsson, M. Glynn, G. M. Tocci, P. E. Kruger and F. M. Pfeffer, *Coord. Chem. Rev.*, 2006, **250**, 3094-3117.
127. T. Gunnlaugsson, P. E. Kruger, T. C. Lee, R. Parkesh, F. M. Pfeffer and G. M. Hussey, *Tetrahedron Letters*, 2003, **44**, 6575-6578.
128. G. A. Crosby, W. G. Perkins and D. M. Klassen, *J. Chem. Phys.*, 1965, **43**, 1498-&.
129. P. D. Beer, F. Szemes, V. Balzani, C. M. Sala, M. G. B. Drew, S. W. Dent and M. Maestri, *J. Am. Chem. Soc.*, 1997, **119**, 11864-11875.
130. M. S. Vickers, K. S. Martindale and P. D. Beer, *J. Mater. Chem.*, 2005, **15**, 2784-2790.

131. E. Berni, I. Gosse, D. Badocco, P. Pastore, N. Sojic and S. Pinet, *Chemistry – A European Journal*, 2009, **15**, 5145-5152.
132. W. Goodall and J. A. G. Williams, *Journal of the Chemical Society, Dalton Transactions*, 2000, 2893-2895.
133. R. Krapf, N. P. Illsley, H. C. Tseng and A. S. Verkman, *Anal. Biochem.*, 1988, **169**, 142-150.
134. C. M. G. dos Santos, A. J. Harte, S. J. Quinn and T. Gunnlaugsson, *Coord. Chem. Rev.*, 2008, **252**, 2512-2527.
135. C. P. Montgomery, B. S. Murray, E. J. New, R. Pal and D. Parker, *Accounts Chem. Res.*, 2009, **42**, 925-937.
136. S. J. Butler and D. Parker, *Chem. Soc. Rev.*, 2013, **42**, 1652-1666.
137. D. Parker and J. H. Yu, *Chem. Commun.*, 2005, 3141-3143.
138. R. M. Duke, E. B. Veale, F. M. Pfeffer, P. E. Kruger and T. Gunnlaugsson, *Chem. Soc. Rev.*, 2010, **39**, 3936-3953.
139. M. E. Moragues, R. Martinez-Manez and F. Sancenon, *Chem. Soc. Rev.*, 2011, **40**, 2593-2643.
140. A. Metzger and E. V. Anslyn, *Angew. Chem.-Int. Edit.*, 1998, **37**, 649-652.
141. B. T. Nguyen and E. V. Anslyn, *Coord. Chem. Rev.*, 2006, **250**, 3118-3127.
142. L. Fabbrizzi, N. Marcotte, F. Stomeo and A. Taglietti, *Angew. Chem.-Int. Edit.*, 2002, **41**, 3811-3814.
143. J. J. Lavigne and E. V. Anslyn, *Angew. Chem.-Int. Edit.*, 1999, **38**, 3666-3669.
144. K. S. Lee, H. J. Kim, G. H. Kim, I. Shin and J. I. Hong, *Org. Lett.*, 2008, **10**, 49-51.
145. P. D. Beer, J. Cadman, J. M. Lloris, R. Martinez-Manez, M. E. Padilla, T. Pardo, D. K. Smith and J. Soto, *J. Chem. Soc.-Dalton Trans.*, 1999, 127-133.
146. A. E. J. Broomsgrove, D. A. Addy, C. Bresner, I. A. Fallis, A. L. Thompson and S. Aldridge, *Chem.-Eur. J.*, 2008, **14**, 7525-7529.
147. D. M. Rudkevich, J. D. Mercerchalmers, W. Verboom, R. Ungaro, F. Dejong and D. N. Reinhoudt, *J. Am. Chem. Soc.*, 1995, **117**, 6124-6125.
148. D. J. White, N. Laing, H. Miller, S. Parsons, S. Coles and P. A. Tasker, *Chem. Commun.*, 1999, 2077-2078.
149. C. A. Hunter and H. L. Anderson, *Angew. Chem.-Int. Edit.*, 2009, **48**, 7488-7499.
150. A. P. de Silva and N. D. McClenaghan, *Chem.-Eur. J.*, 2004, **10**, 574-586.
151. V. Amendola, L. Fabbrizzi, C. Mangano, P. Pallavicini, A. Poggi and A. Taglietti, *Coord. Chem. Rev.*, 2001, **219**, 821-837.
152. J. M. Lehn, *Pure Appl. Chem.*, 1980, **52**, 2441-2459.
153. J. Comarmond, P. Plumere, J. M. Lehn, Y. Agnus, R. Louis, R. Weiss, O. Kahn and I. Morgensternbadarau, *J. Am. Chem. Soc.*, 1982, **104**, 6330-6340.
154. L. Fabbrizzi, I. Faravelli, G. Francese, M. Licchelli, A. Perotti and A. Taglietti, *Chem. Commun.*, 1998, 971-972.
155. J. M. Chen, W. Wei, X. L. Feng and T. B. Lu, *Chem.-Asian J.*, 2007, **2**, 710-719.
156. M. M. El-Hendawy, N. J. English and D. A. Mooney, *Inorganic Chemistry*, 2012, **51**, 5282-5288.
157. T. Nagasaki, H. Fujishima, M. Takeuchi and S. Shinkai, *J. Chem. Soc.-Perkin Trans. 1*, 1995, 1883-1888.

158. M. A. Hossain, J. M. Llinares, S. Mason, P. Morehouse, D. Powell and K. Bowman-James, *Angew. Chem.-Int. Edit.*, 2002, **41**, 2335-2338.
159. V. Valderrey, E. C. Escudero-Adán and P. Ballester, *Angewandte Chemie International Edition*, 2013, **52**, 6898-6902.
160. J. Scheerder, J. P. M. vanDuynhoven, J. F. J. Engbersen and D. N. Reinhoudt, *Angew. Chem.-Int. Edit. Engl.*, 1996, **35**, 1090-1093.
161. D. M. Rudkevich, Z. Brzozka, M. Palys, H. C. Visser, W. Verboom and D. N. Reinhoudt, *Angew. Chem.-Int. Edit. Engl.*, 1994, **33**, 467-468.
162. T. Tozawa, Y. Misawa, S. Tokita and Y. Kubo, *Tetrahedron Letters*, 2000, **41**, 5219-5223.
163. J. K. Choi, K. No, E. H. Lee, S. G. Kwon, K. W. Kim and J. S. Kim, *Supramolecular Chemistry*, 2007, **19**, 283-286.
164. G. Reeske, G. Bradtmöller, M. Schürmann and K. Jurkschat, *Chemistry – A European Journal*, 2007, **13**, 10239-10245.
165. G. Reeske, M. Schuermann and K. Jurkschat, *Dalton Trans.*, 2008, 3398-3400.
166. CCDC Number: 671304. Generated using CrystalMaker, CrystalMaker Software Ltd., Oxford, England (www.crystalmaker.com)
167. S. K. Kim, B. P. Hay, J. S. Kim, B. A. Moyer and J. L. Sessler, *Chem. Commun.*, 2013, **49**, 2112-2114.
168. S. K. Kim, G. I. Vargas-Zúñiga, B. P. Hay, N. J. Young, L. H. Delmau, C. Masselin, C.-H. Lee, J. S. Kim, V. M. Lynch, B. A. Moyer and J. L. Sessler, *J. Am. Chem. Soc.*, 2011, **134**, 1782-1792.
169. S. S. Flack, J. L. Chaumette, J. D. Kilburn, G. J. Langley and M. Webster, *J. Chem. Soc.-Chem. Commun.*, 1993, 399-401.
170. J. M. Mahoney, A. M. Beatty and B. D. Smith, *J. Am. Chem. Soc.*, 2001, **123**, 5847-5848.
171. A. Lascaux, S. Le Gac, J. Wouters, M. Luhmer and I. Jabin, *Org. Biomol. Chem.*, 2010, **8**, 4607-4616.
172. E. R. Kay, D. A. Leigh and F. Zerbetto, *Angew. Chem.-Int. Edit.*, 2007, **46**, 72-191.
173. W. R. Dichtel, O. S. Miljanic, W. Y. Zhang, J. M. Spruell, K. Patel, I. Aprahamian, J. R. Heath and J. F. Stoddartt, *Accounts Chem. Res.*, 2008, **41**, 1750-1761.
174. J. F. Stoddart, *Chem. Soc. Rev.*, 2009, **38**, 1802-1820.
175. J. Y. Li, P. F. Wei, X. J. Wu, M. Xue, X. Z. Yan and Q. Z. Zhou, *RSC Adv.*, 2013, **3**, 21289-21293.
176. C. O. Dietrichbuchecker, J. P. Sauvage and J. M. Kern, *J. Am. Chem. Soc.*, 1984, **106**, 3043-3045.
177. G. Koshkakaryan, D. Cao, L. M. Klivansky, S. J. Teat, J. L. Tran and Y. Liu, *Org. Lett.*, 2010, **12**, 1528-1531.
178. O. S. Miljanic, W. R. Dichtel, S. I. Khan, S. Mortezaei, J. R. Heath and J. F. Stoddart, *J. Am. Chem. Soc.*, 2007, **129**, 8236-8246.
179. M. R. Sambrook, P. D. Beer, J. A. Wisner, R. L. Paul and A. R. Cowley, *J. Am. Chem. Soc.*, 2004, **126**, 15364-15365.
180. L. M. Hancock and P. D. Beer, *Chem.-Eur. J.*, 2009, **15**, 42-44.

181. T. H. Ho, C. C. Lai, Y. H. Liu, S. M. Peng and S. H. Chiu, *Chem.-Eur. J.*, 2014, **20**, 4563-4567.
182. A. Brown and P. D. Beer, *Dalton Trans.*, 2012, **41**, 118-129.
183. J. P. Collin, F. Durola, V. Heitz, F. Reviriego, J. P. Sauvage and Y. Trolez, *Angew. Chem.-Int. Edit.*, 2010, **49**, 10172-10175.
184. A. Joosten, Y. Trolez, J. P. Collin, V. Heitz and J. P. Sauvage, *J. Am. Chem. Soc.*, 2012, **134**, 1802-1809.
185. P. R. Ashton, M. Belohradsky, D. Philp and J. F. Stoddart, *Journal of the Chemical Society, Chemical Communications*, 1993, 1269-1274.
186. X. H. Huang, S. Y. Huang, B. Q. Zhai, Y. Zhang, Y. A. Xu and Q. C. Wang, *Tetrahedron Letters*, 2012, **53**, 6414-6417.
187. S. H. Chiu, S. J. Rowan, S. J. Cantrill, P. T. Glink, R. L. Garrell and J. F. Stoddart, *Org. Lett.*, 2000, **2**, 3631-3634.
188. P. R. Ashton, M. C. T. Fyfe, C. Schiavo, J. F. Stoddart, A. J. P. White and D. J. Williams, *Tetrahedron Letters*, 1998, **39**, 5455-5458.
189. E. Wasserman, *J. Am. Chem. Soc.*, 1960, **82**, 4433-4434.
190. H. L. Frisch and E. Wasserman, *J. Am. Chem. Soc.*, 1961, **83**, 3789-&.
191. I. T. Harrison and S. Harrison, *J. Am. Chem. Soc.*, 1967, **89**, 5723-&.
192. J. F. Stoddart, *Chem. Soc. Rev.*, 2009, **38**, 1521-1529.
193. C. O. Dietrichbuchecker, J. P. Sauvage and J. P. Kintzinger, *Tetrahedron Letters*, 1983, **24**, 5095-5098.
194. A. M. Fuller, D. A. Leigh, P. J. Lusby, I. D. H. Oswald, S. Parsons and D. B. Walker, *Angew. Chem.-Int. Edit.*, 2004, **43**, 3914-3918.
195. S. M. Goldup, D. A. Leigh, P. J. Lusby, R. T. McBttrney and A. M. Z. Slawin, *Angew. Chem.-Int. Edit.*, 2008, **47**, 6999-7003.
196. L. Hogg, D. A. Leigh, P. J. Lusby, A. Morelli, S. Parsons and J. K. Y. Wong, *Angew. Chem.-Int. Edit.*, 2004, **43**, 1218-1221.
197. D. A. Leigh, P. J. Lusby, R. T. McBurney, A. Morelli, A. M. Z. Slawin, A. R. Thomson and D. B. Walker, *J. Am. Chem. Soc.*, 2009, **131**, 3762-3771.
198. S.-T. Tung, C.-C. Lai, Y.-H. Liu, S.-M. Peng and S.-H. Chiu, *Angewandte Chemie International Edition*, 2013, **52**, 13269-13272.
199. J. D. Crowley, S. M. Goldup, A. L. Lee, D. A. Leigh and R. T. McBurney, *Chem. Soc. Rev.*, 2009, **38**, 1530-1541.
200. V. Aucagne, K. D. Hanni, D. A. Leigh, P. J. Lusby and D. B. Walker, *J. Am. Chem. Soc.*, 2006, **128**, 2186-2187.
201. S. M. Goldup, D. A. Leigh, T. Long, P. R. McGonigal, M. D. Symes and J. Wu, *J. Am. Chem. Soc.*, 2009, **131**, 15924-15929.
202. J. Berna, J. D. Crowley, S. M. Goldup, K. D. Hanni, A. L. Lee and D. A. Leigh, *Angew. Chem.-Int. Edit.*, 2007, **46**, 5709-5713.
203. M. V. MartinezDiaz, N. Spencer and J. F. Stoddart, *Angew. Chem.-Int. Edit. Engl.*, 1997, **36**, 1904-1907.
204. S. Y. Hsueh, K. W. Cheng, C. C. Lai and S. H. Chiu, *Angew. Chem.-Int. Edit.*, 2008, **47**, 4436-4439.

205. E. N. Guidry, S. J. Cantrill, J. F. Stoddart and R. H. Grubbs, *Org. Lett.*, 2005, **7**, 2129-2132.
206. C. Clavel, K. Fournel-Marotte and F. Coutrot, *Molecules*, 2013, **18**, 11553-11575.
207. C. Romuald, A. Arda, C. Clavel, J. Jimenez-Barbero and F. Coutrot, *Chemical Science*, 2012, **3**, 1851-1857.
208. P. R. Ashton, T. T. Goodnow, A. E. Kaifer, M. V. Reddington, A. M. Z. Slawin, N. Spencer, J. F. Stoddart, C. Vicent and D. J. Williams, *Angew. Chem.-Int. Edit. Engl.*, 1989, **28**, 1396-1399.
209. D. B. Amabilino, P. R. Ashton, A. S. Reder, N. Spencer and J. F. Stoddart, *Angew. Chem.-Int. Edit. Engl.*, 1994, **33**, 1286-1290.
210. J. D. Badjic, C. M. Ronconi, J. F. Stoddart, V. Balzani, S. Silvi and A. Credi, *J. Am. Chem. Soc.*, 2006, **128**, 1489-1499.
211. C. A. Hunter, *J. Am. Chem. Soc.*, 1992, **114**, 5303-5311.
212. F. Vogtle, S. Meier and R. Hoss, *Angew. Chem.-Int. Edit. Engl.*, 1992, **31**, 1619-1622.
213. F. G. Gatti, D. A. Leigh, S. A. Nepogodiev, A. M. Z. Slawin, S. J. Teat and J. K. Y. Wong, *J. Am. Chem. Soc.*, 2001, **123**, 5983-5989.
214. R. Ahmed, A. Altieri, D. M. D'Souza, D. A. Leigh, K. M. Mullen, M. Papmeyer, A. M. Z. Slawin, J. K. Y. Wong and J. D. Woollins, *J. Am. Chem. Soc.*, 2011, **133**, 12304-12310.
215. H. Y. Au-Yeung, G. D. Pantos and J. K. M. Sanders, *Proceedings of the National Academy of Sciences of the United States of America*, 2009, **106**, 10466-10470.
216. F. B. L. Cougnon, H. Y. Au-Yeung, G. D. Pantos and J. K. M. Sanders, *J. Am. Chem. Soc.*, 2011, **133**, 3198-3207.
217. F. B. L. Cougnon, N. A. Jenkins, G. D. Pantos and J. K. M. Sanders, *Angew. Chem.-Int. Edit.*, 2012, **51**, 1443-1447.
218. M. D. Lankshear and P. D. Beer, *Accounts Chem. Res.*, 2007, **40**, 657-668.
219. G. M. Hubner, J. Glaser, C. Seel and F. Vogtle, *Angew. Chem.-Int. Edit.*, 1999, **38**, 383-386.
220. P. Ghosh, O. Mermagen and C. A. Schalley, *Chem. Commun.*, 2002, 2628-2629.
221. E. Arunkumar, C. C. Forbes, B. C. Noll and B. D. Smith, *J. Am. Chem. Soc.*, 2005, **127**, 3288-3289.
222. S. Lee, C. H. Chen and A. H. Flood, *Nat. Chem.*, 2013, **5**, 704-710.
223. J. A. Wisner, P. D. Beer, M. G. B. Drew and M. R. Sambrook, *J. Am. Chem. Soc.*, 2002, **124**, 12469-12476.
224. N. H. Evans, C. J. Serpell and P. D. Beer, *Angew. Chem.-Int. Edit.*, 2011, **50**, 2507-2510.
225. N. H. Evans, C. J. Serpell and P. D. Beer, *Chem. Commun.*, 2011, **47**, 8775-8777.
226. G. T. Spence and P. D. Beer, *Accounts Chem. Res.*, 2013, **46**, 571-586.
227. L. M. Hancock, E. Marchi, P. Ceroni and P. D. Beer, *Chem.-Eur. J.*, 2012, **18**, 11277-11283.
228. L. M. Hancock and P. D. Beer, *Chem. Commun.*, 2011, **47**, 6012-6014.
229. G. T. Spence, M. B. Pitak and P. D. Beer, *Chem.-Eur. J.*, 2012, **18**, 7100-7108.
230. N. Hirokawa, *Science*, 1998, **279**, 519-526.
231. J. E. Walker, *Angew. Chem.-Int. Edit.*, 1998, **37**, 2309-2319.

232. Z.-J. Zhang, M. Han, H.-Y. Zhang and Y. Liu, *Org. Lett.*, 2013, **15**, 1698-1701.
233. A. Livoreil, C. O. Dietrichbuchecker and J. P. Sauvage, *J. Am. Chem. Soc.*, 1994, **116**, 9399-9400.
234. D. A. Leigh, J. K. Y. Wong, F. Dehez and F. Zerbetto, *Nature*, 2003, **424**, 174-179.
235. F. Lohmann, D. Ackermann and M. Famulok, *J. Am. Chem. Soc.*, 2012, **134**, 11884-11887.
236. M. J. Barrell, D. A. Leigh, P. J. Lusby and A. M. Z. Slawin, *Angew. Chem.-Int. Edit.*, 2008, **47**, 8036-8039.
237. C. Romuald, E. Busseron and F. Coutrot, *J. Org. Chem.*, 2010, **75**, 6516-6531.
238. A. S. Lane, D. A. Leigh and A. Murphy, *J. Am. Chem. Soc.*, 1997, **119**, 11092-11093.
239. M. R. Panman, B. H. Bakker, D. den Uyl, E. R. Kay, D. A. Leigh, W. J. Buma, A. M. Brouwer, J. A. J. Geenevasen and S. Woutersen, *Nat. Chem.*, 2013, **5**, 929-934.
240. L. Garcia-Rio, F. J. Otero-Espinar, A. Luzardo-Alvarez and J. Blanco-Mendez, *Curr. Top. Med. Chem.*, 2014, **14**, 478-493.
241. K. Hara, T. Beppu, M. Kimura, Y. Fujita, T. Takata, K. Nishio and N. Ono, *J. Pharmacol. Sci.*, 2013, **122**, 153-157.
242. X. Y. Wang and D. B. Smithrud, *Bioorg. Med. Chem. Lett.*, 2011, **21**, 6880-6883.
243. C. G. Collins, E. M. Peck, P. J. Kramer and B. D. Smith, *Chemical Science*, 2013, **4**, 2557-2563.
244. J. M. Baumes, J. J. Gassensmith, J. Giblin, J. J. Lee, A. G. White, W. J. Culligan, W. M. Leevy, M. Kuno and B. D. Smith, *Nat. Chem.*, 2010, **2**, 1025-1030.
245. J.-J. Lee, A. G. White, D. R. Rice and B. D. Smith, *Chem. Commun.*, 2013, **49**, 3016-3018.
246. B. Lewandowski, G. De Bo, J. W. Ward, M. Papmeyer, S. Kuschel, M. J. Aldegunde, P. M. E. Gramlich, D. Heckmann, S. M. Goldup, D. M. D'Souza, A. E. Fernandes and D. A. Leigh, *Science*, 2013, **339**, 189-193.

Chapter 2: Interlocked Structures for Ion-pair Recognition

2.1 Introduction

Borne out of the prevalence of monotopic hosts for cation and anion recognition there has, in recent years, been considerable attention focused on the synthesis of heteroditopic receptors for the simultaneous recognition of both cationic and anionic species.[1] These ion-pair receptors, examples of which were discussed in Section **1.4.5** of the introductory chapter, have shown considerable promise in applications of industrial relevant processes such as salt solubilisation and extraction, as well as medically pertinent membrane-transport research.[1, 2]

This chapter describes the synthesis and ion-pair recognition properties of novel heteroditopic interlocked receptors that contain the calix[4]diquinone motif as the cation recognition unit. The following sections give a brief introduction to both calix[4]arene and calix[4]diquinone chemistry and their previous use in the area of ion-pair recognition.

2.1.1 Introduction to the Calix[4]arene and Calix[4]diquinone Motifs

Calix[4]arene is a cyclic oligomer that has been used extensively in supramolecular chemistry by exploiting its properties both as a functional macrocycle[3] and as a useful molecular scaffold.[4] The first of such compounds to be reported was *p*-tert-butyl-calix[4]arene by Zinke in 1941,[5] although unambiguous determination of the structure was not confirmed until some years later.[6] These semi-rigid macrocycles are able to adopt a variety of conformations by virtue of the methylene linkers that bridge between the phenyl rings (Figure **2.1**).

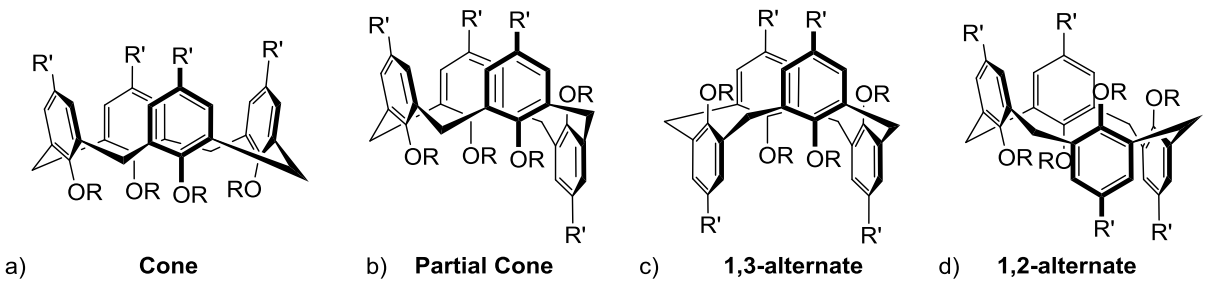

Figure 2.1: Calix[4]arene conformations a) cone b) partial cone c) 1,3-alternate d) 1,2-alternate

In substituted calix[4]arenes these conformations are locked when the lower rim substituent R is more bulky than an *n*-propyl group. Functionalisation of the lower rim of calix[4]arene is readily accomplished *via* an S_N2 reaction with an alkyl halide under basic conditions (Figure **2.2**). The tetra-substituted product may be obtained using an excess of a strong base and four equivalents of an appropriate electrophile. Importantly the substitution pattern can be influenced by the choice of base where mono- di- and tri-substitution is possible. In addition the regioselectivity of the disubstituted product can be controlled by the strength of base. Strong bases such as NaH favour 1,2-proximal substitution whereas weak bases such as K_2CO_3 afford the 1,3-distal product. This is a result of the stabilisation of the mono-substituted intermediate by intramolecular hydrogen-bonding.[7]

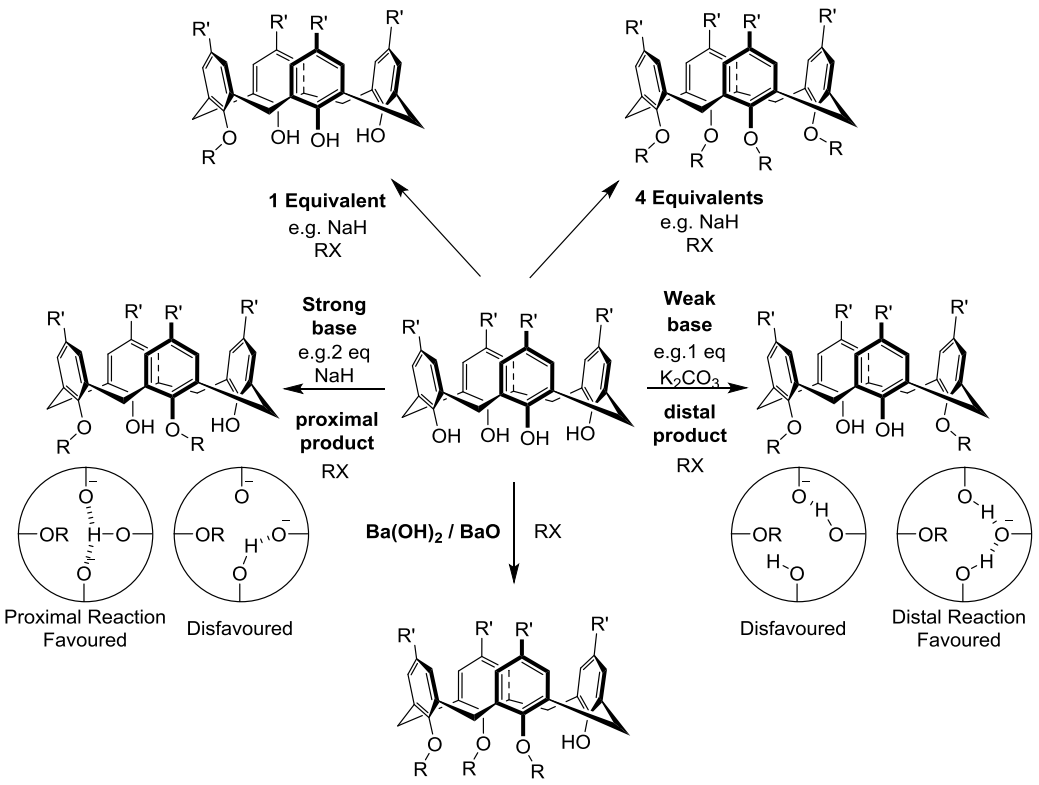

Figure 2.2: Effect of reaction conditions on regioselectivity of calix[4]arene functionalisation (X = leaving group e.g. halide)

Calixquinones are a family of compounds related to the calixarenes in which one or more of the phenol groups are oxidised to the corresponding quinone. Although many strong oxidising reagents have been used to perform this transformation[8, 9] the use of a thallium (III) salt is often preferred as it is capable of the simultaneous cleavage of alkyl substituents *para*- to the phenoxy group, as demonstrated by the mechanism proposed by McKillop (Scheme **2.3**).[10]

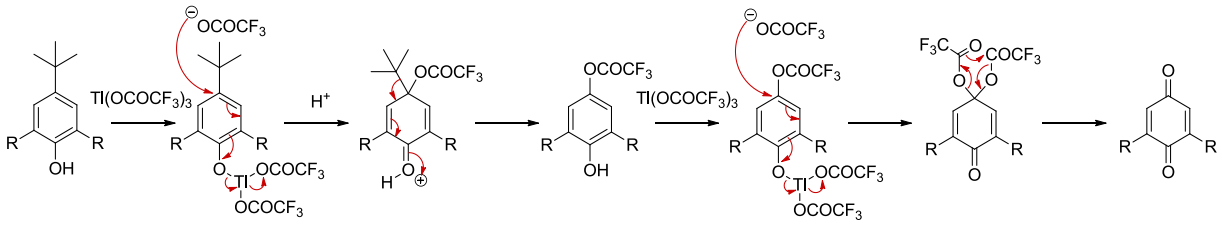

Scheme 2.3: Mechanism of oxidation of *p*-tert-butylphenol by thallium (III) trifluoroacetate

2.1.2 Calixarene Receptors for Cations, Anions and Ion-pairs

Calixarenes and calixquinones have been exploited as molecular scaffolds for a multitude of supramolecular hosts due to their ease of synthesis and functionalisation. Many calixarene-based cation, anion and ion-pair receptors have been reported and were introduced in Section **1.4.5**. This section provides a brief overview of examples that are particularly relevant to the research projects undertaken in this chapter.

The calix[4]arene framework has been shown to form inclusion complexes with alkali metal[11] and organic cations[12, 13] due to favourable cation–**π** interactions. The calix[4]diquinone motif, which contains two convergent quinone oxygen donors, has been employed in the construction of cation hosts. The quinone groups can act as reporter groups and allow ratiometric determination of cationic analytes by UV/visible and electrochemical methods.[14, 15] For example, the calix[4]diquinone receptor reported by Tokita is capable of binding alkali and alkaline earth metals within the macrocyclic cavity (Figure **2.4a**).[16] The receptor undergoes a colour change from blue to green in the presence of calcium cations in ethanol, which was attributed to efficient ion-dipole interactions between the Ca^{2+} ion and the quinone groups. Importantly this behaviour was not observed for potassium as a result of a weaker interaction with the quinone chromophore. Through the incorporation of anion-binding urea groups, Jeon demonstrated the redox-active quinone units of the calix[4]diquinone receptor (Figure **2.4b**) were capable of electrochemically sensing sulphate anions in acetonitrile *via* a cathodic shift of 180 mV in the reduction potential of the quinone groups.[17]

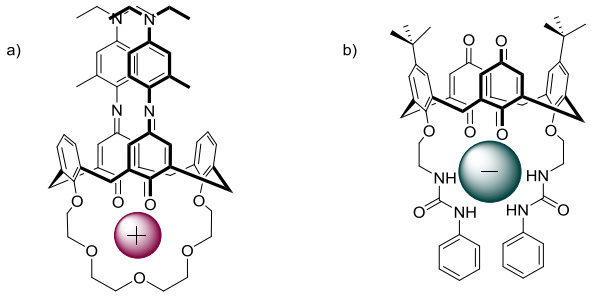

Figure 2.4: Monotopic calixdiquinone ion receptors for a) calcium and b) sulphate

Kilburn's heteroditopic calix[4]arene receptor exhibited ion-pair binding (Figure **2.5a**) where the presence of an alkali metal cation modulated the binding affinity of a range of anions in acetonitrile solution. In the absence of the metal the host was selective for acetate anions whereas upon prior addition of sodium cation the receptor displayed a strong selectivity for diphenyl phosphate.[18] Nabeshima's tritopic ion receptor achieved enhanced anion binding through allosteric effects. The preorganisation of the host was modulated by sodium and/or silver cations which produced a chelating urea cleft for anion binding (Figure **2.5b**). The association constants for nitrate and trifluorosulphonate in chloroform/acetonitrile (9:1) were enhanced by three orders of magnitude in the presence of both sodium and silver cations.[19] Beer and co-workers have reported a contact AND calix[4]diquinone ion-pair receptor which displays positive cooperativity for both charged species (Figure **2.5c**).[20] The host exhibited little affinity for the cation or anion alone but strong binding of ion-pairs in acetonitrile. This was due to an intramolecular hydrogen bond between the quinone oxygen and the isophthalamide motif disfavouring the binding of either guest. The binding of the ion-pair was sufficiently strong to overcome this interaction and thus only ion-pair binding was observed for NH_4Cl and NaCl ion-pairs.[21]

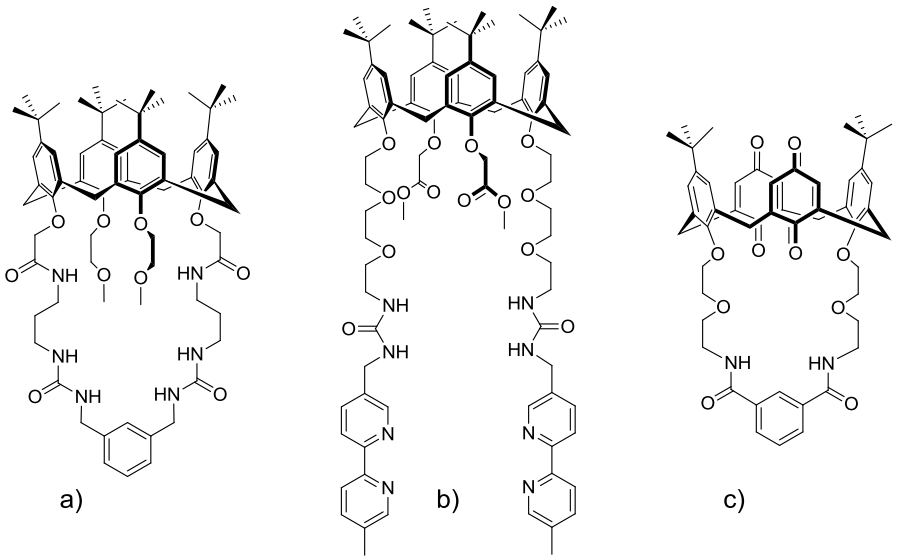

Figure 2.5: Ion-pair receptors by a) Kilburn b) Nabeshima c) Beer

2.1.3 Introduction to the pyridine *N*-oxide motif

The pyridine *N*-oxide motif has been used extensively in a wide range of applications such as asymmetric catalysts,[22, 23] antibacterial agents[24] and as ligands for coordination chemistry.[25, 26] Recently it has also been exploited to form interpenetrated structures. Jiang and co-workers demonstrated the formation of a [2]pseudorotaxane assembly in chloroform between a 3,5-bis-amide pyridine *N*-oxide threading moiety and an isophthalamide macrocycle, stabilised by hydrogen-bonding and favourable aromatic donor-acceptor interactions (Figure **2.6**).[27] The threading-dethreading process could also be controlled *via* pH whereby addition of trifluoroacetic acid (TFA) protonated the pyridine *N*-oxide oxygen and resulted in expulsion of the thread.

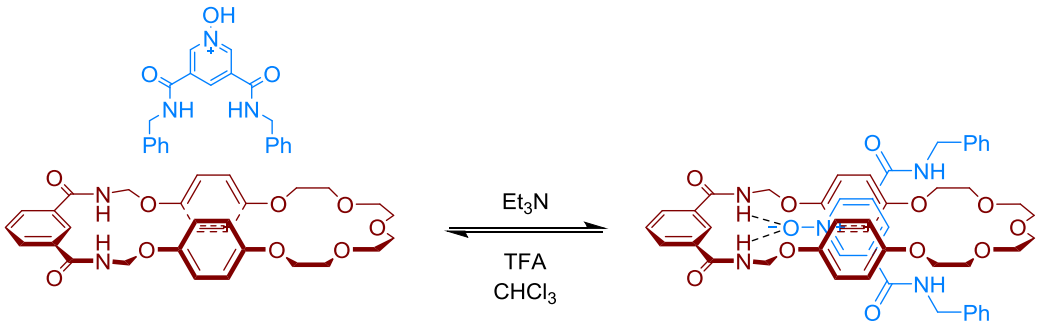

Figure 2.6: Jiang's pH switchable [2]pseudorotaxane

Ballester has used anions such as azide and thiocyanate to augment the assembly of a [2]pseudorotaxane between a bis-calix[4]pyrrole containing macrocycle and a pyridine *N*-oxide thread *via* complementary hydrogen bonding interactions in chloroform solution (Figure **2.7**)[28].

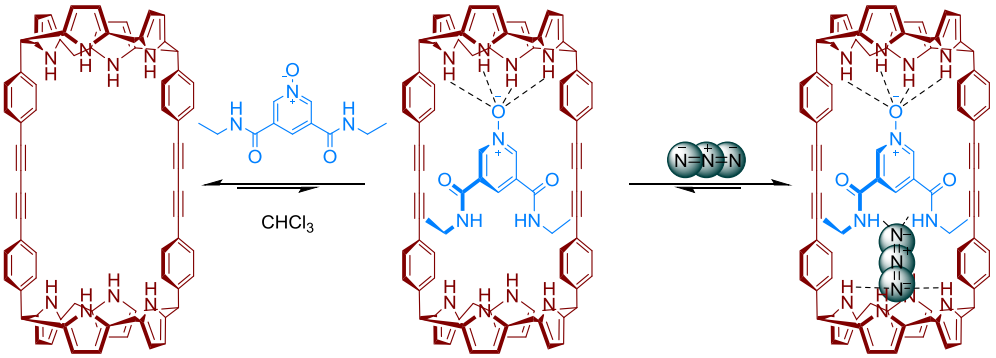

Figure 2.7: Ballester's polyatomic anion-assisted formation of a [2]pseudorotaxane

Beer and co-workers have also demonstrated the versatility of the pyridine *N*-oxide motif to prepare interlocked hosts *via* both sodium cation[28] and halide anion templation.[29] Additionally lanthanide cation-templation was used by the same group to construct a [2]rotaxane containing a pyridine *N*-oxide axle component (Figure **2.8**).[29]

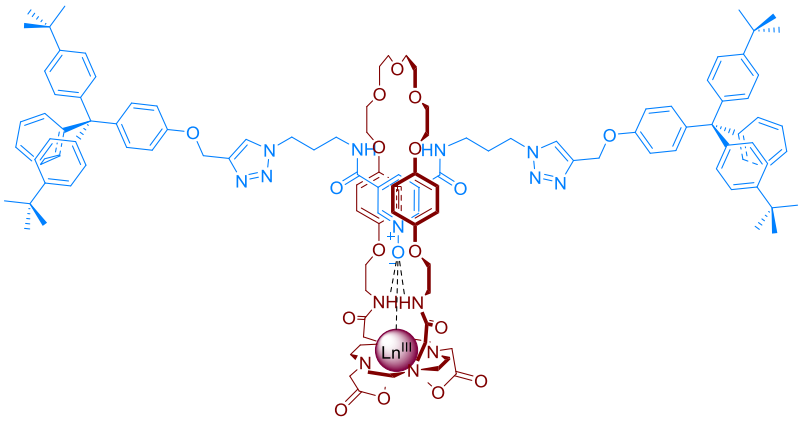

Figure 2.8: Beer's lanthanide cation-templated [2]rotaxane

2.1.4 Chapter Objectives

The research aims of this chapter were to synthesise unprecedented interlocked 'axle separated' ion-pair receptors capable of ion-pair recognition. The target interlocked structures contained a heteroditopic macrocycle consisting of a calix[4]diquinone cation recognition site covalently linked to a 3,5-bis-amide functionalised pyridine anion binding motif. This macrocycle was combined with a ditopic 3,5-bis-amide pyridine *N*-oxide axle component to produce a rotaxane host system designed to recognise alkali metal cation - halide anion ion-pairs in an 'axle-separated' binding fashion (Figure **2.9a**).

A cation templated threading followed by stoppering or clipping reaction was investigated initially for interlocked structure formation. The synthetic methodology adopted focused on using the well known copper-catalysed azide-alkyne cycloaddition (CuAAC) 'click' reaction as the bond-forming stoppering reaction for [2]rotaxane synthesis.[30] The use of activated esters as precursors to interlocked structure formation was also explored in rotaxane and catenane ion-pair host construction (Figure **2.9b**). An investigation into the anion templated

synthesis of a 2-methylimidazolium functionalised axle rotaxane for anion recognition applications was also undertaken (Figure **2.9c**).

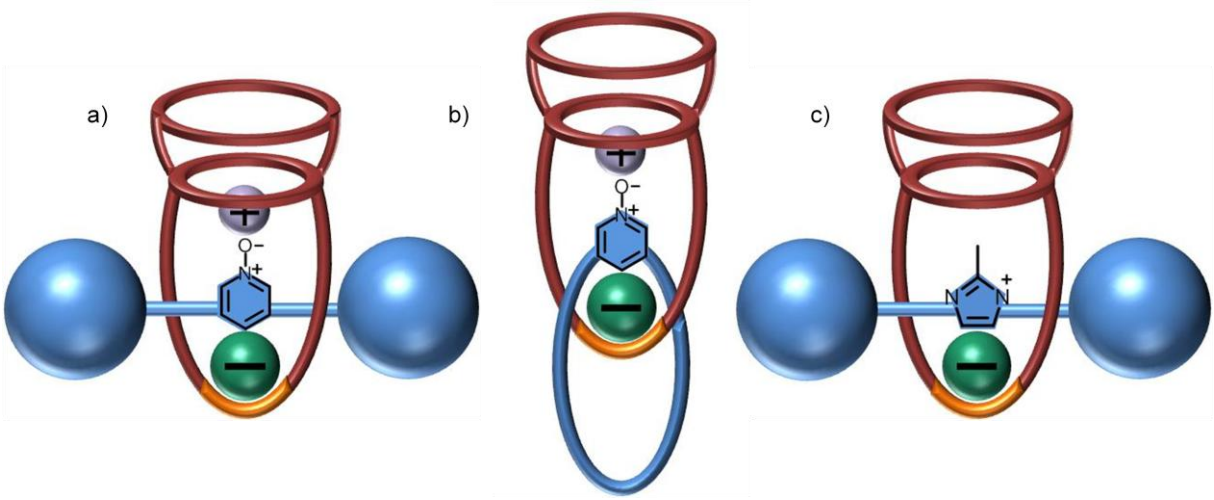

Figure 2.9: Cartoon representation of target a) 'axle separated' rotaxane ion-pair receptor b) catenane ion-pair receptor c) imidazolium rotaxane anion receptor

2.2 Ion-pair binding interlocked structures

2.2.1 Heteroditopic Calix[4]diquinone Macrocycle Synthesis

A multi-step procedure was undertaken to synthesise the target calix[4]diquinone macrocycle **1**. This required the prior synthesis of *p*-tert-butylcalix[4]arene **2** and a phthalimide functionalised hydroquinone synthon **4**. The synthesis of *p*-tert-butylcalix[4]arene was performed according to a literature procedure *via* condensation of formaldehyde with *p*-tert-butyl phenol in the presence of potassium hydroxide.[31] Pyrolysis of the calix[8]arene intermediate and subsequent recrystallisation afforded *p*-tert-butylcalix[4]arene **2** as the toluene adduct in 43% yield (Scheme **2.10**).

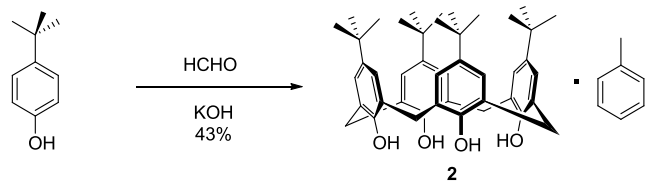

Scheme 2.10: Synthesis of *para*-^{t}butylcalix[4]arene **2**

Two differing synthetic strategies were undertaken as potential routes to the synthon **4** of the target calix[4]diquinone macrocycle (Scheme **2.11**). The first route involved the reaction of commercially available 2,2'-(1,4-phenylenebis(oxy))diethanol with mesyl chloride, in the presence of triethylamine, to afford compound **3** in quantitative yield. A statistical S_N2 reaction of **3** with one equivalent of potassium phthalimide in toluene in the presence of a phase-transfer reagent (aliquat336®) gave, after column chromatography, the mono-substituted precursor **4** in 24% yield. Due to the low yield of this second step an alternative synthesis was explored where mono-tosylation of 2,2'-(1,4-phenylenebis(oxy))diethanol afforded compound **5** in 48% yield. Displacement of the tosylate by potassium phthalimide in *N,N*-dimethylformamide (DMF) gave **6** in 69% yield. Compound **6** was subsequently converted to the mesylate with mesyl chloride, giving the precursor **4** (94%). Despite the additional step it allowed precursor **4** to be synthesised in larger quantities and as such this route was chosen for the synthesis of the target calix[4]diquinone macrocycle.

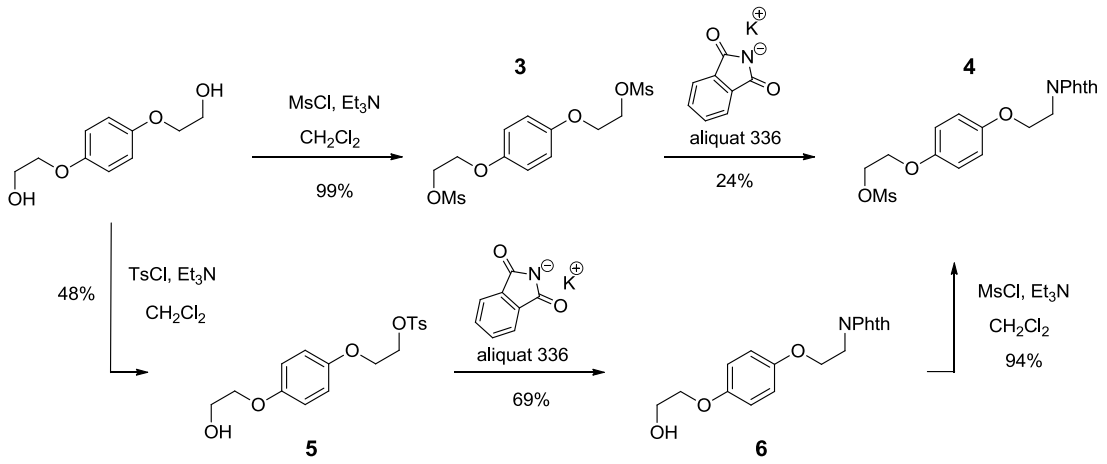

Scheme 2.11: Synthetic routes to precursor **4**

The target calix[4]diquinone receptor **1** was synthesised by modifying an established synthetic strategy (Scheme **2.12**).[32] The lower rim 1,3-disubstituted protected amine calixarene compound **7** was prepared by heating a suspension of *p*-tert-butylcalix[4]arene **2**, an excess of **4** and two equivalents of potassium carbonate in acetonitrile under reflux for four days. Purification by column chromatography gave the synthon **7** (60%). Deprotection of the phthalimide groups by heating compound **7** with hydrazine monohydrate in ethanol, under microwave radiation for 15 minutes at 100°C afforded the bis-amine compound **8** (92%). Bis-chlorocarbonyl pyridine was synthesised from the corresponding bis-acid by activation with oxalyl chloride. The condensation reaction of bis-amine **8** with bis-chlorocarbonyl pyridine in dry dichloromethane under basic high-dilution conditions gave the calix[4]arene macrocycle **9** in 93% yield. Oxidation of macrocycle **9** was accomplished using an alternative strategy to that previously described.[33] Ten equivalents of $Tl^{III}(CF_3CO_2)_3$ were added to macrocycle **10** in dry dichloromethane/trifluoroacetic acid (5:1) at 0°C for 30 minutes to afford the target calix[4]diquinone macrocycle **1** in 42% isolated yield. It was

found that longer reaction times or higher temperatures significantly decreased the yield of the calix[4]diquinone product due to competing oxidation of the hydroquinone groups.

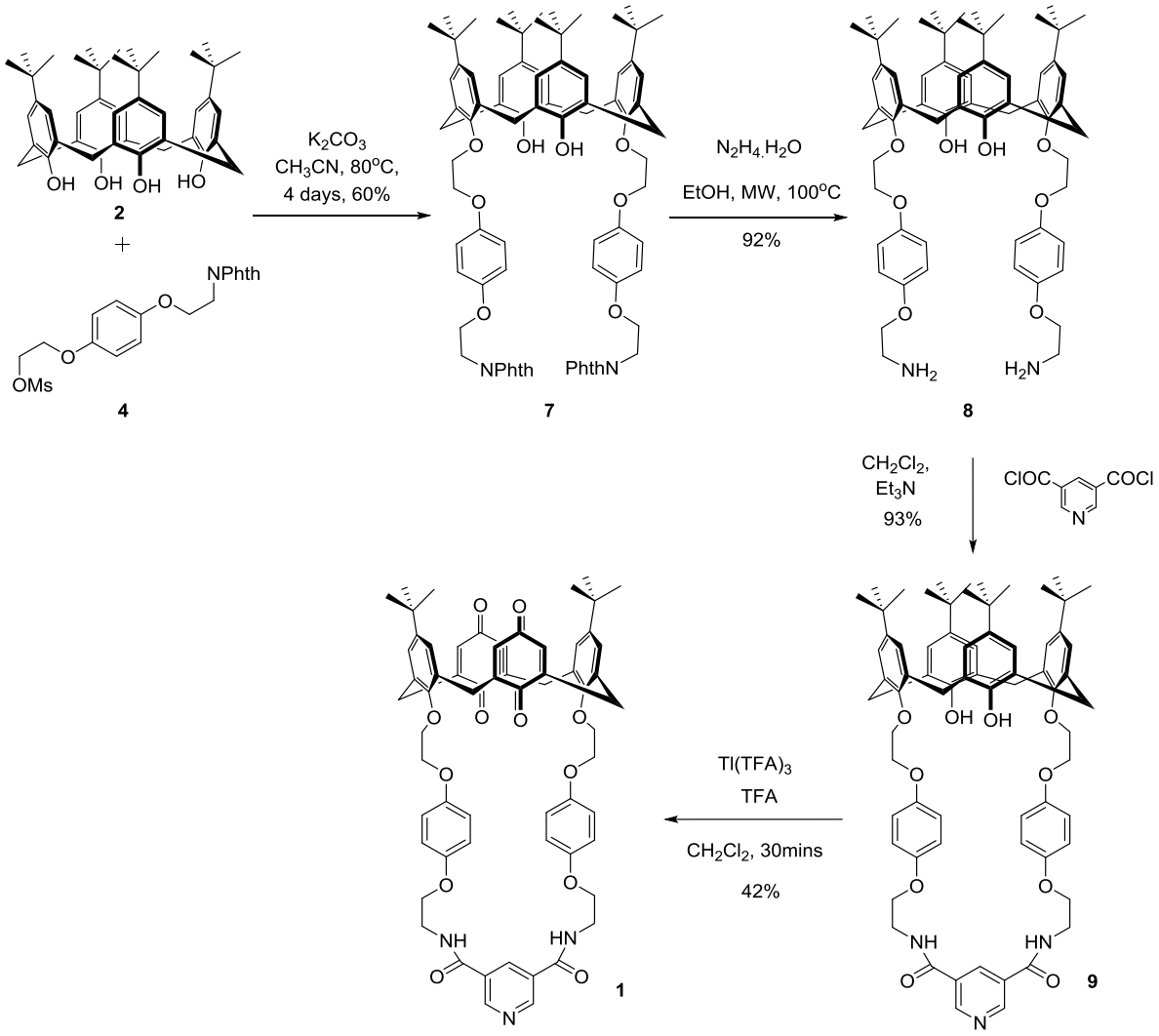

Scheme 2.12: Synthesis of calix[4]diquinone macrocycle **1**

Single crystals of the calix[4]diquinone macrocycle **1** suitable for X-ray diffraction structural analysis (all crystal structure determinations in this thesis were solved by the thesis author R. C. Knighton) were obtained by vapour diffusion of diisopropyl ether into a dilute chloroform solution of the receptor. The structure, collected using synchrotron radiation, shows a DMSO solvate within the macrocyclic cavity (Figure **2.13**). As a result the

calix[4]diquinone moiety adopts a partial cone conformation where one quinone group is hydrogen bonded to the solvent molecule (C-O distance of 3.198 Å). The DMSO oxygen is also hydrogen-bonded to the isophthalamide motif with N-O distances of 3.039(5) Å and 3.188(5) Å, illustrating the ditopic character of the macrocycle.

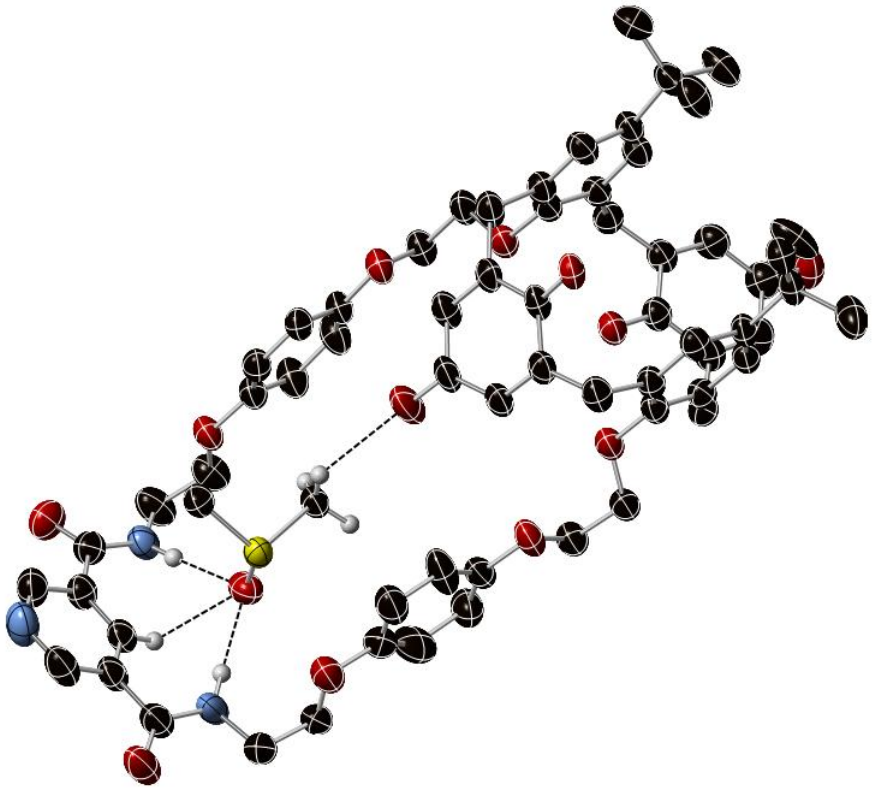

Figure 2.13: Single crystal X-ray structure of calix[4]diquinone macrocycle **1** (Ellipsoid probability at 50%, non-hydrogen bonding hydrogen atoms omitted for clarity)

2.2.2 Preliminary Pseudorotaxane Study

In order to assess the viability of a metal cation-templation strategy for interlocked structure formation, a preliminary ^{1}H NMR pseudorotaxane study was undertaken. The ^{1}H NMR spectrum of an equimolar mixture of calix[4]diquinone macrocycle **1**, 3,5-bis-hexyl-amide pyridine *N*-oxide thread **10**, kindly donated by Dr. J. M. Mercurio, and sodium tetraphenylborate in $CDCl_3$ is shown in Figure **2.14b**. In comparison to the individual ^{1}H

NMR spectra of the macrocycle and thread, significant upfield perturbations of the macrocycle hydroquinone and pyridine *N*-oxide thread protons are observed as a result of favourable aromatic donor-acceptor interactions between the electron rich hydroquinone groups of the macrocycle and the electron deficient pyridine *N*-oxide motif. In addition the quinone protons θ and calixarene resonances shift upfield upon sodium cation binding. These spectral changes confirm the concomitant binding of the metal cation and interpenetration of the thread into the macrocycle to form the [2]pseudorotaxane assembly.

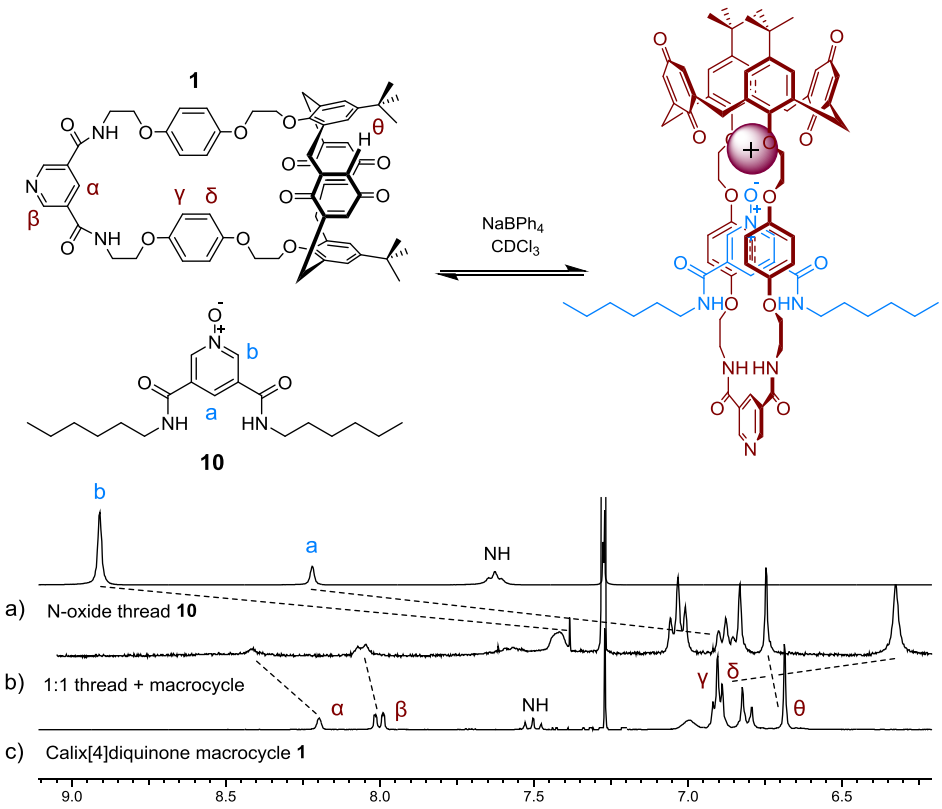

Figure 2.14: ^{1}H NMR (300 MHz, $CDCl_3$, 298 K) of a) N-oxide thread **10** b) 1:1:1 N-oxide thread **10**, calix[4]diquinone macrocycle **1** and $NaBPH_4$ c) calix[4]diquinone macrocycle **1**[34]

2.2.3 Synthesis of the target heteroditopic [2]rotaxane

Having demonstrated the sodium cation-templated pseudorotaxane assembly of pyridine *N*-oxide thread **10** with the calix[4]diquinone macrocycle **1**, it was envisaged that the synthesis of the target heteroditopic [2]rotaxane *via* a copper(I) catalysed azide-alkyne cycloaddition (CuAAC) click stoppering strategy would be possible. This necessitated the synthesis of a bis-azide terminated pyridine *N*-oxide thread derivative for [2]pseudorotaxane formation and an alkyne functionalised terphenyl stopper compound.

2.2.3.1 Axle precursor synthesis

The bis-azide functionalised pyridine *N*-oxide axle precursor was synthesised according to Scheme **2.15**.[30] The bis-chlorocarbonyl pyridine compound was first condensed with two equivalents of 3-bromopropylamine hydrobromide and triethylamine in dry dichloromethane to afford compound **11** (32%). Reaction with sodium azide in dry DMF at 80°C gave the bis-azide compound **12** in 86% yield. Oxidation of the pyridine group with Oxone and $NaHCO_3$ in 2-butanone/water (1:1) afforded the axle precursor **13** (74%) (Scheme **2.15**).

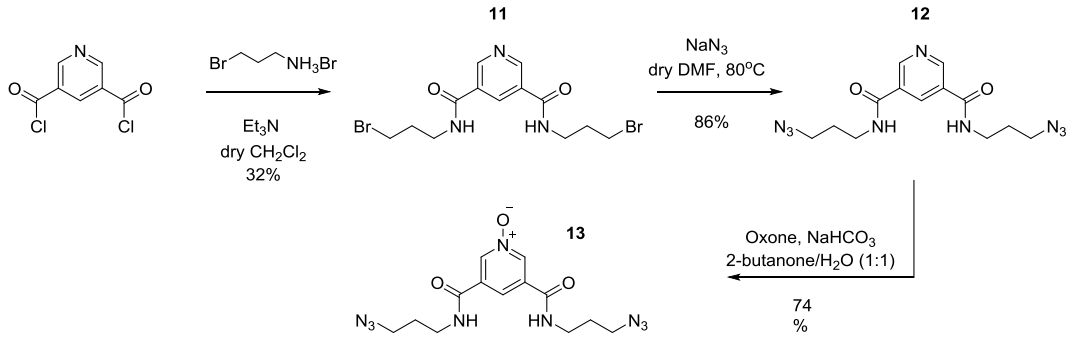

Scheme 2.15: Synthesis of pyridine N-oxide axle precursor **13**

The synthesis of the alkyne terphenyl stopper **16**[35] began with a Grignard reaction between commercially available 4-bromo-*tert*-butylbenzene and methyl benzoate in dry THF to obtain bis(4-(tert-butyl)phenyl)(phenyl)methanol **14** in 66% yield. This was then heated in phenol at 140°C in the presence of catalytic hydrochloric acid to afford the phenol stopper **15** (45%). Functionalisation of **15** with propargyl bromide under basic conditions gave the alkyne terminated terphenyl stopper **16** in 78% yield (Scheme **2.16**).

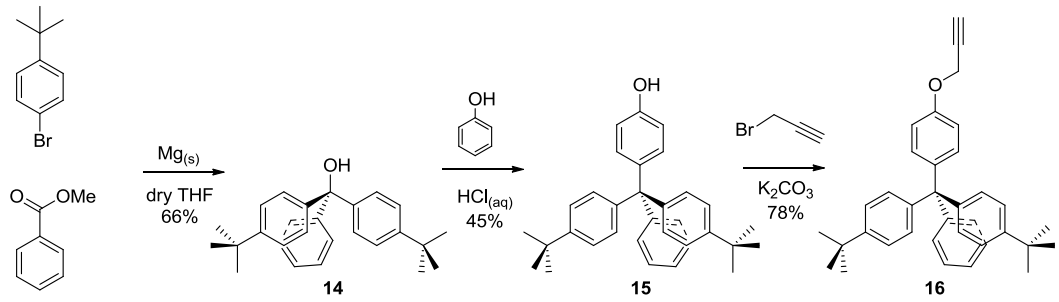

Scheme 2.16: Synthesis of alkyne functionalised stopper **16**

In order to test the viability of the axle synthesis using click reaction conditions, bis-azide **13** and two equivalents of alkyne stopper **16** were subjected to a CuAAC reaction using $Cu^{I}(MeCN)_4PF_6$ as a catalyst, tris[(1-benzyl-1*H*-1,2,3-triazol-4-yl)methyl]amine (TBTA) as a stabilising ligand and diisopropylethylamine (DIPEA) as a base. Purification by silica gel column chromatography afforded the target pyridine *N*-oxide axle **17** in 65% yield (Scheme **2.17**).

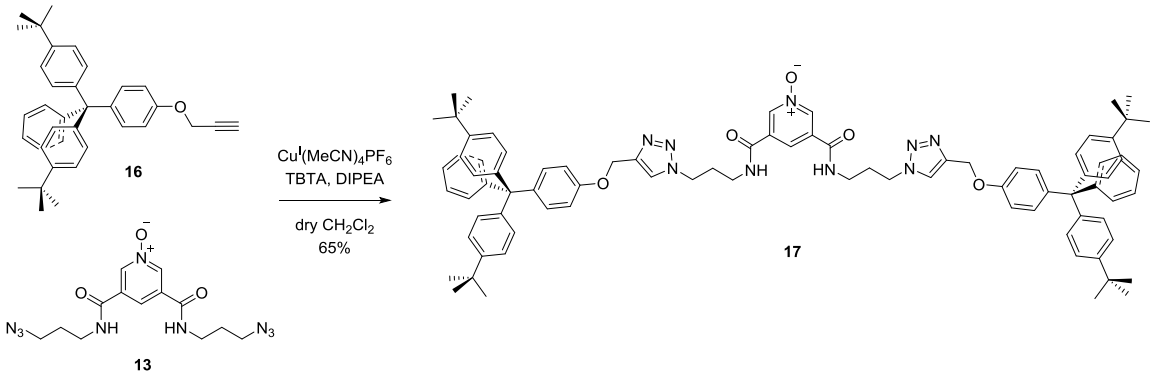

Scheme 2.17: Synthesis of pyridine N-oxide axle **17**

2.2.3.1 [2]Rotaxane Synthesis and Characterisation

Following the successful preparation of the component synthons for rotaxane formation, the synthesis of the rotaxane interlocked structure was undertaken. Chloroform was chosen as the solvent for the rotaxanation reaction due to the limited solubility of bis-azide **13** in dichloromethane. Calix[4]diquinone macrocycle **1** was combined with sodium triflate, bis-azide **13** and two equivalents of alkyne stopper **16** in chloroform and subjected to CuAAC reaction conditions using $Cu^{I}(MeCN)_4PF_6$ as catalyst, TBTA and DIPEA as base. After washing with aqueous ethylenediaminetetraacetic acid ($EDTA_{(aq)}$) the rotaxane **18** was purified by size-exclusion chromatography and preparative TLC (gradient elution DCM/MeOH 98:2→96:4) and isolated in 20% yield. It was found that by allowing the [2]pseudorotaxane components to stir overnight the solubility of the metal salt in chloroform improved significantly and the corresponding yield of the rotaxane was increased to an impressive 62% (Scheme **2.18**). It is noteworthy that the templating role of the metal cation was found to be crucial in the formation of the interlocked structure; when the synthesis was repeated in the absence of the sodium cation the yield of rotaxane was reduced to <10%.[36]

The rotaxane synthesis was also attempted in the presence of one equivalent of sodium triflate and one equivalent of TBA · Cl to ascertain whether chloride recognition would enhance the yield, however, no significant increase was observed.[37]

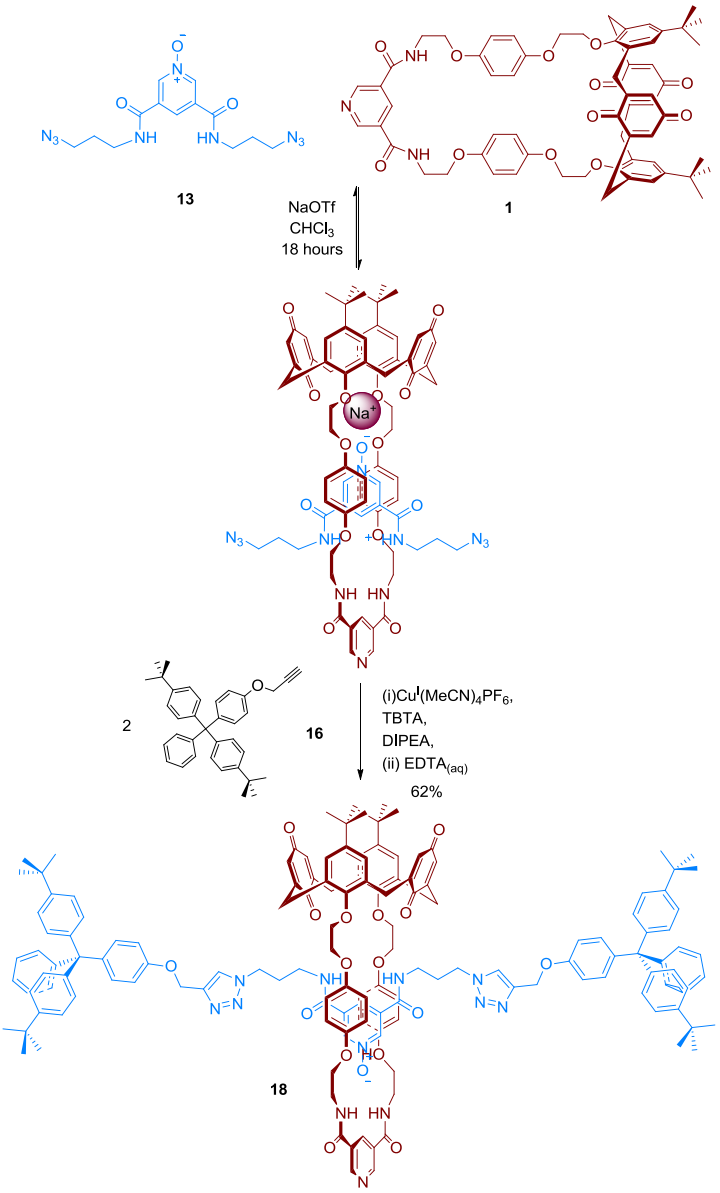

Scheme 2.18: Synthesis of ion-pair binding [2]rotaxane **18** by a threading followed by stoppering strategy

The rotaxane was characterised by ^{1}H, ^{13}C NMR and by high resolution mass spectrometry. The ESI-HRMS analysis of the rotaxane gave the expected peak as m/z = 1210.0753

corresponding to $[M+2Na]^{2+}$ and the ^1H NMR spectrum, together with that of calix[4]diquinone macrocycle **1** and pyridine *N*-oxide axle **17**, is shown in Figure **2.19**.

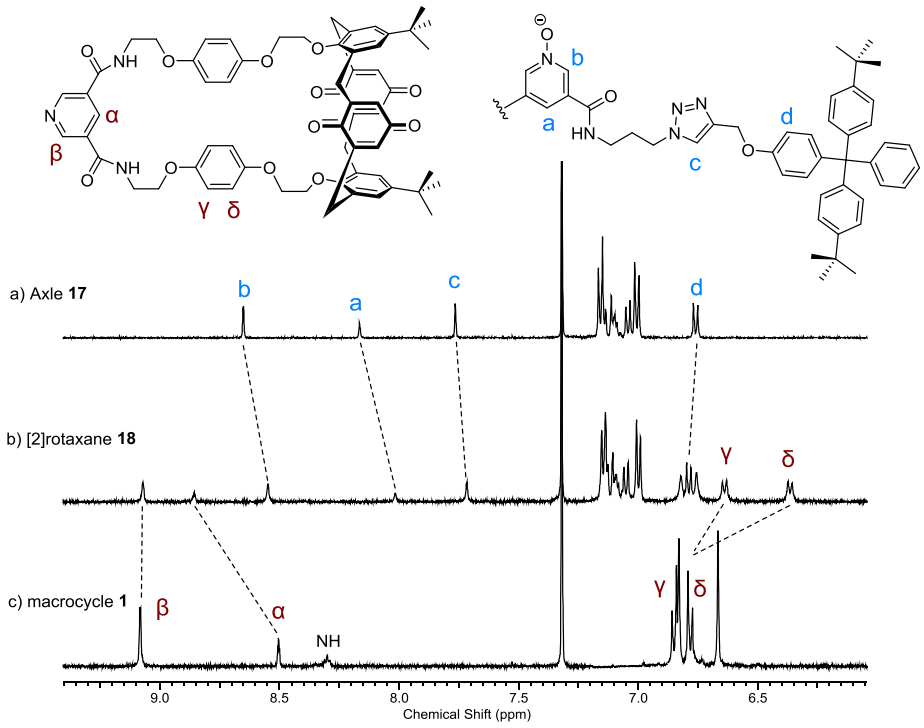

Figure 2.19: ^1H NMR (500 MHz, $CDCl_3/CD_3OD$ 4:1, 298 K) of aromatic region of a) N-oxide axle **17** b) [2]rotaxane **18** c) calix[4]diquinone macrocycle **1**

It can be seen from the spectra that, upon rotaxane formation, the splitting and shifting of hydroquinone protons γ and δ and upfield shift of axle protons *a* and *b* are due to favourable aromatic donor-acceptor interactions between the electron rich hydroquinone groups of the macrocycle and the electron deficient pyridine *N*-oxide component of the axle. This is diagnostic of axle interpenetration of the macrocycle and hence formation of the interlocked structure. Importantly the resonance of the *internal* macrocycle proton α can be seen to shift significantly downfield in the interlocked species. This is likely due to an inter-component hydrogen-bonding interaction between the oxygen of the pyridine *N*-oxide and the 3,5-bis-amide pyridine portion of the macrocycle, indicating the axle adopts an 'axle down'

conformation in the absence of a metal cation. The rotaxane was also characterised by two-dimensional ^{1}H-^{1}H ROESY NMR which provided further evidence of interlocked structure formation (Figure **2.20**). Interactions were observed between the hydroquinone protons *γ* and *δ* with axle protons *b* and *c*, confirming the interlocked product. Additionally couplings are observed between pyridine *N*-oxide protons *b* and the *internal* macrocycle *α*, providing further evidence that the [2]rotaxane adopts the 'axle down' conformation in the absence of metal cations.

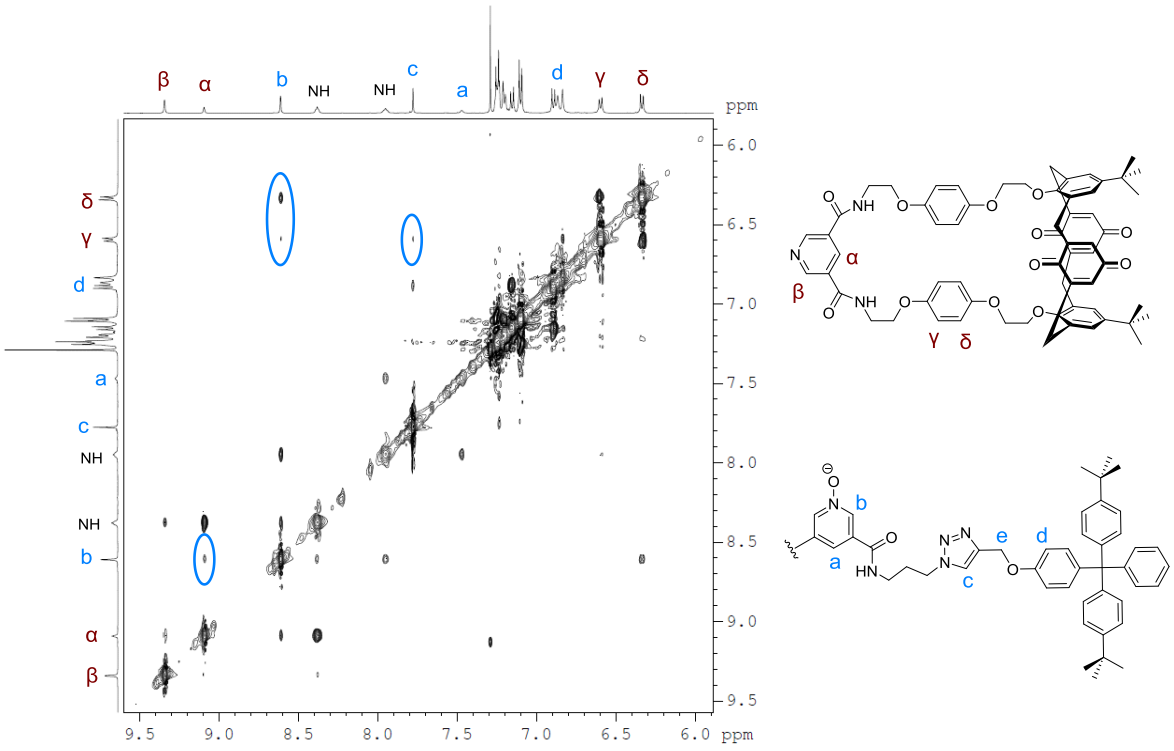

Figure 2.20: truncated ^{1}H-^{1}H ROESY NMR (500 MHz, $CDCl_3$, 298 K) of [2]rotaxane **18**

2.2.3.2 Molecular Motion Investigation

In order to confirm the orientation of the axle with respect to the macrocycle in the presence of metal cations a simple ^{1}H NMR sodium cation titration experiment was undertaken. Spectra of the rotaxane were recorded in $CDCl_3$ as the free host and upon addition of one equivalent of sodium triflate (Figure **2.21**).

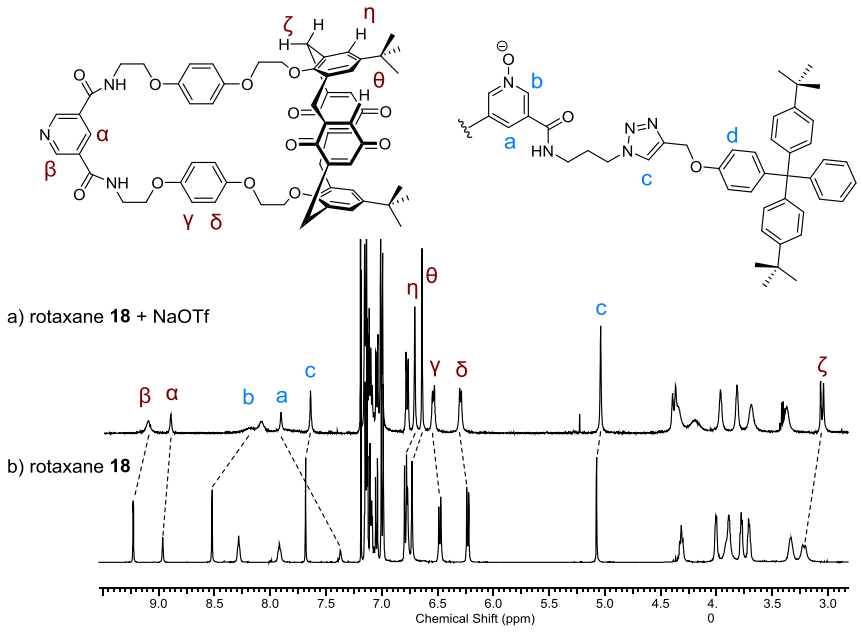

Figure 2.21: ^{1}H NMR (500 MHz, $CDCl_3$, 298 K) spectra of a) [2]rotaxane **18** and one equivalent of NaOTf b) [2]rotaxane **18**

As can be seen, significant perturbations occur upon the addition of sodium cation. The hydroquinone protons γ and δ shift downfield as a result of sodium coordination. The two peaks corresponding to the macrocycle's 3,5-bis-amide pyridine moiety α and β shift upfield upon addition of the cation. This is evidence for the pirouetting motion of the axle pyridine *N*-oxide motif within the macrocyclic cavity to coordinate to the calix[4]diquinone bound metal, which results in the pyridine *N*-oxide-amide hydrogen bonding interactions being broken.

In order to further elucidate the orientation of the interlocked receptor in the presence of sodium cation a two-dimensional ^{1}H-^{1}H ROESY NMR in $CDCl_3$ was undertaken. The spectrum of [2]rotaxane **18** in the presence of one equivalent of sodium triflate is shown in Figure **2.22**.

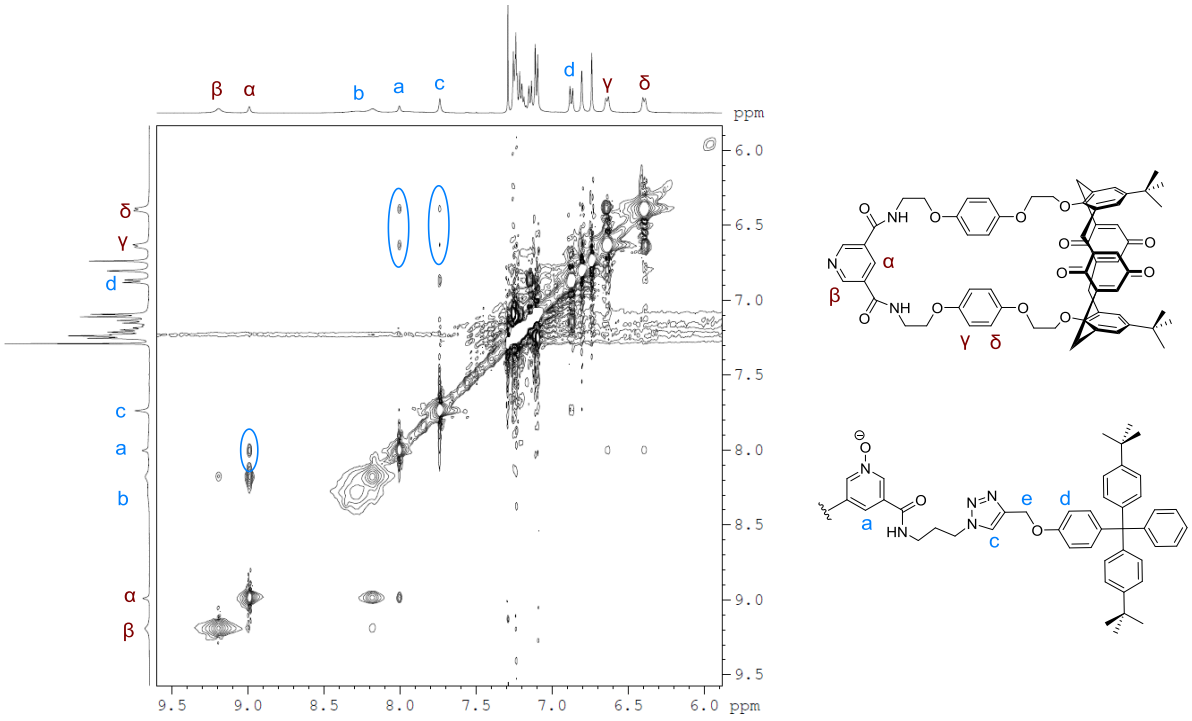

Figure 2.22: ^{1}H-H ROESY (500 MHz, $CDCl_3$, 298 K) of rotaxane **18** in the presence of one equivalent of NaOTf

Cross-couplings can be observed between the hydroquinone protons *γ* and *δ* and the axle pyridine *N*-oxide protons *a* and *b*, confirming that the *N*-oxide component resides within the macrocyclic cavity. Crucially an additional interaction is evident between *α* and *a,* the *internal* proton of the 3, 5-bis-amide pyridine and the pyridine *N*-oxide respectively. This confirms that upon addition of sodium cations the pyridine *N*-oxide pirouettes to coordinate to the metal centre and adopts the 'axle up' conformation (Figure **2.23**). Importantly upon

sequestration of the sodium cations with $EDTA_{(aq)}$ the pyridine *N*-oxide returns to the original 'axle down' conformer.

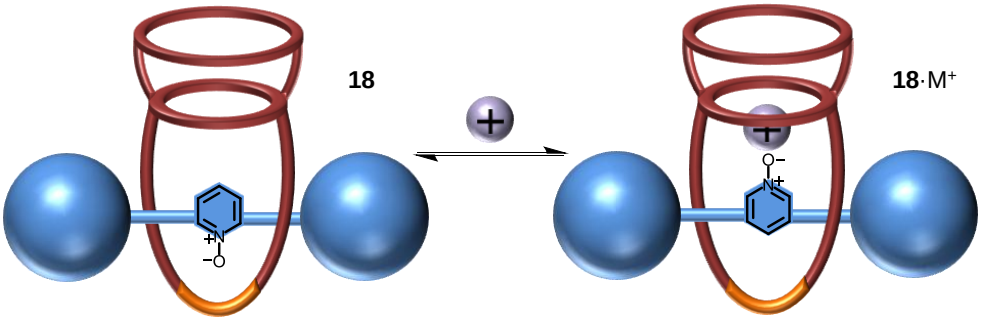

Figure 2.23: Schematic representation of sodium cation-induced molecular pirouetting

2.2.3.3 Anion and ion-pair recognition properties

Preliminary ^{1}H NMR anion titration experiments were undertaken to determine the affinity of the rotaxane to halides in the absence of a metal cation. Titrations were carried out by monitoring the chemical shifts of the pyridine macrocycle protons (α, β) and pyridine *N*-oxide (a, b) protons upon addition of chloride as the tetrabutylammonium (TBA) salt in $CDCl_3/CD_3OD$ (4:1) (Figure **2.24**).

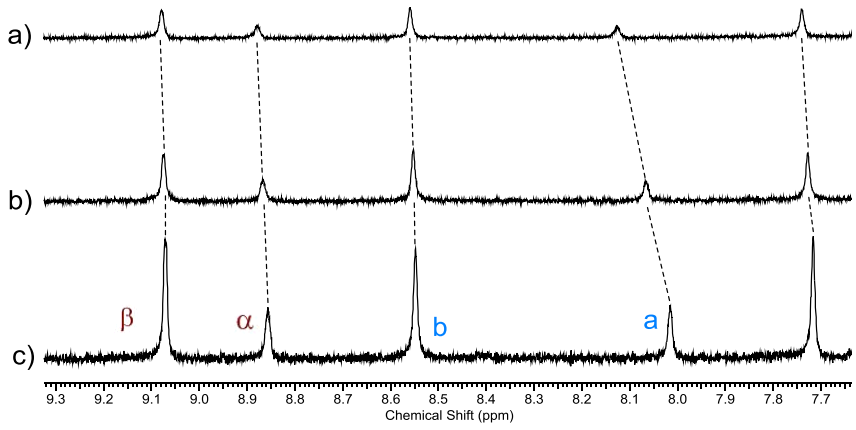

Figure 2.24: ^{1}H NMR (500 MHz, $CDCl_3/CD_3OD$ 4:1, 298 K) spectra of a) rotaxane **18** plus 3 equivalents of TBA · Cl b) rotaxane **18** plus 1 equivalent of TBA · Cl c) rotaxane **18**

The downfield shifts of *a* and *α* are indicative of a polarising hydrogen bonding interaction of these protons with the chloride anion. The shift of both of these protons suggests the halide anion is binding within the interlocked amide cavity of the rotaxane formed between the axle and macrocycle components. The smaller shift of the macrocycle proton *α* with respect to *a* is a reflection of the fact that in the free rotaxane this proton is already hydrogen bonding to the pyridine *N*-oxide oxygen. Similar downfield shifts of *a*, *b* and *α*, *β* were also observed on addition of bromide and iodide. The titration data was analysed using the WinEQNMR2[38] program, monitoring the internal axle proton *a* (Figure **2.25**), to determine 1:1 stoichiometric association constants shown in Table **2.26**.

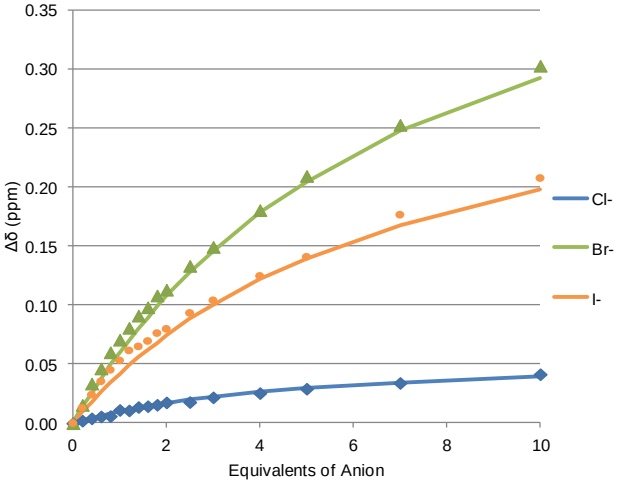

Figure 2.25: Changes in the chemical shift of proton a upon addition of increasing amounts of halide in $CDCl_3/CD_3OD$ (4:1), 298 K

Anion	K_a/ M^{-1}
Chloride	71 (7)
Bromide	88 (8)
Iodide	92 (12)

Table 2.26:Association constants ($CDCl_3/CD_3OD$ 4:1, 298) *Ka* (M^{-1}) obtained for rotaxane 18; fitting errors in parentheses

As can be seen from the tabulated data, rotaxane **18** displays modest halide binding affinities with the association constant values all being of similar magnitude. This may reflect the rotaxane having to undergo a conformational reorganisation in order to bind the halide guest which also requires the breaking of axle pyridine *N*-oxide - amide macrocycle intercomponent hydrogen bonds (Figure **2.27a**).

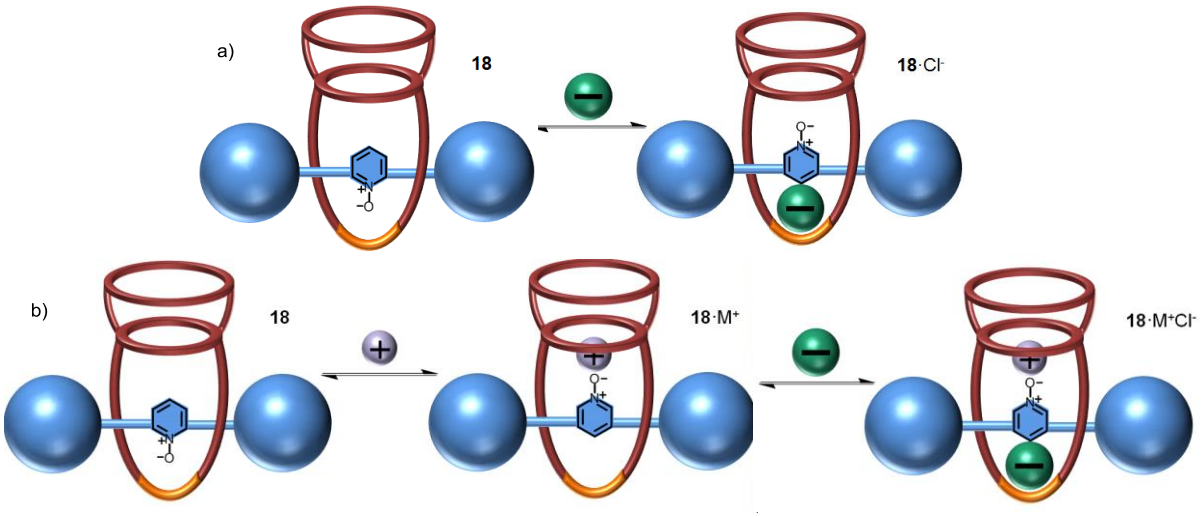

Figure 2.27: Simplified equilibria of rotaxane **18** in the presence of a) halide anion b) metal cation and anion

Analogous halide anion titration experiments were undertaken in the presence of an alkali metal cation with the expectation that the bound metal would help preorganise the rotaxane through conformational reorganisation and, in addition to favourable electrostatic interactions, increase the interlocked host's anion binding affinity (Figure **2.27b**). Anion titration experiments were performed in the presence of one equivalent of an alkali metal cation added as non-coordinating hexafluorophosphate and triflate salts. Figure **2.28** shows ^{1}H NMR spectra of the change in chemical shift of the rotaxane's macrocycle protons (a, b) and axle protons (α, β) upon the addition of chloride to **18** · NaOTf.

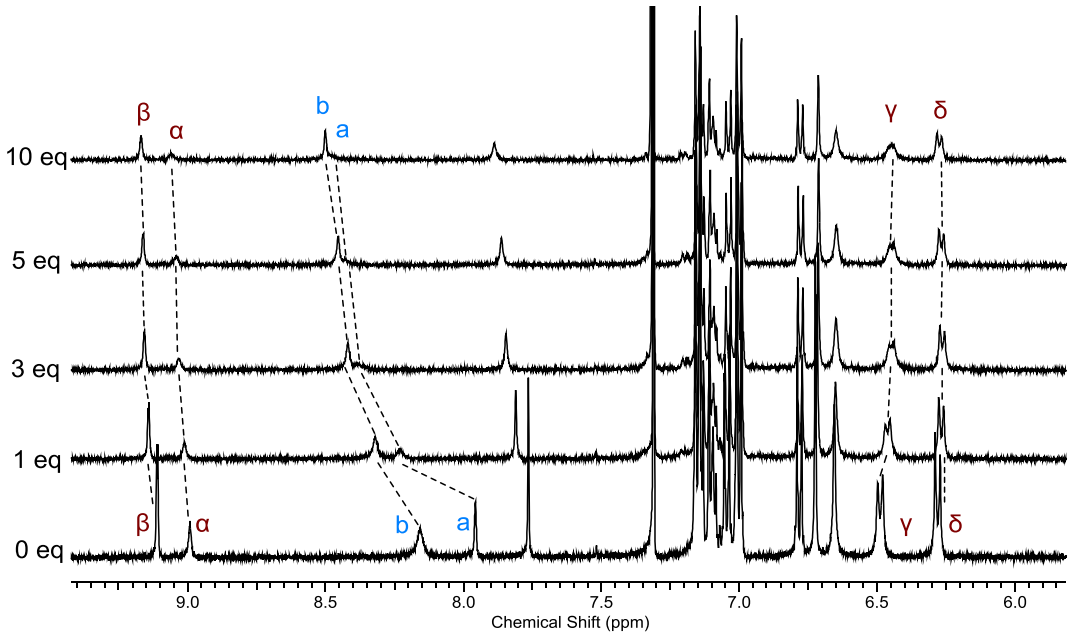

Figure 2.28: ^{1}H NMR (500 MHz, $CDCl_3/CD_3OD$ 4:1, 298 K) of rotaxane **18** · NaOTf in the presence of increasing amounts of TBA · Cl

The macrocycle protons (*a*, *b*) and axle protons (*α*, *β*) can be seen to shift downfield upon the addition of TBA · Cl. This indicates that the chloride anion is binding within the interlocked cavity of the rotaxane and thus the sodium cation –chloride ion-pair is being bound in an 'axle separated' binding arrangement. Additionally the hydroquinone protons *γ* and *δ* can be seen to shift upfield with a concomitant decrease in the splitting of the peaks. This arises as a result of reorganisation of the central axle component to accommodate both the sodium cation and chloride anion within the rotaxane cavity. Analogous spectra were obtained for all chloride and bromide titrations with co-bound alkali metal cations; however titrations with iodide in the presence of alkali metals resulted in precipitation. WinEQNMR2 analysis of the chloride and bromide titration data (Figure **2.30)** determined 1:1 stoichiometric association constant values shown in Table **2.29**. It is noteworthy that a significant increase in the magnitudes of chloride and bromide anion association constants are

observed in the presence of sodium and potassium. In the case of chloride the cooperativity factor in the presence of sodium cations is over 15-fold, suggesting a high degree of host-guest binding complementarity between the heteroditopic rotaxane and the sodium chloride ion-pair. Chloride binding affinity is also enhanced by almost an order of magnitude in the presence of potassium. Large cooperativity factors are also noted for bromide; 10.6 and 7.2 for sodium and potassium respectively. With lithium, a modest increase in the strength of bromide anion binding was observed although no significant enhancement of the binding affinity of chloride was noted.

	Cation	Association Constant/ M^{-1}	Cooperativity Factor[a]
Cl^-	None	71 (7)	-
	Li^+	80 (3)	1.1
	Na^+	1079 (33)	15.1
	K^+	676 (85)	9.5
Br^-	None	88 (8)	-
	Li^+	166 (6)	1.9
	Na^+	930 (134)	10.6
	K^+	633 (91)	7.2

Table 2.29: Association constants Ka (M^{-1}) for rotaxane **18** in the presence of a metal cation (4:1 $CDCl_3/CD_3OD$, 298 K); errors in parentheses; Alkali metals cations added as $LiPF_6$, NaOTf and KPF_6; [a]cooperativity factor calculated by K_a (anion, ion pair)/K_a (anion, free)

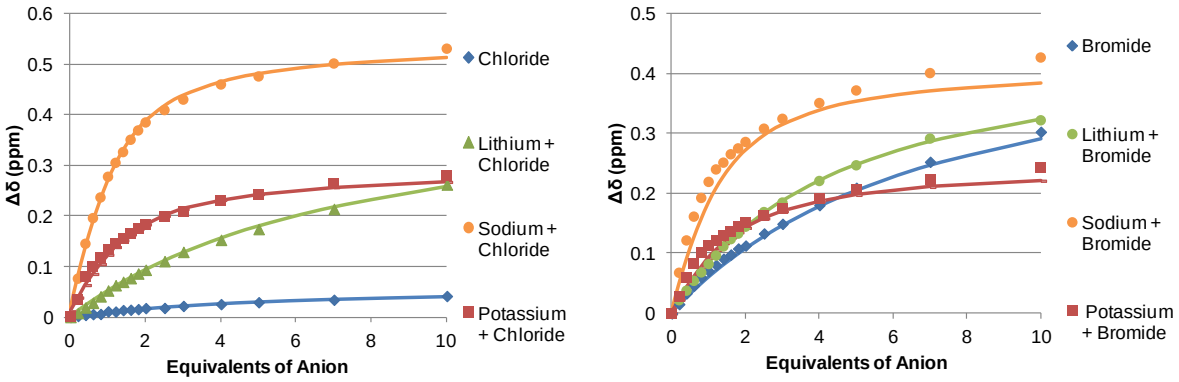

Figure 2.30: changes in the chemical shift of proton a upon addition of increasing amounts halide to a solution of rotaxane **18** · Na^+ in $CDCl_3/CD_3OD$ (4:1), 298 K

2.2.3.4 Extraction Studies

Heteroditopic receptors for ion-pair recognition have applications in the areas of salt solubilisation and extraction as well as in membrane transport research.[1, 2] The capability of rotaxane **18** for extracting alkali metal-halide salts into organic solution was investigated. In a solid-liquid extraction experiment, ten equivalents of dried metal chloride salts (M = Na, K) were added to a 2 mM $CDCl_3$ solution of receptor **18**. The resulting samples were subjected to ^{1}H NMR analysis over the period of twelve days which confirmed the uptake of the metal salt by the receptor (Figure **2.31**).

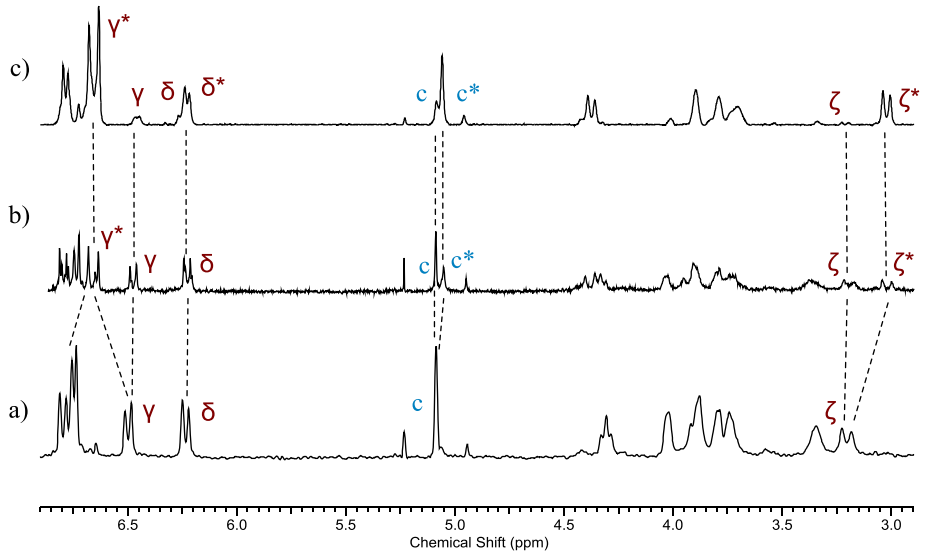

Figure 2.31: ^{1}H NMR (500 MHz, $CDCl_3$, 298 K) spectra of rotaxane **18** a) in the absence of KCl b) after 2 days c) after 12 days equilibration with 10 equivalents of $KCl_{(s)}$; peaks corresponding to bound receptor marked with an asterisk

Monitoring the relative integrals of ζ and ζ*, corresponding to the calix[4]diquinone methylene resonances of the free and bound receptor respectively, it was possible to determine the percentage uptake of the metal salts over time (Figure **2.32**). It can clearly be seen from this data that solubilisation of the alkali metal chloride salts is a slow process although the rate of uptake by the interlocked host compares favourably with related macrocyclic systems.[20] The

extraction of KCl and NaCl reaches a maximum of ca. 70% and ca. 40% respectively. The increased efficiency of potassium chloride uptake is likely to be due to the salt's lower lattice energy compared to sodium chloride.

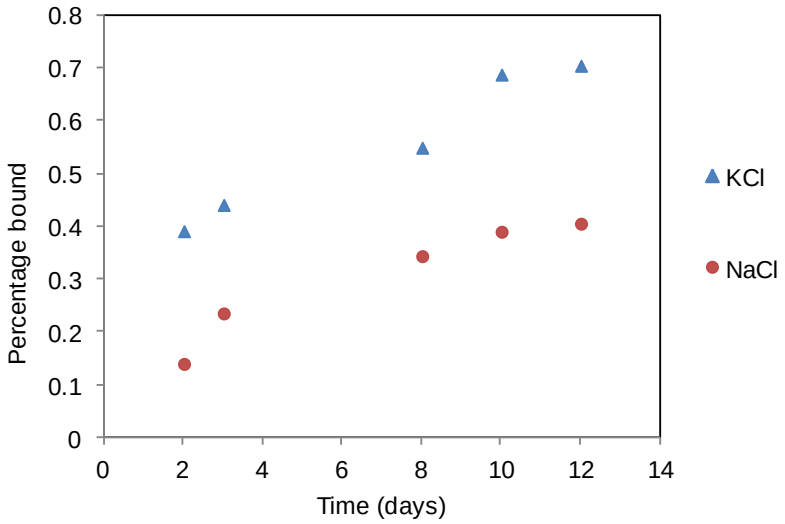

Figure 2.32: Time dependence of the extraction of MCl salts by **18** in $CDCl_3$. Ratio of bound and unbound receptor deduced by integration of the peak integrals belonging to proton ζ

2.2.4 Attempted synthesis of a pH-dependent rotaxane molecular shuttle

Encouraged by the metal cation induced pirouetting of [2]rotaxane **18**, it was anticipated that related pyridine *N*-oxide axle containing rotaxanes may be capable of translational motion upon protonation of the *N*-oxide functional group. As discussed previously in Section **2.1.3**, Jiang[27] demonstrated that pseudorotaxane formation between a pyridine *N*-oxide thread and an isophthalamide macrocycle was pH dependent. The synthesis of a pH-dependent molecular shuttle rotaxane was undertaken which upon protonation has the potential of breaking the intercomponent hydrogen-bonding interactions between the pyridine *N*-oxide axle and the macrocycle's isophthalamide motif, resulting in translation of the macrocycle along the axle (Figure **2.33**).

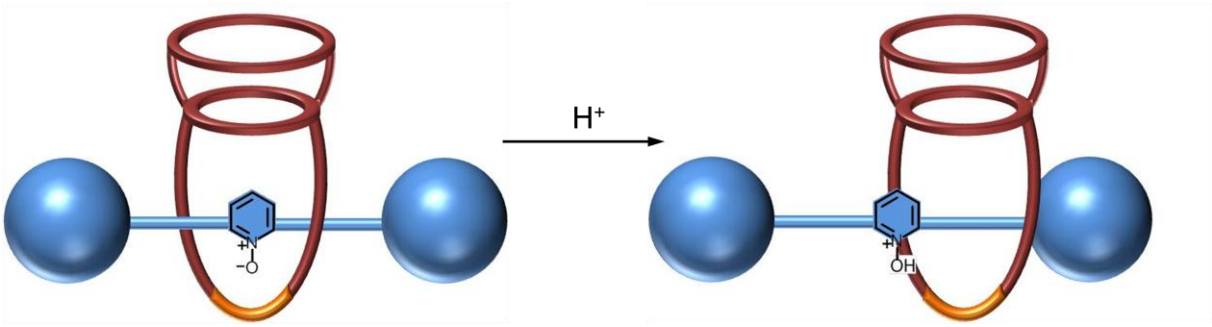

Figure 2.33: Cartoon representation of pH-induced shuttling

This required the synthesis of a pH-independent calix[4]diquinone isophthalamide macrocycle and an extended pyridine *N*-oxide axle precursor.

2.2.4.1 [2]Rotaxane Precursor Syntheses

The isophthalamide containing macrocycle **19** was synthesised under high dilution conditions in dry dichloromethane *via* condensation of bis-amine **8** with isophthaloyl dichloride to afford the product in 81% yield. Oxidation of the calix[4]arene unit was performed with thallium trifluoroacetate in dry dichloromethane for 30 minutes which, after chromatographic purification, furnished the target calix[4]diquinone macrocycle **20** in 38% yield (Scheme **2.34**).

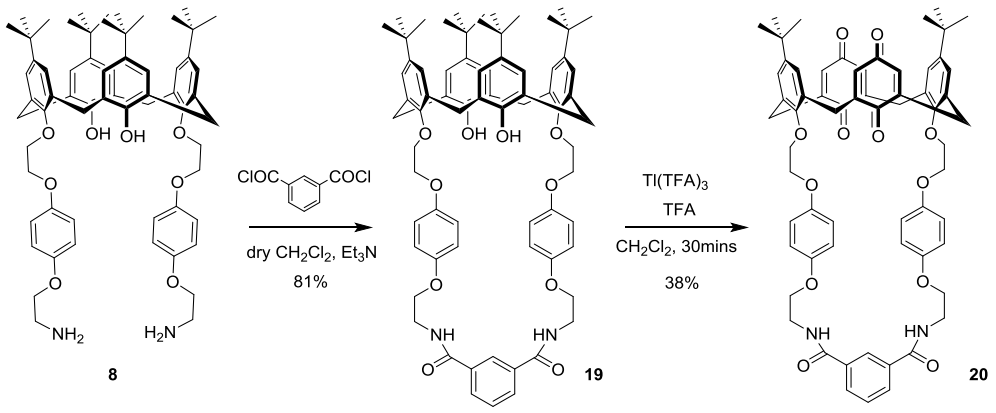

Scheme 2.34: Synthesis of isophthlamide calix[4]diquinone macrocycle **20**

The synthesis of the pyridine *N*-oxide axle precursor began with reaction of tetraethylene glycol with two equivalents of mesyl chloride to furnish the activated bis-mesylate **21** in near quantitative yield (>98%). Subsequent reaction of bis-mesylate **21** with sodium azide in DMF afforded the bis-azide **22** in 82% yield. Mono-reduction of **22** with triphenylphosphine in a biphasic mixture yielded the amino-azide synthon **23** (81%). Condensation of two equivalents of amine **23** with 3,5-bis-chlorocarbonyl pyridine in dry dichloromethane produced bis-amide **24** (74%) which upon oxidation with Oxone in 2-butanone/H_2O (1:1) gave the axle precursor **25** in 62% yield (Scheme **2.35**).

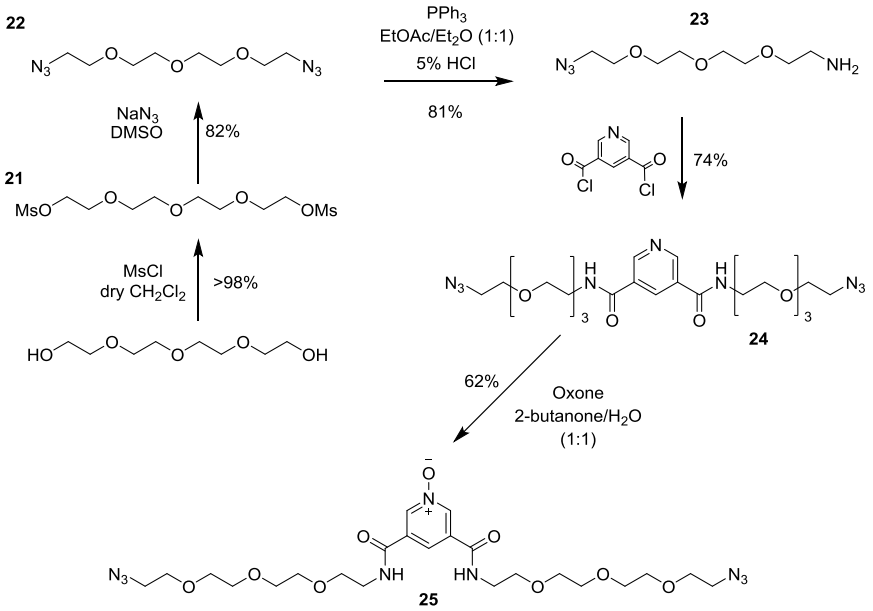

Scheme 2.35: Synthesis of pyridine *N*-oxide axle precursor **25**

2.2.4.2 Rotaxane Synthesis

The target interlocked [2]rotaxane was synthesised using an analogous sodium cation-templated click stoppering procedure to that used for the preparation of rotaxane **18**. (Scheme **2.36**). Equimolar amounts of calix[4]diquinone macrocycle **20**, the pyridine *N*-oxide

axle precursor **25** and sodium triflate were stirred overnight in dry dichloromethane to form the [2]pseudorotaxane assembly. The addition of two equivalents of alkyne functionalised terphenyl stopper **16**, $Cu^{I}(MeCN)_4PF_6$, TBTA and DIPEA and subsequent removal of the sodium cation template by washing with aqueous EDTA gave a crude product which inspite of repeated attempts at purification by preparative thin layer chromatography gave the [2]rotaxane **26** in *ca.* 4% yield (95% purity). Unfortunately the [2]rotaxane sample was contaminated with a macrocyclic impurity – indicated from the presence of calix[4]arene methylene protons in the ^{1}H NMR - that could not be separated from the target compound. However, the ESI-HRMS confirmed formation of the interlocked product, $m/z = 2631.2802$, corresponding to $[M+Na]^+$. Analysis by ^{1}H NMR spectroscopy indicated the interlocked nature of the product (Figure **2.37**).

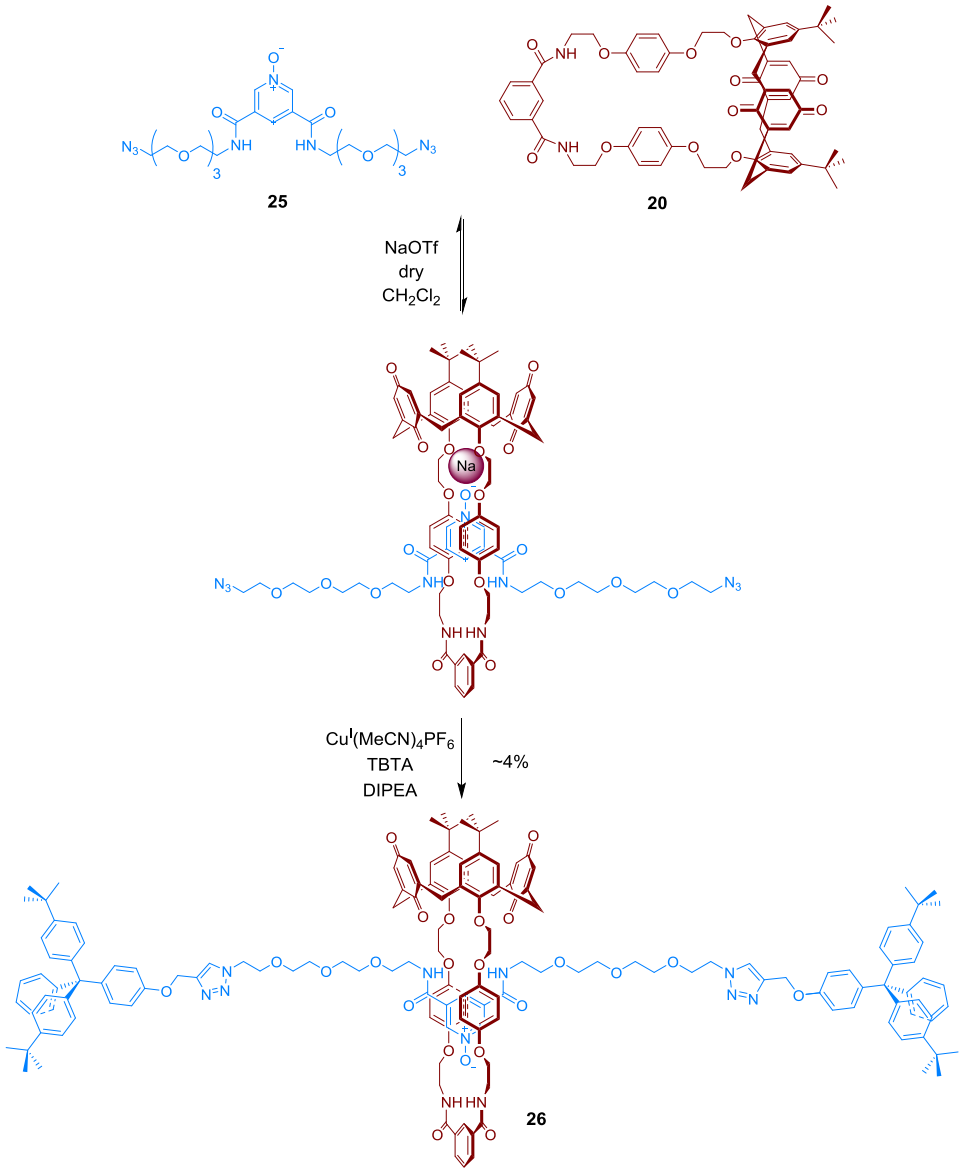

Scheme 2.36: Synthesis of pyridine *N*-oxide [2]rotaxane **26**

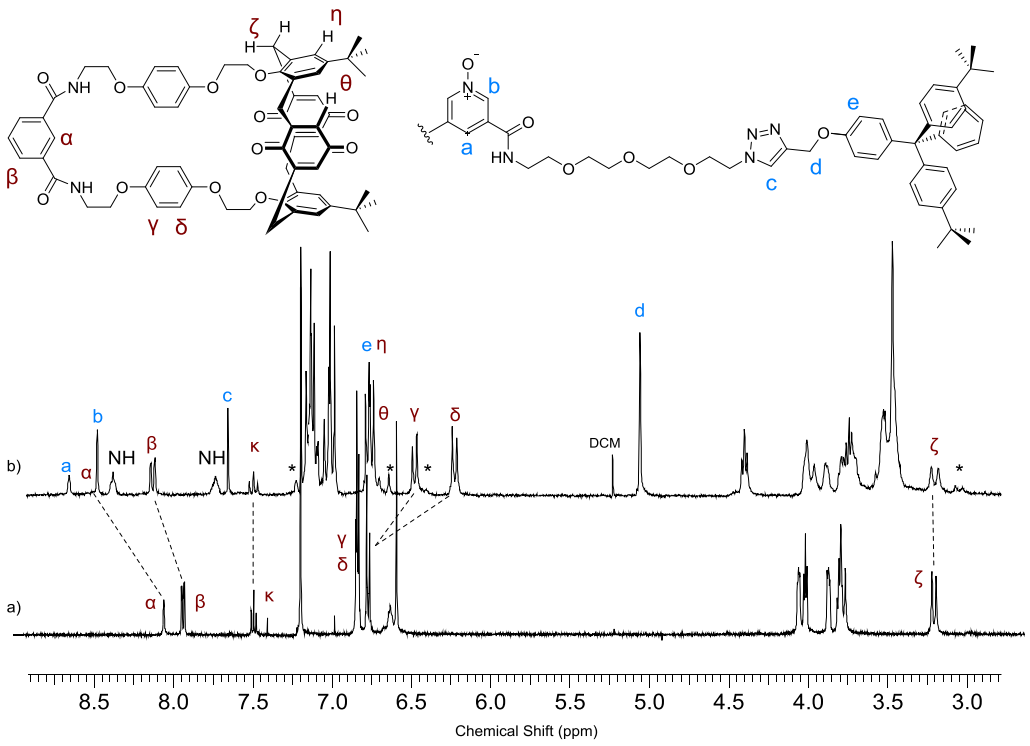

Figure 2.37: ^{1}H NMR (500 MHz, $CDCl_3$, 298 K) spectra of a) calix[4]diquinone macrocycle **20** b) [2]rotaxane **26** (impurities marked with an asterisk)

The hydroquinone protons of the calix[4]diquinone macrocycle γ and δ are split and perturbed upfield in the interlocked structure due to aromatic donor-acceptor interactions with the pyridine *N*-oxide axle. Additionally the *internal* isophthalamide proton α and *external* β proton are shifted downfield, indicative of the hydrogen-bonding with the pyridine *N*-oxide oxygen atom.

The yield obtained for rotaxane **26** is very low compared to the analogous synthesis of rotaxane **18** which is thought to be due to the difficulties experienced in purification. The inability to purify the rotaxane product fully, coupled with the inherently low yield of the rotaxanation precluded pH-shuttling studies of [2]rotaxane **26**.

2.2.4.3 Summary

The sodium cation-templated synthesis of a novel heteroditopic rotaxane **18** was accomplished. The rotaxane was demonstrated to be capable of alkali metal cation, halide anion and most importantly ion-pair recognition through an unprecedented 'axle separated' binding arrangement. The interlocked host displayed a modest affinity for halide anions in the absence of metal cations, however, in the presence of sodium or potassium alkali metal cations the affinities for chloride and bromide were dramatically enhanced due to conformational reorganisation and favourable electrostatic contributions. The rotaxane receptor was found to be most complementary for sodium chloride ion-pairs exhibiting a cooperativity factor of over 15 for chloride binding.

The synthesis of the related heteroditopic rotaxane **26**, containing an isophthalamide macrocycle and extended axle component, was also attempted. Spectroscopic evidence indicated the formation of the interlocked product; however, the low yield and problems encountered with purification negated any pH-dependent ^{1}H NMR shuttling investigations being carried out.

2.2.5 Synthesis of Interlocked Structures Using Activated Esters

2.2.5.1 Introduction

Following the successful synthesis of the ion-pair binding rotaxane **18** attention focused on finding ways to increase the binding affinity for ion-pairs. It has been shown recently that the strength of halide association exhibited by mono-topic interlocked [2]rotaxane receptors

was affected significantly by the length of the axle, where rotaxanes that contain shorter axles exhibited stronger halide anion binding.[39] A shorter axle component reduces the conformational freedom of a rotaxane host system and hence increases the degree of preorganisation of the receptor for binding a guest species. It was envisaged that an amide-bond-forming method could be used in place of the CuAAC click reaction to synthesise a heteroditopic rotaxane that contained a pyridine *N*-oxide axle component of reduced length (Scheme **2.38**).

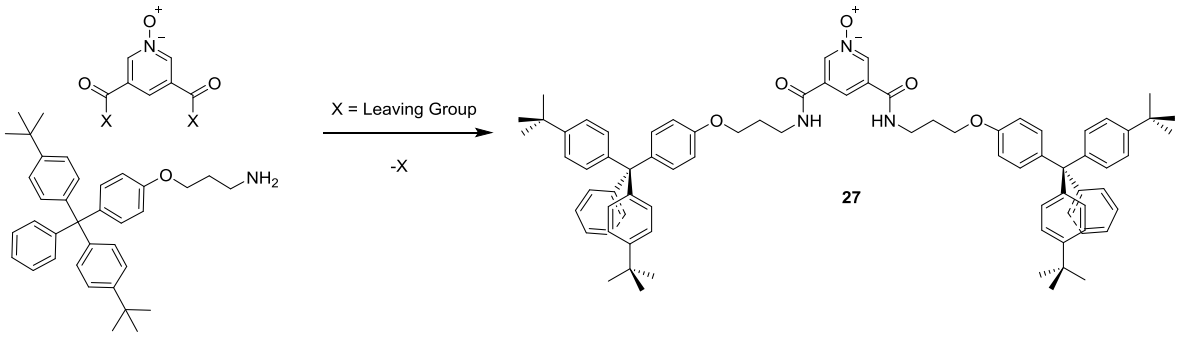

Scheme 2.38: Target shortened pyridine *N*-oxide axle **27**

The use of acid chloride – amine condensation 'clipping' strategies is a well-established method for constructing interlocked architectures.[40] It has shown specific utility in the field of strategic anion templation due to the wide scope of the reaction and the high yields obtained.[41, 42] However, this approach is not compatible with metal-cation templation due to the presence of excess of chloride in solution in the form of triethylammonium chloride which would favour competitive ion-pair precipitation. In order to circumvent this issue, activated esters were explored as a potential alternative to the acid-chloride condensation reaction.

2.2.5.2 Axle Precursor Synthesis

The amine functionalised terphenyl derivative was prepared according to a literature procedure (Scheme **2.39**).[43] Compound **15** was reacted with an excess of 1,3-dibromopropane in acetonitrile under basic conditions to give the bromopropyl stopper derivative **28** (63%). Reaction with sodium azide in dry DMF at 80°C and column chromatographic purification gave azide **29** in 87% yield. Reduction of the azide group with Pd/C under 5 atm $H_{2(g)}$ furnished the aminopropyl stopper **30** in a moderate yield (55%).

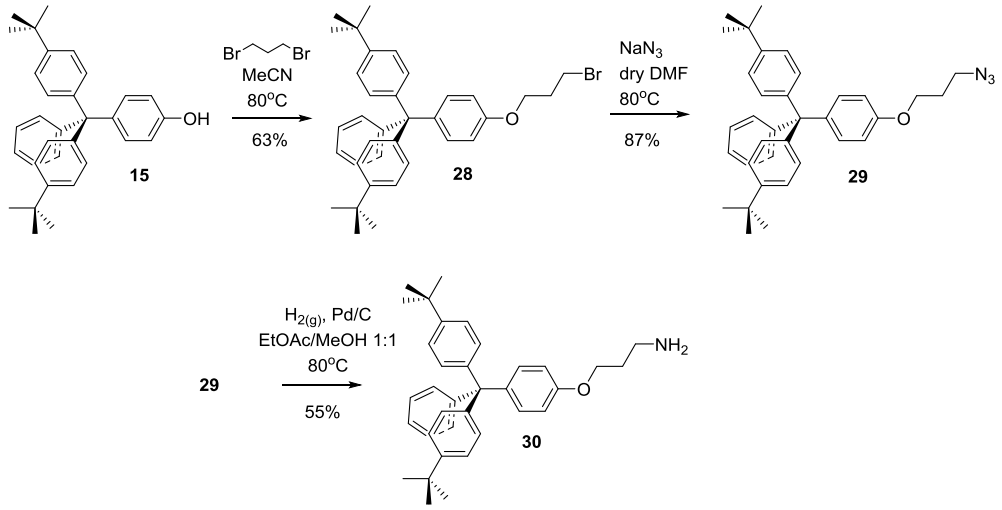

Scheme 2.39: Synthesis of amine-functionalised stopper **30**

The pyridine *N*-oxide activated ester **32** was synthesised from the corresponding acid (Scheme **2.40**). This was prepared by oxidation of commercially available pyridine-3,5-dicarboxylic acid with Oxone in a basic aqueous solution of (1M) sodium hydroxide. Neutralisation afforded the protonated bis-acid **31** in 64% yield. Activation of the acid was accomplished using 1-ethyl-3-(3-dimethylaminopropyl)carbodiimide (EDC) and pentafluorophenol to afford the *N*-oxide activated ester **32** which was used immediately without purification.

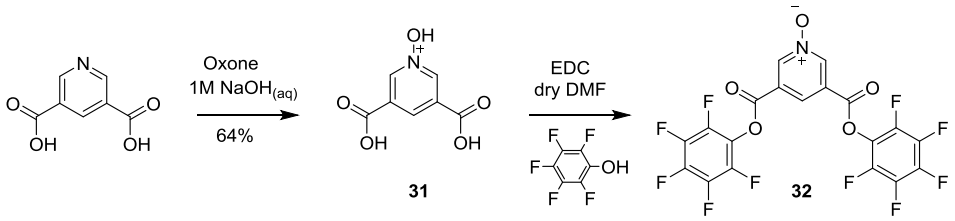

Scheme 2.40: Synthesis of activated ester **32**

2.2.5.3 Attempted Activated Ester [2]rotaxane Synthesis

The synthesis of the rotaxane *via* an activated ester stoppering strategy was attempted using similar sodium cation templated conditions as for the axle triazole-containing rotaxane **18**. The calix[4]diquinone macrocycle **1** was stirred with one equivalent of sodium triflate and pyridine *N*-oxide ester **32** overnight in dry dichloromethane. Following the addition of two equivalents of aminopropyl stopper **30** the reaction mixture was stirred for a further 3 hours (Scheme **2.41**). Disappointingly, mass spectrometric analysis of the reaction mixture gave no evidence for the formation of rotaxane **33**. The high reactivity and susceptibility of the activated ester compound **32** to hydrolysis was thought to be the problem. The reaction was repeated by stirring the [2]pseudorotaxane components **1** and **32** for only 30 minutes in an attempt to minimise degradation of the ester. Thin-layer chromatograph and ESI-LRMS indicated formation of the target rotaxane. Removal of the metal template with $EDTA_{(aq)}$ followed by several iterations of size-exclusion chromatography and preparative TLC (gradient elution DCM/MeOH 100:0→97:3) failed to isolate a pure sample of the rotaxane.

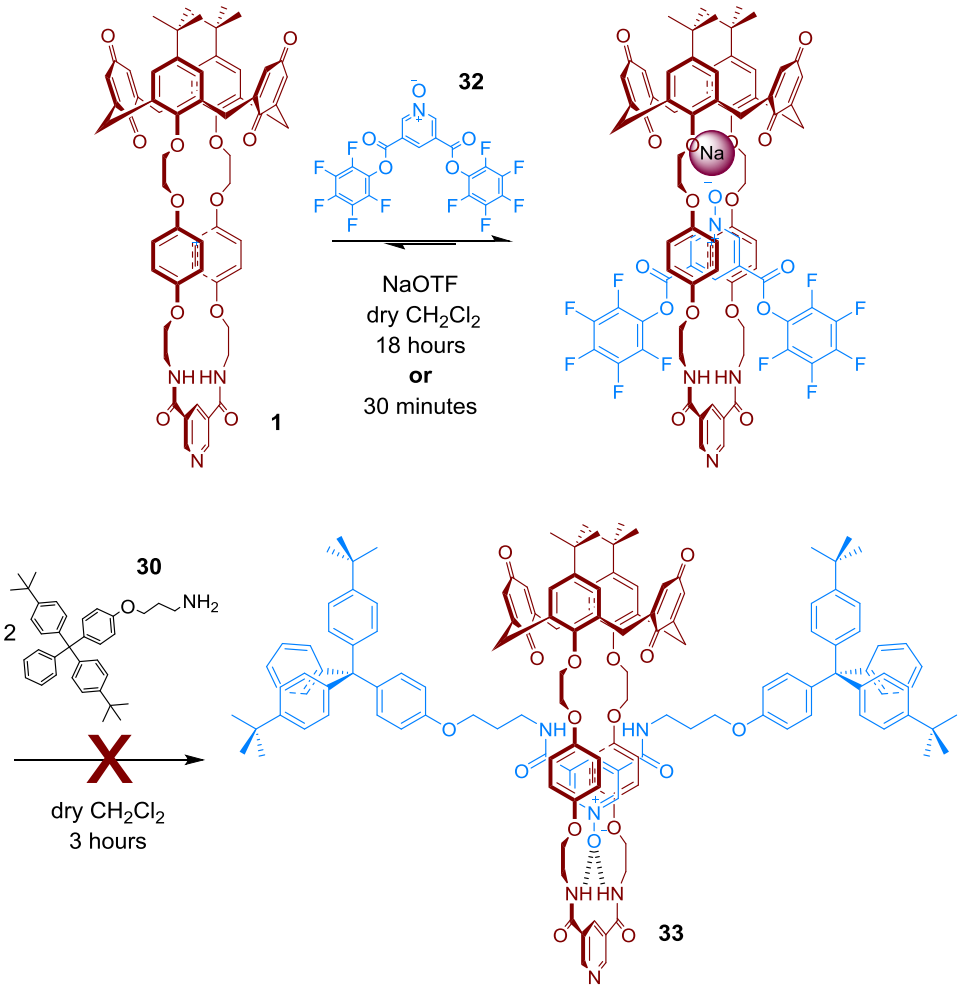

Scheme 2.41: Attempted synthesis of [2]rotaxane **33**

2.2.6 Attempted Activated Ester [2]catenane Synthesis

2.2.6.1 Catenane precursor synthesis

Undeterred by the failure to purify [2]rotaxane **33**, attention turned to the synthesis of a related [2]catenane *via* adaptation of a clipping procedure described by Beer and co-workers.[42] This strategy utilises the coordination of the pyridine *N*-oxide activated ester to the metal cation to form a [2]pseudorotaxane assembly which can subsequently react with a flexible bis-amine and 'clip' around the calix[4]diquinone macrocycle to form the interlinked ringed catenane product (Figure **2.42**).

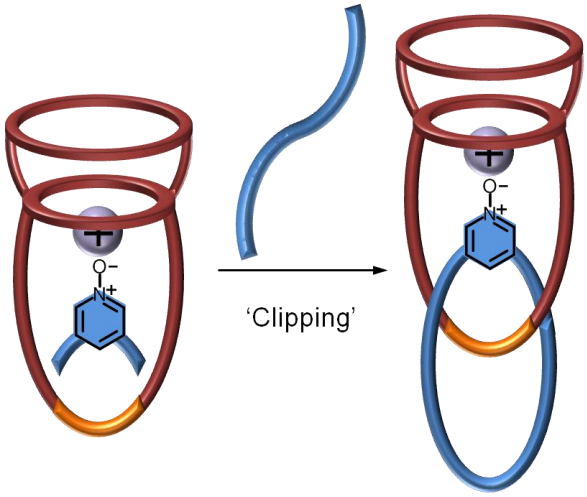

Figure 2.42: Cartoon representation of catenane formation by 'clipping'

This required the preparation of the pyridinium functionalised calix[4]diquinone macrocycle and the synthesis of a hydroquinone functionalised bis-amine macrocycle precursor. Calix[4]diquinone macrocycle **1** was heated with methyl iodide in chloroform to obtain the methylated pyridinium macrocycle **34** · I in quantitative yield (Scheme **2.43**). Due to the very low solubility of the pyridinium macrocycle even as tetrafluoroborate and hexafluorophosphate salts, the compound was anion exchanged to the tetrakis[3,5-bis(trifluoromethyl)phenyl]borate salt via addition of excess $Na[BAr^{F}{}_{4}]$,[40] to obtain **34** · $Na[BAr^{F}{}_{4}]_2$ salt in preparation for cation-templated catenane synthesis.

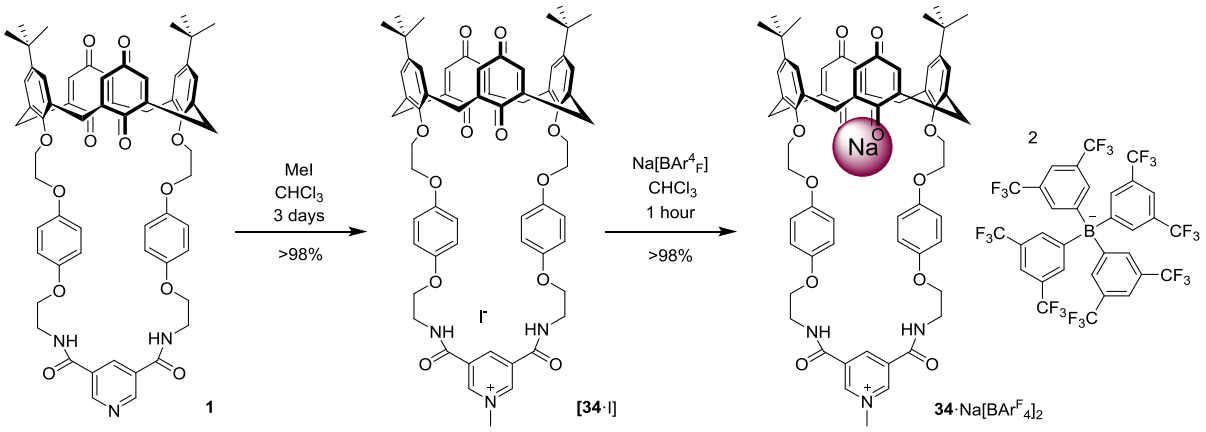

Scheme 2.43: Synthesis of calix[4]diquinone macrocycle **34** · $Na[BAr^{F}{}_{4}]_2$

Single crystals of the pyridinium macrocycle suitable for X-ray diffraction structural determination were obtained by vapour diffusion of diisopropyl ether into a chloroform solution. The data were collected using synchrotron radiation and the resultant structure revealed a chloride complex; it is presumed that chloride was present in the chloroform solution and subsequently crystallised with the macrocycle (Figure **2.44**) The positively charged receptor adopts the partial-cone conformation whereby one quinone is inverted to maximise donor-acceptor interactions with neighbouring molecules in the unit cell. The disordered chloride counteranion resides in the pyridinium-3,5-bis-amide cleft with mean N-Cl and C-Cl distances of 3.31 Å and 3.24 Å respectively.

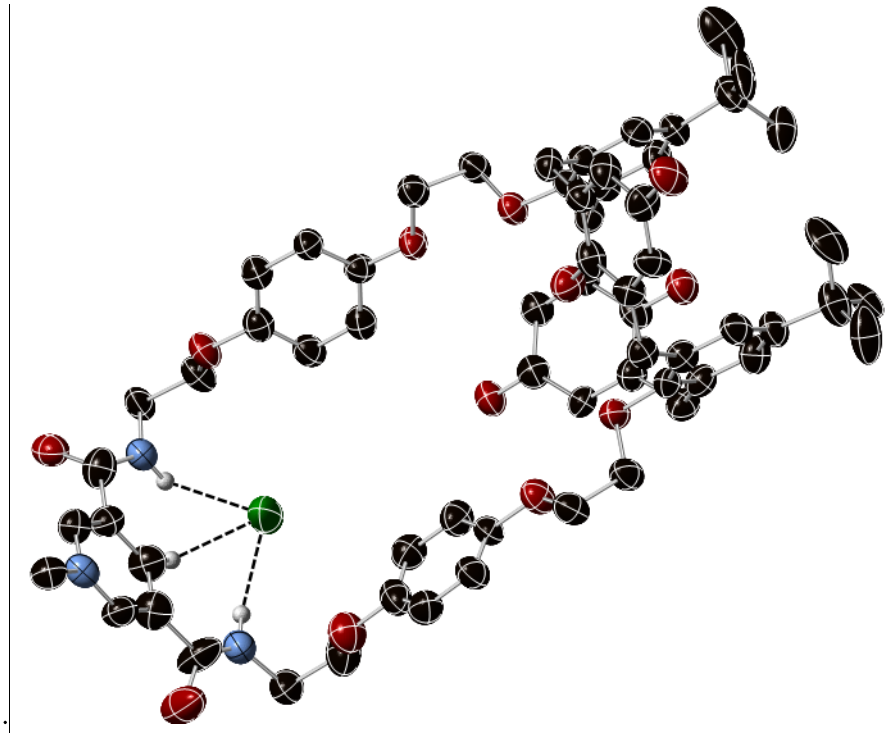

Figure 2.44: Single crystal X-ray crtucture of **34** · Cl (Ellipsoids at 50% probability; disorder and non hydrogen-bonding hydrogen atoms ommitted for clarity)

Bis-amine **37** was prepared *via* a multi-step synthesis outlined in Scheme **2.45**.[41] Monosubstitution of hydroquinone with bromoacetonitrile afforded compound **35** in moderate yield (62%). Reaction of bis-mesylate **21** with two equivalents of **35** in acetonitrile in the presence of potassium carbonate, gave the bis-nitrile compound **36** in 37% yield after column chromatographic purification. Reduction of **36** using 1M $BH_3 \cdot THF$ complex afforded bis-amine macrocycle precursor **37** in 77% yield.

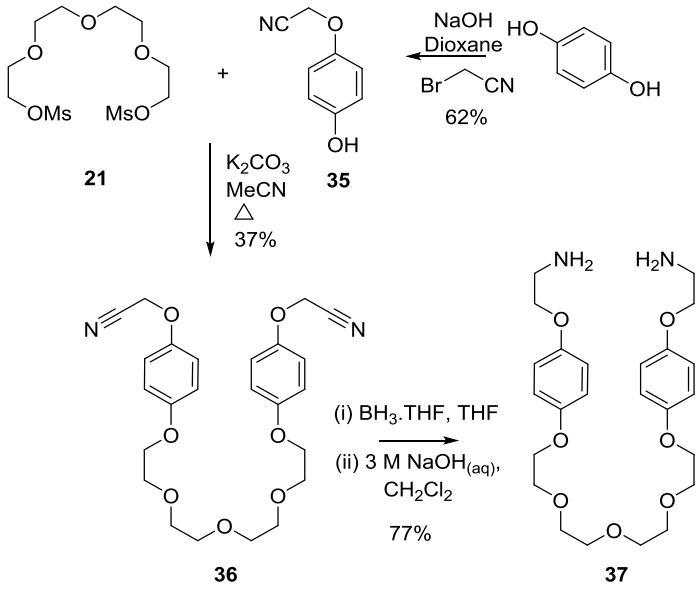

Scheme 2.45: Synthesis of bis-amine macrocycle precursor **37**

In order to determine whether the activated-ester strategy was amenable to interlocked structure formation the corresponding pyridine *N*-oxide macrocycle **40** was prepared. Cyclisation of the macrocycle precursor was preceded by the synthesis of a templating 3,5-bis-hexylamide *N*-methyl pyridinium chloride thread which has been demonstrated to assist macrocyclisation (Scheme **2.46a**).[44] 3,5-Bis-chlorocarbonyl pyridine, prepared *in situ* from the corresponding bis-acid and oxalyl chloride, was reacted with excess hexylamine in dry

dichloromethane to give the bis-amide **38** in 86% yield. Alkylation with methyl iodide, followed by anion exchange gave the chloride salt **39** · Cl.

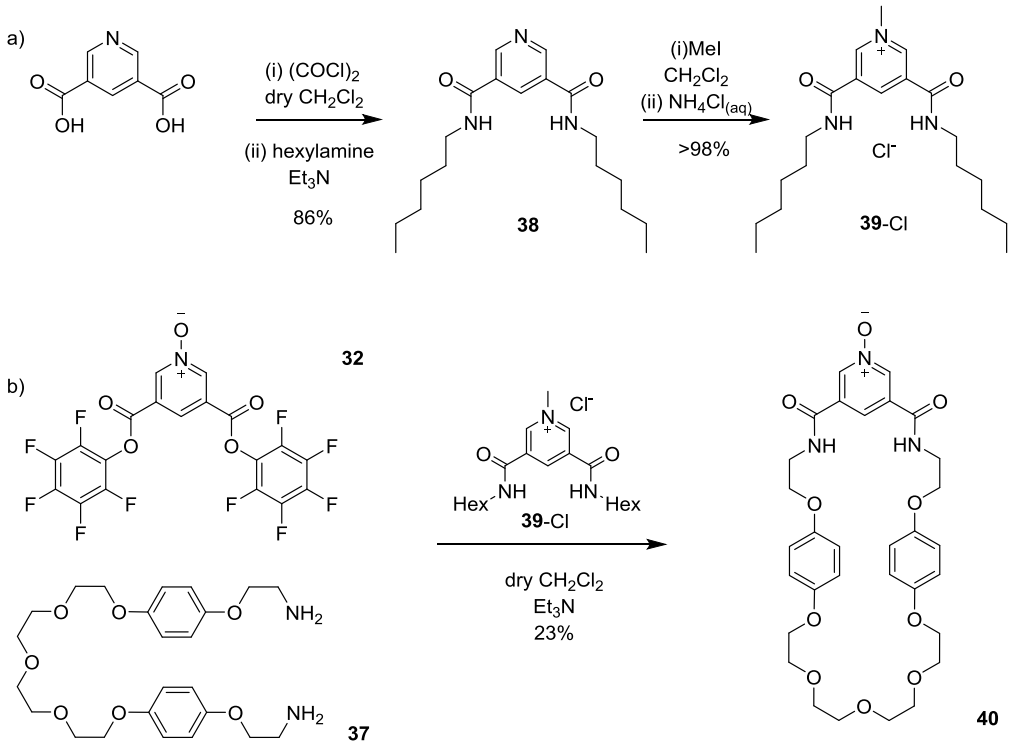

Scheme 2.46: Synthesis of a) pyridinium thread **33** · Cl b) pyridine *N*-oxide macrocycle **40**

The pyridine *N*-oxide macrocycle **40** was prepared by reacting activated ester **32** and bis-amine **37** in the presence of template **39** · Cl in dry dichloromethane to afford the target macrocycle **40** in 23% yield (Scheme **2.46b**).

2.2.6.2 Activated ester [2]catenane synthesis and characterisation

Having successfully prepared pyridine *N*-oxide macrocycle **40**, the formation of the target [2]catenane was attempted. Pyridinium calix[4]diquinone macrocycle **34** · $Na[BAr^F{}_4]_2$ was combined with the pyridine *N*-oxide activated ester **32** in dry dichloromethane to form the pseudorotaxane. Bis-amine **37** was then added dropwise *via* a syringe pump and stirred

overnight (Scheme **2.47**). The reaction was purified by column chromatography, size-exclusion chromatography and finally preparative TLC to afford the target [2]catenane as the sodium adduct **41** · $Na[BAr^F{}_4]_2$ which was contaminated with the metal free compound **41** · $[BAr^F{}_4]$; during the purification by preparative TLC partial decomplexation of sodium was observed but due to very similar R_f values could not be separated from the sodium complex. A number of attempts were made to remove the sodium cation from the [2]catenane cavity, however all proved unsuccessful. These included washing with water, $EDTA_{(aq)}$ and displacement with barium cations followed by precipitation with sulphate. The inability to remove the sodium cation is likely due to the lipophilic nature of the $[BAr^F{}_4]$ anion combined with the strong association of the sodium cation with the interlocked structure.

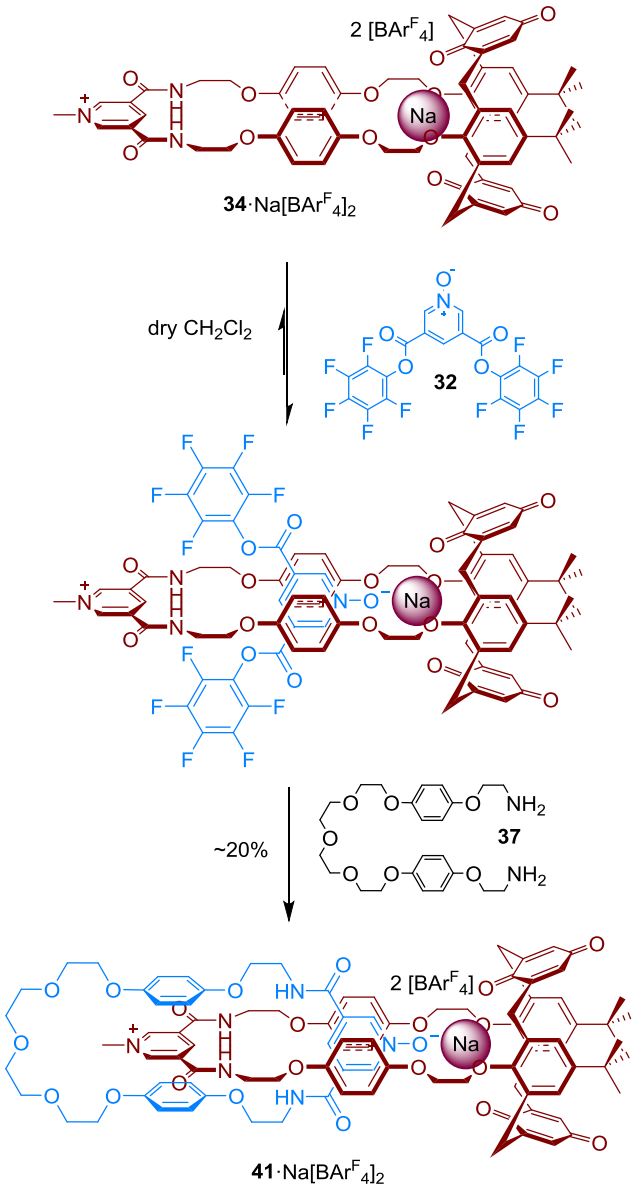

Scheme 2.47: Synthesis of [2]catenane **41** · Na[BAr$^F_4$]$_2$ by a threading followed by clipping strategy

The catenane was characterised by ^{1}H, ^{13}C and by high resolution mass spectrometry. The ESI-HRMS analysis of the catenane gave the expected peak as m/z = 1701.6918 corresponding to [M+Na]$^+$ and the ^{1}H NMR spectrum, together with the spectra of pyridinium calix[4]diquinone macrocycle **34** · Na[BAr$^F_4$]$_2$ and pyridine *N*-oxide maxrocycle **40**, is shown in Figure **2.48**.

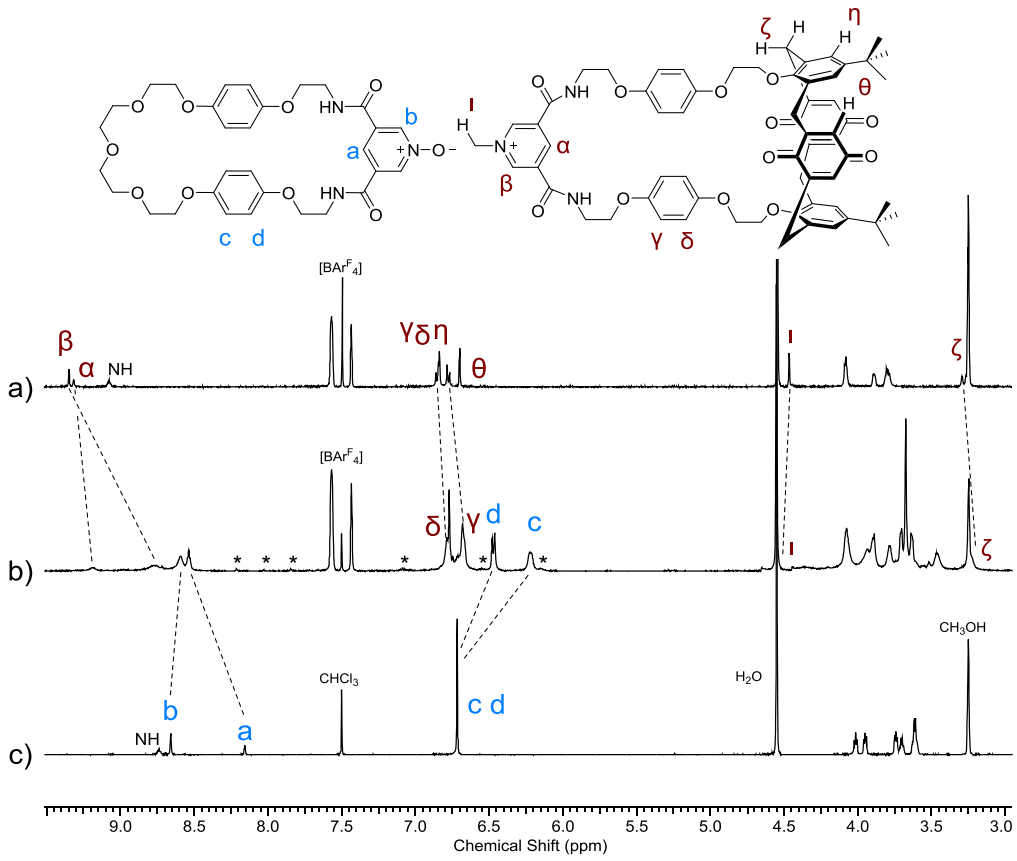

Figure 2.48: ^{1}H NMR (500 MHz, $CDCl_3/CD_3OD$ 1:1, 298 K) spectra of a) calix[4]diquinone macrocycle **34** · $Na[BAr^F_4]_2$ b) [2]catenane **41** · $Na[BAr^F_4]_2$ (peaks corresponding to free [2]catenane **41** · $[BAr^F_4]$ marked with an asterisk *) c) pyridine *N*-oxide macrocycle **40**

The hydroquinone protons of the *N*-oxide macrocycle *c* and *d* and calix[4]diquinone macrocycle *γ* and *δ* can both be seen to shift upfield due to aromatic donor-acceptor interactions present in the [2]catenane. The magnitude of the shift is larger for *c* and *d* as a result of the more favourable stacking interactions with the positively charged pyridinium motif. The methyl pyridinium proton resonances *ι* are shifted downfield in the [2]catenane, a consequence of hydrogen-bonding to the polyether component of the other interlinked macrocycle. The catenane was also characterised by two-dimensional ^{1}H-^{1}H ROESY NMR which provided further evidence for interlocked structure formation (Figure **2.49**). Interactions were observed between the hydroquinone protons of the calix[4]diquinone

macrocycle ***γ*** and *δ* and the pyridine *N*-oxide proton *b* and between protons *β* and *c* and *d* of the pyridinium and hydroquinone groups respectively. Additionally couplings are observed between the pyridinium resonances *β* and the polyether portion of the macrocycle, which provide further evidence of the inter chain linked topology. Cross-coupling peaks are also noted between the *internal* protons of each macrocycle *a* and *α*, indicating the *N*-oxide is in the 'up' conformation and is coordinated to the metal cation.

Unfortunately, due to the inability to obtain a pure sample of **41** · $Na[BAr^F_4]_2$, which was contaminated with **41** · $[BAr^F_4]$ (Figure **2.48b**; peaks corresponding to free catenane marked with an asterisk) ion-binding titrations could not be undertaken.

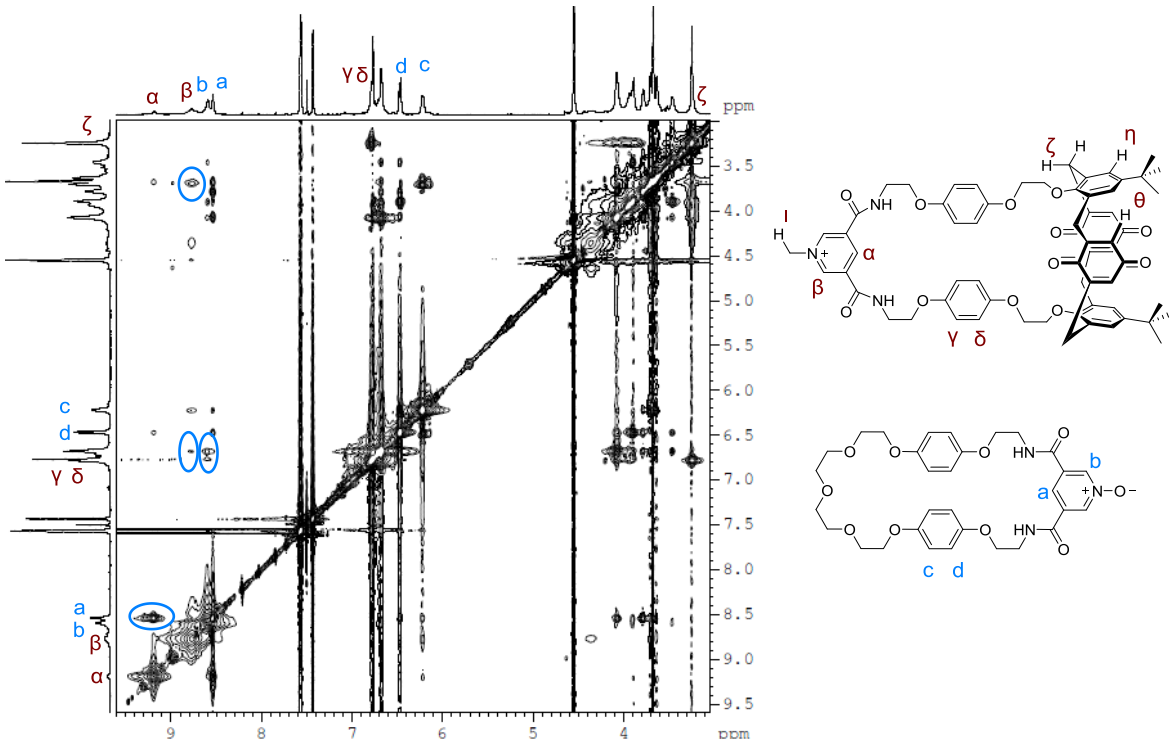

Figure 2.49: truncated ^{1}H-H ROESY (500 MHz, $CDCl_3/CD_3OD$ 1:1, 298 K) of the catenane **41** · $Na[BAr^F_4]_2$

Despite the purification issues, crystals of the catenane suitable for X-ray diffraction structural analysis were obtained by slow diffusion of diisopropyl ether into a chloroform solution of the catenane. Surprisingly the structure was found to contain a sodium cation-chloride halide anion ion-pair within the cavity of the interlocked structure (Figure **2.49a**); the chloride is once again presumed to be present in the chloroform solution. The structure crystallised as a dimer in the solid state whereby the two distorted octahedral sodium metal cations are bridged *via* the pyridine *N*-oxide amide oxygen atoms (O_{amide}-Na = 2.31 Å) (Figure **2.50b**). The calix[4]diquinone unit adopts the cone conformation to chelate the metal cation with mean phenoxy and quinone O-Na bond lengths of 2.68 Å and 2.28 Å respectively. In addition the chloride anion is bound within the tetrahedral array of amide hydrogen-bond donors, displaying a mean $N_{(amide)}$-Cl distance of 3.37 Å.

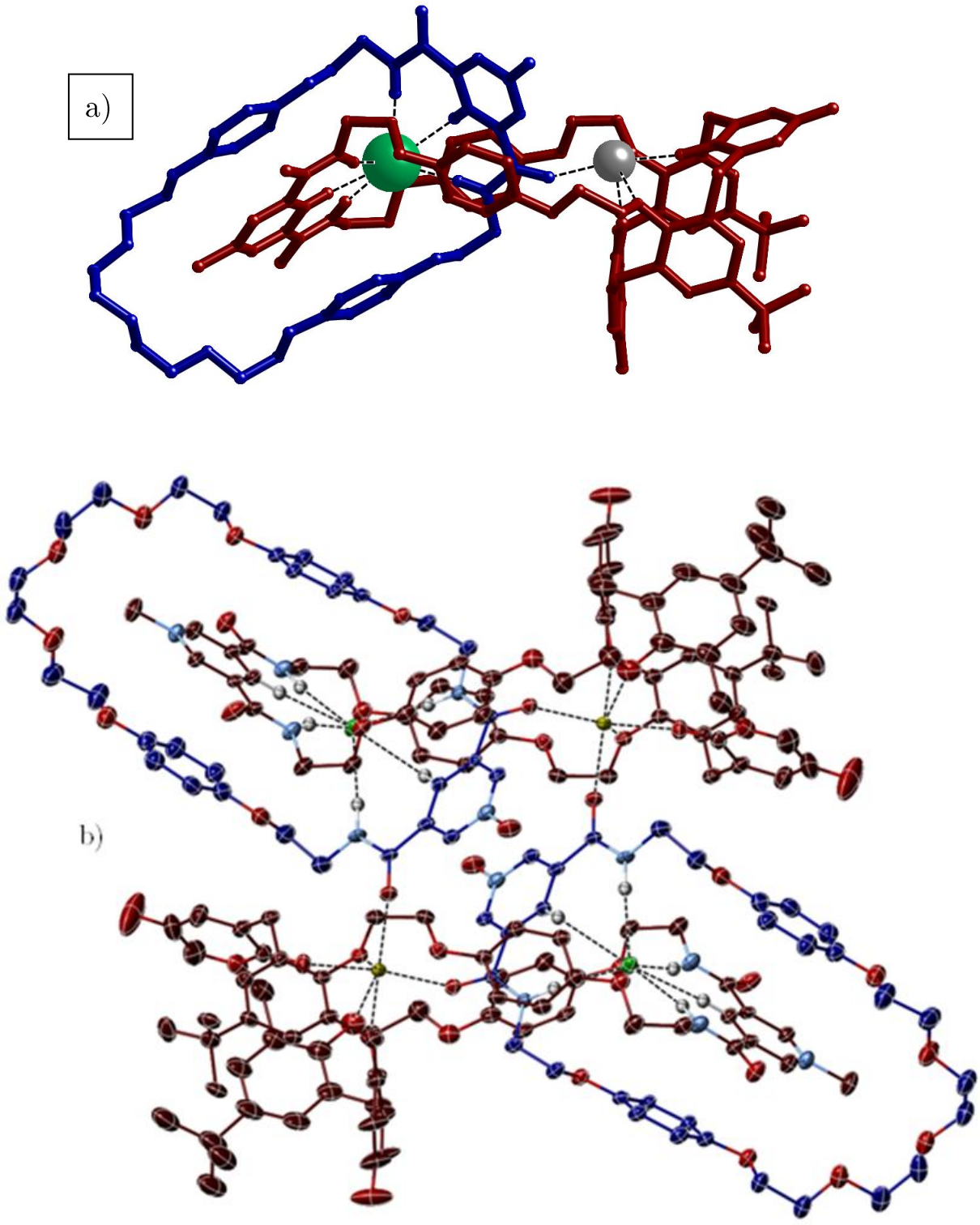

Figure 2.50: Single crystal X-ray structure of **41** · NaCl[BAr^F_4] as a) stick representation b) ellipsoid plot of dimer (Ellipsoids at 20% probability; disorder, [BAr^F_4] anion and non hydrogen-bonding hydrogen atoms omitted for clarity)

2.2.6.3 Summary

The preparation of interlocked structures by using a sodium cation templated activated ester strategy was investigated. The target [2]rotaxane **33** was not isolated due to purification issues, however it was possible to isolate a partially pure sample of a novel [2]catenane. Despite the difficulties encountered during purification, a single crystal X-ray structure of the catenane was obtained. The structure contained a complexed sodium-chloride separated ion-pair; the sodium cation was bound in the calix[4]diquinone fragment of the macrocycle with the chloride anion residing in the 3,5-bis-amide pyridinium cleft.

2.2.7 Imidazolium-containing [2]rotaxane

2.2.7.1 Introduction

The imidazolium group is a versatile and widely employed motif that has been used in ionic liquid chemical research,[45-47] nanoparticle stabilisation[48, 49] and as precusors to *N*-heterocyclic carbene ligands for organometallic chemistry.[50, 51] This group has also found use in supramolecular chemistry as an anion-binding motif in synthetic anion receptors, (see Section **1.4.3.1.4** of Chapter 1). More recently it has been exploited in the construction of pseudorotaxanes,[52-55] rotaxanes[56] and rotaxane linked metal organic frameworks.[57]

As an alternative to previously discussed metal cation-templated synthesis, a strategic anion-templated strategy was envisaged for the preparation of a novel imidazolium axle containing rotaxane. The use of *discrete* anion templated formation of interlocked structures was discussed in the introduction in Section **1.5.2.3**. Although templation using the 3,5-bis-amide

pyridinium motif has been relatively well-explored by Beer,[58] anion templated imidazolium containing interlocked and interpenetrated assemblies are rare.[53, 59-61] One example by Beer and co-workers reports the synthesis of a 2-methylimidazolium axle containing [2]rotaxane with a 3,5-bis-amide functionalised macrocycle by an anion templated clipping strategy (Scheme **2.51**). The rotaxane host was found to discriminate between halides and larger oxoanions such as acetate and dihydrogenphosphate in chloroform/methanol (1:1).

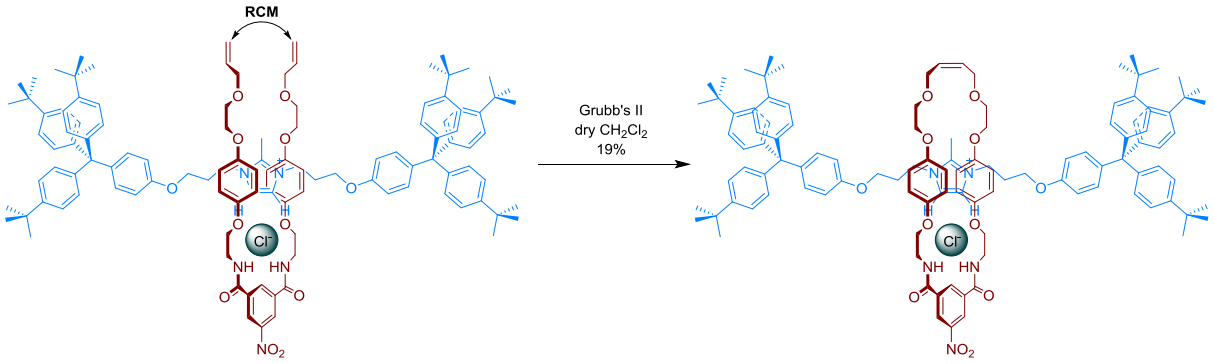

Scheme 2.51: *discrete* anion templated synthesis of 2-methylimidazolium containing [2]rotaxane

2.2.7.2 [2]Rotaxane Precursor Synthesis

In accordance with the work described previously in this chapter, a threading followed by stoppering methodology, ulitilising a copper(I)-catalysed click reaction, was chosen initially as the route to the target [2]rotaxane. As such the synthesis of a bis-alkynyl imidazolium synthon was undertaken (Scheme **2.52**).

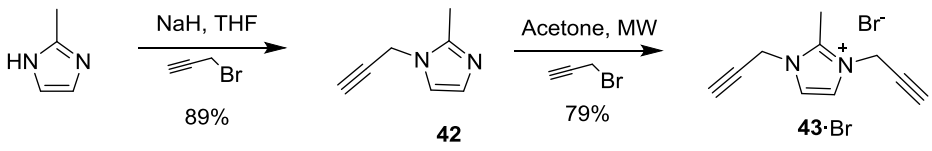

Scheme 2.52: Synthesis of bis-alkynyl 2-methylimidazolium **43** · Br

Commercially available 2-methylimidazole was deprotonated with NaH and reacted with propargyl bromide to afford the mono-functionalised imidazole **42** in high yield (89%). This compound underwent a second alkylation with propargyl bromide under microwave irradiation to obtain the target bis-alkynyl imidazolium axle precursor **43** · Br. As a test reaction for axle formation, **43** · Br was mixed with two equivalents of the azide-terminated terphenyl stopper **29**, in the presence of $Cu^{I}(MeCN)_4PF_6$, TBTA and DIPEA in dry dichloromethane. Unfortunately after 9 days of reaction only trace amounts of the axle product **44** · Br were obtained, most likely due to the low solubility of **43** · Br in dichloromethane (Scheme **2.53**).

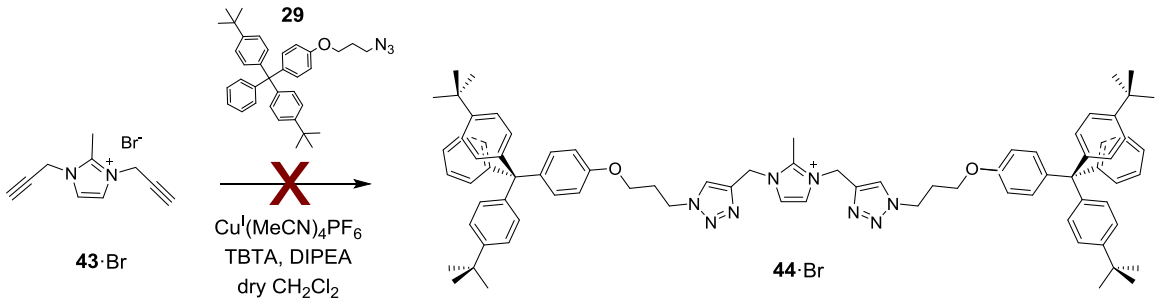

Scheme 2.53: Attempted synthesis of imidazolium axle **44** · Br

The requirement of forming anion-templated interlocked structures in non-competitive solvents such as dichloromethane necessitated the synthesis of an alternative axle precursor with enhanced solubility in organic media. As such the synthesis of a mono-stoppered imidazolium synthon **47** · Cl was attempted (Scheme **2.54**).

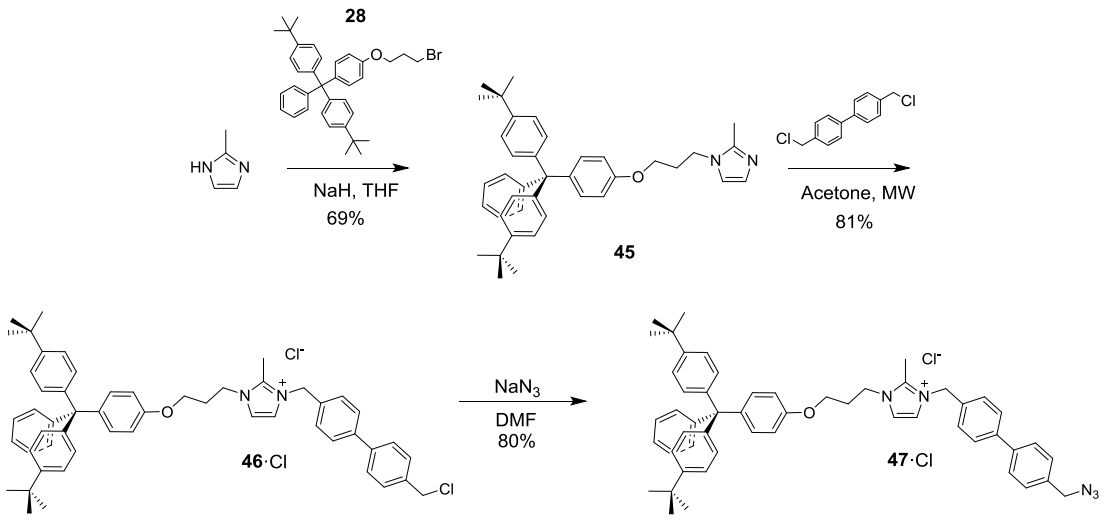

Scheme 2.54: Synthesis of mono-stoppered imidazolium axle precursor **47** · Cl

This was accomplished by first reacting 2-methylimidazole with bromopropyl stopper **28** to afford the mono-stoppered imidazole **45**. Imidazole **45** was subsequently reacted with a large excess of 4,4'-bis(chloromethyl)-1,1'-biphenyl under microwave irradiation, giving the imidazolium compound **46** · Cl in good yield (81%). Substitution of the benzyl chloride with sodium azide afforded the azide-terminated axle precursor **47** · Cl (80%). The resulting compound had excellent solubility in dichloromethane and was subjected to copper (I) catalysis to determine the viability of rotaxane formation by this route. Alkyne terminated stopper **16**, **47** · Cl, $Cu^{I}(MeCN)_4PF_6$, TBTA and DIPEA in dry dichloromethane furnished the asymmetric imidazolium axle **48** · Cl in 54% yield (Scheme **2.55**).

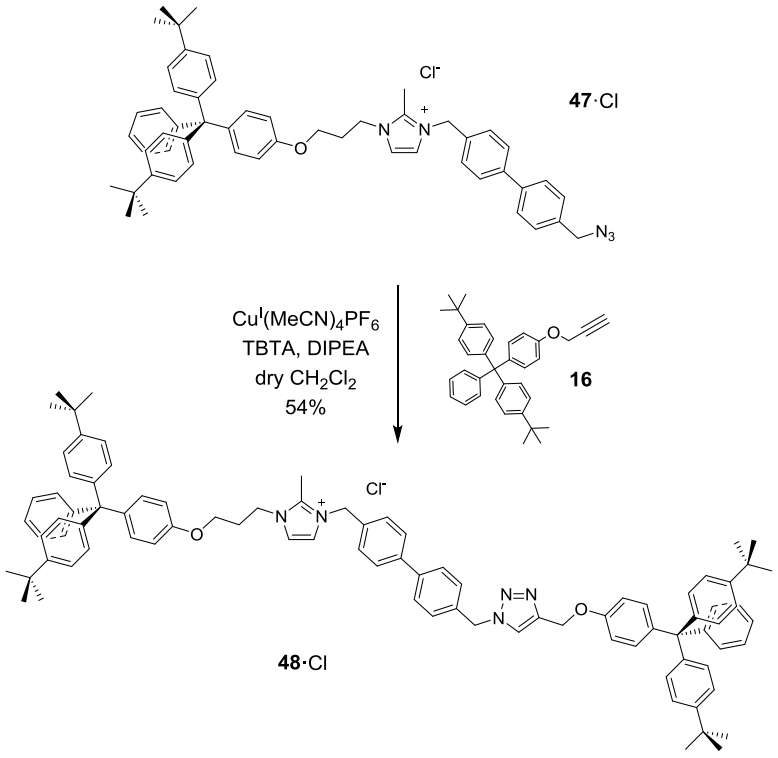

Scheme 2.55: Synthesis of asymmetric imidazolium axle **48** · Cl

2.2.7.3 [2]Rotaxane Synthesis

Having demonstrated the viability of forming the 2-methylimidazolium axle **48** · Cl *via* a CuAAC click stoppering reaction, the corresponding rotaxanation was attempted. Isophthalamide calix[4]diquinone macrocycle **20** was combined with an equimolar amount of axle precursor **47** · Cl in dry dichloromethane (Scheme **2.56**). This was followed by the addition of two equivalents of alkyne terminated stopper **16**, $Cu^{I}(MeCN)_4PF_6$, TBTA and DIPEA and the reaction was allowed to proceed for 24 hours. The crude reaction was purified by three iterations of thin layer chromatography (DCM/MeOH 95:5, DCM/MeCN 1:1, gradient elution DCM/MeOH 99:1→95:5) to obtain the target 2-methylimidazolium rotaxane **49** · Cl in a modest 1% isolated yield.

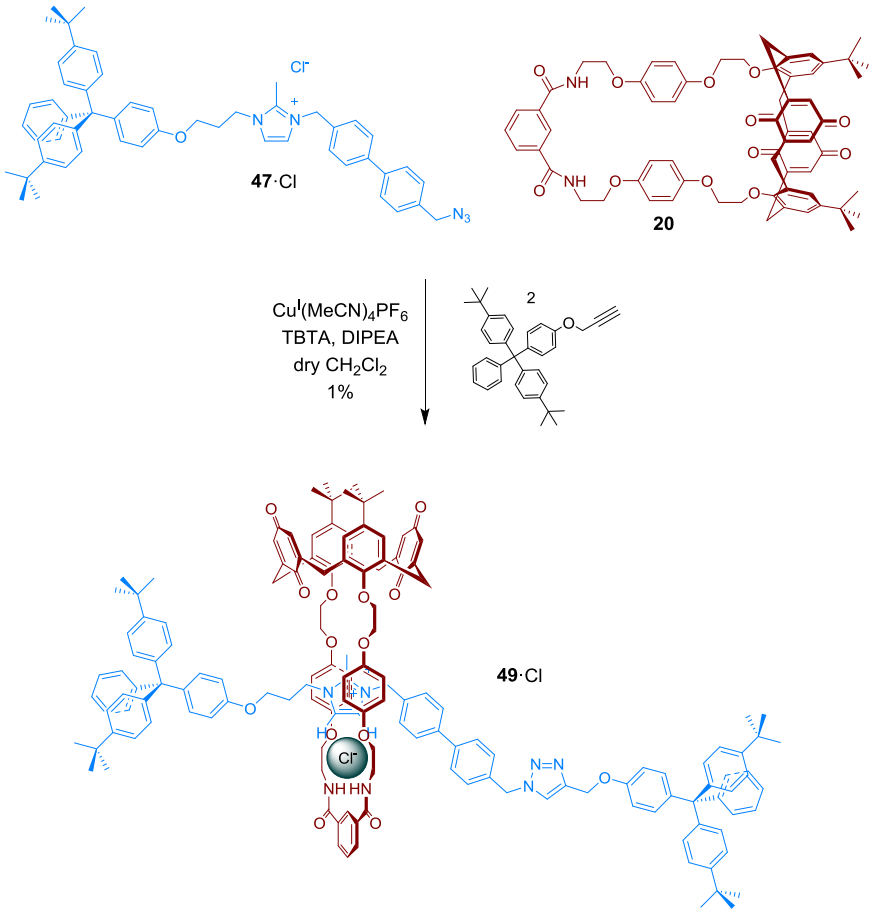

Scheme 2.56: Synthesis of 2-methylimidzolium [2]rotaxane **49** · Cl

The target [2]rotaxane was characterised by ^{1}H NMR spectroscopy and mass spectrometry. The ESI-LRMS spectrum gave a peak at $m/z = 2331.69$ corresponding to [M-Cl]$^+$, consistent with the formation of the interlocked product. Analysis of the ^{1}H NMR spectrum provided further evidence of formation of the target [2]rotaxane (Figure **2.57**). The hydroquinone protons γ and δ shift upfield and split due to aromatic donor-acceptor interactions with the imidazolium axle. There is also a downfield shift of macrocycle proton α upon interlocked structure formation, caused by hydrogen-bonding of the isophthalamide motif with the chloride anion. Additionally the resonance corresponding to the methyl imidazolium proton

a shifts upfield due to the interaction with the calix[4]diquinone component of the macrocycle.

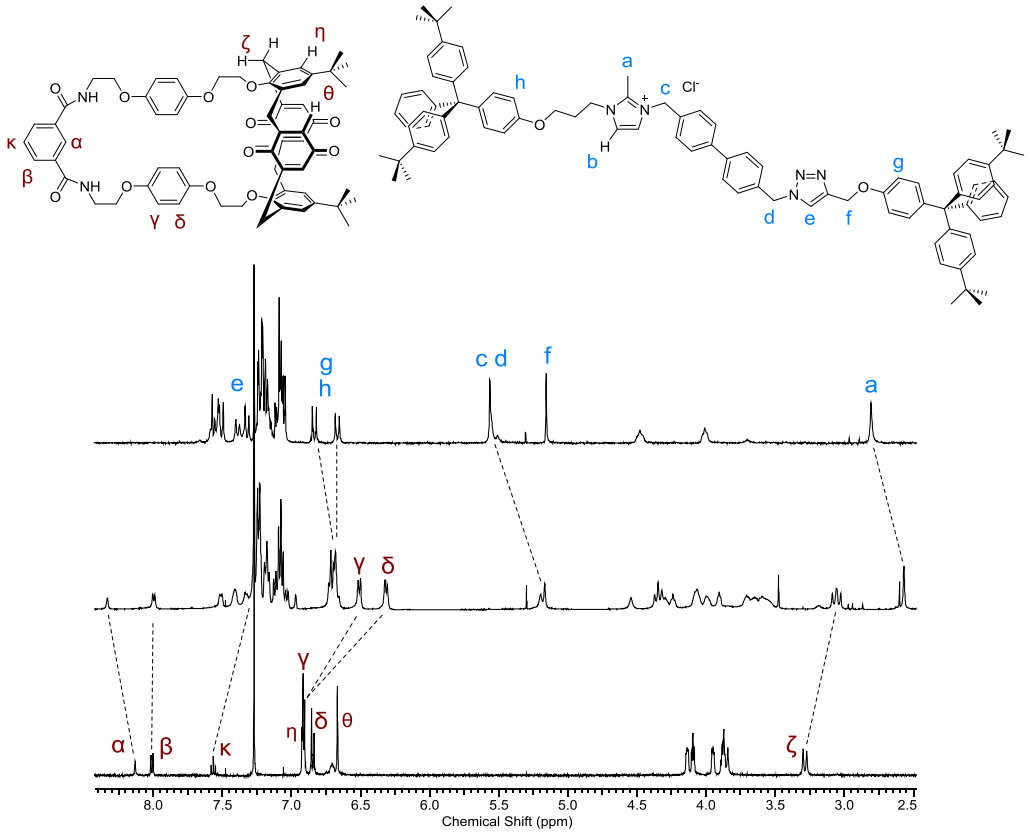

Figure 2.57: ^{1}H NMR (500 MHz, $CDCl_3$, 298 K) spectra of a) calix[4]diquinone macrocycle **20** b) [2]rotaxane **49** · Cl c) 2-methylimidazolium axle **48** · Cl

The low yield of the rotaxanation reaction meant it was not feasible to conduct anion-binding titrations on the interlocked structure.

2.2.7.4 Summary

The ability of the heteroditopic calix[4]diquinone macrocycle **20** to form an anion templated interlocked structure has been demonstrated. The imidazolium motif was chosen as the anion-binding motif for incorporation into the rotaxane structure. The target [2]rotaxane

49 · Cl was successfully synthesised, however, due to the very low isolated yield no anion binding investigations were undertaken.

2.3 Conclusions

The pyridine *N*-oxide motif was successfully incorporated into axle and macrocyclic components of interlocked rotaxane and catenane structural frameworks *via* sodium cation templation. Several differing methods of interlocked structure formation were employed; the 'click' reaction and amide formation using activated esters demonstrated the versatility of the sodium cation templated approach.

The novel ion-pair [2]rotaxane host system **18** displayed weak halide anion binding in the absence of a co-bound alkali metal cation with little discrimination between the halides. Upon sodium or potassium cation complexation, halide anion binding affinities were enhanced significantly, up to a 15-fold enhancement for chloride with a co-bound sodium cation. This interlocked receptor was also found to be capable of solubilising sodium and potassium chloride salts in chloroform solution, indicating its utility to salt extraction research. The synthesis of an extended tetraethylene glycol pyridine N-oxide axle containing rotaxane **33** was attempted in order to investigate potential pH-dependent dynamic molecular motion properties. Unfortunately a pure sample of the rotaxane could not be obtained, precluding any further studies. The synthesis of interlocked rotaxane and catenane targets by a new activated ester methodology were also undertaken. Preliminary investigations suggest interlocked structure formation by this method is viable, indeed a partially pure sample of a [2]catenane was obtained. Importantly a X-ray single crystal

structure determination of the catenane host revealed a bound sodium-chloride ion-pair, illustrating an inter-ring catenane separated ion-pair binding mode.

Finally in this chapter chloride anion templation was used to synthesise an imidazolium axle containing rotaxane, albeit in low yield.

In summary novel heteroditopic rotaxane and catenane interlocked host systems have been prepared and demonstrated to exhibit unprecedented respective axle and inter-ring component separated ion pair recognition.

The preparation and photophysical investigations of luminescent anion sensing rotaxanes are discussed in the next chapter.

2.4 References

1. S. K. Kim and J. L. Sessler, *Chem. Soc. Rev.*, 2010, **39**, 3784-3809.
2. A. J. McConnell and P. D. Beer, *Angew. Chem.Int. Ed.*, 2012, **51**, 5052-5061.
3. T. Nagasaki, H. Fujishima, M. Takeuchi and S. Shinkai, *J. Chem. Soc.-Perkin Trans. 1*, 1995, 1883-1888.
4. F. Szemes, M. G. B. Drew and P. D. Beer, *Chem. Commun.*, 2002, 1228-1229.
5. A. Zinke and E. Ziegler, *Berichte der deutschen chemischen Gesellschaft (A and B Series)*, 1941, **74**, 1729-1736.
6. C. D. Gutsche, B. Dhawan, K. H. No and R. Muthukrishnan, *J. Am. Chem. Soc.*, 1981, **103**, 3782-3792.
7. K. Araki, K. Iwamoto, S. Shigematsu and S. Shinkai, *Chem. Lett.*, 1992, 1095-1098.
8. Y. Morita, T. Agawa, Y. Kai, N. Kanehisa, N. Kasai, E. Nomura and H. Taniguchi, *Chem. Lett.*, 1989, 1349-1352.
9. Y. L. Lin, T. S. Yu, W. Y. Wang and L. G. Lin, *Tetrahedron*, 2006, **62**, 6082-6089.
10. A. McKillop, B. P. Swann and E. C. Taylor, *Tetrahedron*, 1970, **26**, 4031-&.
11. J. M. Harrowfield, M. I. Ogden, W. R. Richmond and A. H. White, *J. Chem. Soc.-Chem. Commun.*, 1991, 1159-1161.
12. K. Araki, K. Hisaichi, T. Kanai and S. Shinkai, *Chem. Lett.*, 1995, 569-570.
13. L. Pescatori, A. Arduini, A. Pochini, A. Secchi, C. Massera and F. Ugozzoli, *Org. Biomol. Chem.*, 2009, **7**, 3698-3708.

14. P. R. A. Webber, P. D. Beer, G. Z. Chen, V. Felix and M. G. B. Drew, *J. Am. Chem. Soc.*, 2003, **125**, 5774-5785.
15. N. Kerdpaiboon, B. Tomapatanaget, O. Chailapakul and T. Tuntulani, *J. Org. Chem.*, 2005, **70**, 4797-4804.
16. Y. Kubo, S. Obara and S. Tokita, *Chem. Commun.*, 1999, 2399-2400.
17. H. Jeong, E. M. Choi, S. O. Kang, K. C. Nam and S. Jeon, *J. Electroanal. Chem.*, 2000, **485**, 154-160.
18. G. Tumcharern, T. Tuntulani, S. J. Coles, M. B. Hursthouse and J. D. Kilburn, *Org. Lett.*, 2003, **5**, 4971-4974.
19. T. Nabeshima, T. Saiki, J. Iwabuchi and S. Akine, *J. Am. Chem. Soc.*, 2005, **127**, 5507-5511.
20. M. D. Lankshear, A. R. Cowley and P. D. Beer, *Chem. Commun.*, 2006, 612-614.
21. M. D. Lankshear, I. M. Dudley, K. M. Chan, A. R. Cowley, S. M. Santos, V. Fejix and P. D. Beer, *Chem.-Eur. J.*, 2008, **14**, 2248-2263.
22. G. Chelucci, G. Murineddu and G. A. Pinna, *Tetrahedron: Asymmetry*, 2004, **15**, 1373-1389.
23. A. V. Malkov, M. Bell, F. Castelluzzo and P. Kocovsky, *Org. Lett.*, 2005, **7**, 3219-3222.
24. M. Kratky and J. Vinsova, *Curr. Pharm. Design*, 2013, **19**, 1343-1355.
25. Z. He, Z. M. Wang, S. Gao and C. H. Yan, *Inorganic Chemistry*, 2006, **45**, 6694-6705.
26. D. Rosario-Amorin, S. Ouizem, D. A. Dickie, Y. F. Wen, R. T. Paine, J. Gao, J. K. Grey, A. de Bettencourt-Dias, B. P. Hay and L. H. Delmau, *Inorganic Chemistry*, 2013, **52**, 3063-3083.
27. M. J. Chen, S. J. Han, L. S. Jiang, S. G. Zhou, F. Jiang, Z. K. Xu, J. D. Liang and S. H. Zhang, *Chem. Commun.*, 2010, **46**, 3932-3934.
28. L. M. Hancock and P. D. Beer, *Chem. Commun.*, 2011, **47**, 6012-6014.
29. J. M. Mercurio, F. Tyrrell, J. Cookson and P. D. Beer, *Chem. Commun.*, 2013.
30. F. Zapata, O. A. Blackburn, M. J. Langton, S. Faulkner and P. D. Beer, *Chem. Commun.*, 2013, **49**, 8157-8159.
31. C. D. Gutsche and M. Iqbal, *Org. Synth*, 1990, **68**, 234-237.
32. M. D. Lankshear, N. H. Evans, S. R. Bayly and P. D. Beer, *Chemistry – A European Journal*, 2007, **13**, 3861-3870.
33. A. V. Leontiev, C. A. Jemmett and P. D. Beer, *Chemistry – A European Journal*, 2011, **17**, 816-825.
34. The appearance of the ortho pyridine proton (beta) of the macrocycle and [2]pseudorotaxane assembly as doublets suggest that the macrocycle is protonated in this titration experiment
35. V. Aucagne, K. D. Hanni, D. A. Leigh, P. J. Lusby and D. B. Walker, *J. Am. Chem. Soc.*, 2006, **128**, 2186-2187.
36. Determined by 1H NMR spectroscopy of the crude reaction
37. Although the chloroform reaction solvent is known to contain chloride anions, possibly explaining the comparable yield.
38. M. J. Hynes, J. Chem. Soc., Dalton Trans., 1993, 311–312

39. N. G. White, P. J. Costa, S. Carvalho, V. Félix and P. D. Beer, *Chemistry – A European Journal*, 2013, **19**, 17751-17765.
40. C. A. Hunter, *J. Am. Chem. Soc.*, 1992, **114**, 5303-5311.
41. L. M. Hancock and P. D. Beer, *Chem.-Eur. J.*, 2009, **15**, 42-44.
42. L. M. Hancock, L. C. Gilday, N. L. Kilah, C. J. Serpell and P. D. Beer, *Chem. Commun.*, 2011, **47**, 1725-1727.
43. H. Y. Zheng, W. D. Zhou, J. Lv, X. D. Yin, Y. J. Li, H. B. Liu and Y. L. Li, *Chem.-Eur. J.*, 2009, **15**, 13253-13262.
44. J. A. Wisner, P. D. Beer and M. G. B. Drew, *Angew. Chem.-Int. Edit.*, 2001, **40**, 3606-+.
45. T. Welton, *Chem. Rev.*, 1999, **99**, 2071-2083.
46. J. P. Hallett and T. Welton, *Chem. Rev.*, 2011, **111**, 3508-3576.
47. R. D. Rogers and K. R. Seddon, *Science*, 2003, **302**, 792-793.
48. J. Dupont and J. D. Scholten, *Chem. Soc. Rev.*, 2010, **39**, 1780-1804.
49. M. Planellas, W. Guo, F. Alonso, M. Yus, A. Shafir, R. Pleixats and T. Parella, *Adv. Synth. Catal.*, 2014, **356**, 179-188.
50. E. Peris and R. H. Crabtree, *Coord. Chem. Rev.*, 2004, **248**, 2239-2246.
51. H. Jacobsen, A. Correa, A. Poater, C. Costabile and L. Cavallo, *Coord. Chem. Rev.*, 2009, **253**, 687-703.
52. A. K. Mandal, M. Suresh and A. Das, *Org. Biomol. Chem.*, 2011, **9**, 4811-4817.
53. C. J. Serpell, N. L. Kilah, P. J. Costa, V. Félix and P. D. Beer, *Angewandte Chemie International Edition*, 2010, **49**, 5322-5326.
54. H. Y. Gong, B. M. Rambo, V. M. Lynch, K. M. Keller and J. L. Sessler, *Chem.-Eur. J.*, 2012, **18**, 7803-7809.
55. N. Farahani, K. L. Zhu, N. Noujeim and S. J. Loeb, *Org. Biomol. Chem.*, 2014, **12**, 4824-4827.
56. S. Dong, J. Yuan and F. Huang, *Chemical Science*, 2014, **5**, 247-252.
57. V. N. Vukotic and S. J. Loeb, *Chem. Soc. Rev.*, 2012, **41**, 5896-5906.
58. G. T. Spence and P. D. Beer, *Accounts Chem. Res.*, 2013, **46**, 571-586.
59. M. R. Sambrook, P. D. Beer, J. A. Wisner, R. L. Paul, A. R. Cowley, F. Szemes and M. G. B. Drew, *J. Am. Chem. Soc.*, 2005, **127**, 2292-2302.
60. C. J. Serpell, R. Chall, A. L. Thompson and P. D. Beer, *Dalton Trans.*, 2011, **40**, 12052-12055.
61. G. T. Spence, C. J. Serpell, J. Sardinha, P. J. Costa, V. Félix and P. D. Beer, *Chemistry – A European Journal*, 2011, **17**, 12955-12966.

Chapter 3: Anion Templated Synthesis of Interlocked Structures Containing *d*- and *f*-Metal Reporter Groups

3.1: Introduction

Through the incorporation of a reporter group into a host structure, the recognition and sensing of a guest species may be achieved. The reporter group is designed to be capable of signalling the binding of a target analyte *via* a macroscopic response such as a change in the colourimetric,[1] luminescent[2] or electrochemical[3] properties of the host. In this regard luminescent probes have proven to be very effective due to their inherent sensitivity and ability to detect at very low concentrations.[4, 5] The most common strategy that has been adopted for the construction of effective sensing hosts is *via* the covalent integration of the reporter group in proximity to the recognition site so that guest binding induces an observable response; for instance the luminescent anion sensor design shown in Figure **3.1**. Examples of sensing systems with covalently integrated reporter groups were discussed in the introduction in Section **1.4.4.1**.

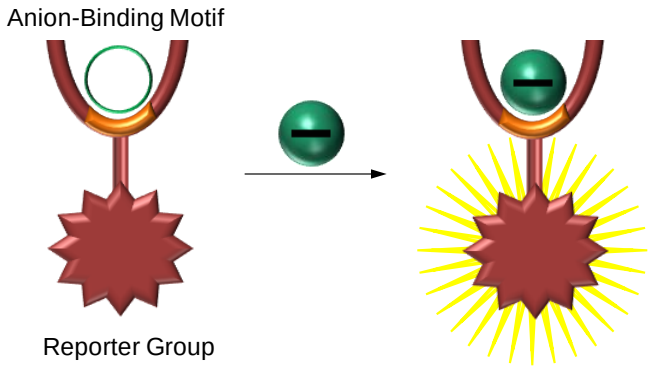

Figure 3.1: Schematic representation of anion-sensing by a covalently bound luminescent reporter group

This chapter investigates the incorporation of luminescent lanthanide and transition-metal reporter groups into interlocked rotaxane structures for anion sensing applications. The following section discusses some relevant examples of interlocked sensory assemblies.

3.1.1 Interlocked Sensors

While there are a plethora of examples of acyclic and macrocyclic supramolecular sensors in the literature,[5, 6] the application of interlocked host architectures for sensing purposes is relatively underexplored.[7] This is in spite of their unique topology which has advantages over acyclic or macrocyclic systems such as increased binding affinities and enhanced selectivity.[8, 9] In recent years however, the area has garnered more attention and effective mechanically bonded sensors have been reported for cationic,[10-12] anionic[13-15] and neutral species.[16] For example Chui's squaraine [2]rotaxane (Figure **3.2a**), upon binding two sodium cations in acetonitrile solution, exhibited an increase in the axle's squaraine dye fluorescence.[17] The addition of chloride in methanol to Smith's anion binding rotaxane triggered a molecular shuttling motion of the macrocycle along the squaraine dye axle component, which caused a 30–40 nm shift in the emission spectrum of the interlocked host (Figure **3.2b**).[14] The capability of interlocked architectures to detect neutral species was realised in Li's cucurbituril surface-assembled [2]rotaxane. Exposure to trinitrotoluene (TNT) vapour caused fluorescence quenching of the naphthalene axle component due to an electron transfer process facilitated by inclusion of the aromatic guest (Figure **3.2c**).[16]

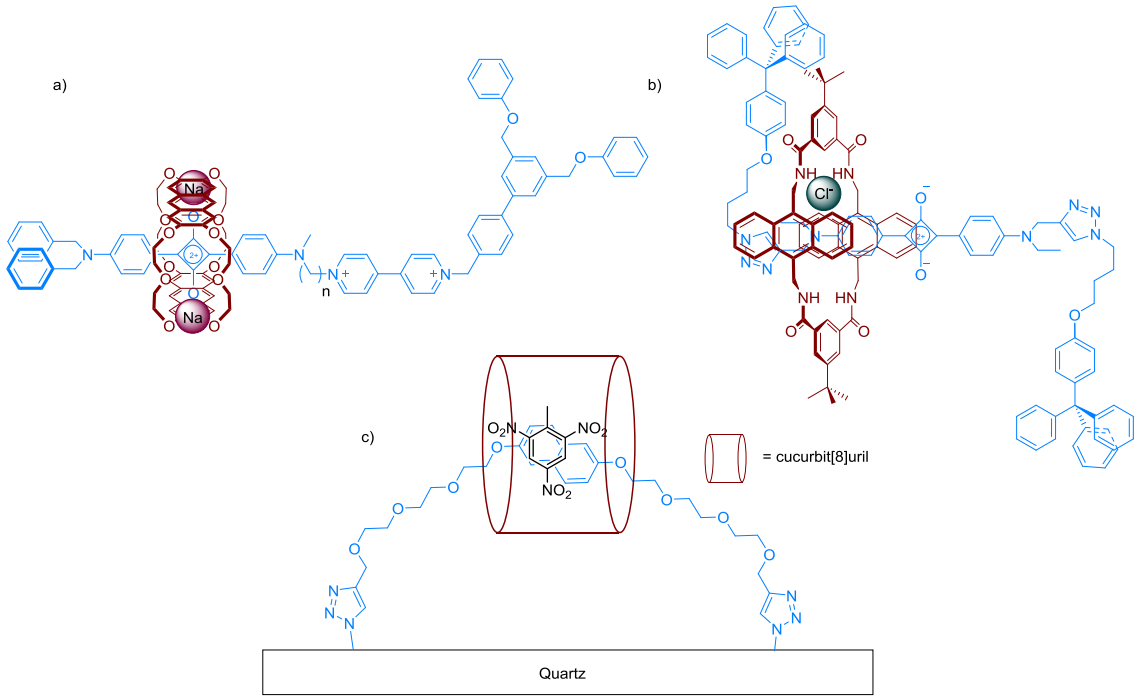

Figure 3.2: interlocked sensors for a) sodium cations b) chloride anions c) trinitrotoluene (TNT) sensor on quartz surface

In additon to using conventional organic fluorophores, the use of transition metal and lanthanide luminophores in interlocked and interpenetrated assemblies has been pioneered within the Beer group. The chloride templated [2]pseudorotaxane in Figure **3.3a** exhibited near-IR emission from the neodymium centre upon excitation of the rhenium (I) bipyridyl luminophore. This is a consequence of energy transfer between the proximal rhenium (I) bipyridyl macrocycle and lanthanide thread, which is only possible in the assembled chloride templated [2]pseudorotaxane.[18] A ruthenium (II) tris-bipyridine macrocycle containing rotaxane (Figure **3.3b**) was demonstrated to selectively complex chloride over dihydrogenphosphate in acetone/water (9:1), displaying MLCT luminesence enhancement of 20% for the halide anion guest.[19]

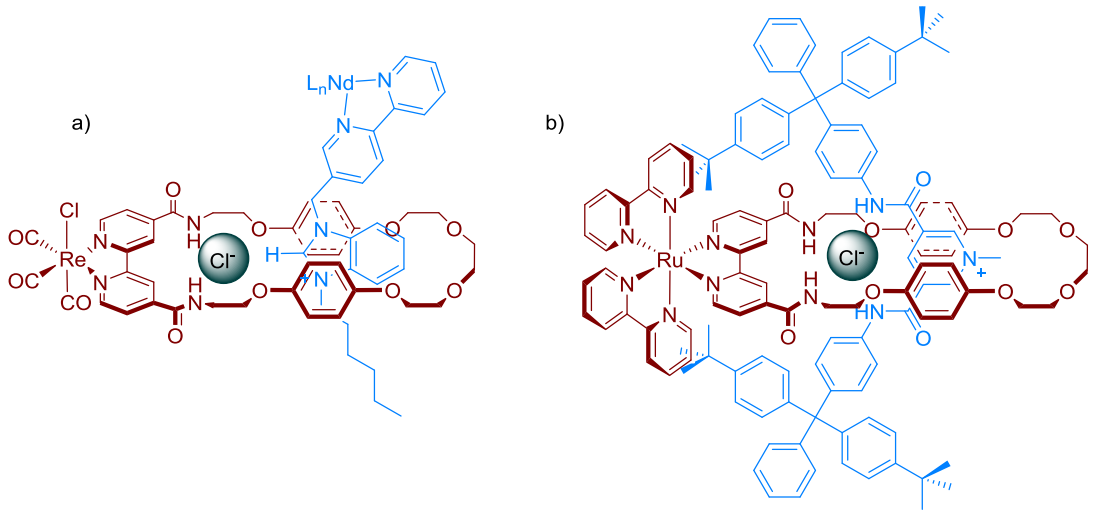

Figure 3.3: Anion-templated assemblies; a) rhenium-neodymium d-f hybrid [2]pseudorotaxane; b) ruthenium (II) tris-bipyridyl [2]rotaxane

3.1.2 Chapter Objectives

This chapter investigates the integration of metal-based luminescent reporter groups into rotaxane anion host structures for the purpose of anion sensing. The target rotaxane assemblies consist of a positively charged pyridinium anion binding axle motif and a luminescent reporter group functionalised macrocycle component. The first part of the chapter focuses on the synthesis of an unprecedented lanthanide appended rotaxane (Figure **3.4a**) which is achieved *via* a CuAAC 'click' post rotaxane-synthetic modification strategy. The second part of this chapter is concerned with the synthesis of transition metal dipyridylbenzene containing macrocycles and their incorporation into rotaxanes (Figure **3.4b**). The anion recognition and sensing capabilities of the lanthanide and transition-metal rotaxanes is also studied to determine their viability as effective anion sensors.

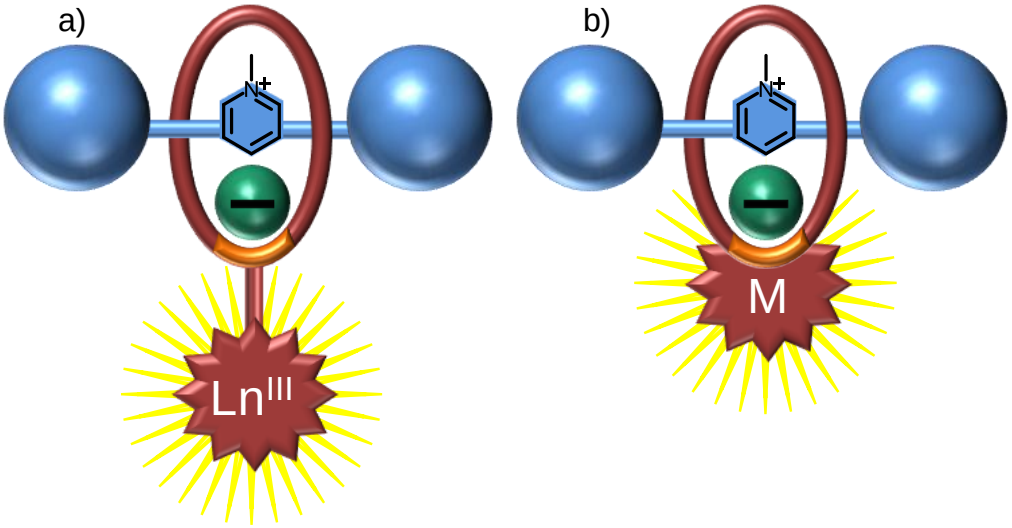

Figure 3.4: Schematic representation of target interlocked anion sensors based upon a) lanthanides b) late transition metals

3.2 [2]Rotaxanes Containing Lanthanide Reporter Groups

The motivation for the incorporation of lanthanide metals into supramolecular assemblies is driven by their unique photophysical properties, which arise from the partially filled 4f orbitals. The electrons in the 4f orbitals are screened by filled $5s^2$ and $5p^6$ shells and as such lanthanide complexes retain many of the spectroscopic and magnetic properties of the parent ion. Another consequence of this is that they display low covalency and typically form labile complexes which, coupled with their inherent toxicity, has lead to the use of highly potent multidentate cyclen based ligands such as 1,4,7,10-tetraazacyclododecane-1,4,7,10-tetraacetic acid (DOTA) (Figure **3.5a**). Lanthanide (III) ions are generally eight- or nine-coordinate and so are rarely coordinatively saturated even when using ligands such as DOTA; these vacant coordination sites are typically occupied by polar solvent molecules such as water (Figure **3.5b**). The presence of vacant sites also presents an opportunity to coordinate other ligands

and is an important tool in lanthanide sensor design, as was discussed in Chapter 1, Section **1.4.4.1**.

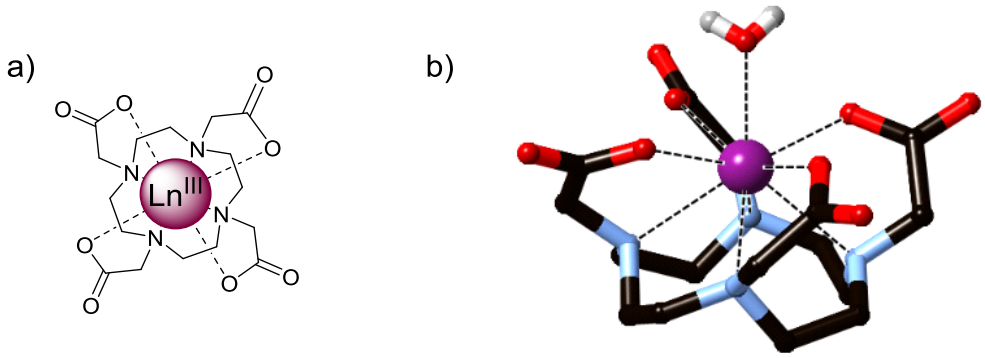

Figure 3.5: a) Lanthanide (III) complex with DOTA b) X-ray crystal structure of Nd(DOTA) · H_2O (non-solvent hydrogen atoms and countercation omitted for clarity)

3.2.1 Lanthanide Photophysics

Lanthanides are unique luminescent metals that emit in aqueous solution with long millisecond lifetimes. They have been used as luminescent probes for cations[20] and anions[21] (discussed in the introduction in Section **1.4.4.1**) but have found particular use in bioimaging[22] and bioassay[23, 24] applications due to their long-lived emission which, in concert with time-gated detection techniques, allows distinction from biological autofluorescence. The emission arises from transitions between 4f orbitals which are Laporte forbidden and as a result $f \rightarrow f$ transitions display very low absorption coefficients. To circumvent this issue the use of a sensitising chromophore is often employed which allows indirect excitation of the lanthanide *via* fluoresent resonant energy transfer, usually from the antenna's triplet state (Figure **3.6**).[25]

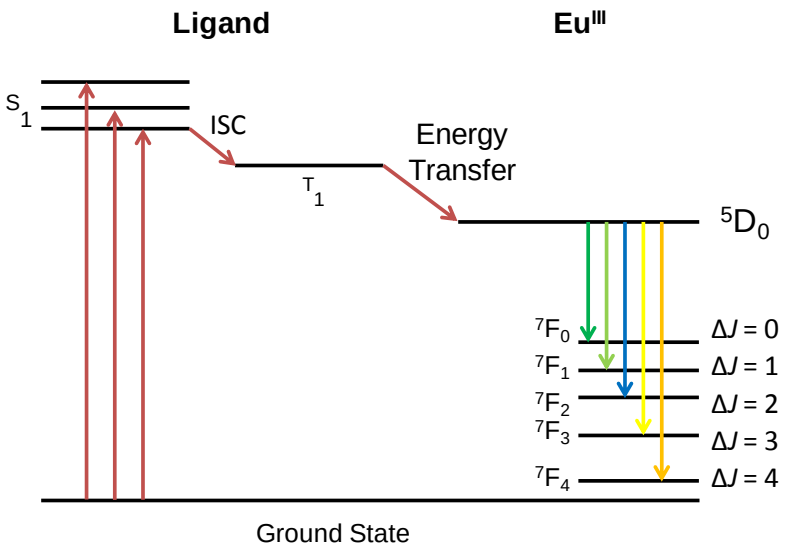

Figure 3.6: Jablonski diagram for excitation of europium by resonant energy transfer

Another consequence of shielded f-orbitals is that lanthanides display well resolved spectra whose wavelength is independent of the coordination environment or solvent. The intensity of the emission is however strongly dependent on the local coordination sphere; bound solvent molecules significantly contribute to the quenching of the lanthanide excited state through O-H and C-H oscillators. This is more profound for some transitions, for example, the hypersensitive $\Delta J = 2$ transition in europium can give a unique insight into the ligand environment of the complex.[22, 26]

3.2.2 Azide Functionalised [2]Rotaxane Synthesis

As mentioned previously, a CuAAC 'click' reaction was envisaged as the method of covalently attaching a lanthanide complex to a preformed [2]rotaxane. This would involve the initial preparation of an azide functionalised macrocycle component containing rotaxane

which could then be subsequently be reacted with an alkyne functionalised lanthanide complex.

The 3,5-bis-amide pyridinium functionalised axle component of the rotaxane was prepared by a literature procedure (Scheme **3.7**),[27] by reacting compound **14** with aniline, after activation with acetyl chloride, to obtain the amine terphenyl stopper **50** in 43% yield. Two equivalents of stopper **50** were condensed with bis-chlorocarbonyl pyridine in dry dichloromethane to afford the pyridine axle precursor **51** in good yield (60%). Alkylation of the pyridine group with methyl iodide gave the pyridinium axle **52** · I which was anion-exchanged with aqueous NH_4Cl to obtain the chloride salt **52** · Cl (93% over 2 steps).

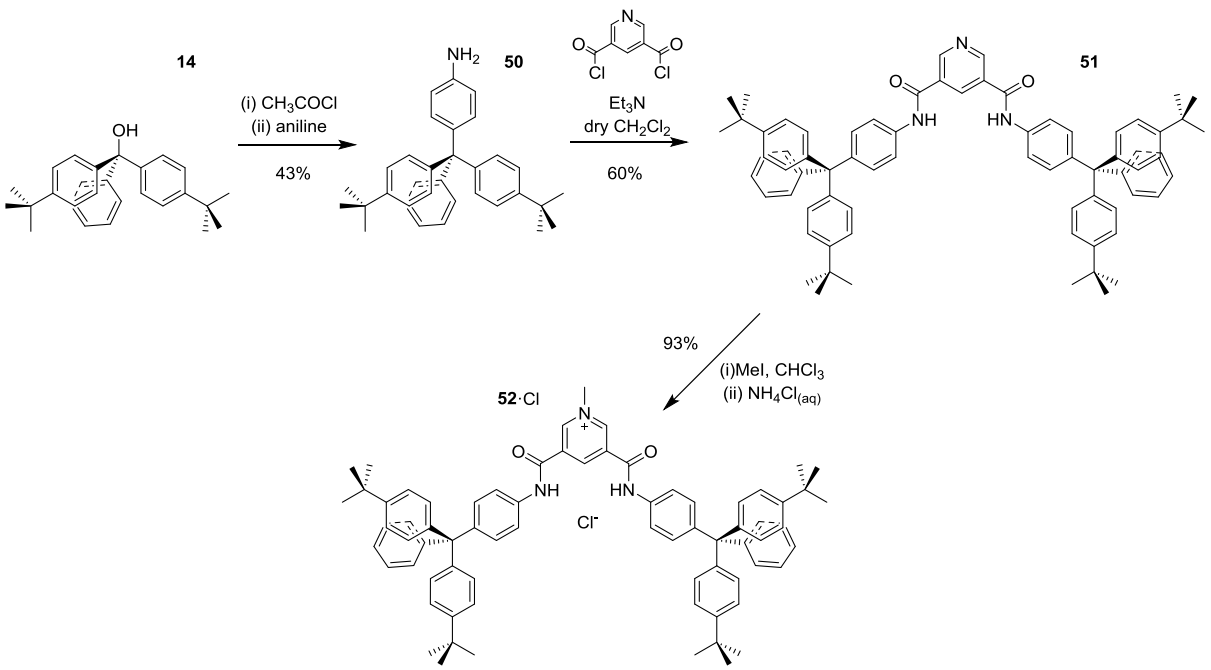

Scheme 3.7: Synthesis of methyl pyridinium axle **52** · Cl

The other synthons necessary for rotaxane formation using the acid chloride 'clipping' methodology[28] were 5-azidoisophthalic acid **53** (kindly donated by Dr. N. L. Kilah) and bis-

amine **37**. After conversion of **53** to 5-azido-isophthaloyl dichloride using oxalyl chloride, it was added to a solution of 3,5-bis-amide pyridinium axle **52** · Cl, bis-amine **37** and triethylamine in dry dichloromethane. Purification by column chromatography (gradient elution DCM/MeOH 99:1→95:5) and preparative thin layer chromatography (DCM/MeOH 95:5) afforded the 5-azido functionalised [2]rotaxane **54** · Cl in 48% yield (Scheme **3.8**).

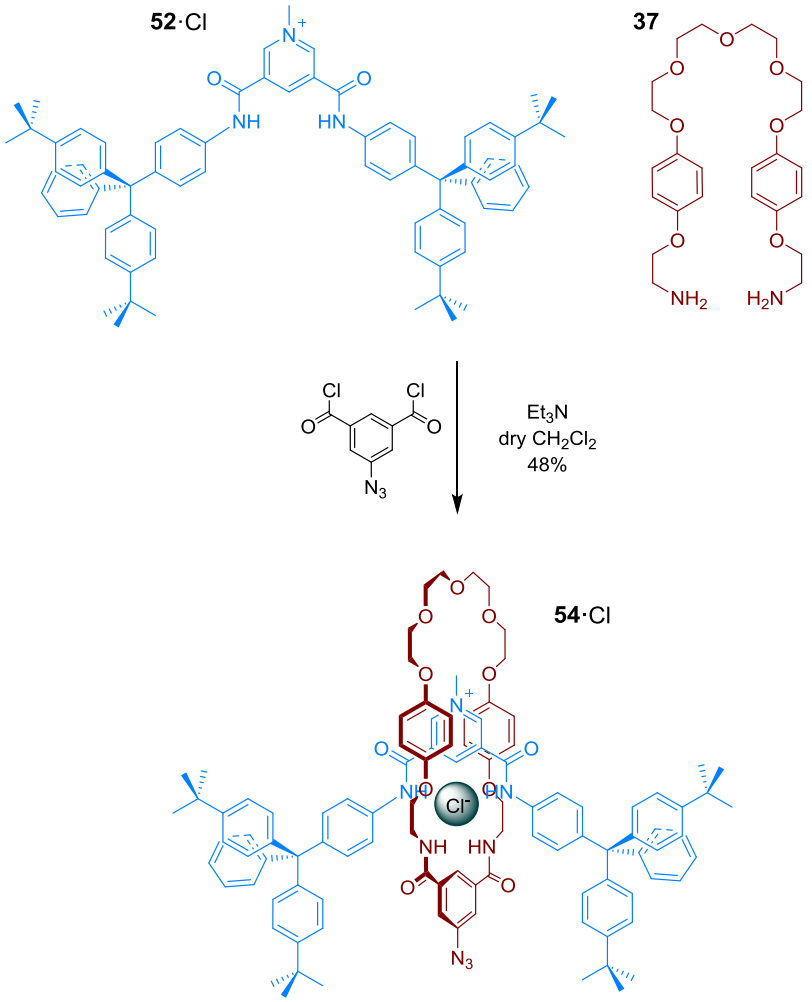

Scheme 3.8: Synthesis of azide functionalised [2]rotaxane **54** · Cl

The novel rotaxane was characterised by ^{1}H and^{13}C NMR spectroscopy and by high resolution mass spectrometry. The ESI-HRMS analysis of the rotaxane gave the expected

peak at $m/z = 1675.8666$ corresponding to $[M-Cl]^+$ and the ^1H NMR spectrum, together with that of the pyridinium axle **52** · Cl is shown in Figure **3.9**.

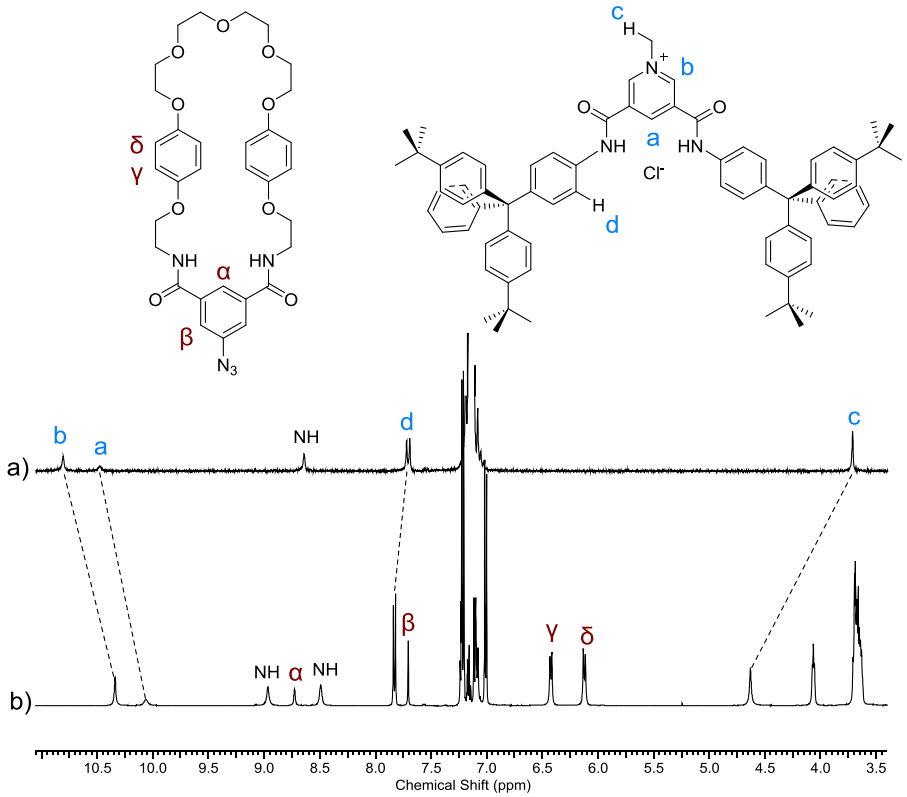

Figure 3.9: ^1H NMR (500 MHz, $CDCl_3$, 298 K) of a) pyridinium axle **52** · Cl b) azide [2]rotaxane **54** · Cl

Comparison of the spectra indicates formation of the interlocked product, the axle 3, 5-bis-amide pyridinium protons *a* and *b* are perturbed upfield due to aromatic donor-acceptor interactions with the electron rich hydroquinones of the macrocycle. The hydroquinone protons γ and δ are split in the interlocked product, which is also indicative of mechanical bond formation. Additionally a large downfield shift is observed for the methyl pyridinium protons *c* of the axle which arises from hydrogen bonding to the polyether portion of the macrocycle.

Further evidence for the interlocked nature of the product was obtained by two-dimensional ^{1}H-^{1}H ROESY NMR spectroscopy (Figure **3.10**). Interactions are observed between the methyl pyridinium protons *c* and the resonances corresponding to the polyether component of the macrocycle. Cross-coupling can also be seen between axle stopper proton *d* and the macrocycle hydroquinone protons γ and δ. Additional crosspeaks are also observed between stopper protons *d* and the NCH_2CH_2O alkyl resonances of the macrocycle.

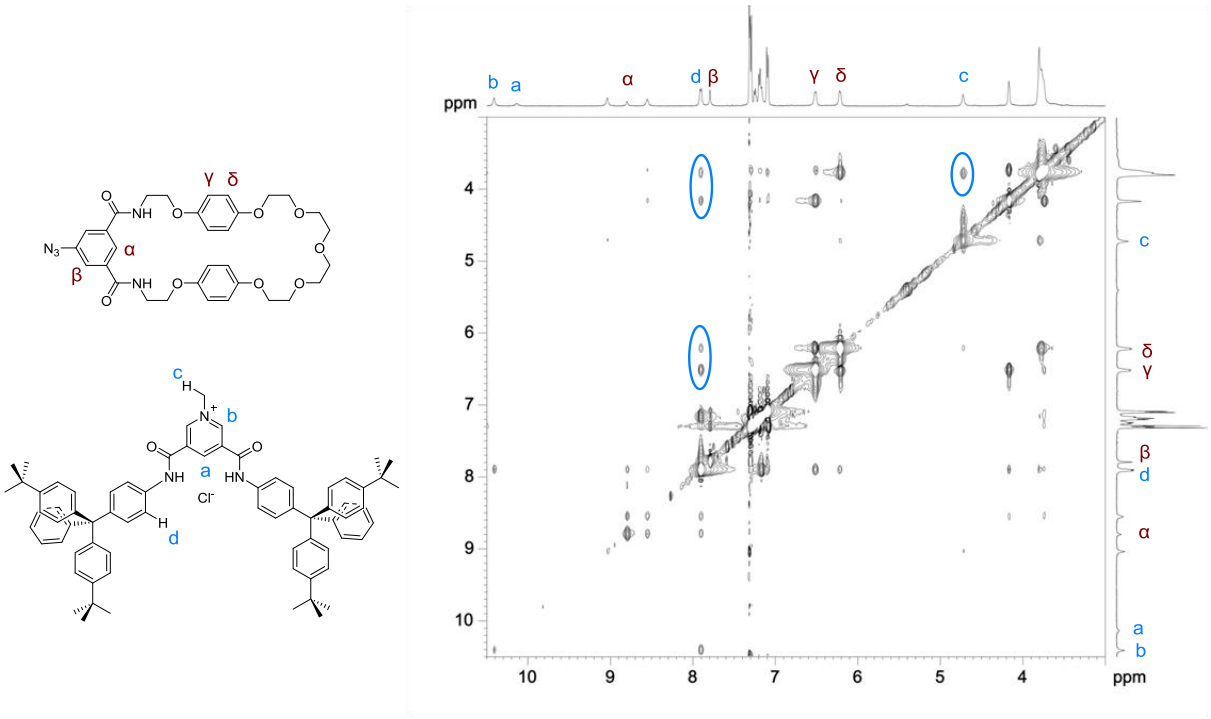

Figure 3.10: ^{1}H-^{1}H ROESY NMR (500 MHz, $CDCl_3$, 298 K) spectrum of **54** · Cl

Crystals suitable for X-ray diffraction structural analysis were obtained by slow diffusion of diisopropyl ether into a chloroform solution of **54** · Cl (Figure **3.11**). The structure confirms the interlocked nature of the system, and the templating chloride anion is encapsulated by the hydrogen bonded amide array, exhibiting mean N-Cl distances of 3.37Å.

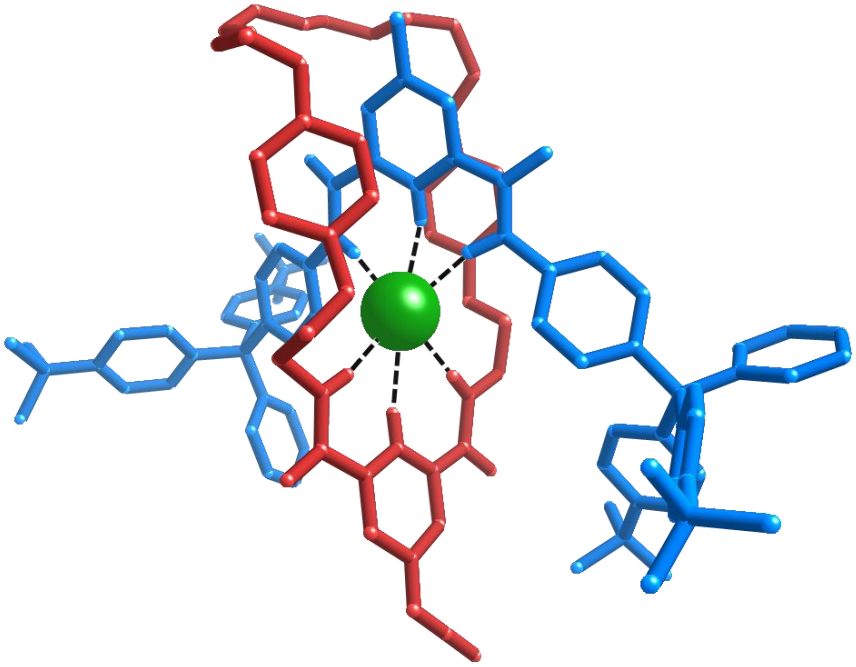

Figure 3.11: Single crystal X-ray structure of **54** · Cl (non-hydrogen bonding hydrogen atoms omitted for clarity)

In order to assess the anion binding properties of the rotaxane the chloride counteranion was exchanged for a non-coordinating hexafluorophosphate anion by washing with NH_4PF_6 to obtain **54** · PF_6 (>98%).

3.2.3 [2]Rotaxane Anion Recognition Properties

^{1}H NMR anion titration experiments were undertaken by monitoring the rotaxane's *internal* macrocycle and axle protons upon increasing equivalents of anion, added as the TBA salt in $CDCl_3/CD_3OD/D_2O$ (45:45:10) The addition of chloride (Figure **3.12**) caused significant downfield shifts of protons *a* and *α* which are a result of the polarising hydrogen bonding interaction with the chloride anion. The shifts of both these protons indicate the chloride is binding within the rotaxane cavity in the tetra-amide cleft. Additionally the hydroquinone

protons are perturbed upfield due to a small conformational change of the rotaxane to accommodate the anionic guest.

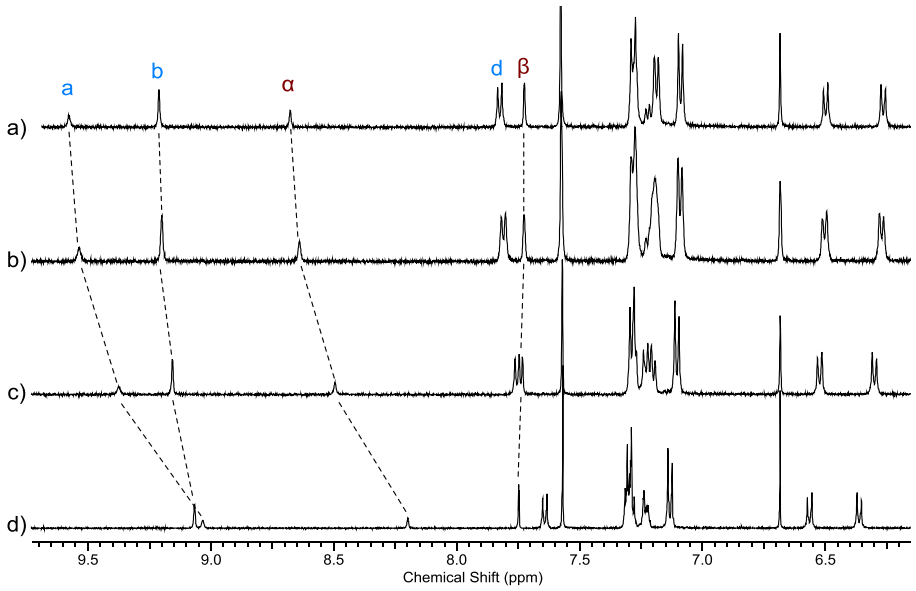

Figure 3.12: ^{1}H NMR (500 MHz, $CDCl_3/CD_3OD/D_2O$ 45:45:10, 298 K) spectra of a) rotaxane **54** plus 5 equivalents of TBA · Cl b) rotaxane **54** plus 3 equivalent of TBA · Cl c) rotaxane **54** plus 1 equivalent of TBA · Cl d) rotaxane **54**

Titrations with the oxoanions acetate and dihydrogenphosphate induced different changes in the ^{1}H NMR spectra. Importantly the *internal* protons *a* and *α* shifted upfield whereas *external* protons *b* and *β* shifted downfield indicating these oxoanions are too large to bind within the cavity and are bound on the periphery of the rotaxane structure, consistent with previous studies.[28] The titration data was analysed using the WinEQNMR2 program by monitoring the *internal* macrocycle proton *α* (Figure **3.13**) to determine 1:1 stoichiometric association constants, shown in Table **3.14**. The rotaxane host displays a strong preference for chloride with an association constant of 1460 M^{-1} in competitive aqueous solvent media. Both the oxoanions acetate and dihydrogenphosphate are bound considerably more weakly (<200 M^{-1}) due to peripheral association. Having demonstrated the high affinity of the

[2]rotaxane host for chloride, attention turned to appending the lanthanide complex in the hope that the strong and selective chloride binding of the rotaxane could be detected *via* the luminescence sensing properties of the lanthanide reporter group.

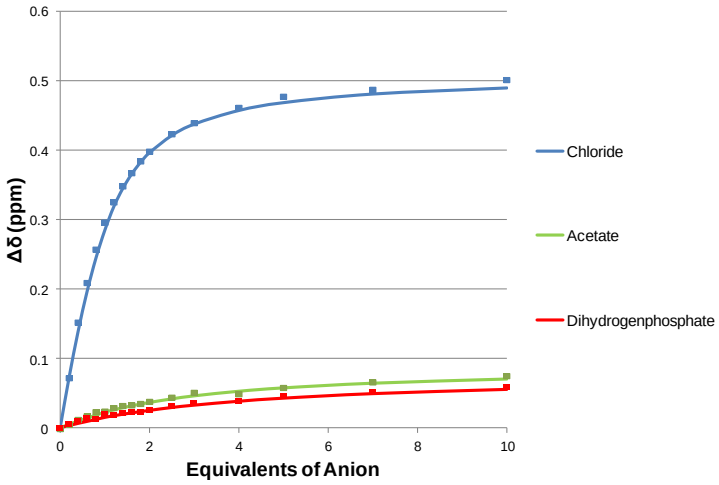

Figure 3.13: Changes in the chemical shift of proton α upon addition of increasing amounts of anion in $CDCl_3/CD_3OD/D_2O$ (45:45:10)

Anion	K_a/ M^{-1}
Chloride	1460 (74)
Acetate	115 (21)
Dihydrogenphosphate	188 (28)

Table 3.14: Association constants ($CDCl_3/CD_3OD/D_2O$ 45:45:10, 298 K) K_a (M^{-1}) obtained for rotaxane **54** · PF_6; errors in parentheses

3.2.4 Lanthanide Appended Rotaxane Preparation *via* Post-synthetic Modification

In order to covalently append a lanthanide ion complex to the azido-[2]rotaxane structure via a post-synthetic CuAAC click strategy, it was necessary to synthesise an alkyne-functionalised lanthanide cyclen complex. Europium DO3A complex (**55**) (Figure **3.15**) was

synthesised by Dr. Manuel Tropiano of the Faulkner research group according to a previously reported method.[29]

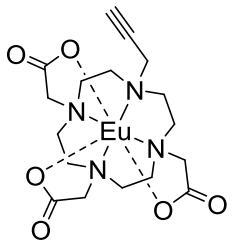

55

Figure 3.15: Alkyne functionalised europium DO3A complex **55**

Despite the versatility of the CuAAC click reaction, it proved difficult to find suitable solvent reaction conditions for the two reactants, azide rotaxane **54** · Cl and **55,** because of their marked differences in polarity and hence solubility characteristics. Using $Cu^{I}(MeCN)_4PF_6$ with TBTA and DIPEA in dichloromethane resulted in no reaction. These copper (I) catalytic conditions were repeated in methanol and acetonitrile with similar results. Reaction of the compounds in DMF with $Cu^{II}SO_4$ and sodium ascorbate as the reductant also gave no reaction, in spite of the good solubility of both compounds. Eventually successful reaction conditions between azide [2]rotaxane **54** · Cl and 3 equivalents of Eu(DO3A) **55** were found using $Cu^{I}(MeCN)_4PF_6$, TBTA and DIPEA in a mixed dichloromethane/methanol (4:1) solvent system (Scheme **3.16**). Complete consumption of the azido [2]rotaxane starting material was observed by TLC and ESI-LRMS after 3 days.

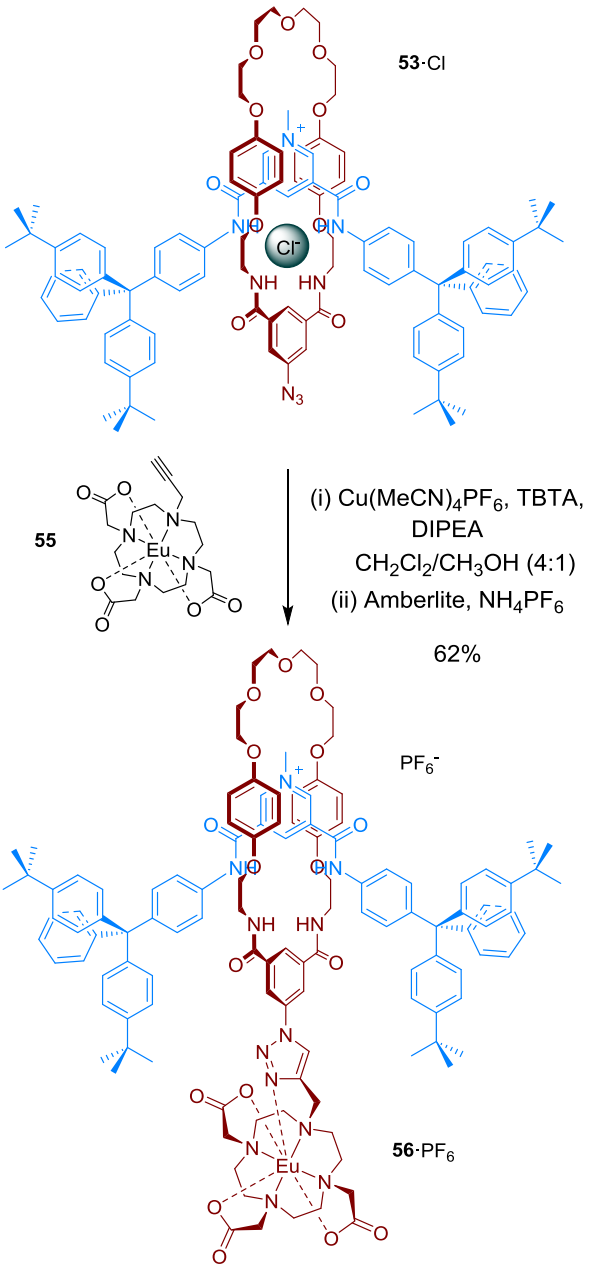

Scheme 3.16: Synthesis of europium rotaxane **56** · PF_6 by a post-synthetic CuAAC methodology

The high affinity of lanthanide complexes for silica and alumina stationary phases precluded purification using traditional column chromatographic methods. Due to the difference in size between the [2]rotaxane product **56** · Cl, europium complex **55** and catalyst side products the crude reaction was purified by size-exclusion chromatography. The chloride complex **56** · Cl was anion exchanged to the non-coordinating hexafluorophosphate salt *via* aqueous washing

with NH_4PF_6 to give **56** · PF_6 in 62% yield. The [2]rotaxane **56** · PF_6 was characterised by ^{1}H NMR spectroscopy and ESI-HRMS spectrometry. The compound gave the expected peak at $m/z = 1116.9766$, corresponding to $[M - PF_6 + Na]^{2+}$ (Figure **3.17**).

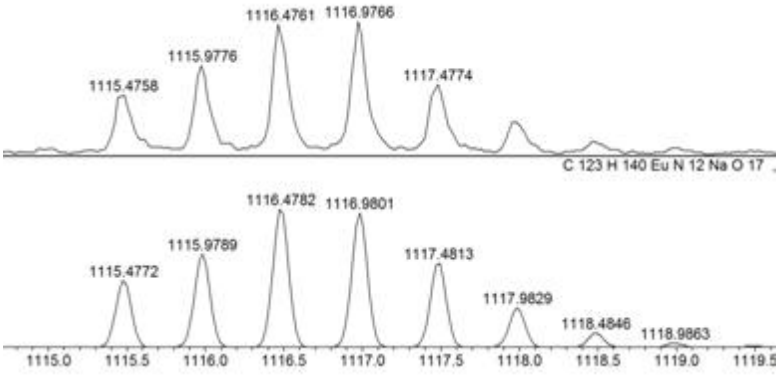

Figure 3.17: Observed (top) and theoretical (bottom) ESI-HRMS spectrum of **56** · PF_6

The ^{1}H NMR spectrum of **56** · PF_6 in CD_2Cl_2/CD_3OD 1:1 (obtained by Dr. A. Kenwright at Durham University) shown in Figure **3.18** is consistent with the covalent incorporation of a paramagnetic lanthanide ion into a [2]rotaxane structure. There are proton peaks belonging to the DO3A ligand which are shifted outside the normal range (0-10ppm). By comparison the [2]rotaxane resonances of the compound are not shifted as a result of the large distance to the paramagnetic ion. The proton shifts of the DO3A ligand are consistent with octadentate binding to the europium, with a predominant square antiprismatic geometry at the lanthanide centre, indicating the triazole is occupying the eighth coordination site of the lanthanide.[29, 30]

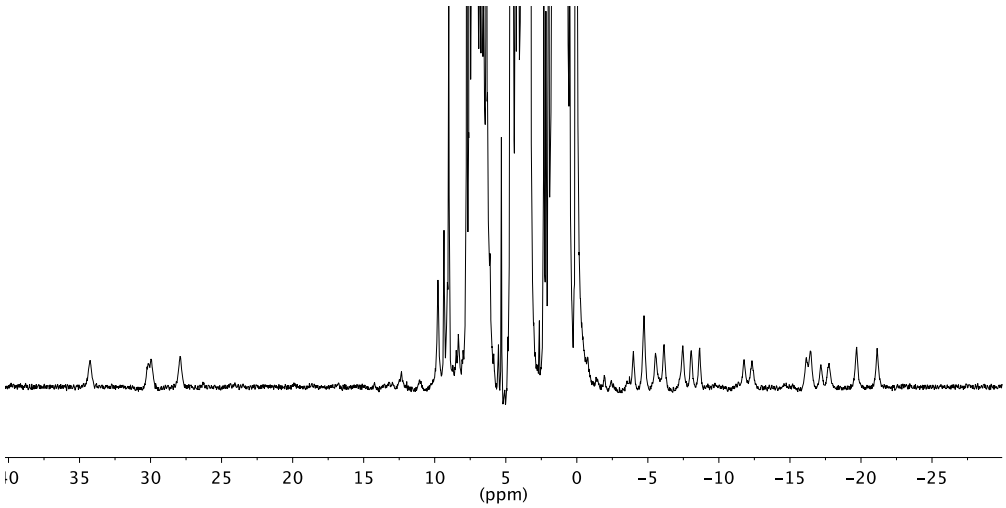

Figure 3.18: ^{1}H NMR (500 MHz, CD_2Cl_2/CD_3OD 1:1, 298 K) spectrum of europium rotaxane **56** · PF_6

3.2.5 Europium Cyclen Appended [2]Rotaxane Photophysical and Anion Sensing Properties

All photophysical measurements and luminescent anion titration experiments were performed by Dr. M. Tropiano of the Faulkner Group in Oxford. The excitation and emission spectra of europium cyclen appended [2]rotaxane **56** · PF_6 is shown in Figure **3.19**. As can be seen, the emission of the europium complex occurs *via* energy transfer from simple aryl chromophores present in the rotaxane. Splitting is observed in the $\Delta J = 2$ transition in the emission spectrum which is indicative of the triazole-europium interaction, as has been previously observed for related complexes.[30]

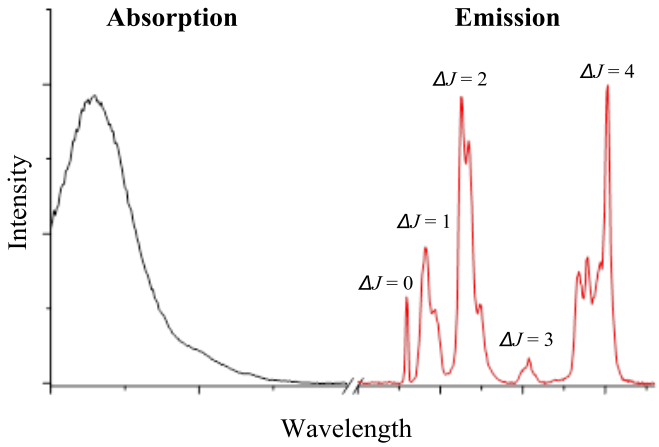

Figure 3.19: Excitation and emission spectra of europium rotaxane **56** · PF_6 in dichloromethane

Luminescent anion titration experiments with chloride, acetate and dihydrogenphosphate were carried out in dichloromethane by addition of the anions as their TBA salts. Upon addition of one equivalent of chloride there was a marked quenching of the europium emission (Figure **3.20**). After addition of chloride beyond one equivalent, a recovery of the emission to the initial luminescence signal was observed, suggesting that two binding processes were occurring. The binding processes are thought to involve binding within the rotaxane cavity but also ligation of the halide anion at the ninth coordination site of the europium by displacement of solvent.

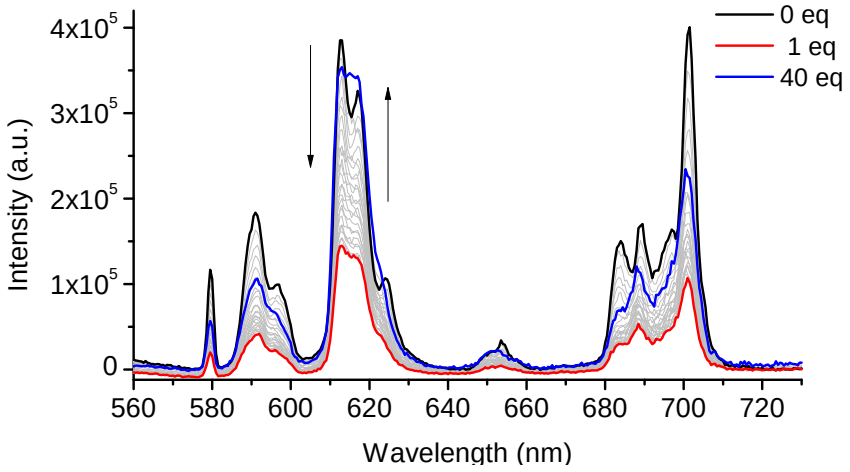

Figure 3.20: Emission spectra of [2]rotaxane **56** · PF_6 in the presence of increasing amounts of TBA · Cl in dichloromethane (λ_{ex} = 270 nm)

Analysis of the spectra shows a greater change in the hypersensitive ΔJ_2 transition, and consequently the $\Delta J_2/\Delta J_1$ ratio, up to one equivalent. Further addition of chloride induced no change in the ratio of $\Delta J_2/\Delta J_1$ (Figure **3.21**). The change in the ΔJ_2 transition is clear evidence for binding of chloride to the ninth donor site on the lanthanide complex[31] indicating that chloride first binds at the axial coordination site of europium, causing a change in the local crystal field environment. Above one equivalent, binding then occurs within the tetra-amide cavity of the rotaxane causing an increase in the rigidity of the receptor. This increased rigidity causes a decrease in the non-radiative vibronic relaxation of the lanthanide and hence an increase in the luminescence intensity of the europium is observed.

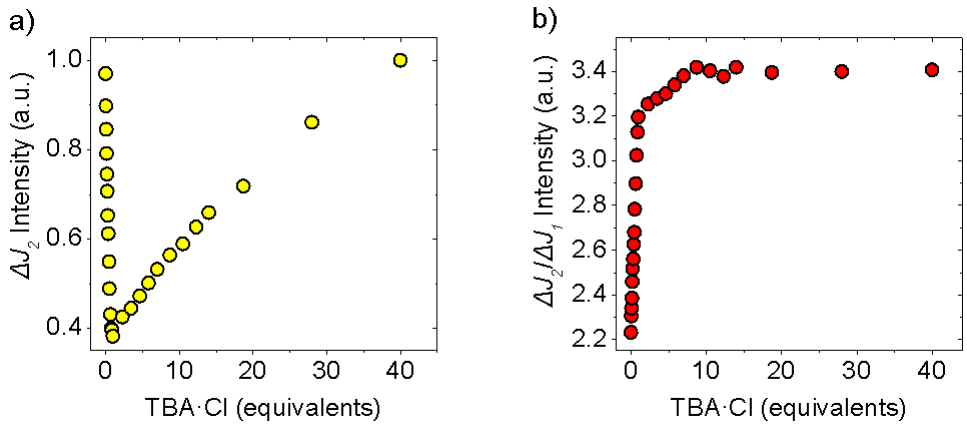

Figure 3.21: Changes in the emission spectrum of **56** · PF_6 upon addtion of TBA · Cl in dichloromethane a) changes in the ΔJ_2 transition b) changes in the ratio of $\Delta J_2/\Delta J_1$

To further probe the chloride binding behaviour of the rotaxane host, time-resolved spectroscopy was employed, monitoring the lifetime of the europium excited state. These data corroborate the steady-state results already obtained; they confirm the presence of two distinct binding events. Initially upon addition of chloride there is a large decrease in the luminescence lifetime of the europium, due to non-radiative quenching of the emission by the

bound anion through a photo-electron transfer (PET) process.[21] Increasing concentrations of chloride then structurally modify and rigidify the rotaxane host which increases the lifetime through reduced probability of non-radiative vibrational quenching (Figure **3.22**).

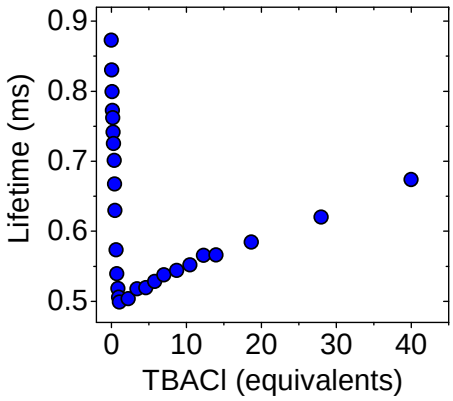

Figure 3.22: Changes in europium luminescence lifetime of [2]rotaxane **56** upon increasing amounts of TBA · Cl in dichloromethane (λ_{ex} = 270 nm, λ_{em} = 616 nm)

In order to determine the affinity of the europium rotaxane host system for chloride it was necessary to invoke a binding model for the two independent binding events (Figure **3.23**). This model assumes that the equilibria are all under thermodynamic control and that no cooperativity is in effect. Modelling of the data was performed using the Dynafit software program.[32] Two association constants were determined for chloride, K_1 = 750,000 M^{-1} and K_2 = 1360 M^{-1}, for binding at the europium and in the rotaxane cavity respectively giving a good correlation between the experimental and calculated values (Figure **3.24**)

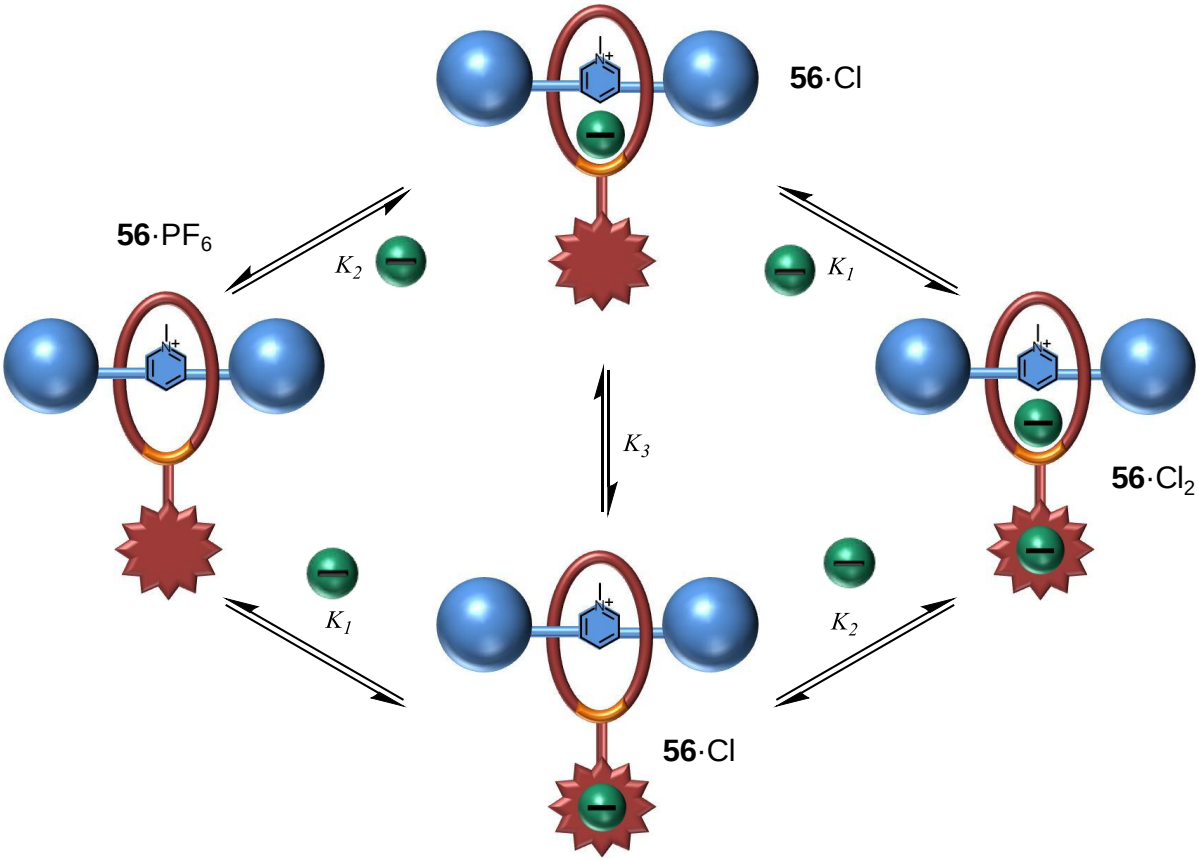

Figure 3.23: Simplified equilibria of chloride binding to [2]rotaxane **56** · PF_6

In addition, plotting of the $\Delta J_2/\Delta J_1$ ratio enabled study of the interaction of chloride only with the lanthanide centre which after Dynafit analysis determined an association constant of 504,000 M^{-1}. This value is in good agreement with the previous modelled data and indicates that in dichloromethane the chloride anion is bound most strongly by the europium centre.

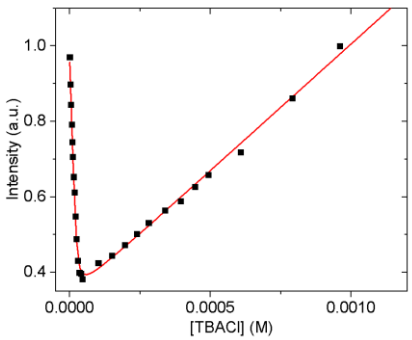

Figure 3.24: Comparison of the experimental and modelled data of the independent binding model of chloride to rotaxane **56** · PF_6

The binding of the oxoanions, acetate and dihydrogenphosphate, displayed different binding behaviour. As demonstrated by the ^{1}H NMR titration experiments with the azido-rotaxane **54** · PF_6, the oxoanions were not bound within the [2]rotaxane cavity and associate on the outside of the structure. The luminescence titration experiments of acetate (Figure **3.25**) and dihydrogenphosphate (Figure **3.26**) support this, showing only one binding event occuring, with significant quenching observed in the ΔJ_2 transition. This quenching was without the accompanying recovery in emission above one equivalent observed for chloride, confirming that the oxoanions only bind at the europium centre and do not induce any structural changes in the rotaxane.

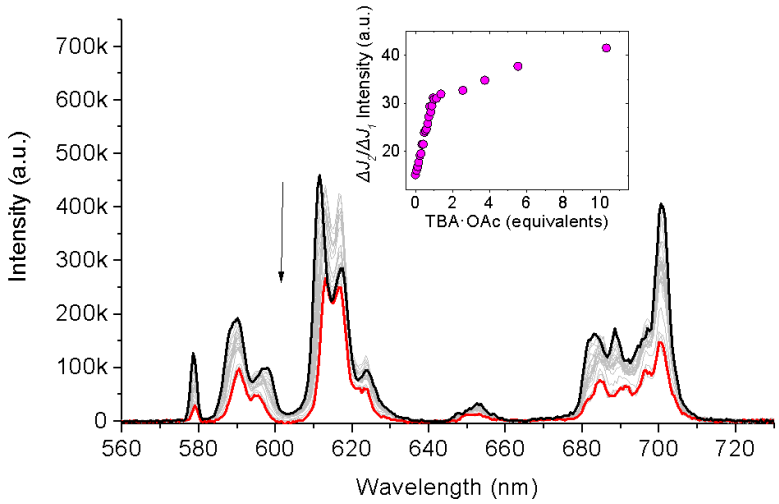

Figure 3.25: Luminescence changes of [2]rotaxane **56** · PF_6 upon addition of TBA · OAc in dichloromethane (black line = 0 equivalents, red line = 10 equivalents, λ_{ex} = 270 nm)

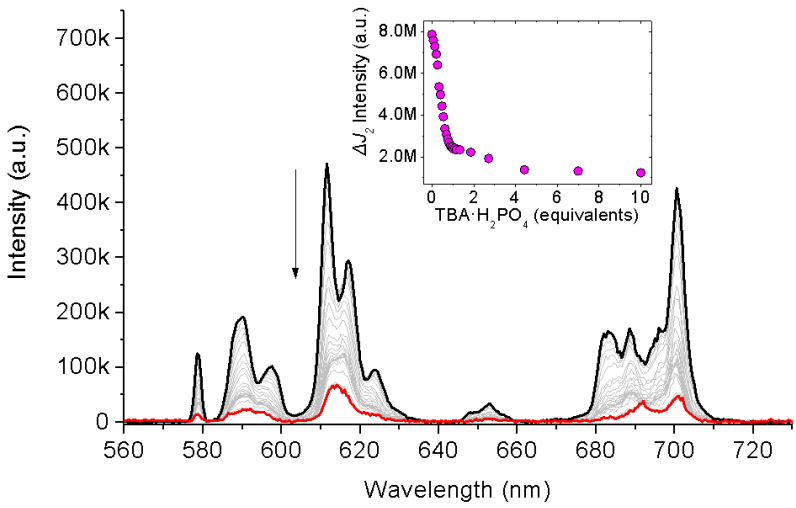

Figure 3.26: Luminescence changes of [2]rotaxane **56** · PF_6 upon addition of TBA · H_2PO_4 in dichloromethane (black line = 0 equivalents, red line = 10 equivalents, λ_{ex} = 270 nm)

Fitting of the data using Dynafit enabled the calculation of 1:1 stoichiometric association constants (Table **3.27)** which indicates rotaxane **56** · PF_6 is selective for chloride over oxoanions in dichloromethane. Importantly the luminescent response in the presence of chloride is unique when compared to acetate and dihydrogenphosphate, demonstrating that the system is able to act as an effective luminescent probe for chloride anions.

Anion	**Association Constant K_1[a]/ M^{-1}**	
Cl	504 000[b]	[298900 – 1014000][c]
H_2PO_4	304 000	[264200 – 354600][c]
OAc	58 000	[52520 – 64300][c]

Table 3.27: Association constants of **56** · PF_6 with chloride, acetate and dihydrogenphosphate in dichloromethane ([a] obtained from ΔJ ratios binding plots, [b]gave two independent association constants of 750000 M^{-1} and 1360 M^{-1}, [c]confidence intervals determined as the values of K that are possible while keeping χ^2 with 99% on the minmum value)

3.2.6 Summary

The synthesis of the first lanthanide-containing interlocked structure was achieved. This was accomplished by a post-rotaxane synthetic modification strategy where an azide functionalised [2]rotaxane was 'clicked' with an alkyne functionalised lanthanide complex. The europium functionalised rotaxane $\mathbf{56} \cdot \mathrm{PF}_6$ was shown to sense chloride selectively in dichloromethane via a two-step halide binding process, occurring first at the lanthanide centre and subsequently in the rotaxane cavity. This resulted in an initial quenching of the lanthanide luminescence followed by recovery of the luminescence which was not observed for oxoanions acetate and dihydrogenphosphate due to the selectivity imparted by the rotaxane cavity.

3.3 [2]Rotaxanes Containing Transition Metal Reporter Groups

The second part of this chapter concerns the incorporation of transition metal reporter groups into acyclic, macrocyclic and interlocked host systems. This involved using a modified dipyridylbenzene ligand as an alternative to the bipyridine based transition metal anion sensors introduced in Section **3.1.1**. Part of the research carried out in this section was undertaken in collaboration with a Part II student, Sophie Dapin.

3.3.1 Dipyridylbenzene Transition Metal Complexes

A diverse range of dipyridylbenzene ligand transition metal complexes (Figure **3.28a**) have shown widespread utility in research areas such as catalysis,[33] organic light emitting diodes (OLEDs)[34] and energy transfer.[35, 36] Related to well-known tridentate terpyridine transition metal complexes, they display a planar N^C^N coordination geometry (Figure **3.28b**). Transition metal dipyridylbenzene complexes are usually extremely stable due to the synergistic combination of σ-donating nitrogen and carbon atoms, and π-accepting aromatic rings.

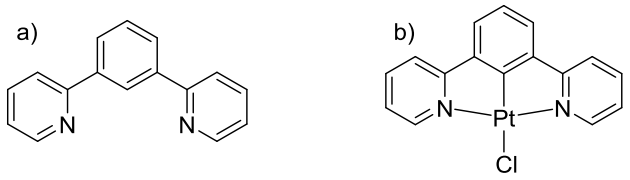

Figure 3.28: a) 1,3-Di(pyridin-2-yl)benzene (dpb) b) [Pt(dpb)Cl]

Complexes containing the dipyridylbenzene ligand have been reported for a range of late second and third row transition metals including Ru (II), Pt (II), Ir (III), Rh (III) and Pd (II).[37] The strong field imparted by the ligand produces photo-active complexes which

typically emit in the visible and near-infrared region. Many of these complexes have been shown to exhibit high levels of luminescence efficiency, including the platinum (II) complex shown in Figure **3.28b**, which has a quantum yield of 60%.[38] In spite of this, the luminescence sensing properties of such systems have yet to be explored. With this in mind, the initial project aim was to incorporate an anion binding isophthalamide group into the dipyridylbenzene ligand structure and investigate the luminescent anion sensing properties of ruthenium (II) and platinum (II) complexes containing this new motif.

3.3.2 Isophthalamide Functionalised Dipyridylbenzene Ligand Synthesis

The synthesis of the key bis-ester functionalised ligand **62** was attempted by adapting a previously reported literature procedure (Scheme **3.29**).[39] meta-Xylene was reacted with bromine to obtain the dibrominated product **57** in 40% yield. 2-Tributylstannyl pyridine **58** was synthesised in 87% yield via lithiation and subsequent transmetallation of 2-bromopyridine.[40] The dimethyl functionalised ligand **59** was then obtained by a Pd-catalysed Stille coupling in toluene (51%). Oxidation of compound **59** was attempted using $KMnO_4$ in pyridine, K_2CrO_7 in ethanol, and $SeO_2/AgNO_3$ but unfortunately it was not possible to obtain the target compound. An alternative route was investigated adapting a literature procedure;[41] oxidation of **57** with $KMnO_4$ in pyridine/water 1:1 for two weeks produced the isophthalic acid synthon **60** in high yield (89%). The long reaction time is likely a result of the hindered reaction site and may explain the failure to oxidise compound **59**. Esterification of **60** with methanol under acidic conditions afforded the dimethyl ester **61** (89%). A Stille reaction between **58** and **61** gave the bis-ester functionalised ligand **62** (58%).

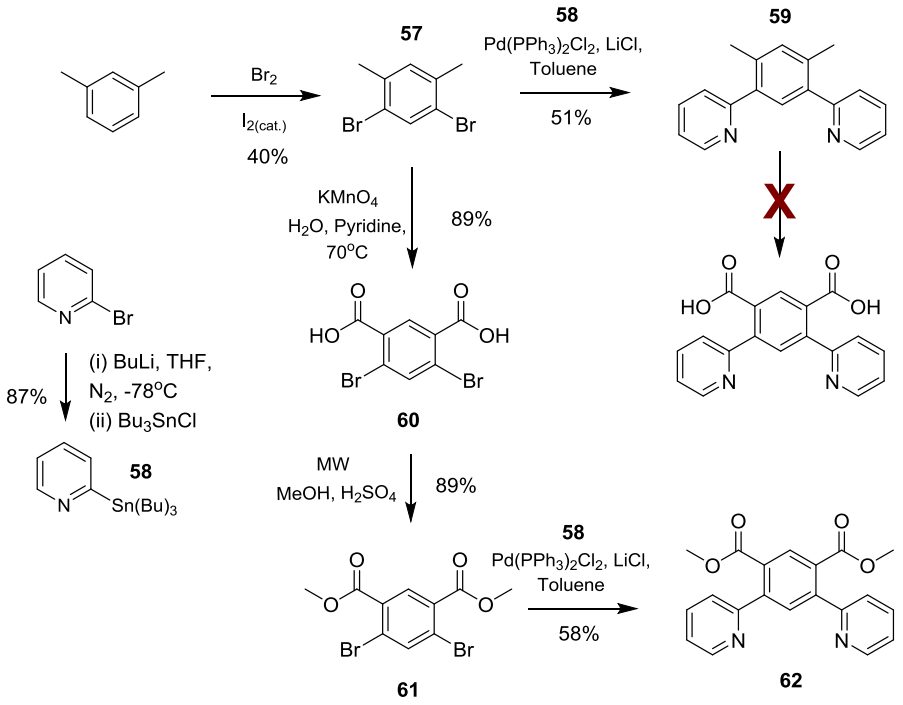

Scheme 3.29: Synthesis of target bis-ester functionalised dipyridylbenzene ligand **62**

Crystals of **62** suitable for X-ray diffraction structural analysis were obtained by diffusion of methanol into a chloroform solution of the ligand, confirming the proposed formulation (Figure **3.30**).

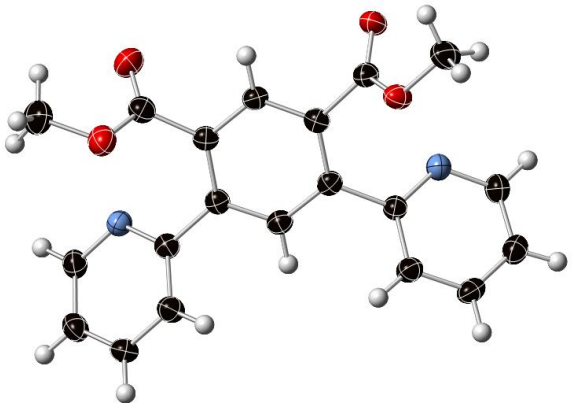

Figure 3.30: Single crystal X-ray crystal structure of bis-ester functionalised dipyridylbenzene ligand **62** (Ellipsoids shown at 50% probability, hydrogen atoms drawn as spheres of arbitrary radius)

3.3.3 Acyclic and Macrocyclic Anion Receptor Synthesis

Reaction between the bis-ester functionalised dipyridylbenzene ligand **62** and K_2PtCl_4 in degassed aqueous acetonitrile afforded the platinum (II) bis-ester complex **63** in 64% yield (Scheme **3.31**). Hydrolysis of the methyl esters was accomplished using KOH in methanol[42] which afforded the platinum (II) bis-acid complex **64**. After reaction with oxalyl chloride, the bis-acid chloride was condensed with two equivalents of hexylamine in dry dichloromethane to afford the platinum (II) acyclic receptor **65** in a 6% yield. The low yield of the reaction is probably a result of the limited solubility of the platinum (II) bis-acid chloride reactant in dichloromethane.

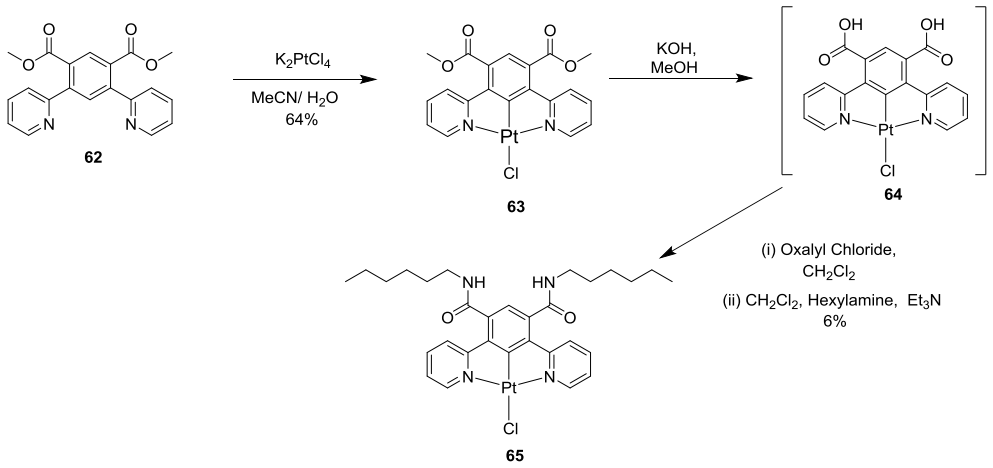

Scheme 3.31: Synthesis of acyclic platinum (II) anion receptor **65**

The preparation of the corresponding ruthenium (II) complex required the synthesis of an additional terpyridine ligand, achieved using a Kröhnke reaction[43] (Scheme **3.32**) which afforded 4-tolyl-terpyridine (ttpy) **66** in moderate yield (20%).

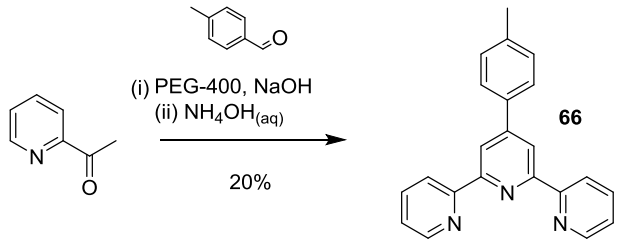

Scheme 3.32: Synthesis of 4-tolylterpyridine **66**

Reaction between terpyridine **66** and $RuCl_3$ hydrate, produced $Ru(ttpy)Cl_3$ **67** in good yield (82%) (Scheme **3.33).** Addition of $AgBF_4$ in acetone generated the labile acetone complex which facilitated complexation to ligand **62**. Addtion of $KPF_{6(aq)}$ gave the ruthenium (II) bis-ester complex $\mathbf{68} \cdot PF_6$ (67%). Deprotection of the ester groups with NaOH in methanol/dioxane afforded the ruthenium (II) bis-acid synthon $\mathbf{69} \cdot PF_6$ (52%), which was activated with oxalyl chloride and condensed with two equivalents of hexylamine in dry dichloromethane. Anion exchange with $NH_4PF_{6(aq)}$ and purification by preparative TLC furnished the target ruthenium (II) acyclic receptor $\mathbf{70} \cdot PF_6$ in good yield (81%) (Scheme **3.33**).

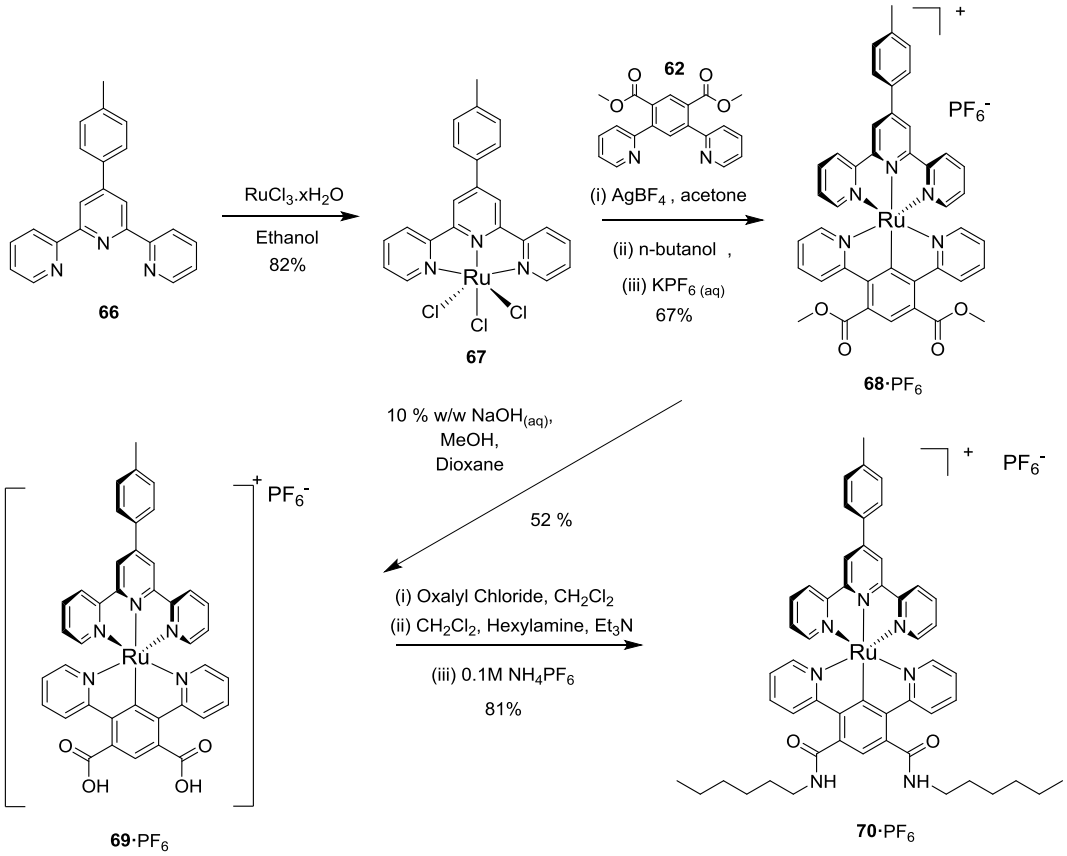

Scheme 3.33: Synthesis of acyclic ruthenium (II) receptor **70** · PF_6

Diffusion of diisopropyl ether into an acetonitrile solution of **70** · PF_6 and excess TBA · Cl yielded crystals of **70** · Cl suitable for X-ray diffraction. The crystal structure shown in Figure **3.34**, reveals the chloride counteranion is bound within the isophthalamide cleft of the receptor with mean N-Cl bond lengths of 3.41 Å. The chloride is bound out of the plane of the bis-amide motif, presumably to satisfy electrostatic interactions between the anion and the positively charged complex. Additionally there are secondary hydrogen-bonding interactions between the dipyridylbenzene ligand and the isophthalamide carbonyl oxygens with mean C-O distances of 3.21 Å.

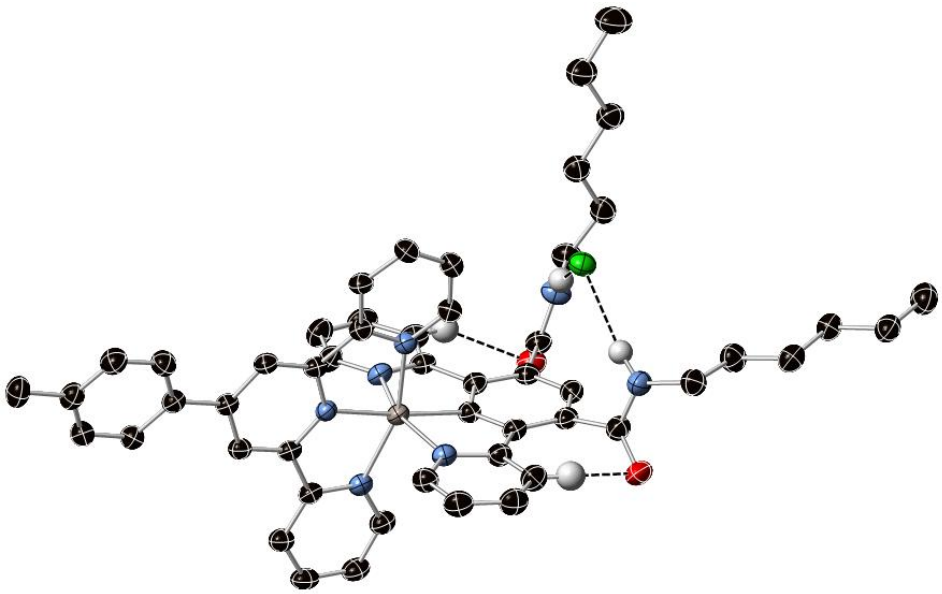

Figure 3.34: Single crystal X-ray structure of acyclic ruthenium (II) receptor **70** · Cl (Ellipsoids displayed at 50% probability, non-hydrogen bonding hydrogen atoms are omitted for clarity)

The macrocyclic anion receptors were synthesised using 3,5-bis-amide pyridinium template using an acid chloride clipping methodology.[28] The platinum (II) bis-acid was converted to the acid chloride using oxalyl chloride and then added dropwise to a solution of bis-amine **37** and 3,5-bis-amide pyridinium template **39** · Cl in dry dichloromethane (Scheme **3.35a**). Purification by preparative TLC afforded to target platinum (II) macrocycle **71** in 24% yield.

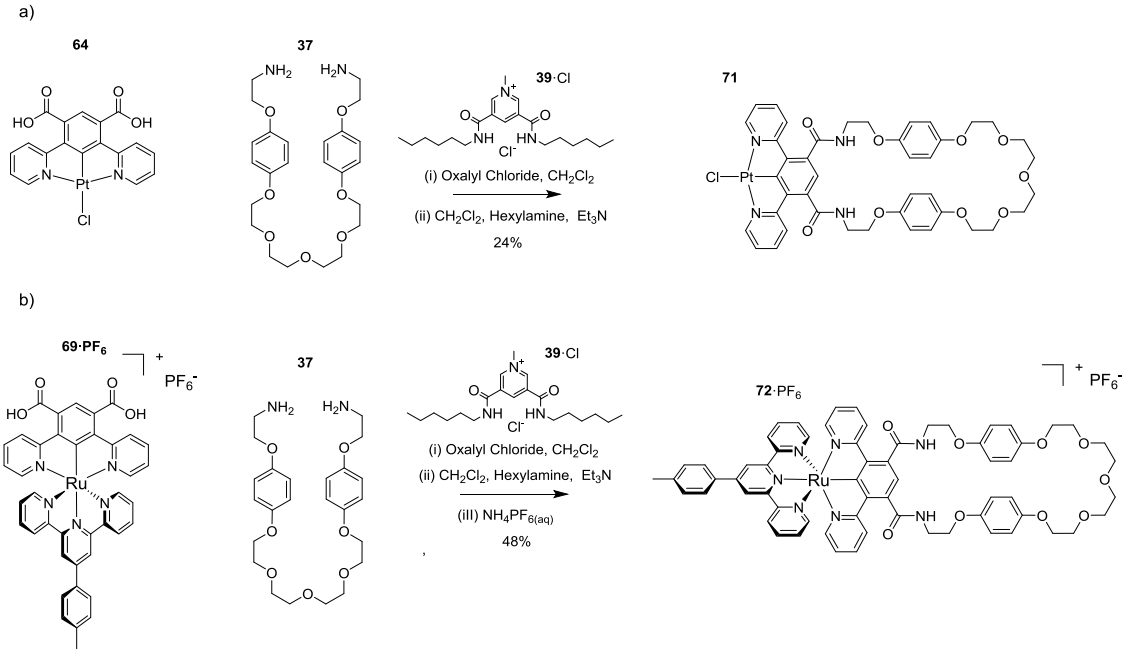

Scheme 3.35: Synthesis of macrocyclic systems a) platinum (II) macrocycle **71** b) ruthenium (II) macrocycle **72** · PF_6

The ruthenium (II) macrocycle **72** · PF_6 was synthesised according to the same procedure as **71** (Scheme **3.35b**), which upon anion exchange with $NH_4PF_{6(aq)}$ and purification by preparative TLC afforded the target macrocycle in 48% yield. The higher yield relative to the platinum derivative may be a consequence of the greater efficiency of the 3,5-bis-amide pyridinium chloride template interacting with the positively charged ruthenium complex. The ESI-HRMS and assigned ^{1}H NMR spectrum of the macrocyclic ruthenium (II) receptor **72** · PF_6 are displayed in Figure **3.36**.

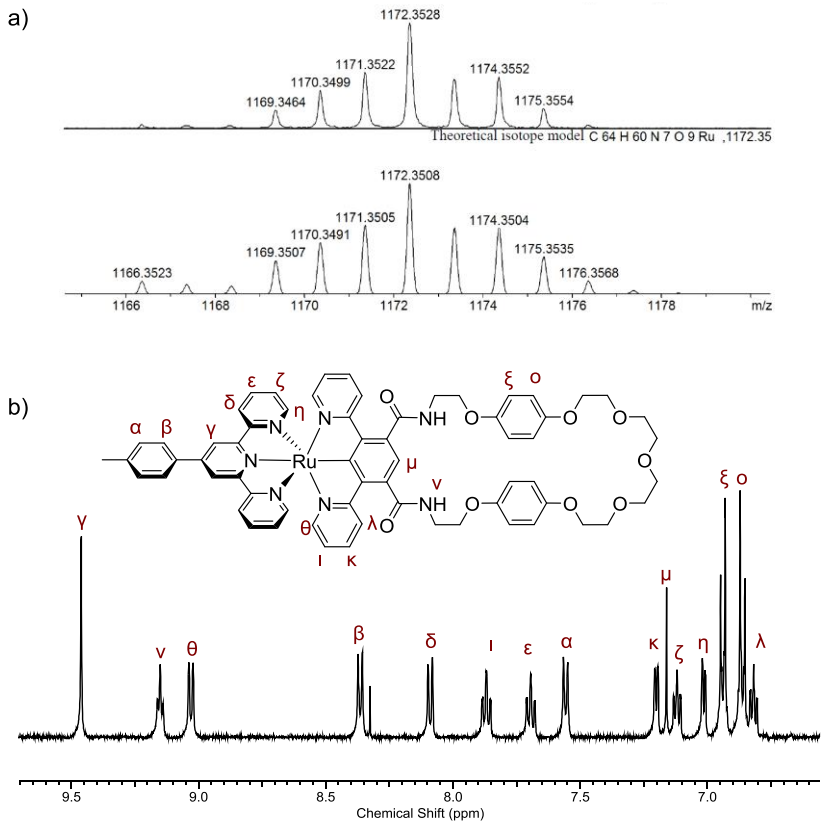

Figure 3.36: a) Electrospray high-resolution mass spectrum of **72** · PF_6 (predicted spectra bottom; obtained spectra top) b) truncated ^{1}H NMR (500 MHz, DMSO-d_6, 298 K) spectrum of **72** · PF_6

Crystals suitable for analysis by X-ray diffraction were obtained for the macrocyclic ruthenium (II) receptor **72** · PF_6. Crystals were grown by vapour diffusion of diisopropyl ether into a chloroform (Figure **3.37a**) or acetone/water (9:1) (Figure **3.37b**) solution of the macrocycle. The two structures exhibit both *syn-* and *anti-* conformations of the isophthalamide and cocrystallise with their respective solvents. It is also noteworthy that both structures also exhibit hydrogen-bonding between the isophthalamide carbonyl oxygens and the dipyridylbenzene ligand with average C-O bond lengths of 3.20 Å and 3.11 Å for the *syn-* and *anti-* conformations respectively.

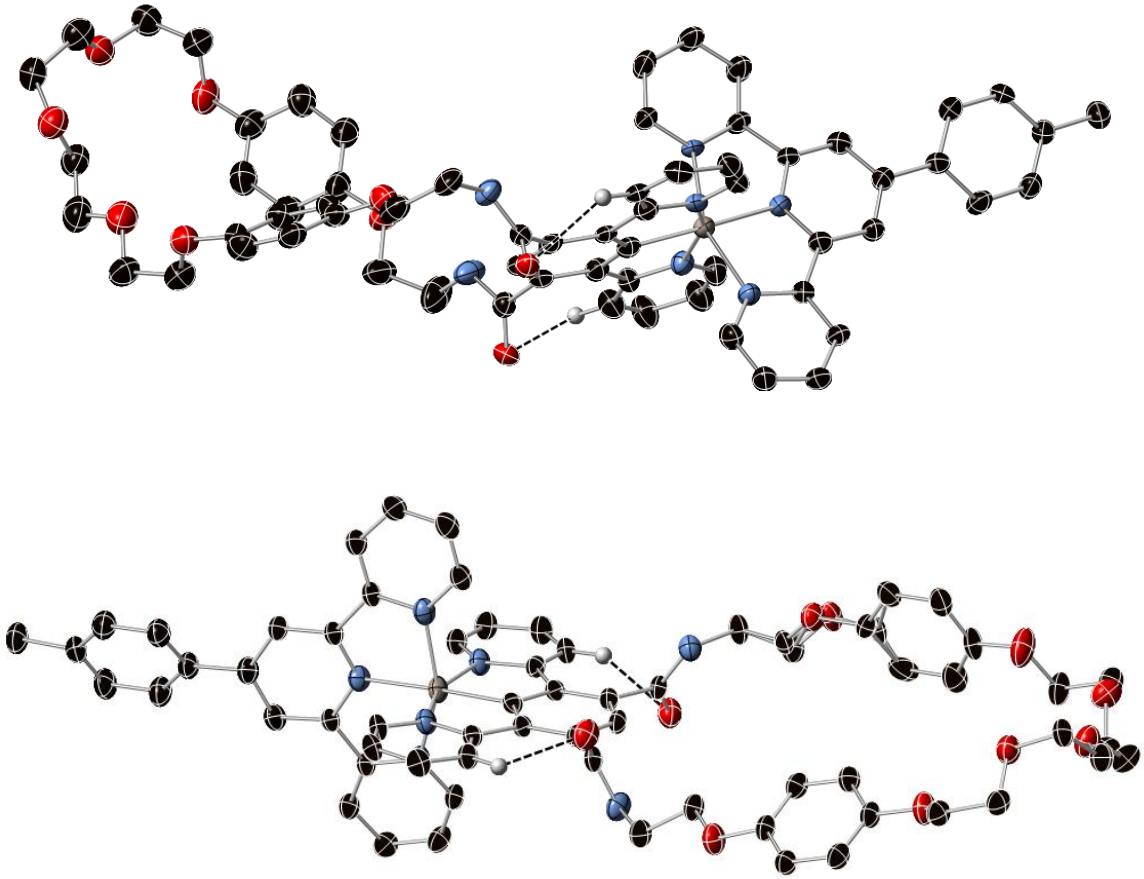

Figure 3.37: Single crystal X-ray structures of ruthenium (II) macrocycle **72** · PF_6 in a) *syn*-conformation b) *anti*-conformation (Ellipsoids at 50% probability, non-hydrogen bonding hydrogen atoms and hexafluorophosphate anion omitted for clarity)

3.3.4 Acyclic and Macrocyclic Luminescent Anion Sensing

Following the successful preparation of the target acyclic and macrocyclic platinum (II) and ruthenium (II) receptors, luminescent anion titrations were undertaken. Ruthenium (II) dipyridylbenzene terpyridine complexes typically display emission from metal-to-ligand charge-transfer (^{3}MLCT) states[44] whereas platinum (II) dipyridylbenzene complexes display ligand centred (π–π^*) phosphorescent emission.[38]

3.3.4.1 Acyclic and macrocyclic platinum (II) receptors

The UV/visible absorption and luminescence spectral studies of the acyclic and macrocyclic platinum (II) receptors **65** and **71** were conducted in dichloromethane; the photophysical data is summarised in Table **3.38**. Both receptors exhibit absorption bands centred around 320 nm, consistent with their characteristic π–π* transitions, and display emission at 504 nm (Figure **3.39**).

	λ_{max} / nm	
	π–π* absorption (ε/dm^3 mol^{-1} cm^{-1})	**π–π* emission** (λ_{ex} = 320 nm)
65	**318** (8,000)	**504**, 535
71	**320** (3,000)	**504**, 535

Table 3.38: Absorption and emission spectra for acyclic and macrocyclic platinum (II) receptors **65** and **71** in dichloromethane at 293 K (highest intensity emission peak shown in bold)

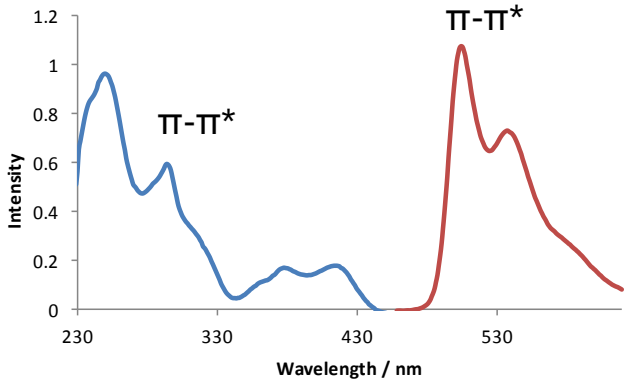

Figure 3.39: Absorption (blue line) and emission (red line) spectra of macrocyclic platinum (II) receptor **71** in dichloromethane at 293 K (spectra have been standardised for clarity)

Luminescence anion titrations were performed in dichloromethane at a receptor concentration of 1×10^{-5} M. Upon addition of chloride there was an observed luminescent enhancement for both acyclic and macrocyclic platinum (II) receptors, with the acyclic derivative exhibiting the largest response (Figure **3.40**).

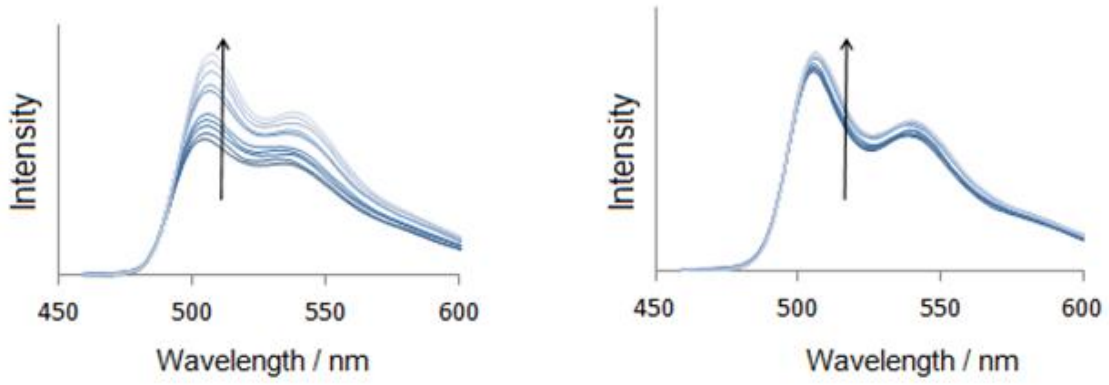

Figure 3.40: Emission spectra (λ_{ex}= 320 nm) of a) acyclic platinum receptor **65** and b) macrocyclic platinum receptor **71** in the presence of 0–100 equivalents of TBA · Cl in dichloromethane at 293 K.

The contrasting percentage emission changes of **65** and **71** with chloride, bromide, iodide, acetate, dihydrogenphosphate and sulphate anions are summarised in Figure **3.41**. With the halides a number of competing factors may account for the changes in luminescence observed. It can be postulated that the enhancement of the emission intensity for chloride binding is due to a rigidification effect which decreases vibrational quenching.

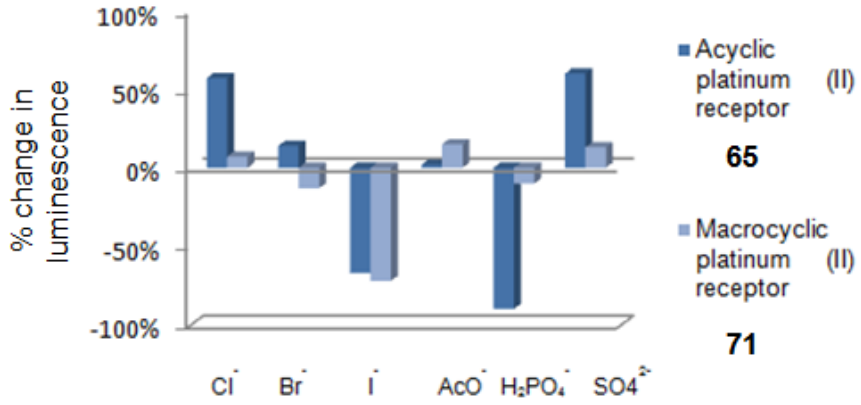

Figure 3.41: Percentage changes in luminescence emission intensity at 504 nm (λ_{ex}=320 nm) between 0–100 equivalents of anion of acyclic platinum receptor **65** and platinum macrocycle **71** at 293 K.

Conversely the decrease in emission intensity for iodide may be the result of collisional quenching. The response therefore from bromide demonstrates the effect of these two

opposing processes. The increase in emission intensity in the presence of sulphate and acetate can also be attributed to rigidity effects. The large decrease in emission intensity upon addition of dihydrogenphosphate ions can be tentatively attributed to PET which is common among basic oxoanions.[45] It is significant that the response of the acyclic derivative **65** is in general greater than the response for the platinum (II) macrocycle **71**. This is consistent with the greater conformational freedom of the acyclic host and hence a greater increase in the rigidity of the receptor when binding anions. Anion association constants were determined by fitting of the titration data using the SPECFIT program.[46] The data confirmed a 1:1 stoichiometric binding model (Figure **3.42**) and the association constants obtained are displayed in Table **3.43**.

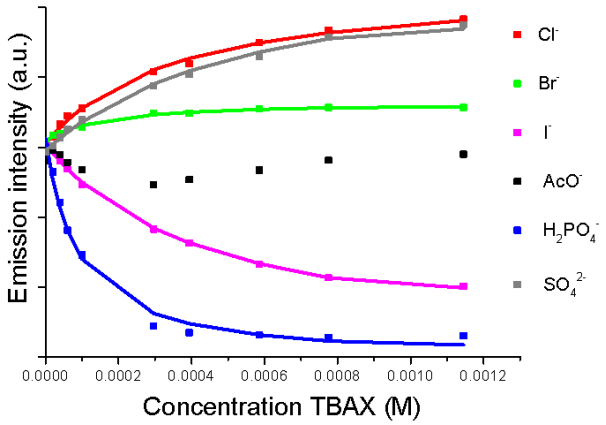

Figure 3.42: Change in the intensity of emission at 504 nm as a function of the concentration of TBA · X (X = anion) for acyclic platinum receptor **65** at 293 K (square data points represent experimental data; continuous lines represent calculated binding isotherms).

	Acyclic Pt (II) receptor 65	Macrocyclic Pt (II) receptor 71
		$\log K_A$
Chloride	3.43 (0.04)	3.43 (0.14)
Bromide	3.83 (0.09)	3.13 (0.48)
Iodide	3.39 (0.03)	3.90 (0.06)
Acetate	[a]	2.27 (0.79)
Dihydrogenphosphate	4.12 (0.04)	2.57 (0.56)
Sulphate	3.28 (0.04)	2.72 (0.54)

Table 3.43: Anion association constant values with errors in parentheses for acyclic platinum receptor **65** and macrocycle **71** in dichloromethane at 293 K ([a] Data could not be fitted to a simple binding model)

In the case of the acyclic receptor **65** the halides are all bound with comparable strength. Dihydrogenphosphate exhibits the strongest association of all the anions which is common for acyclic isophthalamide receptors.[47] Comparison of the magnitudes of halide binding of the acyclic and macrocyclic receptors reveals the acyclic receptor displays a similar strength of binding. This is thought to be due to intramolecular hydrogen bonding interactions of the isophthalamide oxygen atoms with the dipyridylbenzene ligand (Figure **3.44**), as evidenced in the ruthenium receptor crystal structures (See Figures **3.34** and **3.37**). This intramolecular hydrogen-bonding interaction increases the degree of preorganisation in the platinum receptors to such an extent that little or no macrocyclic effect is observed in the anion assocation constants. Additionally the acyclic platinum receptor displays a higher affinity for oxoanions than the corresponding macrocycle, which is typical for simple isophthalamide receptors.[48]

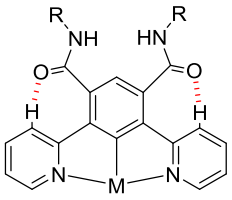

Figure 3.44: Representation of the intramolecular hydrogen-bonding by isophthalamide dipyridylbenzene metal complexes

3.3.4.2 Acyclic and macrocyclic ruthenium (II) receptors

The UV/vis absorption and emission spectra of the acyclic and macrocyclic ruthenium (II) receptors, **70** · PF_6 and **72** · PF_6 in dichloromethane are summarised in Table **3.45**, while the characteristic ^{3}MLCT absorption and near-infrared emission bands are shown in Figure **3.46**.

	λ_{max} / nm	
	MLCT absorption	**MLCT emission**
	(ε/dm^3 mol^{-1} cm^{-1})	(λ_{ex} = 530 nm)
70 · PF_6	516 (7,000)	782
	549 (7,000)	
72 · PF_6	519 (13,000)	782
	543 (13,000)	
74 · $(PF_6)_2$		782

Table 3.45: Absorption and emission data for acyclic ruthenium receptor **70** · PF_6 and macrocycle **72** · PF_6 in dichloromethane at 298 K, and emission data for rotaxane **74** · $(PF_6)_2$ in acetone/water (7:3)

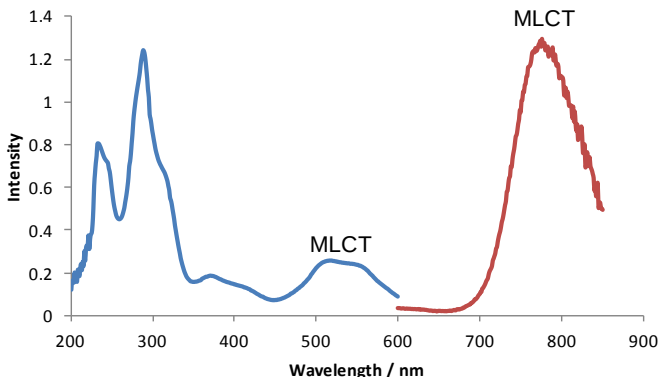

Figure 3.46: Absorption (blue line) and emission (red line) spectra of macrocyclic ruthenium (II) receptor **72** · PF_6 in dichloromethane at 293 K (spectra have been standardised for clarity)

An analogous luminescence anion titration protocol to that used for the platinum receptors was undertaken, initially in dichloromethane and then in the more competitive dichloromethane/methanol (95:5). Titrations were performed at a higher concentration of 1 × 10^{-4} M due to the lower emission intensity of the ruthenium complexes. The changes in the emission spectra, upon increasing amounts (0–30 equivalents) of TBA · Cl, of the complexes in dichlormethane/methanol (95:5) are shown in Figure **3.47**. Upon additon of chloride both systems display a decrease in the emission intensity, accompanied by a bathochromic shift for both acyclic and macrocyclic systems. The percentage change in the luminescence on addition of various anions is compiled in Figure **3.48**.

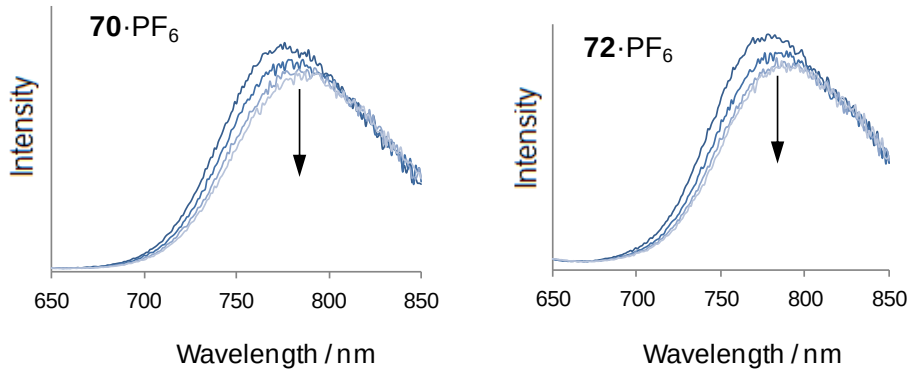

Figure 3.47: Emission spectra (λ_{ex}=530 nm) with 0–30 equivalents of TBA · Cl in dichlormethane/methanol (95:5) at 293 K of a) acyclic ruthenium receptor **70** · PF_6 and b) ruthenium macrocycle **72** · PF_6

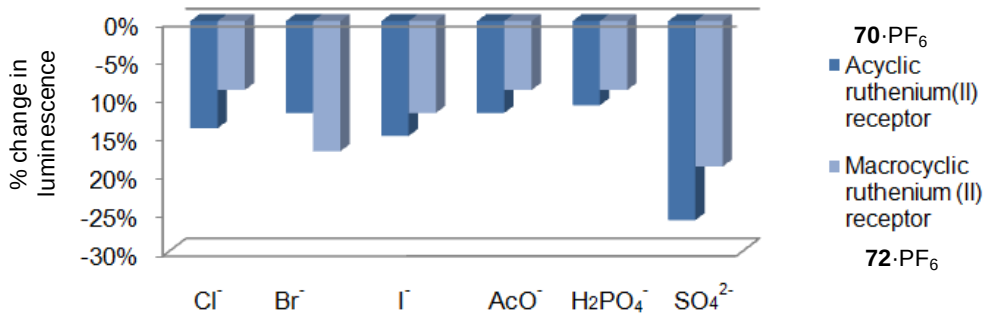

Figure 3.48: Percentage changes in luminescence emission intensity at 782nm (λ_{ex}=530 nm) between 0-30 equivalents of anion in dichloromethane/methanol (95:5) at 293K

In both receptors quenching of the luminescence was observed in the presence of all anions, which is in contrast to the behaviour observed for the platinum systems. SPECFIT analysis of the data determined 1:1 stoichiometric anion association constants which are summarised in Table **3.49**. In the case of the initial titrations in dichloromethane association constants were determined to be $\log K_a > 5$. The stronger association for the ruthenium systems is a result of the positive charge and consequent additional electrostatic contributions between host and guest. In the more competitive dichloromethane/methanol (95:5) both receptors display a modest preference for bromide among the halides. The sulphate anion has the strongest association, particularly for the acyclic ruthenium receptor, which can be rationalised on electrostatic grounds. In analogy to the platinum systems, there is again little evidence for a discernible macrocyclic effect which may be attributed to the high degree of preorganisation of the acyclic receptor due to the intramolecular hydrogen-bonding in the isophthalamide functionalised dipyridylbenzene ligand.

	70 · PF_6		**72** · PF_6
		$\log K_A$	
	DCM	**DCM/MeOH (95:5)**	**DCM/MeOH (95:5)**
Chloride	>5	3.89 (0.07)	3.65 (0.08)
Bromide	>5	4.16 (0.14)	4.09 (0.12)
Iodide	>5	3.90 (0.08)	3.77 (0.08)
Acetate	>5	3.25 (0.16)	3.34 (0.13)
Dihydrogenphosphate	>5	3.34 (0.17)	3.41 (0.07)
Sulfate	>5	4.82 (0.14)	4.08 (0.06)

Table 3.49: Anion association constant values with errors in parentheses for acyclic ruthenium receptor **70** · PF_6 and macrocycle **72** · PF_6 in dichloromethane at 293 K

3.3.5 Preliminary [2]pseudorotaxane Studies

The possibility of forming a [2]pseudorotaxane assembly between the transition metal macrocyclic receptors and a 3,5-bis-amide pyridinium chloride threading component was explored as a preliminary step towards the synthesis of target rotaxanes by a stoppering method. Quantitative [2]pseudorotaxane studies were prevented due to the insolubility of both macrocycles at concentrations required for the ^{1}H NMR titration experiments. However, a qualitative pseudorotaxane study was undertaken by mixing equimolar amounts of ruthenium macrocycle **72** · PF_6 and pyridinium thread **39** · Cl in acetonitrile-d_3 (Figure **3.50**).

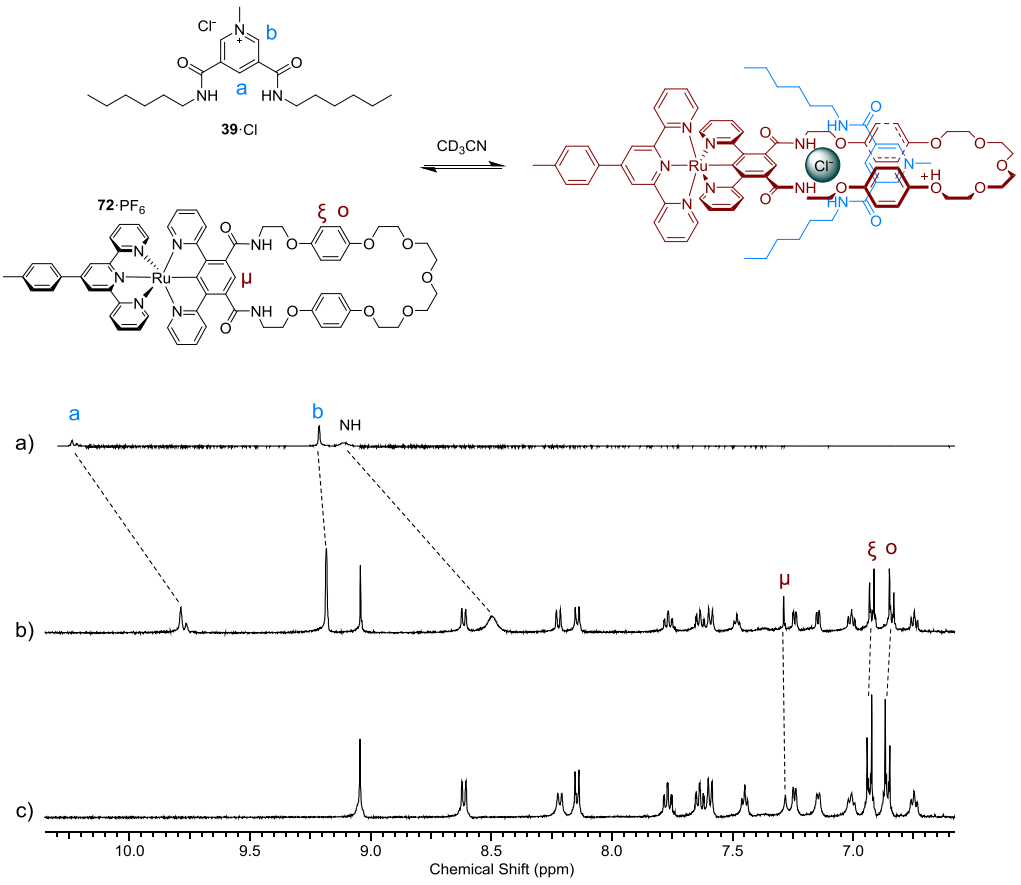

Figure 3.50: ^{1}H NMR (300 MHz, CD_3CN, 298 K) of a) 3,5-bis-amide pyridinium thread **39** · Cl b) 1:1 3,5-bis-amide pyridinium thread **39** · Cl, ruthenium macrocycle **72** · PF_6 c) ruthenium macrocycle **72** · PF_6

Significant upfield perturbations of the pyridinium thread's *a* and NH protons are observed due to the sharing of the chloride anion with the isophthalamide macrocycle. The changes in the macrocycle protons are less pronounced, the hydroquinones shift slightly upfield indicating formation of the [2]pseudorotaxane. However, the *internal* isophthalamide macrocycle proton μ shifts slightly upfield, indicating that it does not interact strongly with the halide anion, and may adopt the out of plane binding mode exhibited in the crystal structure of the acyclic ruthenium receptor (See Figure **3.34**).

3.3.6 Rotaxane Synthesis

The low solubility of the platinum and ruthenium macrocycles meant they were not compatible with a stoppering rotaxane synthesis, and as a consequence an acid chloride clipping method was chosen, using a similar protocol to that described for the preparation of the azido [2]rotaxane **54** · Cl (Scheme **3.51**). For the platinum interlocked receptor, platinum (II) bis-acid **64** was activated with oxalyl chloride and then subsequently added to a dry dichloromethane solution of bis-amine **37** and 3,5-bis-amide pyridinium axle **52** · Cl. Purification by column chromatography (DCM/MeOH 99:1→95:5), size-exclusion chromatography and preparative TLC (gradient elution DCM/MeOH 99:1→95:5) afforded the target interlocked receptor **73** · Cl in a low isolated yield of 3%.

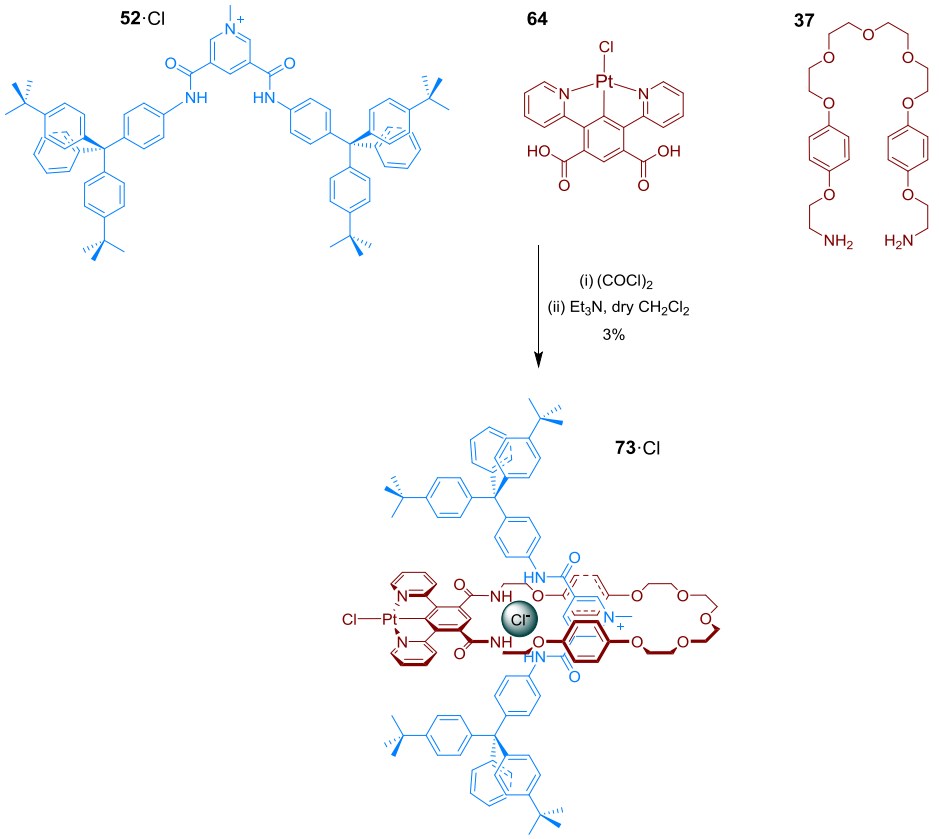

Scheme 3.51: Synthesis of platinum (II) interlocked anion receptor **73** · Cl

The rotaxane product was characterised by ^{1}H and ^{13}C NMR spectroscopy and mass spectrometry. The peak in the MALDI-MS mass spectrum was at the expected m/z = 2018.89, corresponding to $[M-Cl]^{+}$. The ^{1}H NMR spectrum of **73** · Cl, together with that of 3,5-bis-amide pyridinium axle **52** · Cl is displayed in Figure **3.52**.

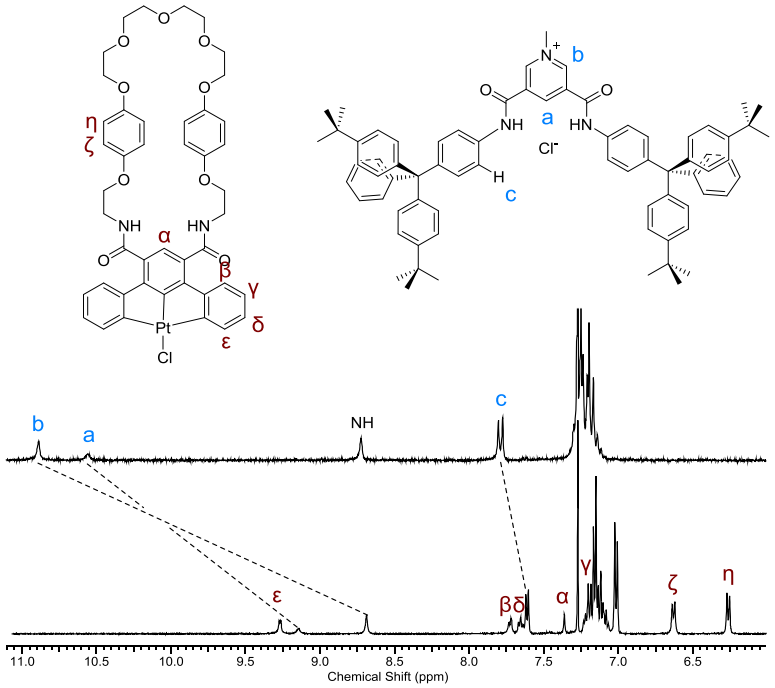

Figure 3.52: ^{1}H NMR (500 MHz, $CDCl_3/CD_3OD$ 9:1, 298 K) spectra of a) 3,5-bis-amide pyridinium axle **52** · Cl b) platinum [2]rotaxane **73** · Cl

Upon formation of the interlocked structure axle protons *a* and *b* are perturbed significantly upfield due to the sharing of the chloride anion guest, which forms additional hydrogen bonds to the macrocycle isophthalamide group in the rotaxane. Additionally the macrocycle hydroquinone protons *ζ* and *η* are split due to aromatic donor–acceptor interactions, indicative of interlocked structure formation. Two-dimensional ^{1}H-^{1}H ROESY NMR studies were undertaken to prove formation of the interlocked host (Figure **3.53**). Cross-couplings were observed between the hydroquinone protons *ζ* and *η* and the stopper protons of the axle *c*. Additional interactions are observed between *c* and the polyether region of the macrocycle. Notably there is a cross peak between the pyridinium proton *b* and the hydroquinone *η*, supporting the existence of stabilising donor–acceptor interactions between the [2]rotaxane's pyridinium and hydroquinone moieties

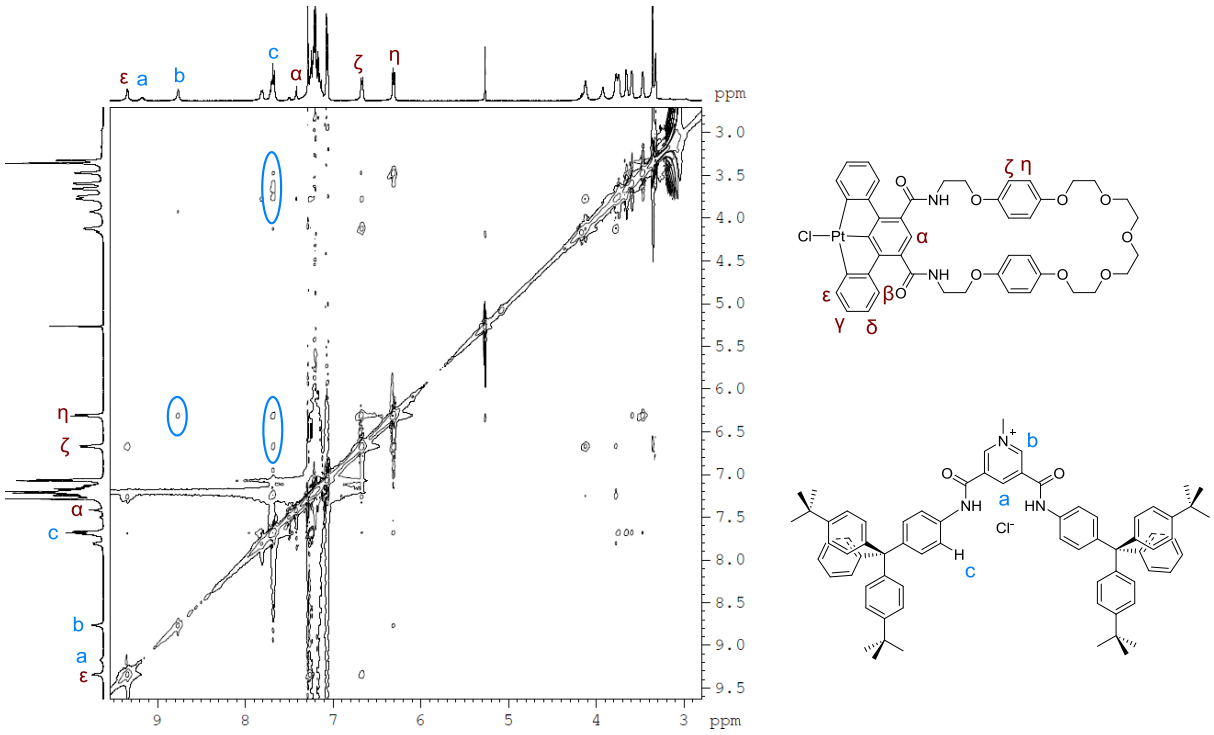

Figure 3.53: Truncated ^{1}H-^{1}H ROESY (500 MHz, $CDCl_3/CD_3OD$ 1:1, 298 K) spectrum of platinum [2]rotaxane **73** · Cl

In order to perform anion binding titrations with the rotaxane **73** · Cl , attempts were made to anion exchange to the hexafluorophosphate salt by washing a chloroform solution of the rotaxane with aqueous NH_4PF_6. Unfortunately upon washing significant degradation of the product occurred, which has been reported for analogous platinum dipyridylbenzene complexes in aerated solvents.[38] As a result of this, coupled with the inherently low yield of the interlocked product, no luminescence anion titration experiments were performed.

An analogous synthetic procedure was undertaken for the preparation of the corresponding ruthenium (II) rotaxane. (Scheme **3.54**). Purification of the crude reaction mixture by column chromatography (DCM/MeOH 95:5), size exclusion chromatography and preparative

TLC (gradient elution EtOAc/MeOH 100:0→98:2) afforded the target receptor **74** · Cl_2 in a modest isolated yield of 8%.

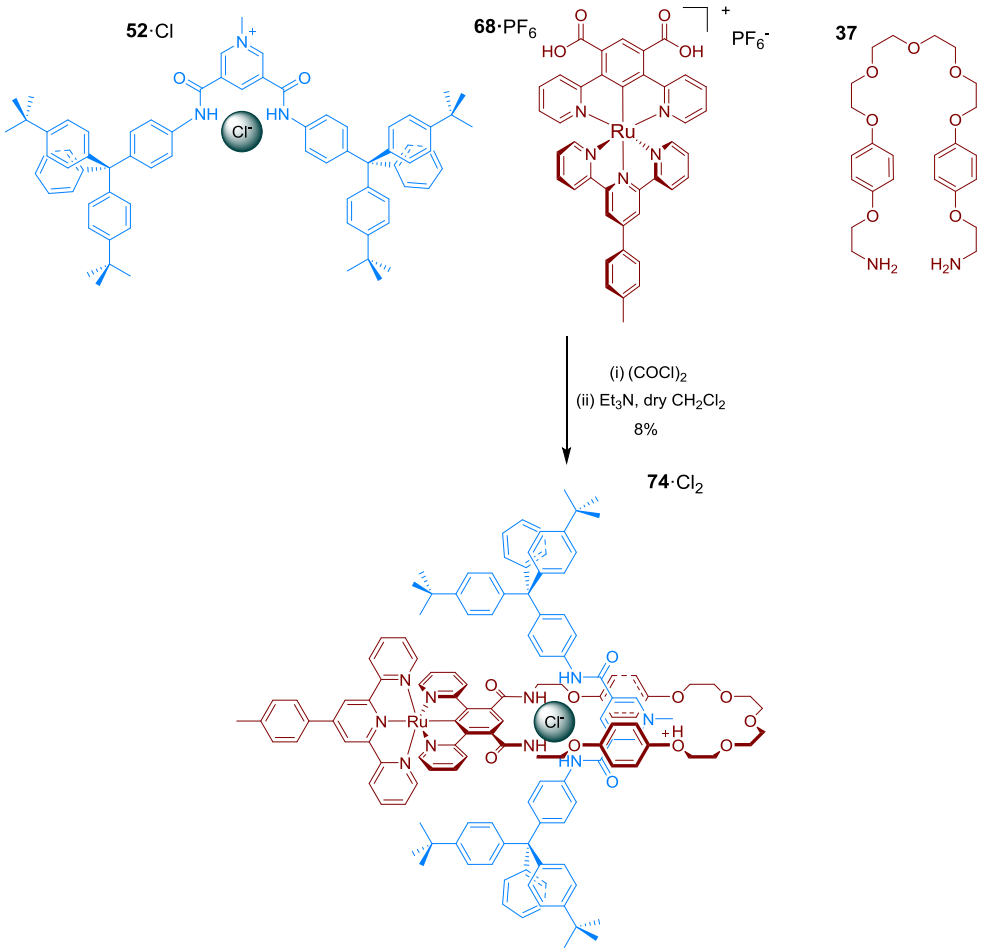

Scheme 3.54: Synthesis of ruthenium [2]rotaxane **74** · Cl_2

The ruthenium (II) rotaxane **74** · Cl_2 was characterised by ^{1}H and ^{13}C NMR spectroscopy and high-resolution mass spectrometry. The ESI-HRMS gave the expected peak at m/z = 1106.4795 which corresponds to $[M-Cl_2]^{2+}$ (Figure **3.55**).

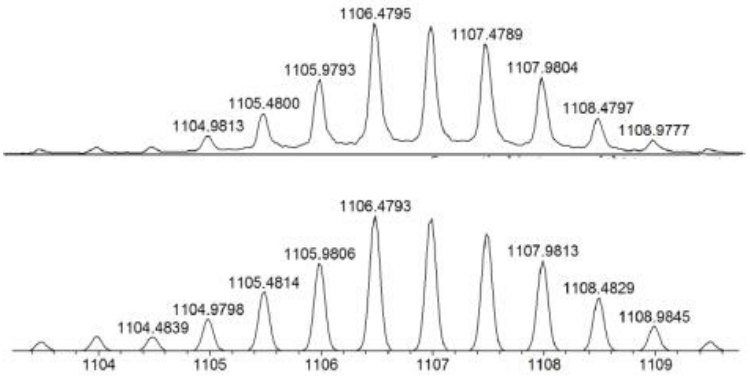

Figure 3.55: Electrospray high-resolution mass spectrum of ruthenium rotaxane **74** · Cl_2 (predicted spectrum bottom, obtained spectrum top)

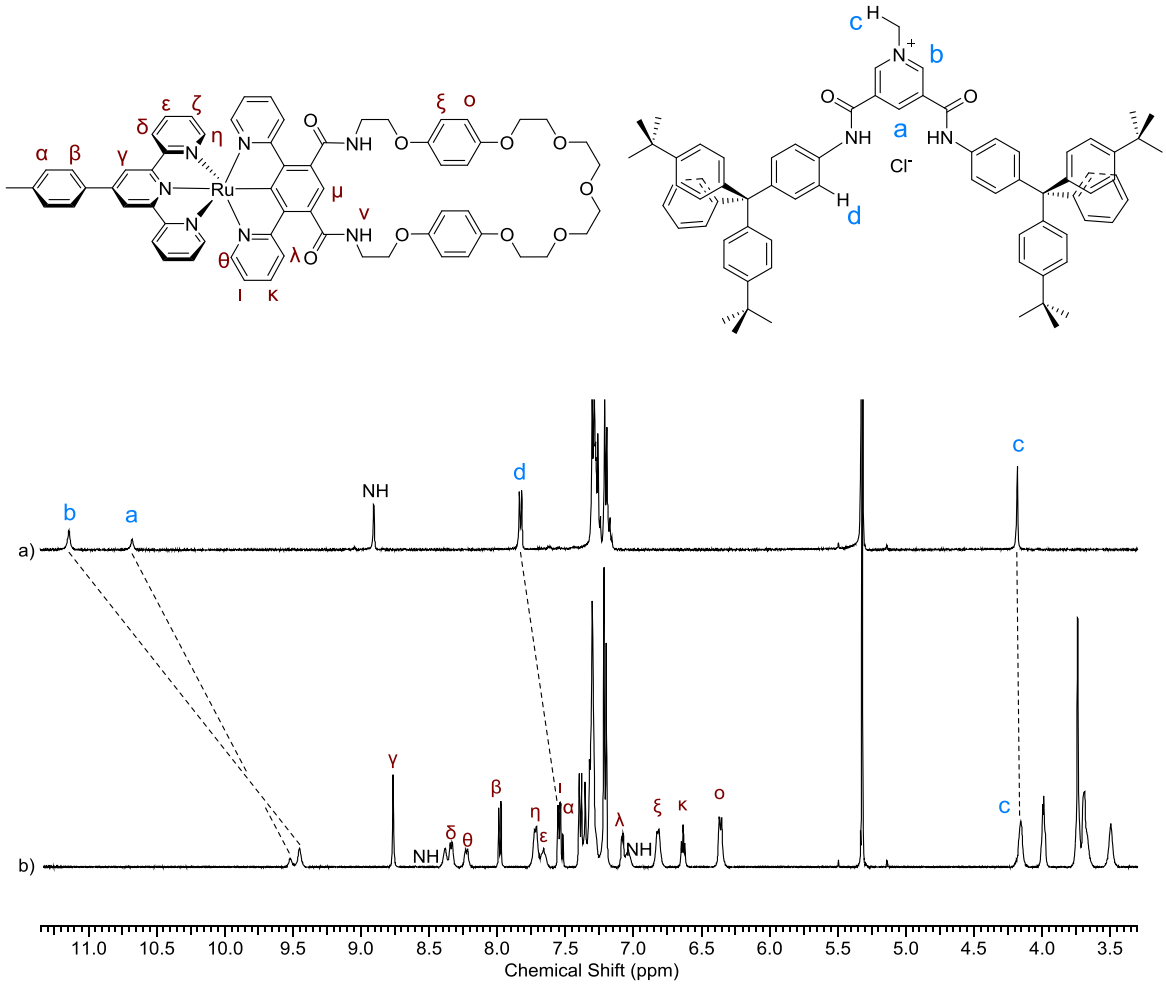

Figure 3.56: Truncated ^{1}H NMR (500 MHz, CD_2Cl_2, 298 K) spectrum of a) methyl pyridinium axle **52** · Cl b) ruthenium [2]rotaxane **74** · Cl_2

The assigned ^{1}H NMR spectrum of the rotaxane in dichloromethane-d_2 is shown in Figure **3.56**, the split hydroquinone protons *ξ* and *o* indicate donor–acceptor interactions with the pyridinium thread. A small upfield shift of the methyl pyridinium proton *c* is also observed as a result of hydrogen-bonding with the polyether portion of the macrocycle. Additionally upfield perturbations are observed in the aryl pyridinium resonances *a* and *b* upon rotaxane formation due to the chloride anion interacting with the macrocycle isophthalamide motif. ^{1}H-^{1}H two-dimensional ROESY NMR was again employed to confirm the interlocked topology of the receptor (Figure **3.57**).

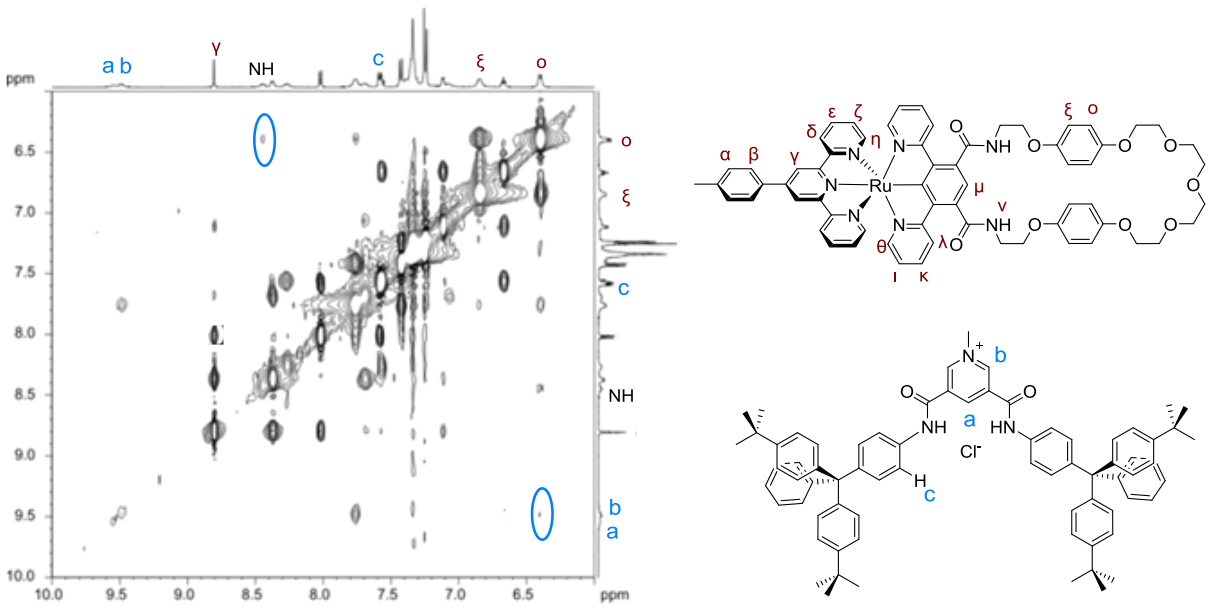

Figure 3.57: Truncated ^{1}H-^{1}H ROESY (500 MHz, CD_2Cl_2, 298 K) spectrum of ruthenium [2]rotaxane **74** · Cl_2

The two-dimensional spectrum reveals key interactions between the axle pyridinium proton *b* and the macrocycle hydroquinone proton **o**, confirming interpenetration of the assembly. There are also interactions observed between the hydroquinone proton **o** and the axle amide

protons. Additonally cross-peaks are observed between the methyl pyridinium protons and the polyether of the macrocycle (not pictured).

3.3.7 Ruthenium (II) Rotaxane Anion Binding and Luminescence Titrations

The ruthenium rotaxane chloride salt was anion exchanged to the hexafluorophosphate derivative **74** · $(PF_6)_2$ by washing with aqueous NH_4PF_6 (81%) in preparation for anion binding studies. ^{1}H NMR anion titration experiments were undertaken to determine the affinity of the rotaxane for halides and oxoanions. Titrations were carried out by monitoring the *internal* macrocycle and axle protons upon increasing equivalents of anion in the competitive aqueous solvent mixture $(CD_3)_2CO/D_2O$ (7:3). The changes in the ^{1}H NMR spectra upon the addition of chloride are displayed in Figure **3.58**.

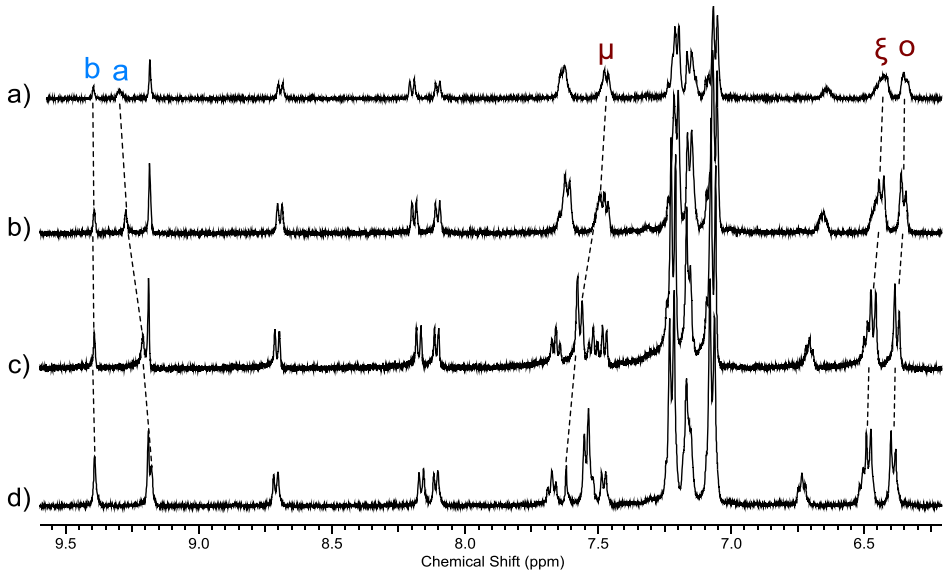

Figure 3.58: ^{1}H NMR (500 MHz, $(CD_3)_2CO/D_2O$ (7:3), 298 K) spectra of a) rotaxane **74** · $(PF_6)_2$ plus 10 equivalents of TBA · Cl b) rotaxane **74** · $(PF_6)_2$ plus 5 equivalent of TBA · Cl c) rotaxane **74** · $(PF_6)_2$ plus 1 equivalent of TBA · Cl d) rotaxane **74** · $(PF_6)_2$

The downfield shifts of the pyridinium axle protons *a* and *b* are indicative of chloride binding within the rotaxane cavity. However, the shifts of the *internal* macrocycle resonance *μ* are perturbed upfield which suggests little interaction of this proton with the chloride anion. Likewise upfield shifts of the macrocycle hydroquinone protons ζ and o are observed upon addition of chloride. This behaviour, in addition to the X-ray single crystal analysis of compound **70**·Cl and [2]pseudorotaxane studies, suggests that chloride is bound only partially within the rotaxane cavity to maximise the electrostatic interactions with the cationic ruthenium complex. The rotaxane host proton signal changes upon acetate and dihydrogenphosphate addition were negligible, which indicates these oxoanions are not bound in this aqueous solvent mixture. The titration data for chloride was analysed using the WinEQNMR2 program by monitoring the *internal* axle proton *a* (Figure **3.59**) to determine a 1:1 stoichiometric association constant of 196 ± 13 M^{-1}. Hence the rotaxane is capable of binding chloride selectively in a highly competitive aqueous solvent system that contains 30% water.

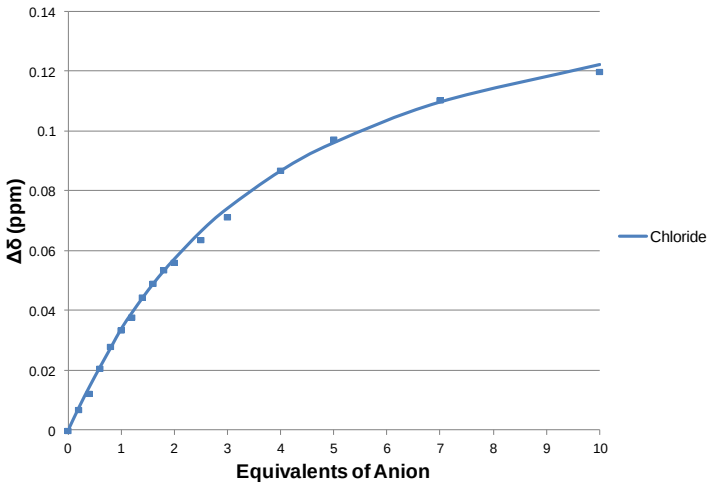

Figure 3.59: Changes in the chemical shift of proton *a* upon addition of increasing amounts of anion in $(CD_3)_2CO/D_2O$ (7:3)

In order to assess the capability for the interlocked ruthenium receptor **74** · $(PF_6)_2$ to act as an effective sensor for chloride, qualitative luminescence titrations were undertaken. The rotaxane host retained all the photophysical properties of the parent macrocycle, exhibiting emission at 782 nm (Table **3.4**5). The changes in the emission spectra upon addition of increasing amounts (0–30 equivalents) of TBA · Cl in acetone/water (7:3) are shown in Figure **3.60**. As was observed with the acyclic and macrocyclic ruthenium receptors, the interlocked host exhibits a modest quenching of the MLCT emission band in response to chloride, with a concomitant bathochromic shift. Analogous preliminary luminescence titrations with acetate and dihydrogenphosphate also resulted in modest quenching. Given the ^{1}H NMR titration results indicated the oxoanions are not bound in the rotaxane cavity in this competitive aqueous solvent mixture, the observed luminescence quenching is unexpected and suggests that chloride and oxoanion induced responses of the rotaxane may be a result of simple collisional quenching between the anion and the positively charged complex as opposed to recognition within the interlocked binding cleft.

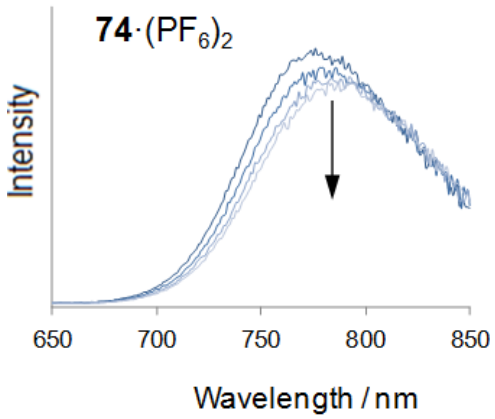

Figure 3.60: Emission spectra (λ_{ex}=530 nm) with 0–30 equivalents of TBA · Cl in acetone/water (7:3) at 293 K of ruthenium rotaxane **74** · $(PF_6)_2$

3.3.8 Summary

The synthesis of a new class of transition metal dipyridylbenzene anion receptor was accomplished. Luminescent platinum (II) and ruthenium (II) dipyridylbenzene ligand complexes were incorporated into acyclic, macrocyclic and interlocked structures *via* an acid chloride condensation strategy.

The acyclic and macrocyclic platinum (II) receptors were shown to bind halides and oxoanions in dichloromethane. The macrocyclic platinum host also displayed selectivity for the halides over oxoanions. The ruthenium (II) analogues had a greater affinity for anions due to the positive charge of the complex. Both receptors were selective for halides over acetate and dihydrogenphosphate in dichloromethane/methanol (95:5); however sulphate was bound most strongly on electrostatic grounds. In addition both platinum and ruthenium receptors were found to display a luminescent response in the presence of halides and oxoanions. The acyclic and macrocyclic platinum (II) sensors gave a range of luminescence responses that depended upon the nature of the receptor and anion guest species, with the acyclic host exhibiting a 50% increase in the emission intensity in the presence of chloride. By contrast the corresponding acyclic and macrocyclic ruthenium (II) systems demonstrated a quenching of MLCT emission upon addition of all anions.

Rotaxane platinum (II) and ruthenium (II) receptors were successfully synthesised *via* an acid chloride clipping methodology and isolated in modest yields. ^{1}H NMR anion titrations revealed the interlocked ruthenium (II) host to be selective for chloride with no evidence of binding oxoanions in the highly competitive aqueous solvent (acetone/water 7:3). Preliminary

luminescence titrations demonstrated that the ruthenium (II) rotaxane exhibited modest quenching of the MLCT luminescence upon addition of chloride and unexpectedly oxoanions which, taking into account the NMR binding results, is most likely to be due to collisional quenching effects and not binding in the interlocked cavity.

3.4 Conclusions

In this chapter the use of metal-based luminophores as reporter groups for anion receptors was explored. The first lanthanide-containing rotaxane was sucessfully synthesised and, in addition, ruthenium and platinum complexes were incorporated into acyclic, macrocyclic and rotaxane hosts. The method of incorporation for the lanthanide complex was *via* a post-synthetic modification strategy which used a CuAAC click reaction to covalently attach a lanthanide cyclen complex after [2]rotaxane synthesis. In the case of the transition metal receptors the dipyridylbenzene ligand was functionalised with a 3,5-bis-amide motif and macrocyclic and interlocked hosts were synthesised by metal complexed reactant acid-chloride clipping reactions.

The europium containing [2]rotaxane was shown to bind and sense chloride in dichloromethane solution. In the case of chloride the luminescence was dramatically quenched followed by a gradual enhancement. This is due to a two-step binding process for chloride which occurs at the ninth axial coordination site of the lanthanide and in the [2]rotaxane cavity. Due to the selecivity imparted by the [2]rotaxane cavity the binding of acetate and dihydrogenphosphate occured only at the lanthanide metal centre, enabling luminescent discrimination between chloride and the oxoanions.

Platinum (II) and ruthenium (II) dipyridylbenzene complex functionalised acyclic and macrocyclic receptors were successfully prepared. The platinum (II) receptors were found to exhibit varied spectroscopic changes in their emission spectra upon anion binding, demonstrating their ability to discriminate between anionic guests by luminescence. The emissive response of the acyclic and macrocyclic ruthenium (II) receptors was less pronounced; all anions induced a small quenching and bathochromic shift. In addition [2]rotaxanes incorporating the platinum (II) and ruthenium (II) dipyridylbenzene complexes were successfully prepared. Anion ^{1}H NMR titration experiments demonstrated the ruthenium [2]rotaxane has a high affinity for chloride in highly competitive aqueous solvent media (acetone/water 7:3). The MLCT luminescence response of the interlocked receptor, however, was similar for chloride and the oxoanions which suggests that the emissive behaviour is due to collisional processes rather than modulation through binding in the rotaxane cavity. The range of luminescent responses exhibted by the acyclic and macrocyclic platinum (II) indicates that platinum dipyridylbenzene complexes are more promising candidates for constructing effective halide sensors than their ruthenium congeners. As such future investigations should focus on interlocked platinum dipyridylbenzene complexes as luminescent probes for anions if the problem of stability could be circumvented and the yield of rotaxanation improved through use of a different synthetic method such as stoppering.

Exploiting the post-synthetic rotaxane click methodology which was used to covalently attach a lanthanide cyclen complex to the periphery of the rotaxane framework, the next chapter discusses related synthetic strategies as potential routes to the construction of higher order interlocked assemblies.

3.5 References

1. H. N. Kim, W. X. Ren, J. S. Kim and J. Yoon, *Chem. Soc. Rev.*, 2012, **41**, 3210-3244.
2. G. DeSantis, L. Fabbrizzi, M. Licchelli, A. Poggi and A. Taglietti, *Angew. Chem.-Int. Edit. Engl.*, 1996, **35**, 202-204.
3. F. Zapata, A. Caballero, A. Espinosa, A. Tarraga and P. Molina, *Org. Lett.*, 2008, **10**, 41-44.
4. A. P. de Silva, H. Q. N. Gunaratne, T. Gunnlaugsson, A. J. M. Huxley, C. P. McCoy, J. T. Rademacher and T. E. Rice, *Chem. Rev.*, 1997, **97**, 1515-1566.
5. R. M. Duke, E. B. Veale, F. M. Pfeffer, P. E. Kruger and T. Gunnlaugsson, *Chem. Soc. Rev.*, 2010, **39**, 3936-3953.
6. T. Gunnlaugsson, M. Glynn, G. M. Tocci, P. E. Kruger and F. M. Pfeffer, *Coord. Chem. Rev.*, 2006, **250**, 3094-3117.
7. M. J. Langton and P. D. Beer, *Acc. Chem. Res.*, 2014, **47**, 1935-1949.
8. G. T. Spence and P. D. Beer, *Acc. Chem. Res.*, 2013, **46**, 571-586.
9. K. M. Mullen, J. Mercurio, C. J. Serpell and P. D. Beer, *Angew. Chem.-Int. Ed.*, 2009, **48**, 4781-4784.
10. G. Kaiser, T. Jarrosson, S. Otto, Y. F. Ng, A. D. Bond and J. K. M. Sanders, *Angew. Chem.-Int. Edit.*, 2004, **43**, 1959-1962.
11. S.-Y. Hsueh, C.-C. Lai, Y.-H. Liu, S.-M. Peng and S.-H. Chiu, *Angew. Chem.-Int. Ed.*, 2007, **46**, 2013-2017.
12. Y. Nakatani, Y. Furusho and E. Yashima, *Angew. Chem.-Int. Ed.*, 2010, **49**, 5463-5467.
13. J. J. Gassensmith, S. Matthys, J. J. Lee, A. Wojcik, P. V. Kamat and B. D. Smith, *Chem.-Eur. J.*, 2010, **16**, 2916-2921.
14. C. G. Collins, E. M. Peck, P. J. Kramer and B. D. Smith, *Chem. Sci.*, 2013, **4**, 2557-2563.
15. N. H. Evans, C. J. Serpell and P. D. Beer, *Chem. Commun.*, 2011, **47**, 8775-8777.
16. W. Zhu, W. Li, C. Wang, J. Cui, H. Yang, Y. Jiang and G. Li, *Chem. Sci.*, 2013, **4**, 3583-3590.
17. S.-Y. Hsueh, C.-C. Lai and S.-H. Chiu, *Chem.–Eur. J.*, 2010, **16**, 2997-3000.
18. M. R. Sambrook, D. Curiel, E. J. Hayes, P. D. Beer, S. J. A. Pope and S. Faulkner, *New J. Chem.*, 2006, **30**, 1133-1136.
19. L. M. Hancock, E. Marchi, P. Ceroni and P. D. Beer, *Chem.-Eur. J.*, 2012, **18**, 11277-11283.
20. C. E. Felton, L. P. Harding, J. E. Jones, B. M. Kariuki, S. J. A. Pope and C. R. Rice, *Chem. Commun.*, 2008, 6185-6187.
21. D. Parker, *Coord. Chem. Rev.*, 2000, **205**, 109-130.
22. C. P. Montgomery, B. S. Murray, E. J. New, R. Pal and D. Parker, *Acc. Chem. Res.*, 2009, **42**, 925-937.
23. D. G. Smith, R. Pal and D. Parker, *Chem.-Eur. J.*, 2012, **18**, 11604-11613.

24. E. G. Moore, A. P. S. Samuel and K. N. Raymond, *Acc. Chem. Res.*, 2009, **42**, 542-552.
25. S. Faulkner, S. J. A. Pope and B. P. Burton-Pye, *Appl. Spectrosc. Rev.*, 2005, **40**, 1-31.
26. D. Parker and J. H. Yu, *Chem. Commun.*, 2005, 3141-3143.
27. J. A. Wisner, P. D. Beer, M. G. B. Drew and M. R. Sambrook, *J. Am. Chem. Soc.*, 2002, **124**, 12469-12476.
28. L. M. Hancock and P. D. Beer, *Chem.-Eur. J.*, 2009, **15**, 42-44.
29. M. Tropiano, N. L. Kilah, M. Morten, H. Rahman, J. J. Davis, P. D. Beer and S. Faulkner, *J. Am. Chem. Soc.*, 2011, **133**, 11847-11849.
30. M. Jauregui, W. S. Perry, C. Allain, L. R. Vidler, M. C. Willis, A. M. Kenwright, J. S. Snaith, G. J. Stasiuk, M. P. Lowe and S. Faulkner, *Dalton Trans.*, 2009, 6283-6285.
31. R. S. Dickins, D. Parker, J. I. Bruce and D. J. Tozer, *Dalton Trans.*, 2003, 1264-1271.
32. P. Kuzmic, *Anal. Biochem.*, 1996, **237**, 260-273.
33. B. Soro, S. Stoccoro, G. Minghetti, A. Zucca, M. A. Cinellu, M. Manassero and S. Gladiali, *Inorg. Chim. Acta*, 2006, **359**, 1879-1888.
34. R. C. Evans, P. Douglas and C. J. Winscom, *Coord. Chem. Rev.*, 2006, **250**, 2093-2126.
35. A. Auffrant, A. Barbieri, F. Barigelletti, J. P. Collin, L. Flamigni, C. Sabatini and J. P. Sauvage, *Inorg.Chem.*, 2006, **45**, 10990-10997.
36. F. Barigelletti, L. Flamigni, V. Balzani, J. P. Collin, J. P. Sauvage, A. Sour, E. C. Constable and A. Thompson, *Coord. Chem. Rev.*, 1994, **132**, 209-214.
37. J. A. G. Williams, *Chem. Soc. Rev.*, 2009, **38**, 1783-1801.
38. J. A. G. Williams, A. Beeby, E. S. Davies, J. A. Weinstein and C. Wilson, *Inorg. Chem.*, 2003, **42**, 8609-8611.
39. A. J. Wilkinson, H. Puschmann, J. A. K. Howard, C. E. Foster and J. A. G. Williams, *Inorg.Chem.*, 2006, **45**, 8685-8699.
40. H. Nierengarten, J. Rojo, E. Leize, J.-M. Lehn and A. Van Dorsselaer, *Eur. J. Inorg. Chem.*, 2002, **2002**, 573-579.
41. L. Chardonnens, P. Sunderplassmann and T. Stauner, *Helv. Chim. Acta*, 1979, **62**, 657-666.
42. B. Wieczorek, B. Lemcke, H. P. Dijkstra, M. R. Egmond, R. J. M. Klein Gebbink and G. van Koten, *Eur. J. Inorg. Chem.*, 2010, **2010**, 1929-1938.
43. A. Winter, A. M. J. van den Berg, R. Hoogenboom, G. Kickelbick and U. S. Schubert, *Synthesis*, 2007, 642-642.
44. S. H. Wadman, R. W. A. Havenith, F. Hartl, M. Lutz, A. L. Spek, G. P. M. van Klink and G. van Koten, *Inorg. Chem.*, 2009, **48**, 5685-5696.
45. E. B. Veale, G. M. Tocci, F. M. Pfeffer, P. E. Kruger and T. Gunnlaugsson, *Org. Biomol. Chem.*, 2009, **7**, 3447-3454.
46. SPECFIT, 2.02, Spectrum Software Associates, Chapel Hill, NC.
47. K. Kavallieratos, C. M. Bertao and R. H. Crabtree, *J. Org. Chem.*, 1999, **64**, 1675-1683.
48. P. A. Gale, *Acc. Chem. Res.*, 2006, **39**, 465-475.

Chapter 4: Higher Order Interlocked Structures

4.1: Introduction to Higher Order Interlocked Assemblies

Since the synthesis of the first interlocked structures in the 1960s,[1-3] chemists have sought to prepare ever more exotic and impressive interlocked and interlinked assemblies. These include complex architectures such as trefoil knots (Figure **4.1a**),[4-6] Solomon's links[7, 8] and borromean rings.[9-11] Recent work by Leigh has built upon the pioneering studies by Lehn on metal helicates to construct the first pentafoil knot by reversible imine bond formation (Figure **4.1b**).[12, 13]

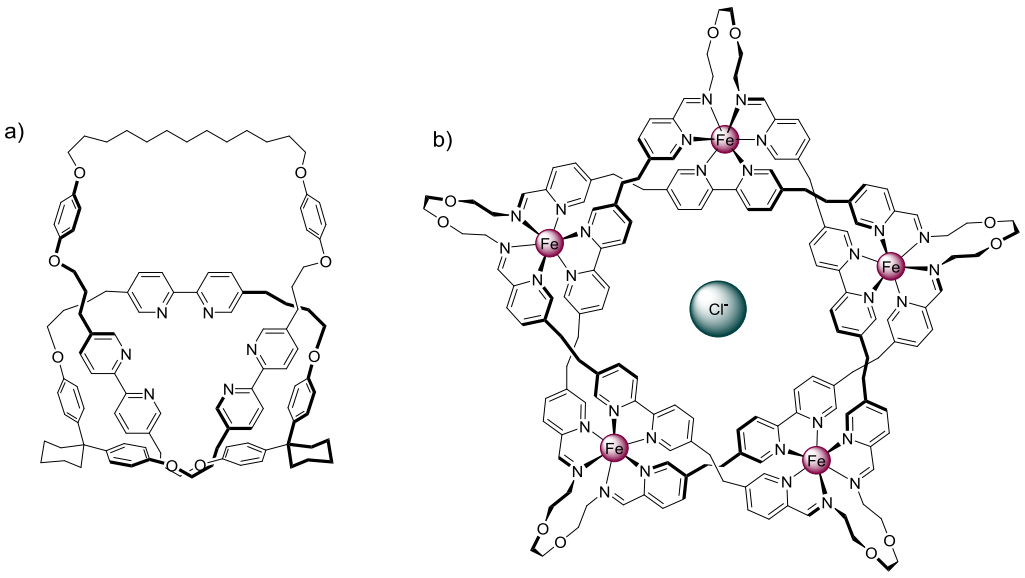

Figure 4.1: Interlocked and Interlinked Assemblies; a) Hunter's trefoil knot b) Leigh's pentafoil knot

The interest in these impressive interlocked structures stems not only from their synthetic complexity; many higher order switchable devices have been realised, such as molecular elevators,[14, 15] synthetic muscles[16, 17] and molecular lassos.[18] The unique topology of these complex interlocked architectures enables switchable motion that is not possible in simple

[2]rotaxanes or [2]catenanes. For example Sauvage has reported a [4]rotaxane molecular 'press' that is switched in the presence and absence of copper (I) ions (Figure **4.2**).[19, 20]

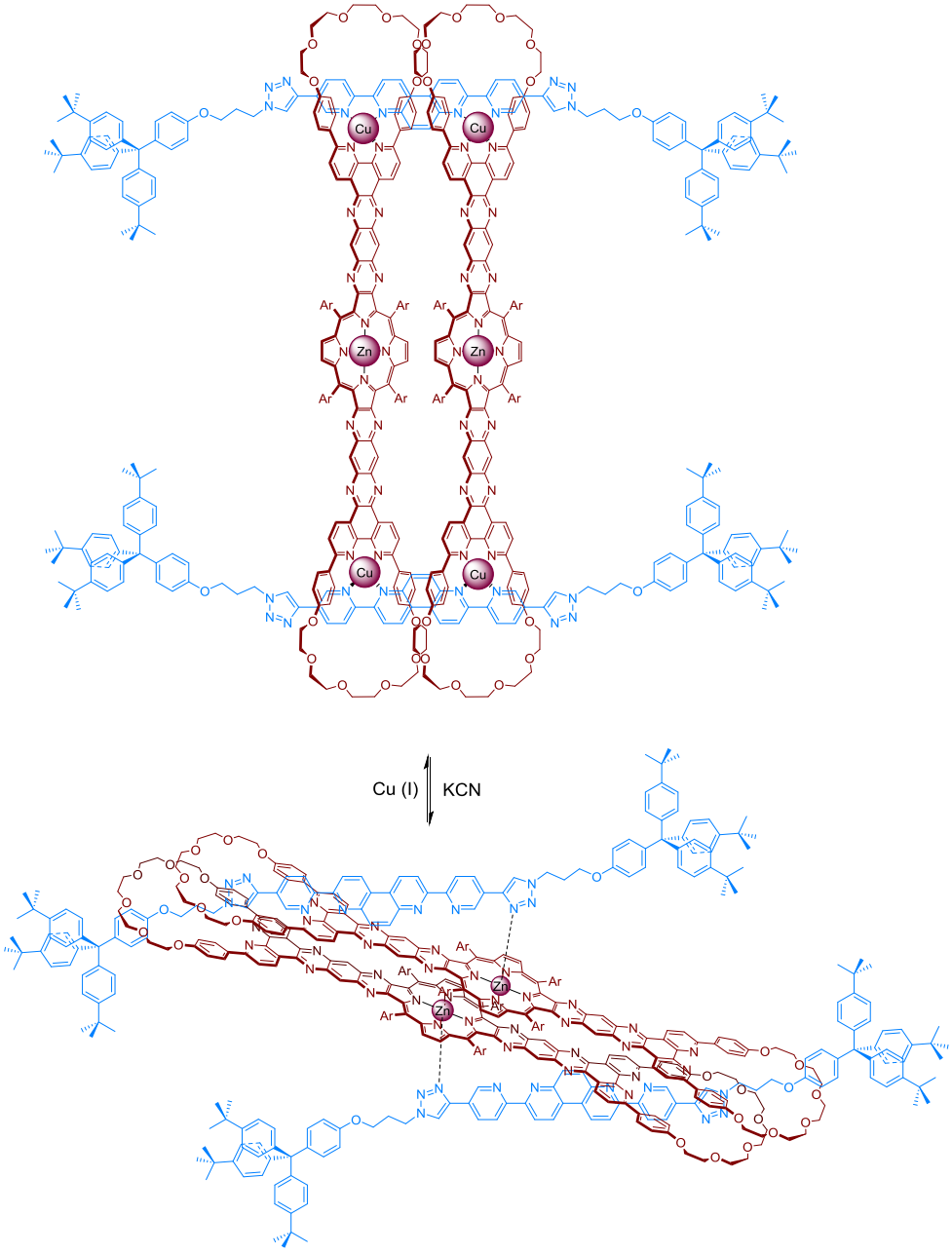

Figure 4.2: Sauvage's [4]rotaxane molecular press

In the presence of copper (I) ions the [4]rotaxane is in an extended conformation; however upon removal of the metal with cyanide the structure collapses. Ligation of the axle triazole groups to the zinc porphyrin greatly reduces the distance between the two porphyrin centres

and thus the molecule acts as a compressor. Indeed it was found that bridging ligands such as 1,4-diazabicyclo[2.2.2]octane (DABCO) were excluded in the compressed conformer due to the close interatomic zinc–zinc distance.

4.2: Higher Order Anion-Templated Interlocked Assemblies

While the formation of interlocked structures by anion-templation is rare, several examples have appeared recently in the literature. Anion-templated [3]catenanes have been prepared by the Beer group (Figure **4.3a**) [2122] while [3]rotaxanes containing one axle and two threaded macrocycles have been realised in Flood's organophosphate-templated [3]rotaxane[23] (Figure **4.3b**) and Beer's electrochemical[24] and fluorescent[25] anion sensors (Figure **4.3c**).

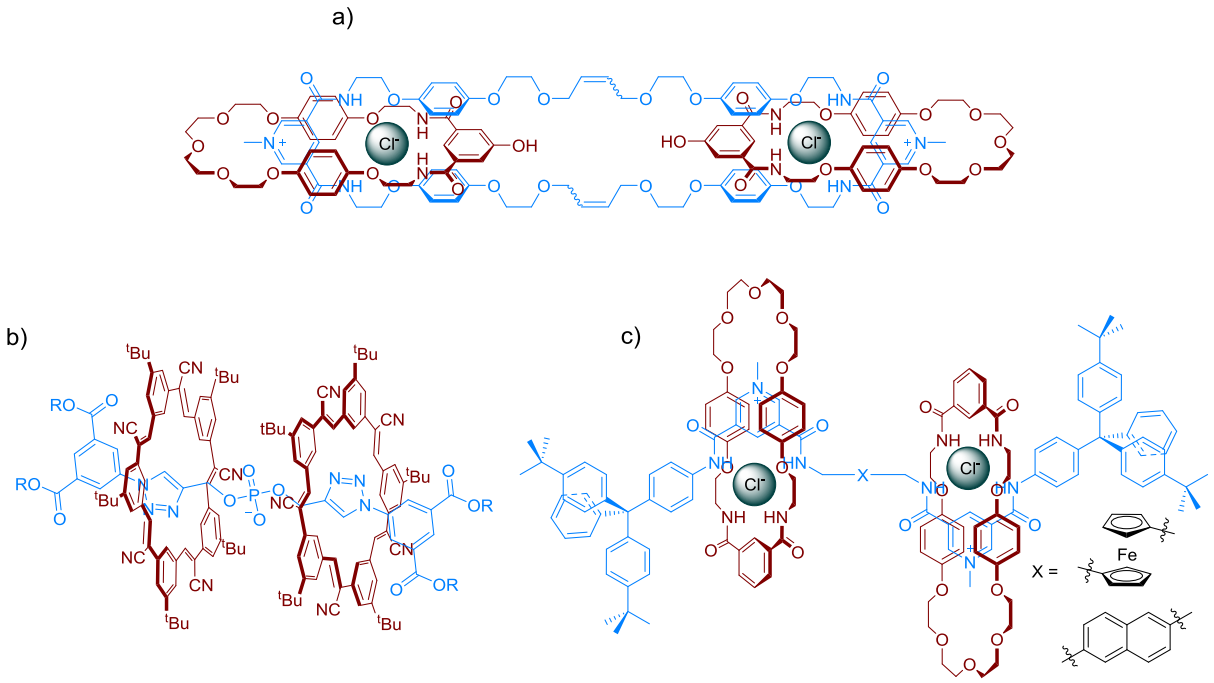

Figure 4.3: Anion-templated higher order interlocked assemblies; a) chloride-templated [3]catenane b) organophosphate-templated [3]rotaxane c) chloride-templated [3]rotaxanes

In an extension of the work on the serendipitous anion-templated [3]catenane in Figure **4.3a,** the first anion-templated 'handcuff' catenane was reported which covalently linked two isophthalamide macrocycles.[26] Forming a [3]pseudorotaxane assembly via chloride anion templation, the bis-vinyl functionalised threading components were subsequently coupled using a double Grubbs' ring closing metathesis (RCM) reaction to produce the handcuff catenane in 30% yield (Scheme **4.4**).

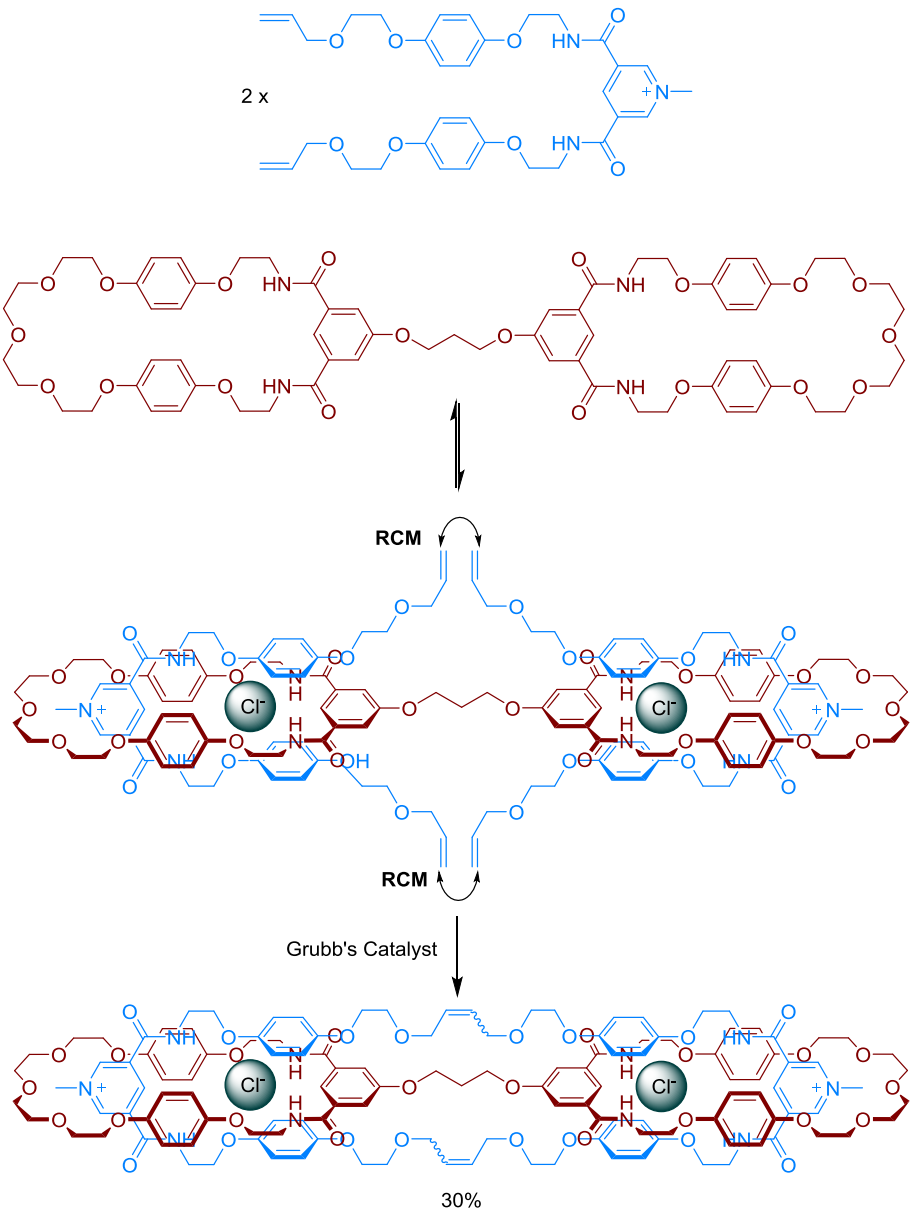

Scheme 4.4: Synthesis of a 'handcuff' catenane by chloride anion-templation and a double Grubbs' ring closing metathesis clipping reaction.

4.3 Chapter Objectives

While 'simple' interlocked structures such as [2]rotaxanes and [2]catenanes have become commonplace within the literature,[27, 28] the synthesis of higher order interlocked architectures have been less well explored.[29] This is partly due to the synthetically onerous nature of preparing such complex assemblies. Given the success in utilising the CuAAC click reaction in post-synthetic modification of an azido [2]rotaxane, discussed in the previous chapter, it was envisaged that this strategy could be employed to prepare higher order interlocked structures by a new facile route (Figure **4.5**). This method would involve the synthesis of an appropriate alkyne functionalised [2]rotaxane which could undergo a copper (I) catalysed click reaction with the corresponding azide-functionalised rotaxane to form a novel triazole-linked 'handcuff' [3]rotaxane. In a more ambitious strategy the preparation of a [4]rotaxane was also attempted. It was anticipated that alkylation of the triazole based [3]rotaxane would provide an additional anion-binding triazolium site which could be exploited to furnish an unprecedented 'rotaxane stoppered' [4]rotaxane via an anion-templated Grubbs' ring closing metathesis clipping reaction[30] (Figure **4.5**).

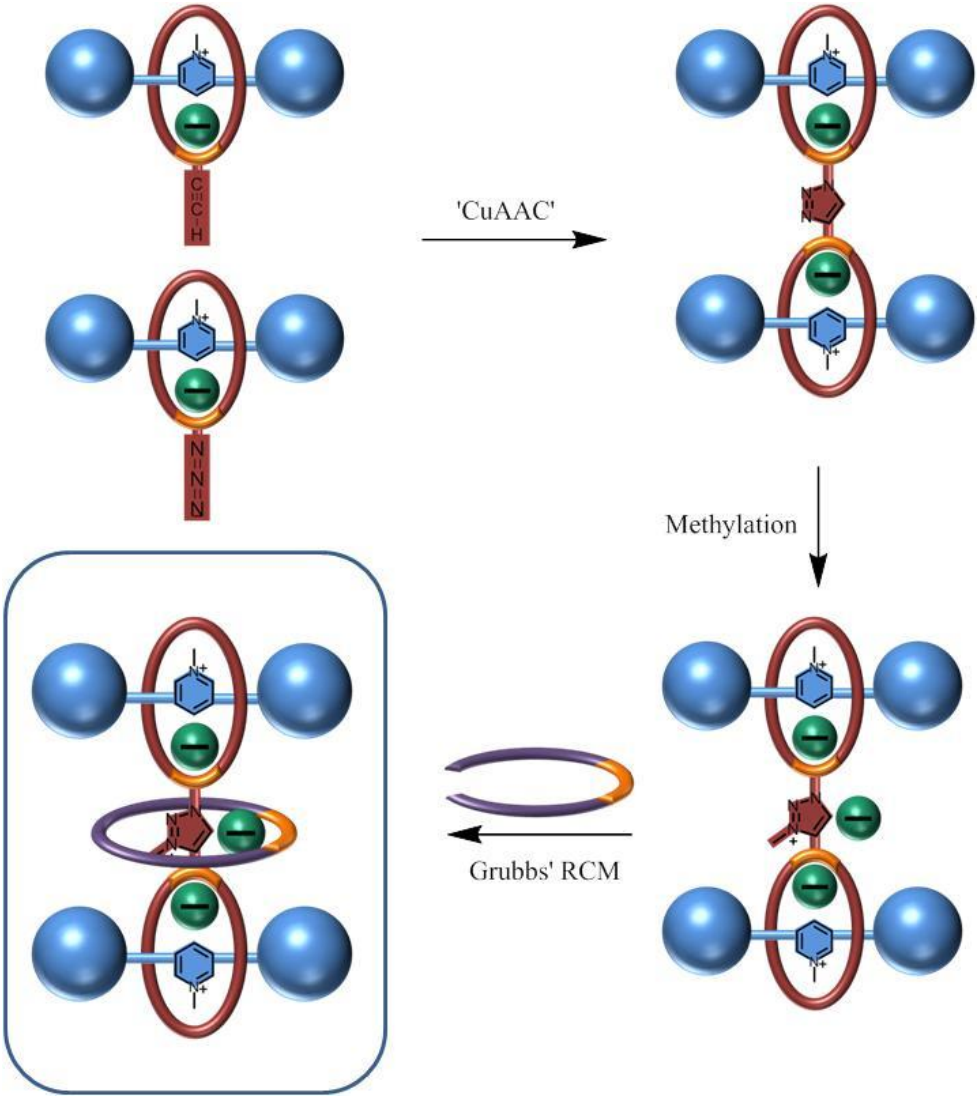

Figure 4.5: Cartoon representation of the synthesis of higher order interlocked structures by 'CuAAC' and anion templation

4.4 Alkyne [2]Rotaxane Synthesis

Having already synthesised the azido functionalised [2]rotaxane **54** · Cl it was necessary to prepare the analogous alkyne appended interlocked structure. This required the synthesis of 5-alkynyl isophthalic acid, which was accomplished according to an adapted literature procedure (Scheme **4.6**).[31] Commercially available 5-bromoisophthalic acid was esterified with

methanol under acidic conditions to obtain compound **75** in high yield (89%). A palladium (II) catalysed Sonogashira reaction between **75** and 2-methylbut-3-yn-2-ol afforded the intermediate **76**. Attempted deprotection of **76** under one-pot basic conditions resulted in only the methyl esters being hydrolysed and so a two step deprotection method was undertaken. The alcohol moiety was first cleaved with NaH in toluene to afford **77** in 80% yield. The bis-ester was then hydrolysed using KOH in *n*-butanol to give the target 5-ethynylisophthalic acid **78**.

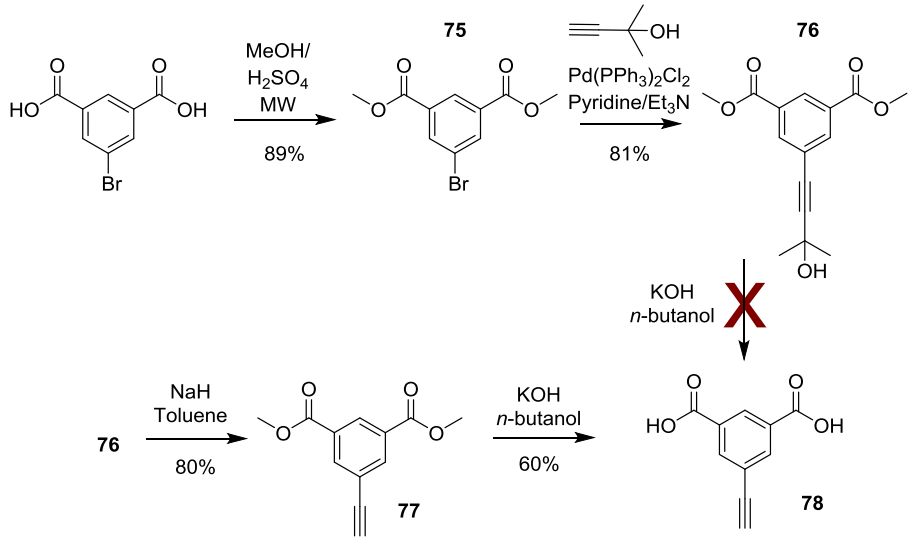

Scheme 4.6: Synthesis of 5-ethynylisophthalic acid **78**

The synthesis of the rotaxane was conducted according to the procedure previously described for the preparation of the azido functionalised [2]rotaxane **54** · Cl. Compound **78** was converted to the bis-acid chloride using oxalyl chloride and added to a solution of bis-amine **37** and 3,5-bis-amide pyridinium axle **52** · Cl in the presence of triethylamine in dry dichloromethane (Scheme **4.7**). Purification of the crude reaction mixture by column chromatography (gradient elution DCM/MeOH 98:2→95:5) and preparative TLC (gradient

elution DCM/MeOH 99:1→97:3) afforded the target alkyne functionalised [2]rotaxane **79** · Cl in 36% yield.

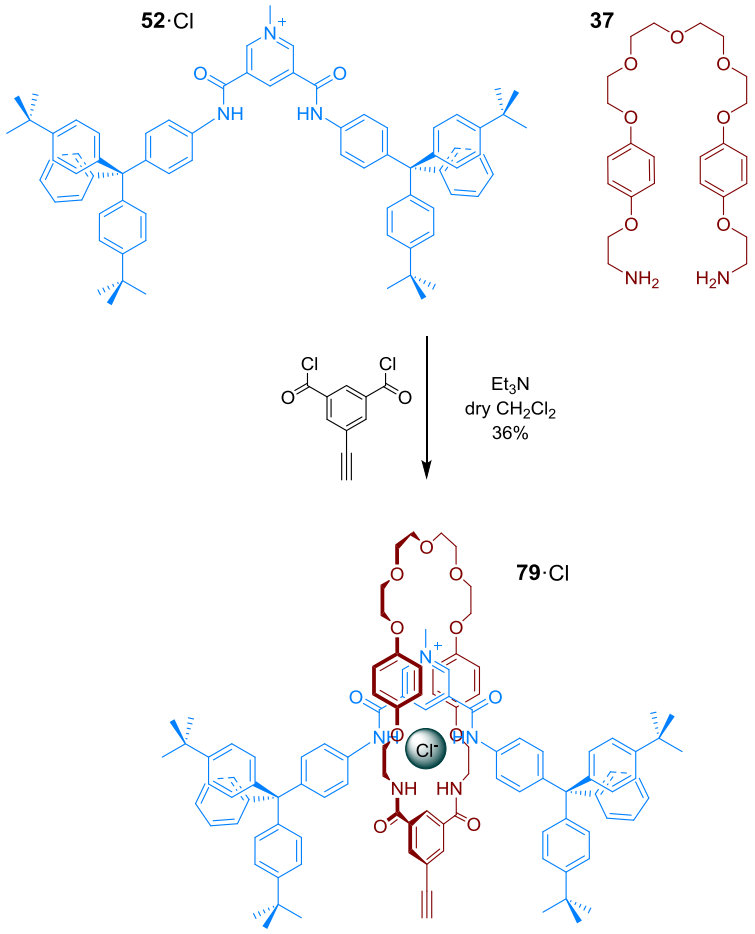

Scheme 4.7: Synthesis of alkyne functionalised [2]rotaxane **79** · Cl

The compound was characterised by ^{1}H NMR, high-resolution mass spectrometry and X-ray diffraction single crystal structural analysis. The compound gave a peak in the mass spectrum at m/z = 1659.8701, which corresponds to [M-Cl]$^+$ (Figure **4.8**). The ^{1}H NMR spectrum is displayed in Figure **4.9** with pyridinium axle **52** · Cl for comparison.

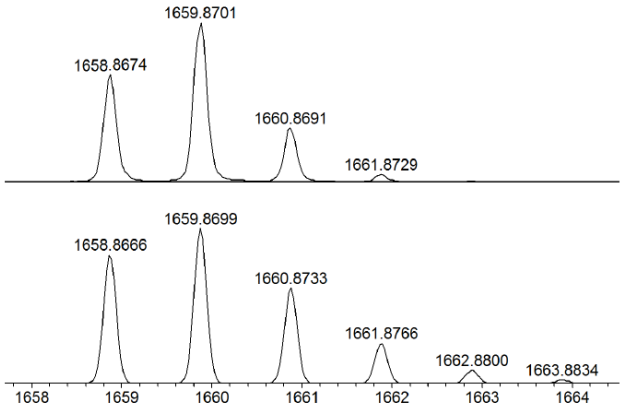

Figure 4.8: Electrospray high-resolution mass spectrum of [2]rotaxane **79** · Cl (predicted spectra bottom; obtained spectra top)

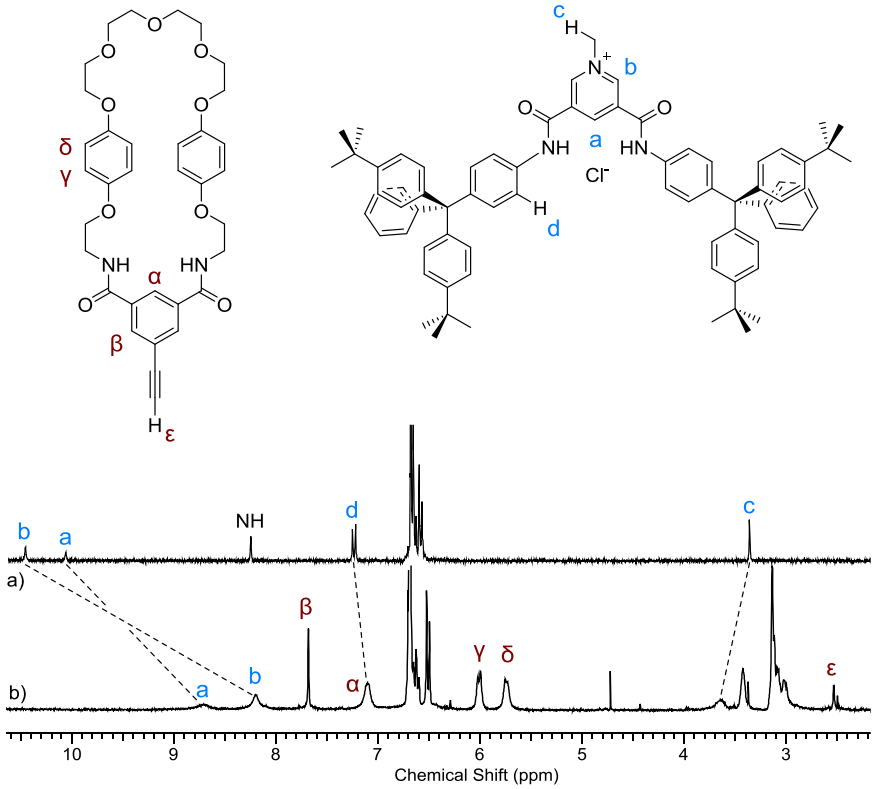

Figure 4.9: ^{1}H NMR (300 MHz, $CDCl_3$, 298 K) spectra of a) methyl pyridinium axle **52** · Cl b) 5-alkynyl [2]rotaxane **79** · Cl

The axle pyridinium protons *a* and *b* are perturbed significantly upfield as a result of hydrogen-bonding of the chloride anion to the macrocycle isophthalamide motif. Importantly the macrocycle hydroquinone protons γ and δ are split in the product which is indicative of a

mechanically bonded assembly. Additional shifts of the axle component are also observed; the methyl pyridinium resonance *c* shifts downfield due to hydrogen bonding to the polyether component of the macrocycle. The resonance *d* is slightly shifted in the interlocked structure due to interaction with the rotaxane cavity.

Crystals suitable for X-ray diffraction structural analysis were obtained by slow diffusion of methanol into a chloroform solution of **79** · Cl (Figure **4.10**). The structure conclusively proves the interlocked nature of the system, and the templating chloride anion is encapsulated by the hydrogen bonded amide array, exhibiting mean N–Cl distances of 3.44 Å. Additionally the bulky terphenyl stopper groups of the [2]rotaxane can be seen to surround the alkyne functionality and may be a factor in preventing reaction at the potentially hindered site (*vide infra*).

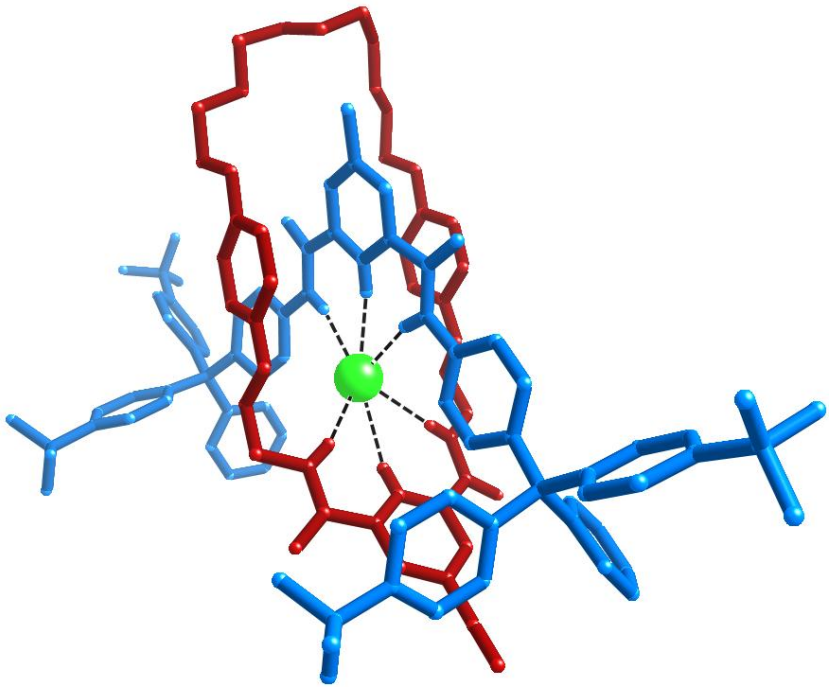

Figure 4.10: Single crystal X-ray structure of 5-alkynyl [2]rotaxane **79** · Cl (non hydrogen-bonding hydrogen atoms omitted for clarity)

4.5 Triazole- and Triazolium-containing [3]Rotaxane Syntheses

4.5.1 Triazole [3]Rotaxane Formation By CuAAC Post-synthetic Modification

Following the successful preparation of the 5-alkynyl functionalised [2]rotaxane **79** · Cl the synthesis of a triazole-linked [3]rotaxane was undertaken. The reaction was performed using standard copper (I) catalysis; alkyne [2]rotaxane **79** · Cl and azide rotaxane **54** · Cl (1.05 equivalents)[32] were dissolved in dry dichloromethane. $Cu(MeCN)_4PF_6$, TBTA and DIPEA were added and stirred overnight (Scheme **4.11**). The reaction mixture was purified by size-exclusion chromatography and preparative TLC (gradient elution; DCM/MeOH 100:0→97:3) to afford the target [3]rotaxane **80** · Cl_2 in high yield (83%).

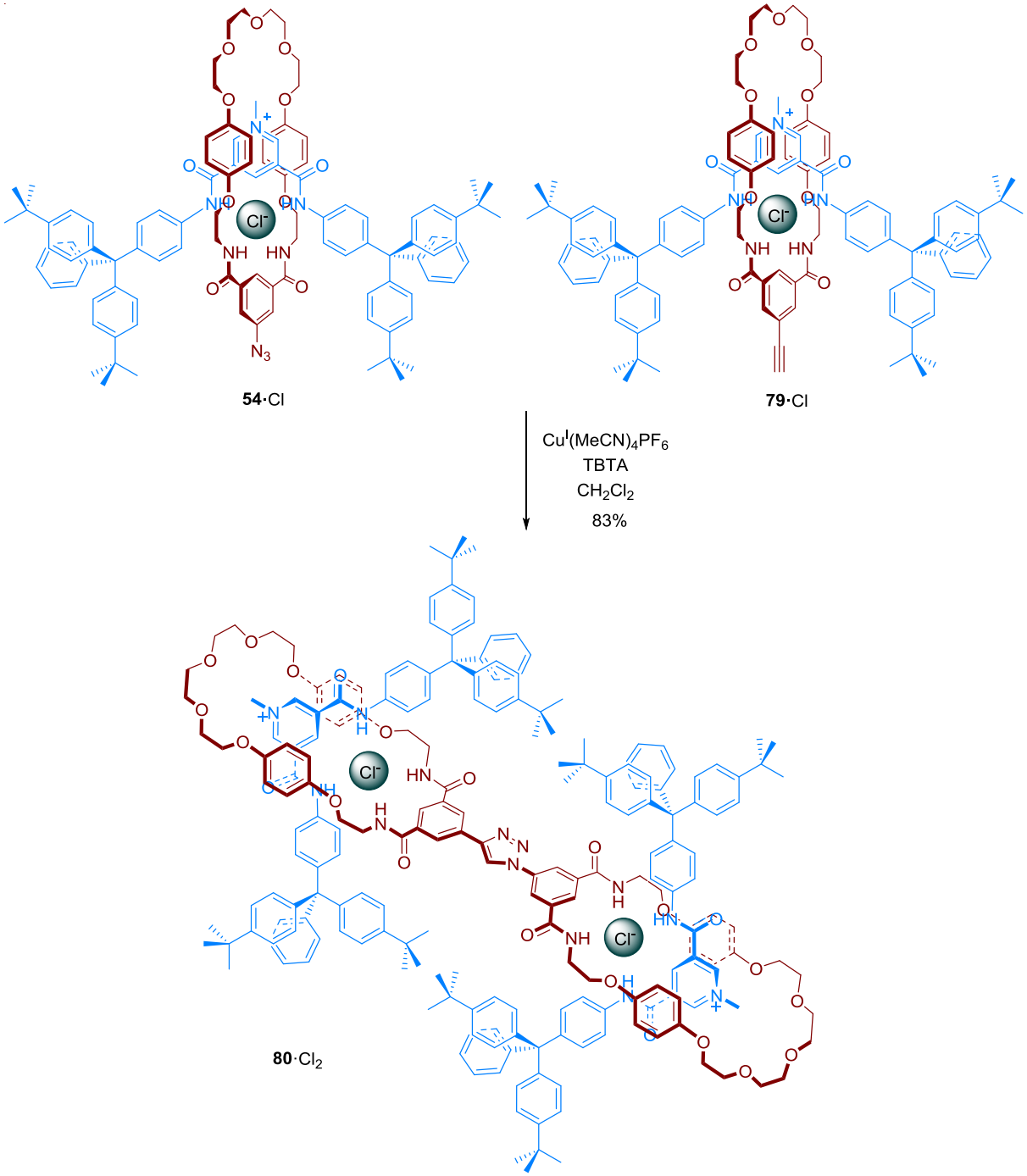

Scheme 4.11: Synthesis of triazole-containing [3]rotaxane **80** · Cl_2 *via* a post-synthetic CuAAC click reaction

The compound was characterised by ^{1}H NMR and high-resolution mass-spectrometry. The mass spectrum of the compound gave the expected peak at $m/z = 1667.3657$ corresponding to $[\text{M-2Cl}]^{2+}$ (Figure **4.12**).

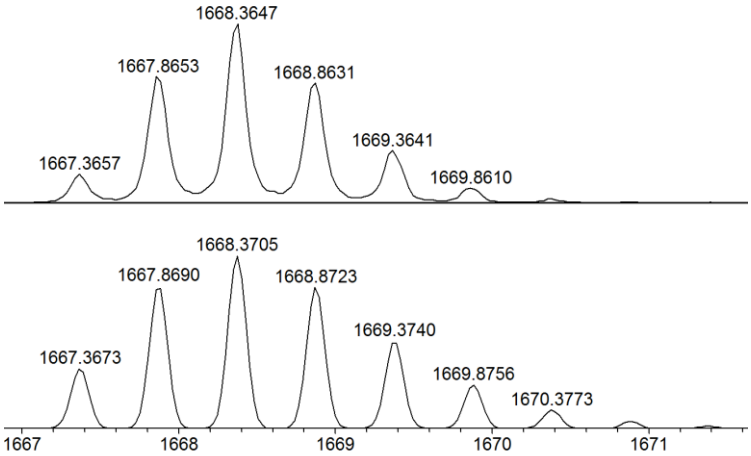

Figure 4.12: Electrospray high-resolution mass spectrum of [3]rotaxane **80** · Cl_2 (predicted spectra bottom; obtained spectra top)

The ^{1}H NMR spectrum of the triazole-linked [3]rotaxane **80** · Cl_2 exhibited very similar shifts to the constituent [2]rotaxanes (Figure **4.13**). Surprisingly the proton resonances *a*, *b* and *c* of the two pyridinium axle components appear at different shifts in the higher order assembly. This is presumably due to steric clashing of the bulky stopper groups which forces the axles to adopt different conformations. The differing position of the axles is also reflected in the split hydroquinone resonances γ and δ of the macrocycles which overlap and appear as multiplets.

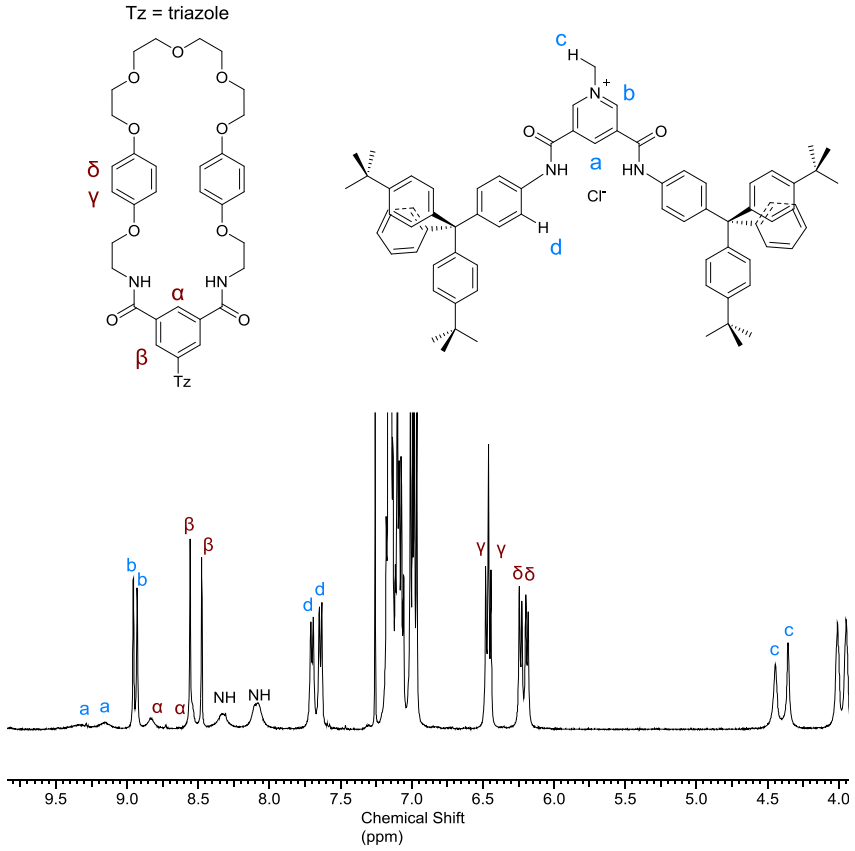

Figure 4.13: ^{1}H NMR (500 MHz, $CDCl_3/CD_3OD$ 9:1, 298 K) spectrum of triazole [3]rotaxane **80** · Cl_2

4.5.2 Triazolium [3]Rotaxane Synthesis

Following the synthesis of the triazole-containing [3]rotaxane assembly a more ambitious anion-templated post-synthetic modification was envisaged whereby alkylation of the triazole linker would furnish a new anion-binding triazolium motif suitable for rotaxane synthesis *via* clipping. The triazole [3]rotaxane **80** · Cl_2 was methylated with trimethyloxonium tetrafluoroborate in dry dichloromethane (Scheme **4.14**). The crude reaction mixture was purified by preparative TLC (gradient elution; DCM/MeOH 96:4→93:7) and subsequently anion exchanged with $NH_4Cl_{(aq)}$ to give the triazolium [3]rotaxane **81** · Cl_3 in high yield (72%).

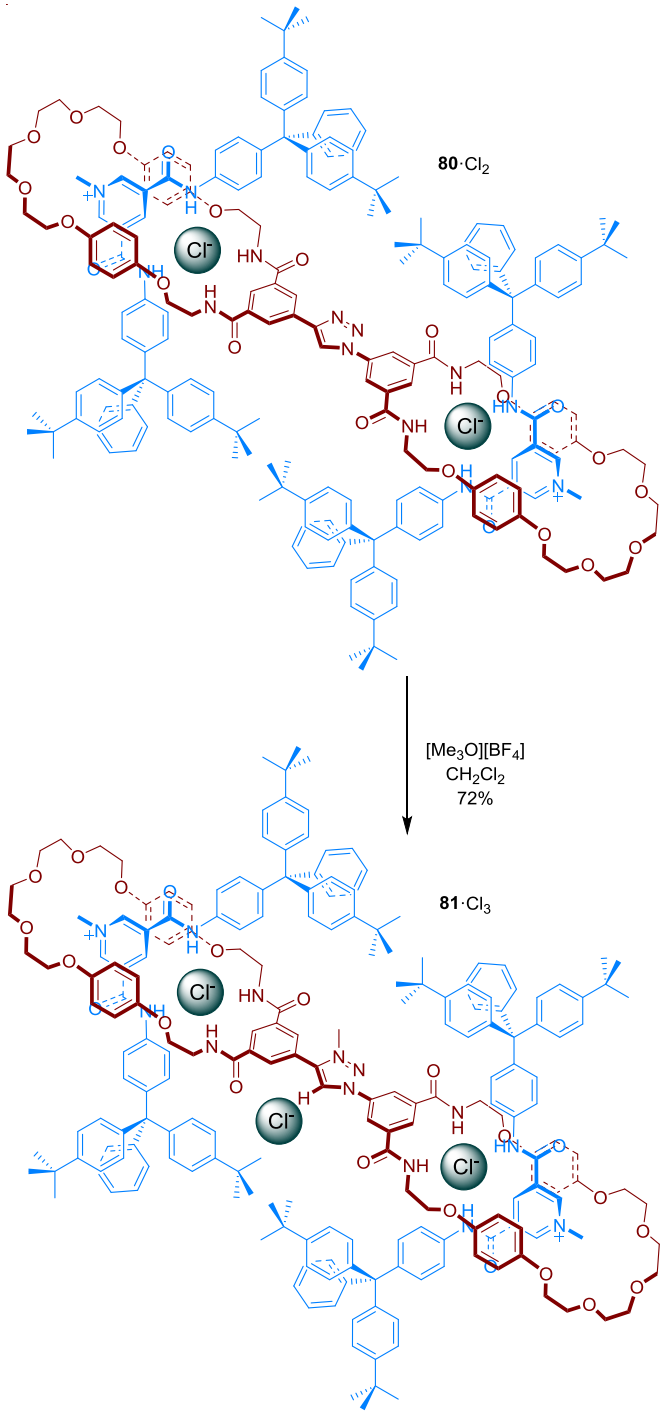

Scheme 4.14: Synthesis of triazolium-containing [3]rotaxane **81** · Cl_3

The triazolium [3]rotaxane product was characterised by ^{1}H, ^{13}C NMR and high-resolution mass spectrometry. The ESI-HRMS showed the expected peak at m/z = 1117.2499 corresponding to $[M - 3Cl]^{3+}$ (Figure **4.15**).

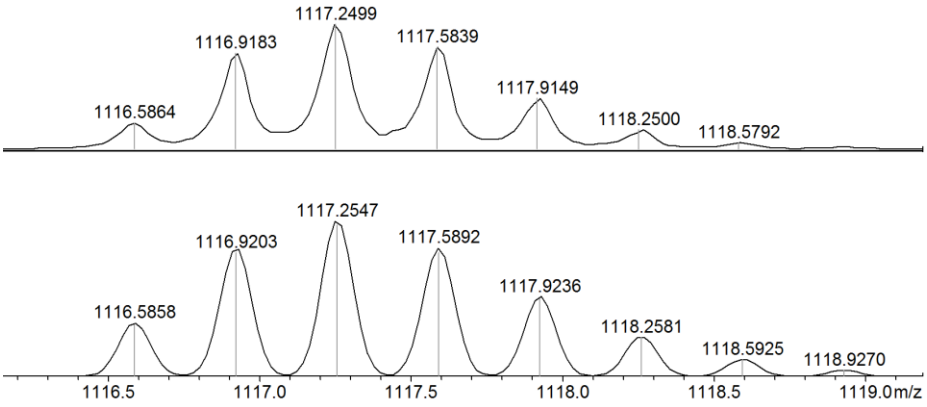

Figure 4.15: Electrospray high-resolution mass spectrum of triazolium-containing [3]rotaxane **81** · Cl_3 (predicted spectra bottom; obtained spectra top)

The ^{1}H NMR spectrum of the triazolium [3]rotaxane **81** · Cl_3 resembled that of the corresponding unmethylated [3]rotaxane but crucially contained an additional methyl triazolium resonance *c* and deshielded triazolium proton *ζ* resulting from methylation (Figure **4.16**). The asymmetry in the ^{1}H NMR spectrum is again observed, indicating conformational differences between the two rotaxane structures.

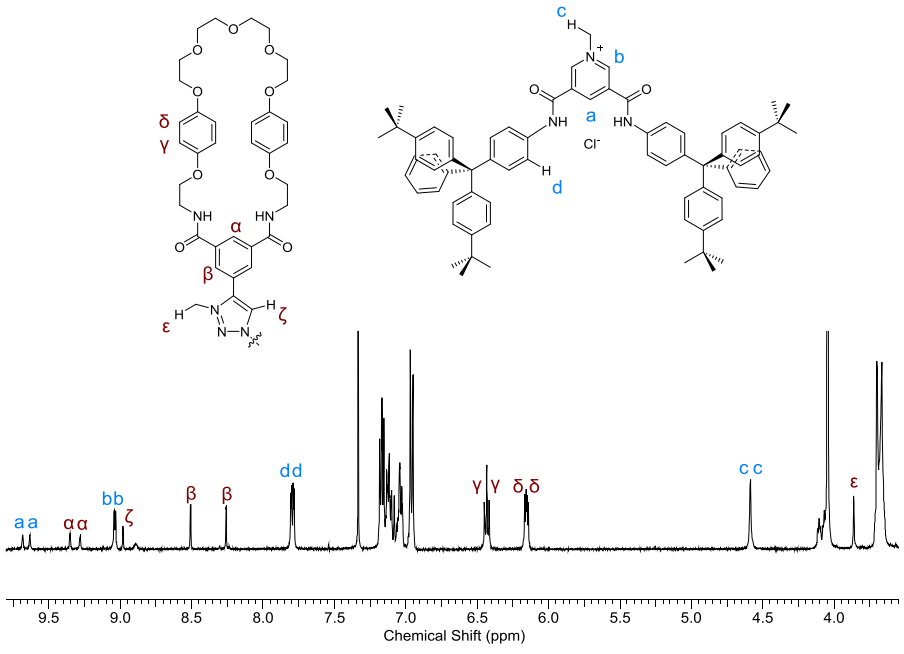

Figure 4.16: ^{1}H NMR (500 MHz, $CDCl_3/CD_3OD$ 9:1, 298 K) spectrum of triazolium [3]rotaxane **81** · Cl_3

4.6 Attempted Synthesis of 'Rotaxane Stoppered' [4]Rotaxane

Following the successful synthesis of the triazolium [3]rotaxane **81** · Cl_3 attempts were made to prepare the target [4]rotaxane. This required a macrocycle precursor suitable for rotaxane formation by ring-closing metathesis (RCM), which was kindly donated by Dr J. M. Mercurio. Rotaxane formation was attempted using the triazolium [3]rotaxane **81** · Cl_3, one equivalent of macrocycle precursor **82** and Grubbs' second generation catalyst in dry dichloromethane (Scheme **4.17**). Analysis of the crude reaction mixture by ^{1}H, ESI-LRMS and TLC only indicated ring-closure of the macrocycle precursor **82** to form the corresponding macrocycle and no evidence for the formation of the desired [4]rotaxane product. This may be attributed to the axle triazolium site in the [3]rotaxane being sterically inaccessible due to the presence of the bulky terphenyl stoppers. In order to alleviate this problem the reaction was repeated with ten equivalents of macrocycle precursor **82** in the presence of Stewart-Grubbs' catalyst, a modified Grubbs'-Hoveyda second generation catalyst which has proven its utility in performing RCM on hindered olefins.[33, 34]

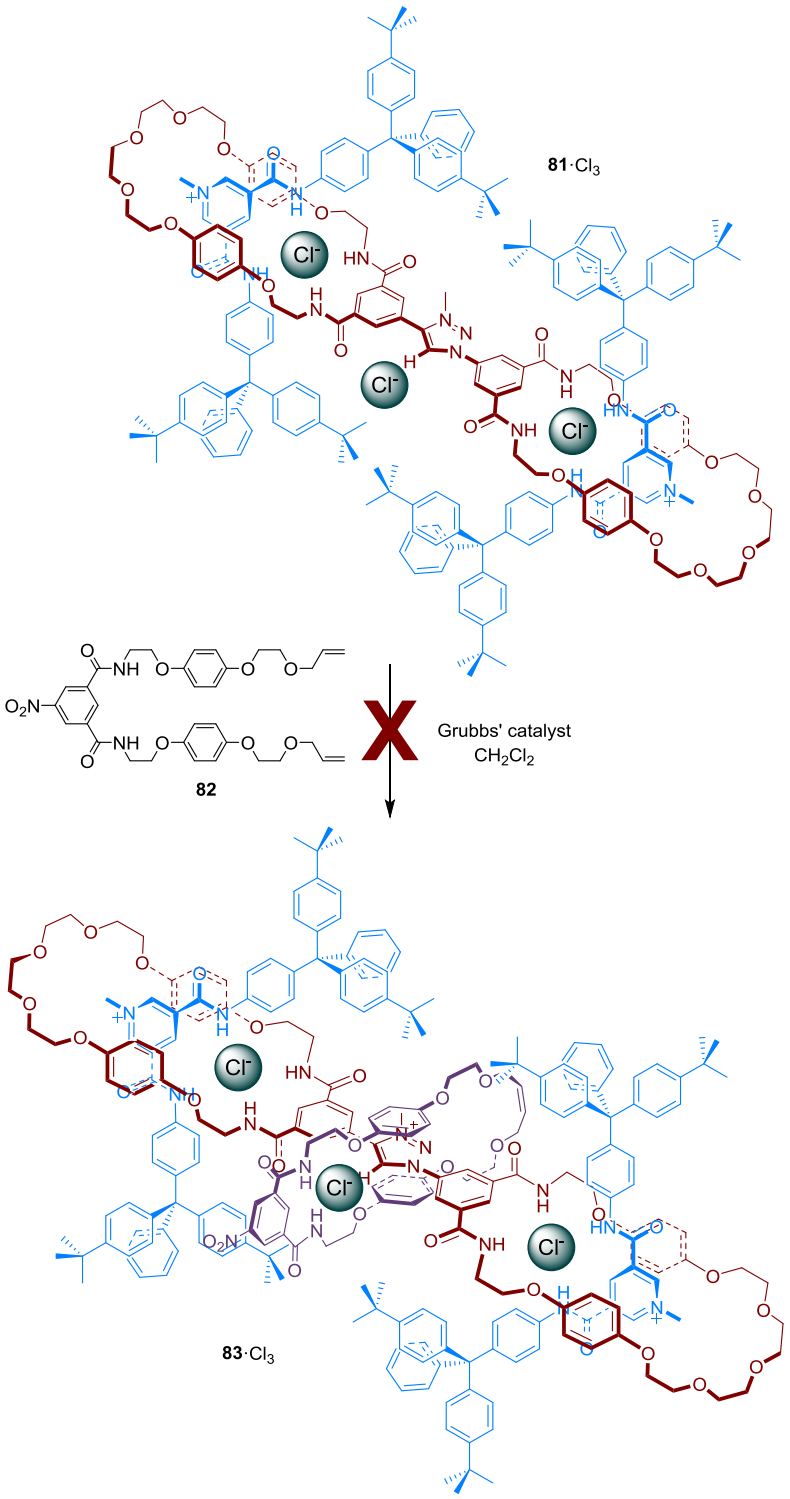

Scheme 4.17: Attempted synthesis of [4]rotaxane **83** · Cl_3 by ring-closing metathesis

Evidence for the [4]rotaxane product was observed in the electrospray low-resolution and high-resolution mass spectrum (Figure **4.18**) of the crude reaction mixture. However, analysis

of the crude reaction mixture by ^{1}H NMR and TLC did not give conclusive evidence for the formation of the [4]rotaxane, indicating the higher order product was only present in trace amounts.

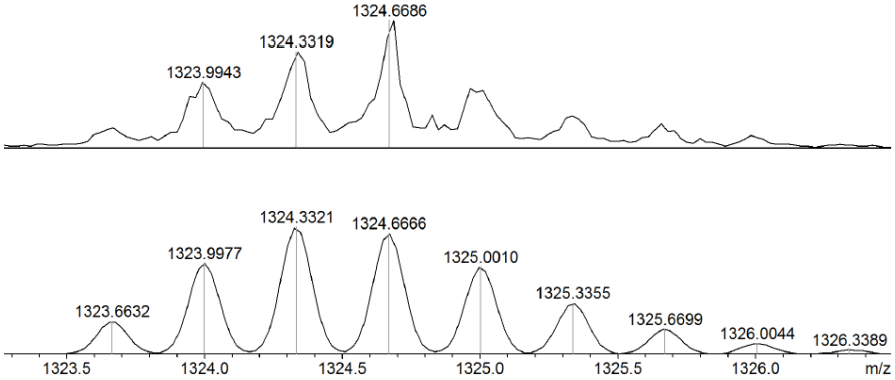

Figure 4.18: Electrospray high-resolution mass spectrum of [4]rotaxane **83** · Cl_3 (predicted spectra bottom; obtained spectra top)

In order to elucidate the processes occurring prior to [4]rotaxane formation a ^{1}H NMR pseudoclipping study was undertaken in dichloromethane-d_2. A stoichiometric amount of the macrocycle precursor was added to the triazolium [3]rotaxane 'axle' **81** · Cl_3 (Figure **4.19**).

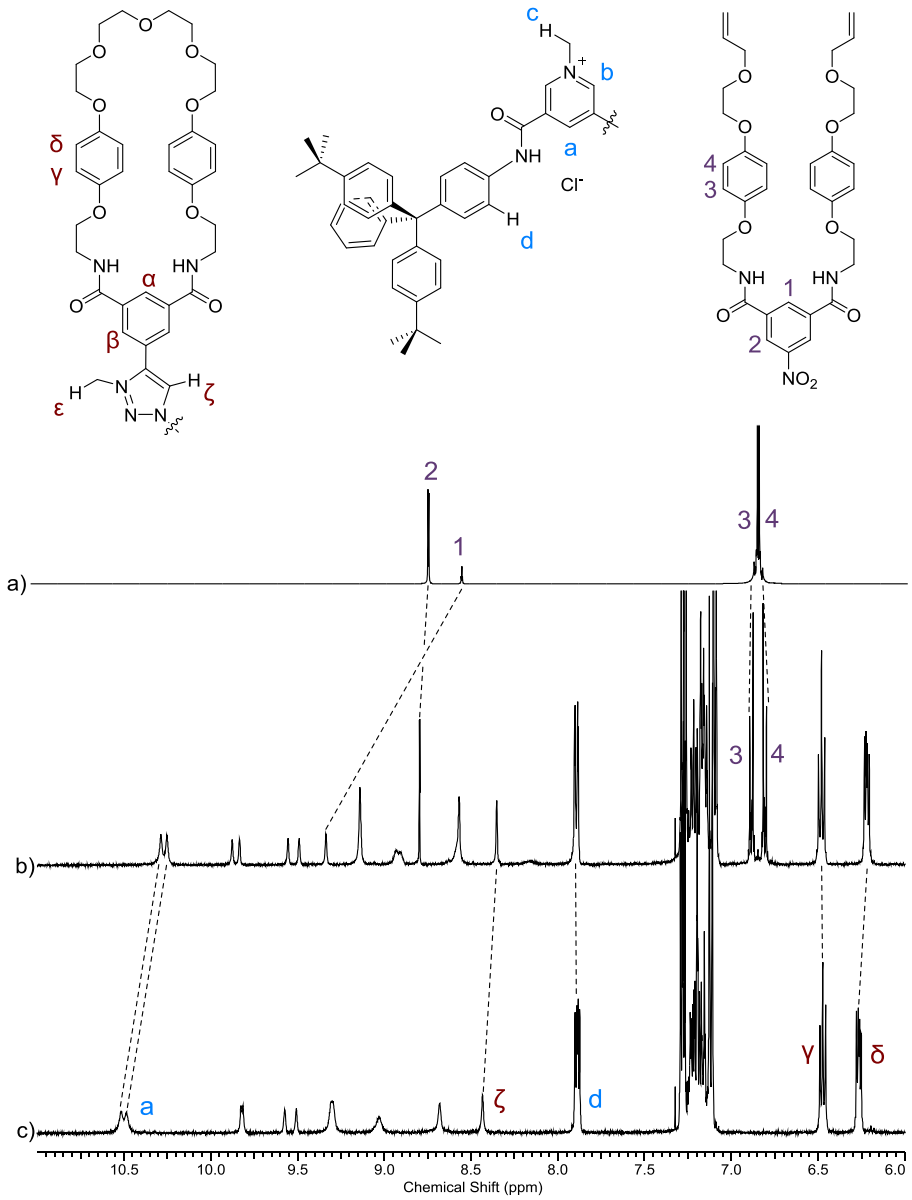

Figure 4.19: ^{1}H NMR (500 MHz, CD_2Cl_2, 298 K) spectra of a) macrocycle precursor **82** b) [3]rotaxane **81** · Cl_3 plus one equivalent of macrocycle precursor **82** c) [3]rotaxane **81** · Cl_3

The ^{1}H NMR spectrum of the [3]rotaxane **81** · Cl_3 plus one equivalent of macrocycle precursor **82** shows significant perturbations with respect to the free components. The isophthalamide protons *1* and *2* of the macrocycle precursor shift downfield upon addition to the 'axle' **81** · Cl_3 due to hydrogen bonding with chloride. Upfield shifts of the triazolium proton *ζ* and splitting of the hydroquinone protons *3* and *4* indicates that the macrocycle isophthalamide group of the macrocycle precursor associates with the central axle triazolium

chloride motif. However, closer analysis of the macrocycle precursor hydroquinone resonances *3* and *4* reveals splitting but not the typical upfield perturbations associated with aromatic donor-acceptor interactions between positively charged axles and hydroquinone motifs. This behaviour implies that rather than adopt the π-stacked arrangement required for [4]rotaxane formation the macrocycle precursor **82** mainly resides on the periphery of the [3]rotaxane **81** · Cl_3 to satisfy the favourable interaction with chloride without wrapping around the central triazolium motif (Figure **4.20**). Despite this there are significant upfield shifts of the pyridinium resonances *a* and the macrocyclic hydroquinone protons *γ* and *δ* which indicate that reorganisation of the pyridinium axles occur to accommodate the macrocycle precursor **82** at the hindered triazolium site.

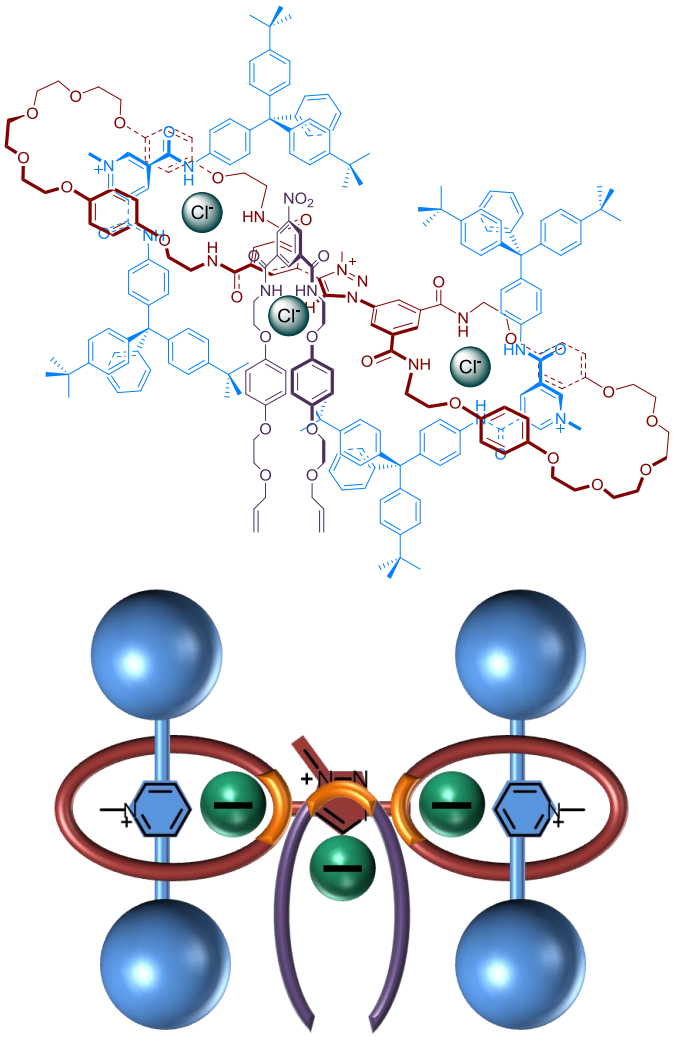

Figure 4.20: Possible conformation of [3]rotaxane **81** · Cl_3 plus one equivalent of macrocycle precursor **82**

It can be concluded that although the steric bulk of the [3]rotaxane's terphenyl stopper groups is not sufficient to prevent interaction of the isophthalamide macrocycle precursor with the central axle triazolium chloride group, it does disfavour formation of the correct conformer required for [4]rotaxane interlocked structure formation which may explain why it was formed in only trace amounts.

4.7 Summary

The synthesis of higher order anion-templated interlocked structures has been demonstrated using a novel post-synthetic modification strategy. Unlike other strategies in which mechanical bond formation is typically the final step, this approach has shown how preformed [2]rotaxane synthons can subsequently be coupled in high yield using the CuAAC click reaction.

The synthesis of the alkyne-functionalised [2]rotaxane was accomplished in good yield using a chloride anion-templated clipping condensation reaction, in an analogous fashion to the corresponding azido-[2]rotaxane preparation introduced in Chapter **3**. The azide and alkyne functionalised [2]rotaxane synthons underwent a copper (I) catalysed click reaction to produce the triazole-containing [3]rotaxane in a high 83% yield. A more adventurous target 'rotaxane stoppered' [4]rotaxane was also envisaged requiring the synthesis of a triazolium [3]rotaxane. This was successfully accomplished using trimethyloxonium tetrafluoroborate, again in high yield (72%), and demonstrates that despite the many functionalities present in anion-templated rotaxanes they are remarkably tolerant to harsh reaction conditions.

The further rotaxanation reaction to produce the desired [4]rotaxane was not successful, possibly due to steric hindrance by the bulky terphenyl stoppering groups. Analysis by mass spectrometry indicated formation of the interlocked assembly but no conclusive evidence of formation by ^{1}H NMR or TLC was obtained. Studies by ^{1}H NMR using the triazolium [3]rotaxane and the macrocycle precursor **82** in dichloromethane-d_2 implied that although the two components appear to associate in solution, the macrocycle precursor was interacting

only with the chloride anion and not with the central axle triazolium group and hence [4]rotaxane formation was highly disfavoured.

4.8 Conclusions

In this chapter the synthesis of higher order interlocked structures using a post-synthetic modification strategy was explored. The utility of this method was demonstrated by using a CuAAC reaction to couple alkyne and azide functionalised [2]rotaxanes together to form a novel triazole [3]rotaxane. The [3]rotaxane was itself tolerant to further reaction; methylation of the triazole group was accomplished using trimethyloxonium tetrafluoroborate, a potent alkylating agent. This is encouraging as it shows that formation of higher order interlocked structures by using this modular approach is not only viable, but presents a new facile route to complex mechanically bonded architectures. Indeed while the synthesis of [3]rotaxane **81** · Cl_3 formally contains 17 steps this is relatively few in number given the complexity of the assembly.

The isolation of the ambitious [4]rotaxane target was not successful. However it was possible to obtain evidence for its formation by mass spectrometry. This was only achievable by using excess macrocycle precursor, which forced the equilibrium towards the desired product, and by using a modified Grubbs' catalyst. The reason for the failed rotaxanation is thought to be due to sterics; the bulky terphenyl stopper groups encumber the axle triazolium binding site and preclude formation of the conformer required for [4]rotaxane formation. Future investigations into [4]rotaxane synthesis would need to avoid this problem by incorporating a

longer axle triazolium linker at the centre of the [3]rotaxane which would allow close approach of the macrocycle precursor.

This chapter concludes the work concerning interlocked host structures, the next chapter will focus on the detection of the chemical warfare agent sulphur mustard by a new nanoparticle-based fluorescent displacement assay approach.

4.9 References

1. E. Wasserman, *J. Am. Chem. Soc.*, 1960, **82**, 4433-4434.
2. H. L. Frisch and E. Wasserman, *J. Am. Chem. Soc.*, 1961, **83**, 3789-&.
3. I. T. Harrison and S. Harrison, *J. Am. Chem. Soc.*, 1967, **89**, 5723-&.
4. C. O. Dietrichbuchecker and J. P. Sauvage, *Angew. Chem.-Int. Edit. Engl.*, 1989, **28**, 189-192.
5. N. Ponnuswamy, F. B. L. Cougnon, J. M. Clough, G. D. Pantos and J. K. M. Sanders, *Science*, 2012, **338**, 783-785.
6. J. Guo, P. C. Mayers, G. A. Breault and C. A. Hunter, *Nat. Chem.*, 2010, **2**, 218-222.
7. C. D. Pentecost, K. S. Chichak, A. J. Peters, G. W. V. Cave, S. J. Cantrill and J. F. Stoddart, *Angew. Chem.-Int. Edit.*, 2007, **46**, 218-222.
8. N. Ponnuswamy, F. B. L. Cougnon, G. D. Pantos and J. K. M. Sanders, *J. Am. Chem. Soc.*, 2014, **136**, 8243-8251.
9. K. S. Chichak, S. J. Cantrill, A. R. Pease, S. H. Chiu, G. W. V. Cave, J. L. Atwood and J. F. Stoddart, *Science*, 2004, **304**, 1308-1312.
10. S. J. Cantrill, K. S. Chichak, A. J. Peters and J. F. Stoddart, *Acc. Chem. Res.*, 2005, **38**, 1-9.
11. C. D. Mao, W. Q. Sun and N. C. Seeman, *Nature*, 1997, **386**, 137-138.
12. J. F. Ayme, J. E. Beves, D. A. Leigh, R. T. McBurney, K. Rissanen and D. Schultz, *Nat. Chem.*, 2012, **4**, 15-20.
13. J. F. Ayme, J. E. Beves, D. A. Leigh, R. T. McBurney, K. Rissanen and D. Schultz, *J. Am. Chem. Soc.*, 2012, **134**, 9488-9497.
14. J. D. Badjić, V. Balzani, A. Credi, S. Silvi and J. F. Stoddart, *Science*, 2004, **303**, 1845-1849.
15. Z.-J. Zhang, M. Han, H.-Y. Zhang and Y. Liu, *Org. Lett.*, 2013, **15**, 1698-1701.
16. C. Romuald, E. Busseron and F. Coutrot, *J. Org. Chem.*, 2010, **75**, 6516-6531.
17. M. C. Jiménez, C. Dietrich-Buchecker and J.-P. Sauvage, *Angew. Chem.-Int. Ed.*, 2000, **39**, 3284-3287.
18. C. Clavel, K. Fournel-Marotte and F. Coutrot, *Molecules*, 2013, **18**, 11553-11575.
19. J. P. Collin, F. Durola, V. Heitz, F. Reviriego, J. P. Sauvage and Y. Trolez, *Angew. Chem.-Int. Ed.*, 2010, **49**, 10172-10175.

20. F. Durola, V. Heitz, F. Reviriego, C. Roche, J.-P. Sauvage, A. Sour and Y. Trolez, *Acc. Chem. Res.*, 2014, **47**, 633-645.
21. M. R. Sambrook, P. D. Beer, J. A. Wisner, R. L. Paul and A. R. Cowley, *J. Am. Chem. Soc.*, 2004, **126**, 15364-15365.
22. Evans, N.H. (2012) , Redox-Active Rotaxanes and Catenanes for Anion Sensing, DPhil, University of Oxford, UK
23. S. Lee, C. H. Chen and A. H. Flood, *Nat. Chem.*, 2013, **5**, 704-710.
24. N. H. Evans, C. J. Serpell and P. D. Beer, *Chem. Commun.*, 2011, **47**, 8775-8777.
25. M. J. Langton and P. D. Beer, *Chem.–Eur. J.*, 2012, **18**, 14406-14412.
26. N. H. Evans, C. J. Serpell and P. D. Beer, *Angew. Chem.-Int. Edit.*, 2011, **50**, 2507-2510.
27. T. J. Hubin and D. H. Busch, *Coord. Chem. Rev.*, 2000, **200**, 5-52.
28. J. P. Collin, V. Heitz and J. P. Sauvage, in *Molecular Machines*, ed. T. R. Kelly, Springer-Verlag Berlin, Berlin, 2005, vol. 262, pp. 29-62.
29. J. E. Beves, B. A. Blight, C. J. Campbell, D. A. Leigh and R. T. McBurney, *Angew. Chem.-Int. Edit.*, 2011, **50**, 9260-9327.
30. J. A. Wisner, P. D. Beer, M. G. B. Drew and M. R. Sambrook, *J. Am. Chem. Soc.*, 2002, **124**, 12469-12476.
31. I. M. Hauptvogel, W. Seichter and E. Weber, *Supramolecular Chem.*, 2011, **23**, 398-406.
32. Due to the similar retention factors on silica between the alkyne [2] rotaxane and the triazole [3]rotaxane an excess of azide [2]rotaxane was used.
33. I. C. Stewart, C. J. Douglas and R. H. Grubbs, *Org. Lett.*, 2008, **10**, 441-444.
34. I. C. Stewart, T. Ung, A. A. Pletnev, J. M. Berlin, R. H. Grubbs and Y. Schrodi, *Org. Lett.*, 2007, **9**, 1589-1592.

Chapter 5: Detection of Sulphur Mustard by Fluorescent Displacement Assay

5.1 Introduction

Chemical warfare agents (CWAs) such as chlorine gas and sulphur mustard (HD) (Figure **5.1a**) were first deployed on a large scale in World War I. Since then the use of CWAs has grown with the introduction of phosphorus-based nerve agents in the 1940s.[1] Phosphorus and sulphur based CWAs have been used in more recent conflicts in Iraq[2] and Syria[3] and in addition, the G-agent sarin (Figure **5.1b**) was released on the Tokyo subway in 1996.[4]

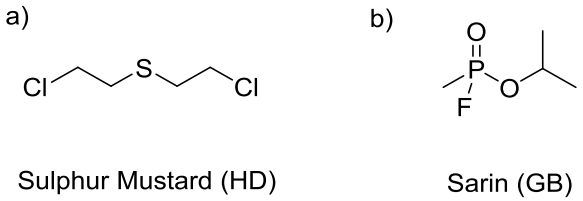

Figure 5.1: Chemical structures of CWAs a) sulphur mustard (HD) b) sarin (GB)

Due to the inherent dangers associated with CWAs it is clearly desirable to be able to detect and deactivate these potent compounds. This chapter investigates the preparation of a new class of fluorescent sensor for sulphur mustard. The following section gives a brief review of examples of CWA receptors and sensors.

5.2 Chemical Warfare Agent Receptors and Sensors

5.2.1 Chemodosimeters

The colourimetric and fluorescent sensing of chemical warfare agents has largely been dominated by the use of chemodosimeter approaches (see Section **1.4.4.1** of the introduction) which generate new molecular species.[5] Swager reported a highly sensitive chemosensor for CWA simulants; the presence of simulant diisopropyl fluorophosphate (DFP) induced cyclisation through alkylation to produce a new highly fluorescent species (Scheme **5.2**).[6]

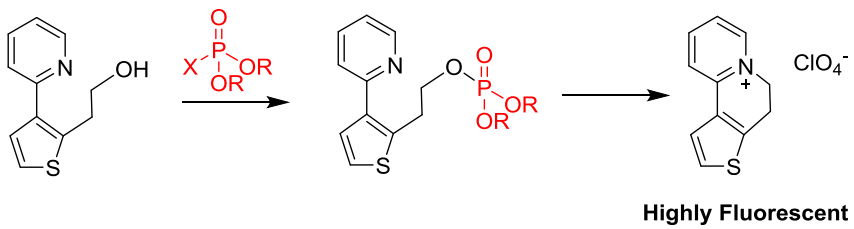

Scheme 5.2: Swager's phosphorus nerve agent chemodosimeter.

The electrophilicity of HD has also been exploited to generate new molecular species. Eichen reported the alkylation of a fluorescent naphthalimide compound (Scheme **5.3**).[7] In the presence of 2-chloroethylethyl sulphide (CEES) in acetonitrile, the tertiary amine was alkylated thereby turning on luminescence due to PET.

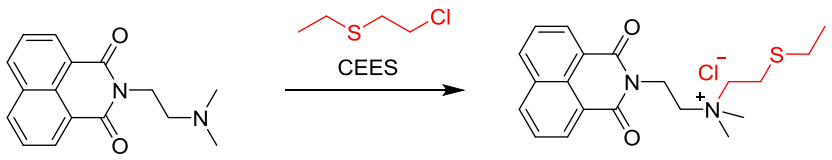

Scheme 5.3: Eichen's PET sensor for sulphur mustard simulants

5.2.2 Supramolecular and Coordination Strategies

While supramolecular and coordination strategies have been widely employed for charged species recognition, the detection of neutral CWAs by this method is underdeveloped.[1] However, phosphorus nerve agents are known to form inclusion complexes with cyclodextrins[8, 9] and cavitands.[10, 11] Hydrogen bond donating interactions are exploited in Gale's acyclic bis-indole based receptor which recognises the nerve agent soman (GD) in acetonitrile-d_3/DMSO-d_6 (98:2) (Figure **5.4a**).[12] A related host, reported by Martinez-Manez, was found to accelerate the deactivation of DFP by increasing the electrophilicity of the phosphorus atom, making it more susceptible to attack by a nucleophile (Figure **5.4b**).[13]

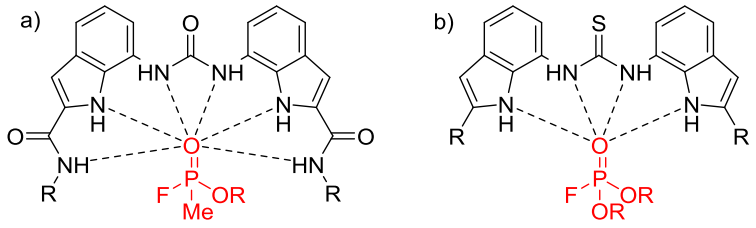

Figure 5.4: Hydrogen-bonded nerve agent receptors by a) Gale b) Martinez-Manez

Coordination to alkali metals,[14] transition metals[15] and lanthanides[16, 17] has also been used to bind and detect nerve agents. This includes the displacement assay approach reported by Weder (Figure **5.5**).[18] Energy transfer from the ligand to the europium centre resulted in quenching of the ligand-based fluorescence in the lanthanide complex. Addition of the simulant triethylphosphate in $CHCl_3$/CH_3CN (9:1) induced decomplexation of the europium by exploiting the high affinity of lanthanide ions for phosphates, and hence a 'switching on' of the ligand fluorescence was observed.[19] Coordination strategies have also been reported for sulphur-based chemical warfare agents. Tilley has demonstrated the high stability of silver (I)

salts with 2-chloroethylmethyl sulphide (CEMS) in polar organic solvents[20] and more recently colourimetric sensing of sulphides by a copper acetate impregnated silica sol-gel matrix was reported by Lin.[21]

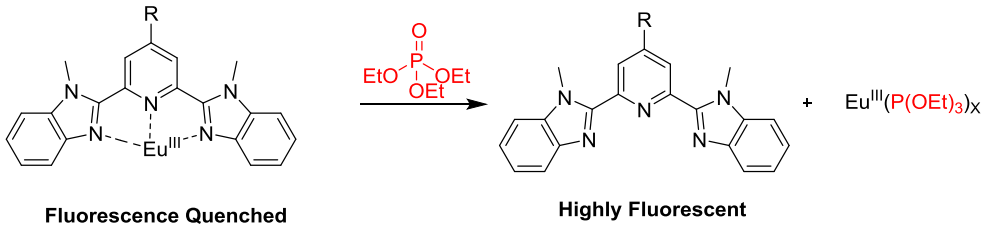

Figure 5.5: Fluorescent displacement assay approach for detection of triethylphosphate

5.3 Chapter Objectives

While research into the detection of multifarious phosphorus-based CWAs has blossomed, the limited functionality of sulphur mustard (HD) means that it's sensing is relatively underexplored. The objective of this chapter was to develop a new class of sensor for HD by using a fluorescent displacement assay (displacement assays were discussed in the introduction Section **1.4.4.1**). The sensor design (Figure **5.6**) uses a fluorescent motif that is functionalised with imidazole or amine groups which are capable of ligating to a gold nanoparticle surface. It was anticipated that the fluorescence of the ligand-nanoparticle conjugates would be low due to the proximity to the metal surface and the well-known quenching effect of gold nanoparticles.[22] The thiophilic properties of gold would then be exploited such that in the presence of sulphur containing analytes the metal surface-stabilising fluorophore is liberated from the surface, triggering a 'switching on' of the fluorescence of the sample. The response of these conjugates to a low toxicity mustard

simulant CEMS and the CWA HD were investigated in collaboration with the Defence and Science and Technology Laboratory (DSTL).

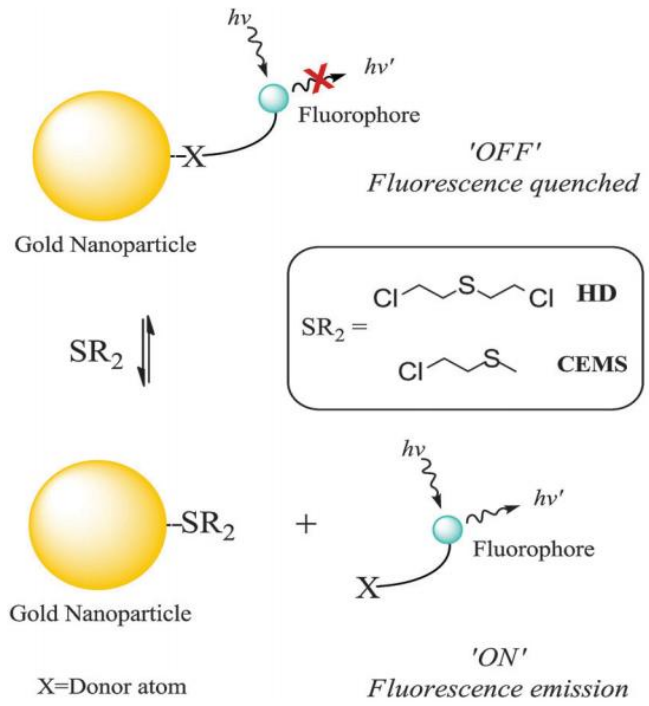

Figure 5.6: Schematic representation of sensing of HD and CEMS sulphides by fluorescent displacement assay

5.4 Nanoparticle Ligand Synthesis

The target ligands chosen for nanoparticle functionalisation incorporated dansyl and 1,8-naphthalimide fluorophores, using both amine and imidazole groups to ligate to the nanoparticle surface. The dansyl ligands were prepared using commercially available dansyl chloride (Scheme **5.7**). Condensation of dansyl chloride with 3-(1H-imidazol-1-yl)propan-1-amine in dry dichloromethane in the presence of triethylamine afforded the target dansyl-imidazole ligand **85** in 77% yield. The amine-functionalised ligand was synthesised first by mono-protection of ethylene diamine with di-*tert*-butyl dicarbonate in dry dichloromethane (67%) to give *tert*-butyloxycarbonyl (BOC) protected ethylene diamine **86**.[23] Dansyl chloride

was condensed with **86** in dry dichloromethane to afford the proligand **87** in 66% yield. Deprotection of the BOC groups was accomplished using TFA in dichloromethane to give the target dansyl-amine ligand **88** (81%).

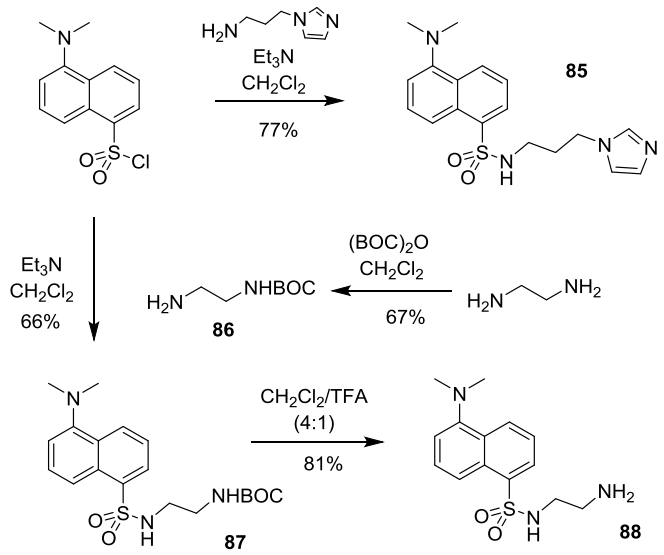

Scheme 5.7: Synthesis of imidazole and amine functionalised dansyl ligands **85** and **88**

Crystals suitable for structural analysis by X-ray diffraction were obtained by slow evaporation of a chloroform solution of ligand **88**, confirming the proposed formulation (Figure **5.8**).

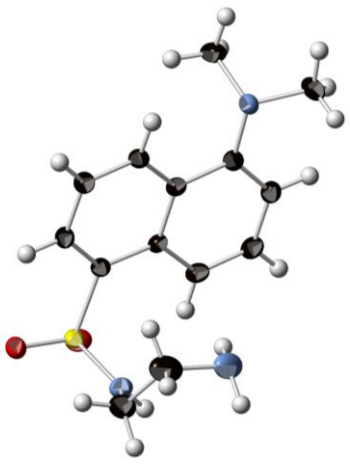

Figure 5.8: Single crystal X-ray structure of dansyl-amine ligand **88** (Ellipsoids plotted at 50% probability, hydrogen atoms shown as spheres of abitrary radius)

The corresponding 1,8-naphthalimide ligands were synthesised by a similar condensation strategy (Scheme **5.9**). Commercially available 4-bromo-1,8-naphthalic anhydride was reacted with 3-(1H-imidazol-1-yl)propan-1-amine in dioxane to obtain synthon **89** in good yield (80%). This was subsequently reacted with piperidine in DMF to give the naphthalimide-imidazole ligand **90** (92%). Crystals of the compound suitable for X-ray single crystal structural analysis were grown by evaporation of water into a DMSO solution of the ligand, confirming the proposed formulation (Figure **5.10**). The amine analogue was prepared first using *N*-BOC-ethylene diamine to afford compound **91** in high yield (85%). Reaction of **91** with piperidine furnished the BOC protected amine precursor **92** (88%). Deprotection of the amine in dichloromethane/trifluoroacetic acid (4:1) gave the naphthalimide-amine ligand **93** in high yield (94%). An alternative naphthalimide ligand with better solubility (*vide infra*) was also prepared; reaction of synthon **89** with dibutylamine afforded the butyl-naphthalimide-imidazole ligand **94** (89%).

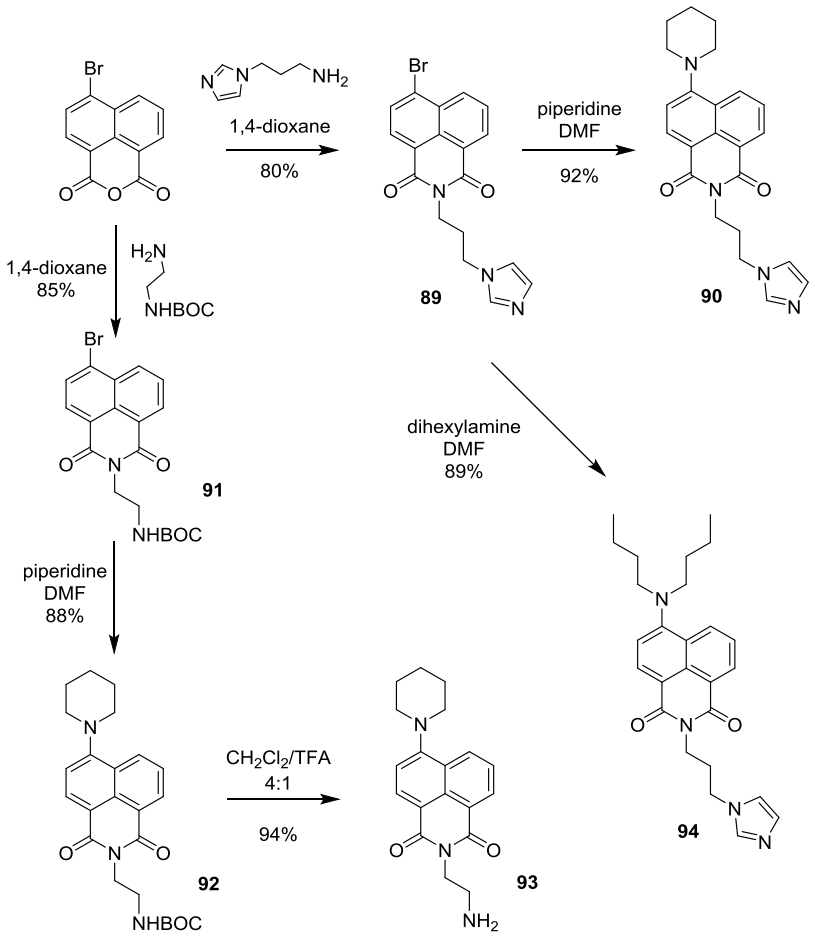

Scheme 5.9: Synthesis of 1,8-naphthalimide functionalised nanoparticle ligands

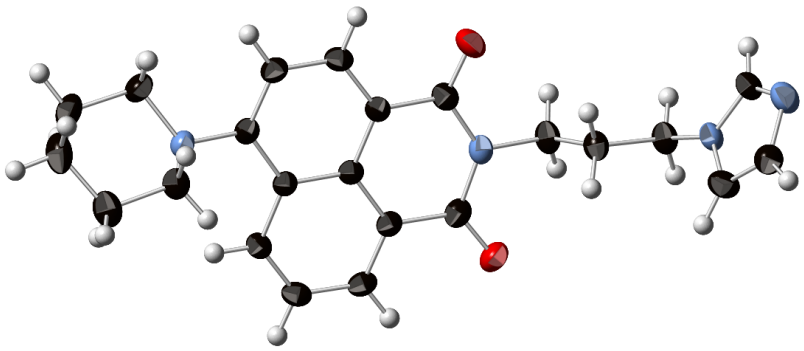

Figure 5.10: Single crystal X-ray structure of naphthalimide-imidazole ligand **90** (Ellipsoids plotted at 50% probability, hydrogen atoms shown as spheres of abitrary radius)

5.5 Nanoparticle Synthesis and Characterisation

5.5.1 Nanoparticle Synthesis

The dansyl ligand nanoparticle syntheses were conducted according to a modified Brüst method (Scheme **5.11**).[24] Aqueous gold (III) tetrachloroaurate was extracted into toluene with the phase transfer reagent Aliquat336. Addition of the dansyl ligand as a dichloromethane solution preceded reduction with sodium borohydride. Purification by dissolution in dichloromethane followed by precipitation with methanol afforded the target dansyl-ligated nanoparticles **Au · 85** and **Au · 88**.

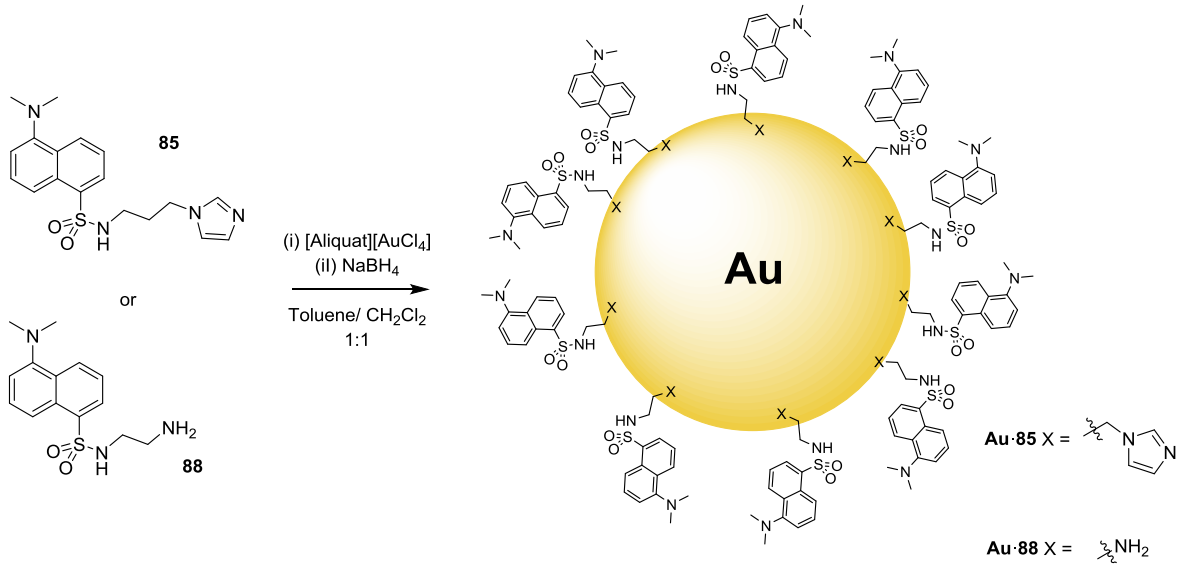

Scheme 5.11: Synthesis of dansyl-ligated gold nanoparticles **Au · 85** and **Au · 88** by a modified Brüst method

The synthesis of the corresponding naphthalimide imidazole- and amine-functionalised nanoparticles was attempted by the same method. Due to the low solubility of **90** and **93** in dichloromethane the ligands were added as a dichloromethane/methanol (9:1) solution.

Reduction of gold in the ternary solvent system gave only insoluble material, indicating that agglomerates were formed. In order to reproduce the conditions used for the dansyl nanoparticle synthesis the dichloromethane soluble butyl-naphthalimide-imidazole ligand **94** was used. However, reduction of $AuCl_4^-$ in the presence of the ligand gave the same results, producing nanoparticles which were insoluble in all common solvents. The reason for this is unknown and as a result characterisation and further studies were only performed on the dansyl-ligated gold nanoparticle **Au · 85** and **Au · 88**.

5.5.2 Nanoparticle Characterisation

The novel dansyl-nanoparticle conjugates **Au · 85** and **Au · 88** were characterised by transmission electron microscopy (TEM), elemental analysis and UV/visible spectroscopy. TEM images and particle sizing analysis (Figure **5.12**) were conducted by Simon Smith at DSTL. It can be noted that using the modified Brüst method very similar nanoparticle sizes are obtained for both samples with mean diameters of 3.1 ± 0.7 nm and 3.2 ± 0.7 nm for the imidazole and amine nanoparticles respectively.

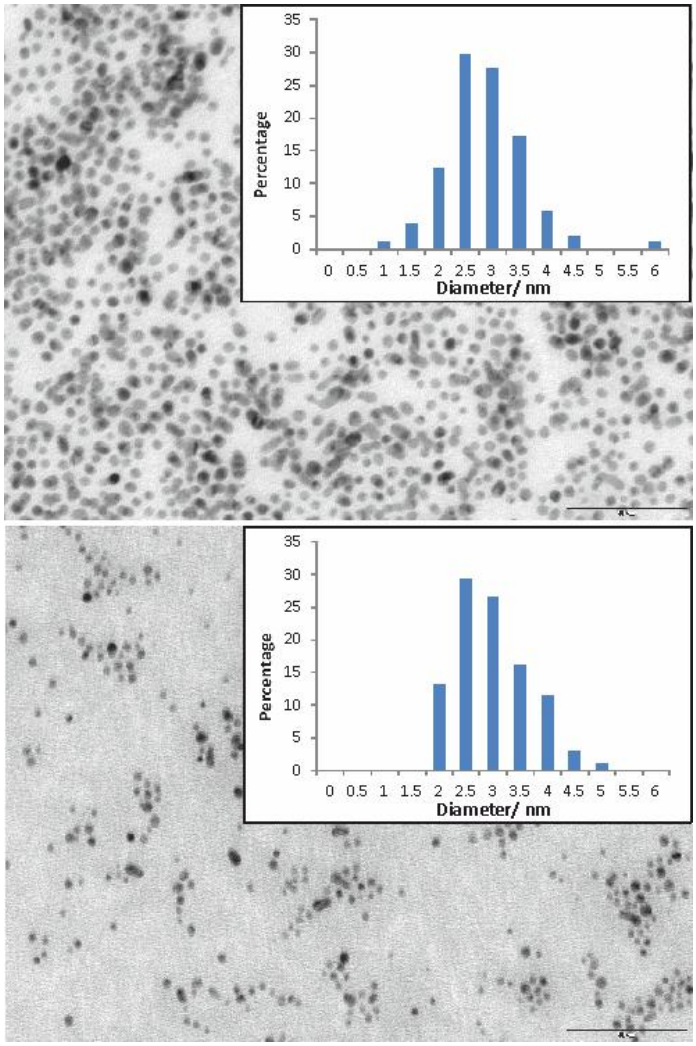

Figure 5.12: Transmission electron microscopy images with inset particle sizing analysis of a) **Au · 85** and b) **Au · 88** (scale bar is at 50 nm)

The elemental C, H, N and S analyses of the gold nanoparticle conjugates are tabulated in Table **5.13**. Using the sulphur analysis, the percentage weights of the ligands were calculated to be 15.7% and 13.5% for **Au · 85** and **Au · 88** respectively.

	Elemental Analysis (% weight)				
	C	**H**	**N**	**S**	**% weight of ligand[a]**
Au · 85	10.5	1.2	2.3	1.4	15.7
Au · 88	7.9	0.9	1.8	1.5	13.5

Table 5.13: Elemental analysis of gold nanoparticle conjugates **Au · 85** and **Au · 88** ([a] weight percentage calculated using sulphur elemental analysis)

The UV/visible absorption properties of the nanoparticles were also investigated in chloroform. Both samples exhibited characteristic absorption bands corresponding to the ligand $n \rightarrow \pi^*$ transition around 350 nm and a broad maxima centred at 520-530 nm attributed to the surface plasmon resonance (SPR) band of the gold nanoparticle (Figure **5.14**).

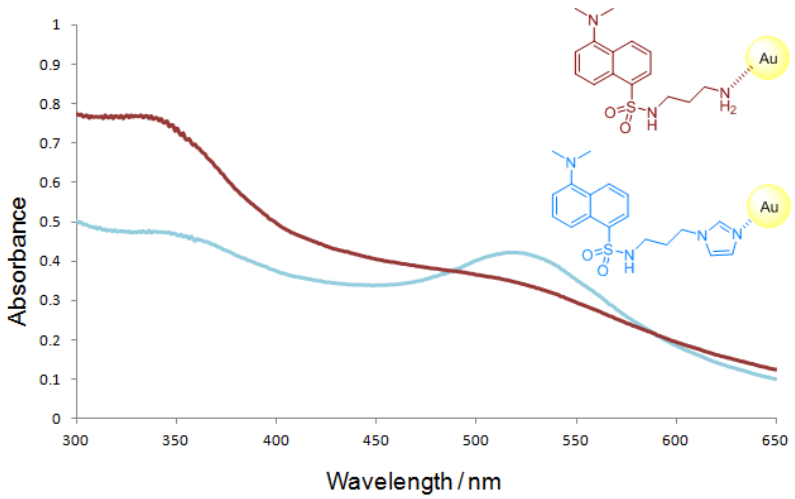

Figure 5.14: UV/visible absorption spectra of dansyl ligated gold nanoparticles (0.04 mg mL^{-1} $CHCl_3$, 298 K)

5.6 Displacement Studies

Following the successful synthesis and characterisation of the novel fluorophore functionalised gold nanoparticle conjugates, their ability to sense sulphur mustard and simulant compound 2-chloroethylmethylsulphide (CEMS) were explored by ^{1}H, UV/vis and fluorescence spectroscopies.

5.6.1 ^{1}H NMR Displacement Study

In order to confirm that displacement of the ligated dansyl fluorophore occurred upon the addition of a sulphur containing compound, a preliminary ^{1}H NMR titration on **Au · 85** was performed. The ^{1}H NMR spectrum of the nanoparticle material was obtained in chloroform; the sample displayed very broad ligand resonances which is consistent with chemical shift anisotropy of the surface bound species as a result of being chemisorbed onto the surface of the gold nanoparticle (Figure **5.15a**).[25] However upon exposure to ten equivalents of the mustard simulant CEMS, new sharp resonances associated with the dansyl moiety were observed (Figure **5.15b**). This observation is evidence of the liberation of the free ligand species **85** by the aurophilic mustard simulant.

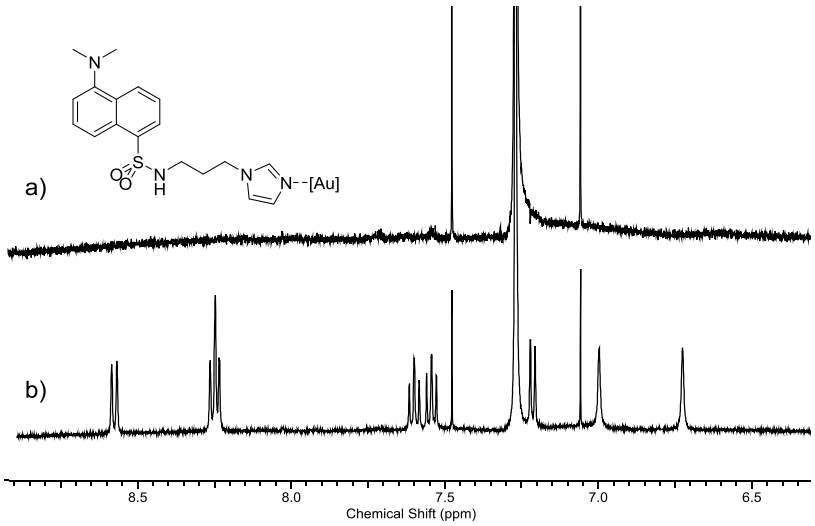

Figure 5.15: ^{1}H NMR (500 MHz, $CDCl_3$, 298 K) spectra of dansyl ligated nanoparticles a) **Au · 85** b) **Au · 85** in the presence of ten equivalents of CEMS ten minutes after addition

5.6.2 UV/visible Absorption Studies

The study of both nanoparticle samples by UV/visible absorption spectroscopy provided further evidence of displacement of the stabilising ligand from the nanoparticle surface upon addition of sulphide analytes. The surface plasmon resonance bands of the nanoparticle samples exhibited significant bathochromic shifts from 528 to 536 nm and 520 to >600 nm for **Au · 85** and **Au · 88** (Figure **5.16a**) respectively upon the addition of excess CEMS. Similar behaviour was also observed in the presence of excess sulphur mustard (HD) with samples **Au · 85** and **Au · 88** (Figure **5.16b**) displaying shifts from 528 to 540 nm and 520 to 540 nm respectively. The observed bathochromic shifting of the SPR band occured over a three hour period and may indicate slow particle agglomeration following the displacement of the stabilising dansyl ligands from the surface. This was particularly evident for **Au · 88** in the presence of CEMS, whereby a colour change was observed from brown to clear with the concomitant formation of a dark precipitate (Figure **5.17**).

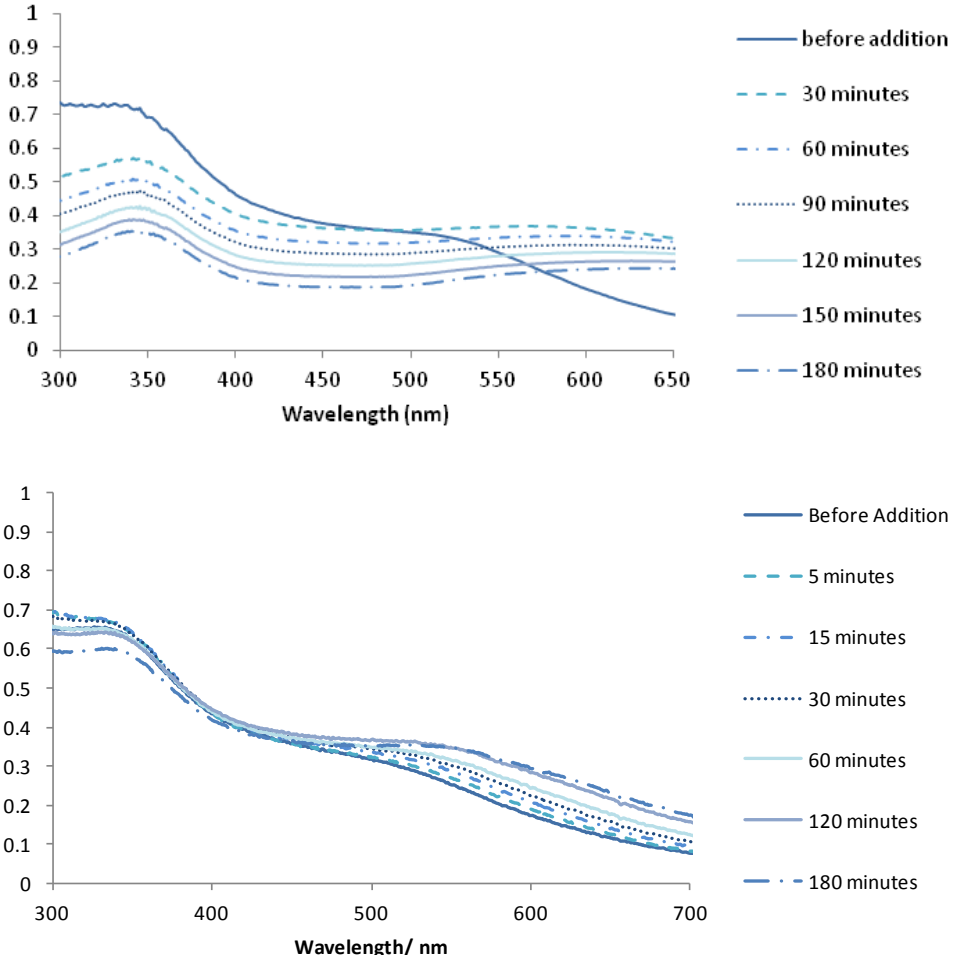

Figure 5.16: Change in UV/vis spectrum of a 0.04 mg mL^{-1} solution of **Au · 88** upon addition of a) 2-chloroethylmethylsulphide (CEMS) 50 µL to 2.5 mL solution b) bis(2-chloroethyl)sulphide (HD) 2 µL to 100 µL solution in $CHCl_3$ (298 K)

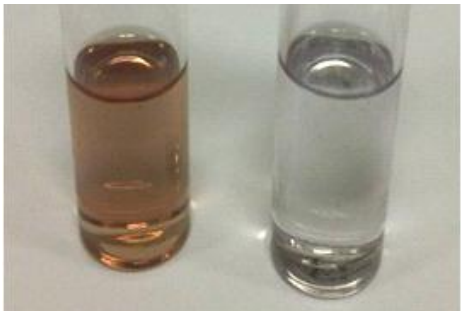

Figure 5.17: Colourimetric response of a chloroform solution **Au · 88** in the presence of CEMS a) 2.5 mL of 0.04 mg mL^{-1} **Au · 88** b) 2.5 mL of 0.04 mg mL^{-1} **Au · 88** plus 50 µL of CEMS after 30 minutes

5.6.3 Luminescence Displacement Studies

Qualitative luminescence studies were performed on both nanoparticle samples in the presence of the mustard simulant CEMS and sulphur mustard (HD). Titrations using sulphur mustard were conducted by Dr M. R. Sambrook and Jack C. Vincent at DSTL. The nanoparticle samples exhibited low intensity emission from the dansyl ligand at around 500 nm. The weak fluorescence is due to quenching of the fluorescence by the gold nanoparticle surface.[22] Spectra were obtained immediately after the addition of sulphur compound and then after five minute intervals, to determine how rapidly the stabilising dansyl ligand was displaced from the nanoparticle surface. The response by the nanoparticles in the presence of the mustard simulant CEMS is shown in Figure **5.18**. Addition of the sulphide induced a significant increase in the luminescence intensity of both samples **Au · 85** and **Au · 88**. This can be rationalised by considering the highly distance dependent nature of the non-radiative processes responsible for the quenching of the luminescence; liberation of the fluorophore from the nanoparticle surface negates quenching and hence an increase in emission is observed.

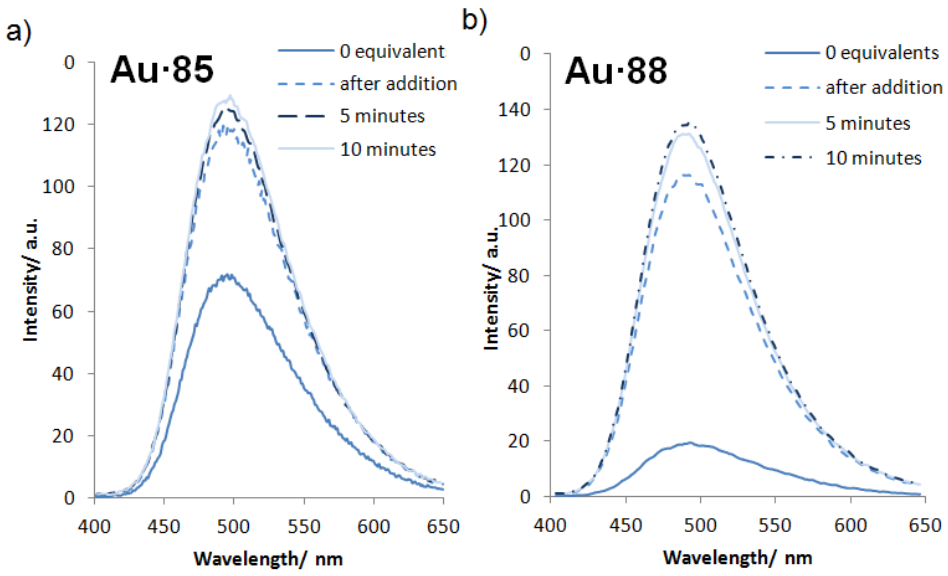

Figure 5.18: Fluorescence spectra of 0.04 mg mL^{-1} solutions of a) **Au · 85** and b) **Au · 88** upon addition of CEMS (50 µL) in $CHCl_3$ at 298 K (λ_{ex} = 345 nm)

As can be seen from the spectra the displacement is almost instantaneous, with maximum emission observed after five minutes, which is in contrast with the slower response detected by UV/vis. Both samples displayed large increases of 100% and 400% for the imidazole and amine samples respectively. Analogous results were obtained for the titrations with sulphur mustard (Figure **5.19**). It can be seen that displacement is rapid, allowing facile detection of HD by the gold nanoparticle conjugates. In this case the fluorescent enhancements are less pronounced than for the simulant compound, approximately an 80% increase in emission intensity was observed for both **Au · 85** and **Au · 88** in the presence of HD. In addition the kinetics are slightly slower for the imidazole variant which required ten minutes to achieve maximum emission. It is noteworthy that analogous titrations experiments with octan-1-ol and di-*n*-butyl ether produced no significant fluorescence change (see Figures **A.23**-**A.26** in the appendix). The selective fluorescent response of both samples to sulphides, coupled with

the rapid kintetics of displacement, suggest that conjugates **Au · 85** and **Au · 88** are promising sensory materials for mustard detection.

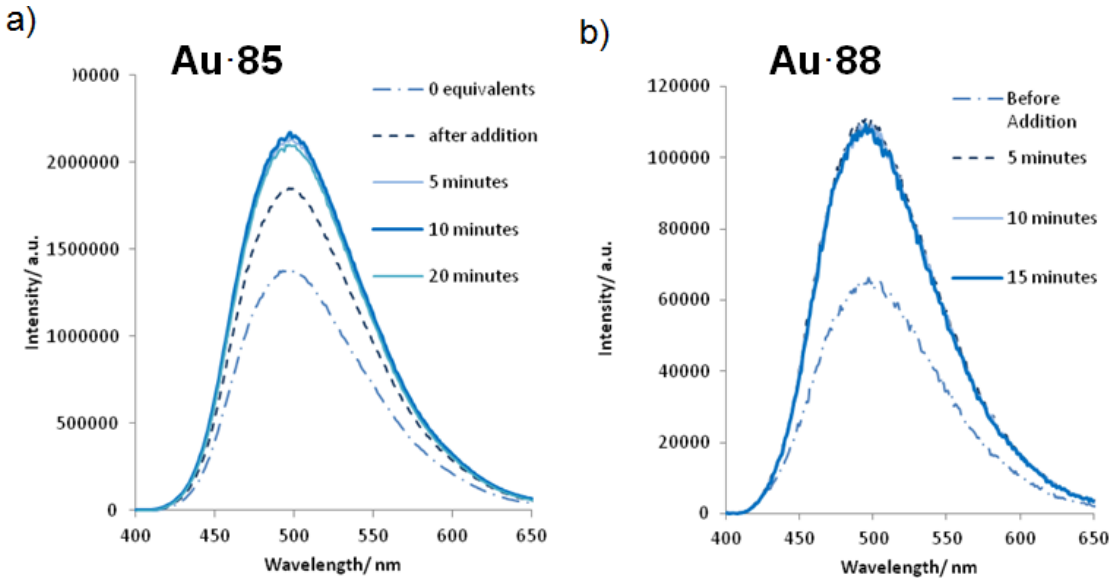

Figure 5.19: Fluorescence spectra of 0.04 mg mL^{-1} solutions of a) **Au · 85** (100 µL) plus 2 µL of HD b) **Au · 88** (100 µL) plus 2 µL of HD in $CHCl_3$ at 298 K (λ_{ex} = 345 nm)

The increase in fluorescence was also observable by the naked eye; Figure **5.20** shows a solution of **Au · 88** upon addition of the mustard simulant compound, CEMS. The luminescence of the sample increases dramatically upon exposure to the sulphide analyte, negating the need for expensive instrumentation for a qualitative analysis.

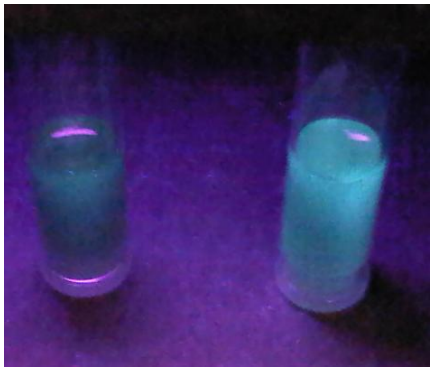

Figure 5.20: Fluorescent response of a chloroform solution **Au · 88** in the presence of CEMS a) 2.5 mL of 0.04 mg mL^{-1} **Au · 88** b) 2.5 mL of 0.04 mg mL^{-1} **Au · 88** plus 50 µL of CEMS after 30 minutes

In order to estimate the binding affinity of the mustard analytes for the nanoparticle surface, quantitative luminescence titrations were undertaken. Due to the slower kinetics of sample **Au · 85** with HD, studies were only conducted with the dansyl-amine derivative **Au · 88**. The surface coverage of **Au · 88** was determined, using sulphur elemental analysis, to be 13.5% dansyl-amine ligand **88** by weight. Titrations were conducted using a 0.04 mg mL^{-1} solution of gold nanoparticles and the change in fluorescence monitored upon addition of increasing equivalents of CEMS or HD (Figure **5.21**). As can be seen from the spectra the ligand-nanoparticle conjugates are extremely sensitive to the presence of either mustard derivative, displaying a response to micromolar concentrations of sulphur mustard.

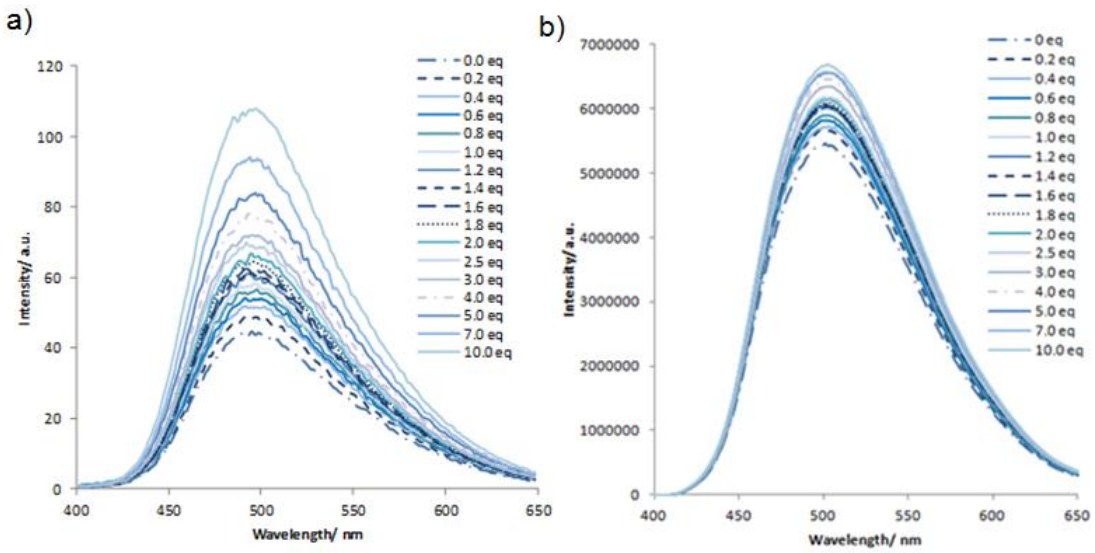

Figure 5.21: Change in emission intensity at 501 nm of a 0.04 mg mL^{-1} solution of **Au · 88** in chlorform at 298 K upon addition of increasing amounts of a) 2-chloroethylmethyl sulphide (CEMS) b) bis(2-chloroethyl)sulphide (HD) (λ_{ex} = 345 nm)

The fluorescence titration data (Figure **5.22**) was subjected to SPECFIT analysis.[26] This assumes the displacement is a 1:1 stoichiometric ligand exchange process with one guest sulphide displacing one surface stabilised ligand, and ignores any cooperativity effects between the surface exchange sites. SPECFIT analysis of the fluorescence titration data determined association constant values of $\log K = 4.65 \pm 0.06$ and $\log K = 4.19 \pm 0.05$ for CEMS and HD respectively, which indicates the binding affinities of the two sulphide analytes are of the same magnitude.

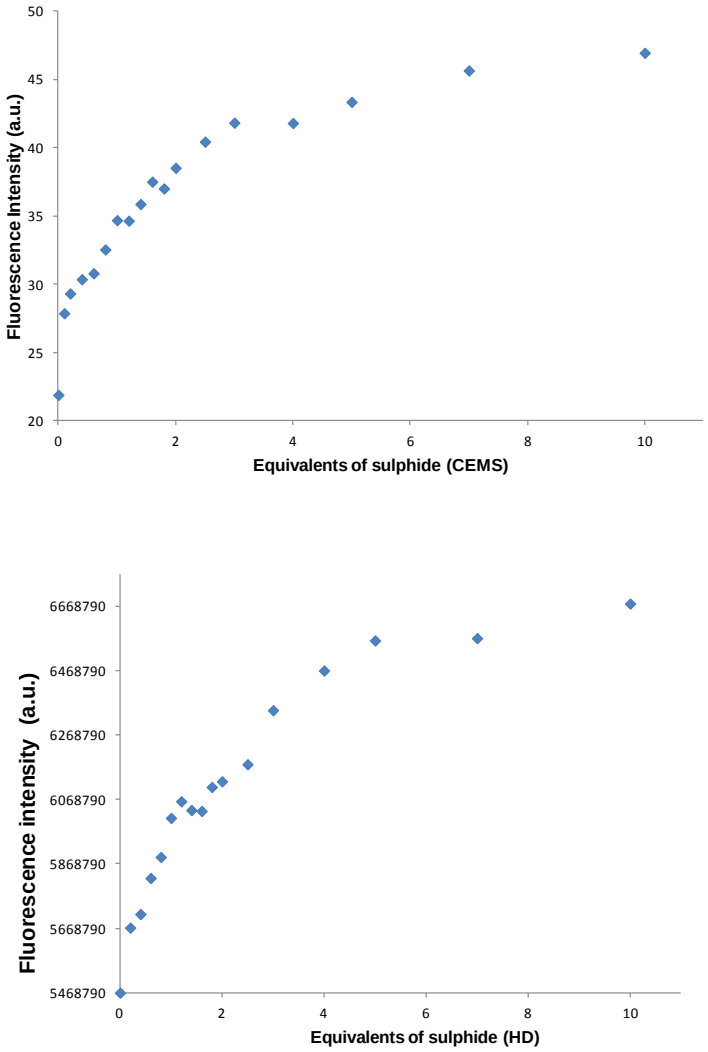

Figure 5.22: Corrected binding curve for the change in emission intensity at 501 nm of **Au · 88** upon addition of a) 2-chloroethylmethyl sulphide b) bis-(2-chloroethyl)sulphide (λ_{ex} = 345 nm)

5.7 Summary

The development of a novel sensing method for the detection of mustard compounds was succesfully accomplished. This was achieved through the use of dansyl-ligated gold nanoparticles which displayed a 'switching on' fluorescent displacement assay response in the presence of CEMS and HD.

Imidazole- and amine-functionalised dansyl and naphthalimide fluorophores were prepared by high-yielding synthetic strategies. Although stable gold nanoparticles with the naphthalimide functionalised ligands were not isolated, dansyl functionalised ligands did produce soluble, stable conjugates.

A preliminary ^{1}H NMR titration experiment indicated that upon addition of CEMS to **Au · 85** the dansyl ligands were displaced from the nanoparticle surface as a result of the highly thiophilic nature of gold. This was corroborated by the UV/visible titrations which showed bathochromic shifts in the SPR absorption band, indicating agglomeration of the nanoparticles. Qualitative titrations of samples **Au · 85** and **Au · 88** with simulant CEMS and sulphur mustard (HD) gave rise to a 'switching on' of the fluorescence of the sample, which was observable by the naked eye. Importantly, analogous titrations with non-sulphur containing alcohol and ether compounds gave no fluorescence response, revealing a degree of selectivity. These results indicate that dansyl-nanoparticle conjugates may be of practical use in real world devices for the detection of HD.

5.8 Conclusions

In this chapter the use of fluorescent ligand-nanoparticle conjugates were explored as potential sensors for sulphur mustard and its derivatives. The work demonstrates that this proof of concept is a viable approach, using a displacment assay to detect HD, which exploits the hierarchy of binding energies of different ligands with gold nanoparticle surfaces. Through the use of weakly stabilising imidazole and amine groups it was possible to readily displace

the fluorescent ligands from the metal nanoparticle surface with rapid kinetics, to produce a detectable increase in the emission response of the samples. It is noteworthy that no emission enhancement was observed for alcohols and ethers. Furthermore in the situations in which these sensory materials may be potentially used it is unlikely that other sulphides will be present, removing the necessity to be able to discriminate between sulphur analytes.

5.9 References

1. M. R. Sambrook and S. Notman, *Chem. Soc. Rev.*, 2013, **42**, 9251-9267.
2. R. M. Black, R. J. Clarke, R. W. Read and M. T. J. Reid, *J. Chromatogr. A*, 1994, **662**, 301-321.
3. H. Thiermann, F. Worek and K. Kehe, *Chem.-Biol. Interact.*, 2013, **206**, 435-443.
4. M. Nagao, T. Takatori, Y. Matsuda, M. Nakajima, H. Iwase and K. Iwadate, *Toxicol. Appl. Pharmacol.*, 1997, **144**, 198-203.
5. K. Kim, O. G. Tsay, D. A. Atwood and D. G. Churchill, *Chem. Rev.*, 2011, **111**, 5345-5403.
6. S. W. Zhang and T. M. Swager, *J. Am. Chem. Soc.*, 2003, **125**, 3420-3421.
7. S. Tal, H. Salman, Y. Abraham, M. Botoshansky and Y. Eichen, *Chem.-Eur. J.*, 2006, **12**, 4858-4864.
8. M. Zengerle, F. Brandhuber, C. Schneider, F. Worek, G. Reiter and S. Kubik, *Beilstein J. Org. Chem.*, 2011, **7**, 1543-1554.
9. F. C. G. Hoskin, D. M. Steeves and J. E. Walker, *Biol. Bull.*, 1999, **197**, 284-285.
10. S. M. Daly, M. Grassi, D. K. Shenoy, F. Ugozzoli and E. Dalcanale, *J. Mater. Chem.*, 2007, **17**, 1809-1818.
11. Y. A. Ruan, H. A. Taha, R. J. Yoder, V. Maslak, C. M. Hadad and J. D. Badjic, *J. Phys. Chem. B*, 2013, **117**, 3240-3249.
12. M. R. Sambrook, J. R. Hiscock, A. Cook, A. C. Green, I. Holden, J. C. Vincent and P. A. Gale, *Chem. Commun.*, 2012, **48**, 5605-5607.
13. A. Barba-Bon, A. M. Costero, M. Parra, S. Gil, R. Martinez-Manez, F. Sancenon, P. A. Gale and J. R. Hiscock, *Chem.-Eur. J.*, 2013, **19**, 1586-1590.
14. I. Bandyopadhyay, M. J. Kim, Y. S. Lee and D. G. Churchill, *J. Phys. Chem. A*, 2006, **110**, 3655-3661.
15. K. Kim, I. Kim, N. Maiti, S. J. Kwon, D. Bucella, O. A. Egorova, Y. S. Lee, J. Kwak and D. G. Churchill, *Polyhedron*, 2009, **28**, 2418-2430.
16. R. Shunmugam and G. N. Tew, *Chem.-Eur. J.*, 2008, **14**, 5409-5412.
17. J. Massue, S. J. Quinn and T. Gunnlaugsson, *J. Am. Chem. Soc.*, 2008, **130**, 6900-6901.

18. M. Burnworth, S. J. Rowan and C. Weder, *Chem.-Eur. J.*, 2007, **13**, 7828-7836.
19. D. Knapton, M. Burnworth, S. J. Rowan and C. Weder, *Angew. Chem.-Int. Edit.*, 2006, **45**, 5825-5829.
20. R. I. Tilley, *Aust. J. Chem.*, 1990, **43**, 1573-1576.
21. J. F. Brinkley, M. L. Kirkey, A. D. S. Marques and C. T. Lin, *Chem. Phys. Lett.*, 2003, **367**, 39-43.
22. T. L. Jennings, M. P. Singh and G. F. Strouse, *J. Am. Chem. Soc.*, 2006, **128**, 5462-5467.
23. E. Riva, D. Comi, S. Borrelli, F. Colombo, B. Danieli, J. Borlak, L. Evensen, J. B. Lorens, G. Fontana, O. M. Gia, L. D. Via and D. Passarella, *Bioorganic & Medicinal Chemistry*, 2010, **18**, 8660-8668.
24. M. Brust, M. Walker, D. Bethell, D. J. Schiffrin and R. Whyman, *J. Chem. Soc.-Chem. Commun.*, 1994, 801-802.
25. R. H. Terrill, T. A. Postlethwaite, C. H. Chen, C. D. Poon, A. Terzis, A. D. Chen, J. E. Hutchison, M. R. Clark, G. Wignall, J. D. Londono, R. Superfine, M. Falvo, C. S. Johnson, E. T. Samulski and R. W. Murray, *J. Am. Chem. Soc.*, 1995, **117**, 12537-12548.
26. SPECTFIT, 2.02, Spectrum Software Associates, Chapel Hill, NC, USA.

Chapter 6: Experimental

6.1 General Information

6.1.1 Solvents and Reagents

Commercially available solvents and chemicals were used without further purification unless stated. Where dry solvents were used, they were degassed with nitrogen, dried by passing through an MBraun MPSP-800 column except in the case of toluene for the Pd-catalysed Stille reaction which was kindly supplied by Remi Tirfoin of the Aldridge group. Water was deionised in all cases and microfiltered prior to use through a Milli-Q® Millipore machine. Where it is not stated acid chlorides were formed using 2 equivalents of oxalyl chloride per acid in dry dichloromethane and catalytic amounts of DMF. This is with the exception of isophthaloyl dichloride which is available commercially. Gaseous hydrogen chloride was prepared by adding concentrated $H_2SO_{4(aq)}$ to sodium chloride. The compounds found within this these were synthesised unless otherwise stated. Tetrabutylammonium (TBA) salts, Grubb's catalysts, $Pd(PPh_3)_2Cl_2$, $[Cu(CH_3CN)_4][PF_6]$, TBTA, $AgPF_6$, $AgBF_4$, $RuCl_3 \cdot xH_2O$, $KtPtCl_4$ and $LiPF_6$ were stored in a vacuum desiccator.

6.1.2 Intrumentation

NMR spectra were obtained using Varian Mercury 300, AVII 500 (for ^{13}C cryoprobe), Unity Plus 500 and AVIII 500 spectrometers at 293 K. The internal standards for ^{19}F and ^{31}P NMR were $CFCl_3$ and H_3PO_4 respectively. Low resolution electrospray mass spectrometry was

performed using a Micromass LCT Premier XE spectrometer and high resolution electrospray mass spectrometry to four decimal places was achieved with Bruker microTOF and Bruker FT-ICR-MS spectrometers. Electron impact and field ionisation mass spectrometry was carried out using a Micromass GCT spectrometer, fitted with a temperature programmed solid probe inlet. MALDI mass spectra were obtained using a Waters MALDI micro spectrometer. Reactions carried out under microwave irradiation used a Biotage Initiator 2.0 microwave. Fluorescence spectra were recorded on a Varian Cary-Eclipse or Yvon-Horiba Fluorolog spectrophotometers. UV-vis spectra were recorded on an Agilent Cary Series UV-Vis-Spectrophotometer at 298 K. Crystal structures were obtained on a Nonius Kappa KCCD diffractometer or using synchrotron radiation on beamline I19 at Diamond Light Source and are discussed later in more detail in the appendix.

6.2 Synthetic Procedures

General Procedure for Anion Exchange

Compound was dissolved in $CHCl_3$ (x mL) and washed with aqueous $NH_4Y_{(aq)}$ (Y = anion) (10 × x mL), dried over $MgSO_4$, filtered and the solvent removed *in vacuo*. Solutions of 1 M of NH_4Y was used except in the case of hexafluorophosphate which was as a 0.l M solution.

Chapter 2 Syntheses

Synthesis of *para*-butylcalix[4]arene 2[1]

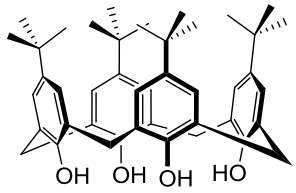

NaOH pellets (0.96 g, 0.024 mol) and p-*tert*-butylphenol (80 g, 0.53 mol) were placed into a 1 litre 3 necked round-bottomed flask, which was fitted with a thermometer, condenser and an overhead mechanical stirrer, and placed within a heating mantle. Formaldehyde (52 mL, 37% w/v, 0.64 mol) was added and the system stirred at 120 °C for 3 hours, after which time a viscous yellow mass had formed. This was allowed to cool to room temperature, then diphenyl ether (400 mL) was added, and the material stirred to aid dissolution. Once the material had dissolved, the flask was fitted with a nitrogen inlet, and the condenser set up for distillation. The stirred solution was then heated to 150 °C to remove H_2O, with N_2 being blown over the solution to aid the process. After *ca.* 3 hours, H_2O was no longer being collected, and a precipitate was observed to have formed in solution. The condenser was then reset for reflux, and the nitrogen inlet replaced with a thermometer. This suspension was then heated under reflux (250-280 °C) for 3 hours, resulting in a dark brown solution. The reaction mixture was allowed to cool to room temperature, then ethyl acetate (400 mL) was added, forming a brown precipitate; this was stirred for a further 30 minutes. The precipitate was collected by filtration then washed with ethyl acetate (2 × 100 mL) and acetic acid (2 × 200 mL). This grey material was recrystallised from toluene and dried to give p-*tert*-butyl calix[4]arene · toluene (1:1) as a white solid (36.9g, 43%); ^{1}H NMR (300MHz, $CDCl_3$) δ_H 10.35

(4H, s, O*H*). 7.06 (8H, s, Ar*H*), 4.26 (4H, d, ^2J = 12.6Hz, C*H*H), 3.52 (4H, d, ^2J = 12.6Hz, CH*H*), 1.19 (36H, s, ^{t}*Bu*).

Synthesis of hydroquinone bis-mesylate 3[2]

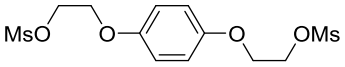

Hydroquinone bis(2-hydroxyethyl)ether (10.0 g, 50 mmol) was dissolved in a solution of dry DCM (200 mL), THF (100 mL) and NEt_3 (17.9 g, 24.6 mL, 176.50 mmol). Methanesulphonyl chloride (12 mL, 155 mmol) dissolved in CH_2Cl_2 (20 mL) was then added dropwise, and the reaction mixture stirred for 1 hour. The solution was then washed with 1 M $HCl_{(aq)}$ (3 × 50 mL), saturated $NaHCO_{3(aq)}$ (3 × 50 mL) and brine (2 × 50 mL). The combined organic layers were dried over anhydrous $MgSO_4$ and filtered before the solvent was removed *in vacuo*. The solid product was recrystallised using chloroform/hexane to give the product as a white solid (17.79 g, 99%). ^{1}H NMR (300 MHz, $CDCl_3$) δ_H 6.85 (4H, s, Ar*H*), 4.55 (4H, t, ^3J = 4.7 Hz, OCH_2), 4.20 (4H, t, ^3J = 4.7 Hz, OCH_2), 3.09 (6H, s, CH_3); ESI-LRMS: found m/z = 377.06, calculated 377.01 for $[M + Na]^+$.

Synthesis of hydroquinone mesylate-phthalimide 4[2]

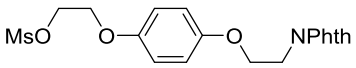

A toluene suspension (60 mL) of **7** (4.0 g, 11.29 mmol), potassium phthalimide (2.3 g, 12.42 mmol) and aliquat336 (1.55 mL, 3.39 mmol) was stirred for 2 hrs at 65 °C. The solution was then filtered and washed with toluene (30 mL) and diethyl ether (30 mL) before the solvent was removed *in vacuo*. The solid product was then recrystallised twice using chloroform/ hexane before it was purified by column chromatography (silica; EtOAc:hexane 1:1) to give

the compound as a white solid (1.69 g, 4.16 mmol, 37%). ^{1}H NMR (300 MHz, $CDCl_3$) δ_H 7.87-7.84 (2H, m, Ar*H*), 7.73-7.70 (2H, m, Ar*H*), 6.80-6.79 (4H, m, Ar*H*), 4.53-4.50 (2H, m, CH_2), 4.19-4.15 (4H, m, OCH_2), 4.09-4.05 (2H, m, OCH_2), 3.06 (3H, s, CH_3); ESI-LRMS: found m/z = 428.11, calculated 428.08 for $[M + Na]^+$.

Synthesis of hydroquinone tosylate-alcohol 5[3]

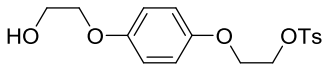

Tosyl chloride (6.06 g, 31.8 mmol) was added to a stirred solution of hydroquinone bis(2-hydroxylethyl)ether (6.00 g, 30.3 mmol), triethylamine (5.5 mL, 39.4 mmol) and *N,N*-dimethyl-4-aminopyridine (DMAP) (cat. 10 mg) in dry THF (150 mL), and the resulting reaction mixture was stirred under N_2 for 16 hours. The white suspension was filtered, and the filtrate was concentrated *in vacuo* to give a crude yellow material that was purified by column chromatography (silica; EtOAc/hexane 1:1) give **5** as a yellow oil (5.13 g, 48%). ^{1}H NMR (300 MHz, $CDCl_3$) δ_H 7.82 (2H, d, ^3J = 8.1 Hz, Ar*H*), 7.36 (2H, d, ^3J = 8.1 Hz, Ar*H*), 6.82 (2H, d, ^3J = 9.4 Hz, Ar*H*), 6.73 (2H, d, ^3J = 9.4 Hz, Ar*H*), 4.34 (2H, t, ^3J = 4.7 Hz, OCH_2), 4.10 (2H, t, ^3J = 4.7 Hz, OCH_2), 4.03 (2H, m, OCH_2), 3.95 (2H, m, OCH_2), 2.46 (3H, s, CH_3); ESI-LRMS: found m/z = 375.09, calculated 375.08 for $[M + Na]^+$.

Synthesis of hydroquinone phthalimide-alcohol 6[3]

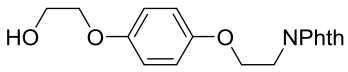

Potassium phthalimide (2.60 g, 14.1 mmol) was added to a solution of **5** (3.30 g, 9.38 mmol) in anhydrous DMF (25 mL), and the resulting suspension was heated to 100 °C for 16 hours, under a nitrogen atmosphere. The reaction mixture was subsequently allowed to cool to room

temperature and was then poured onto H_2O (100 mL). The suspension was extracted with CH_2Cl_2 (3 × 50 mL), before the organic extracts were combined, dried over anhydrous $MgSO_4$, filtered, and the filtrate concentrated *in vacuo*. The crude product was purified by column chromatography (silica; EtOAc/hexane 1:1) to give **6** as a white solid (1.96 g, 64%). ^{1}H NMR (300 MHz, $CDCl_3$) δ_H 7.87 (2H, m, Ar*H*), 7.73 (2H, m, Ar*H*), 4.19 (2H, m, CH_2), 6.82 (4H, m, Ar*H*), 4.03 (2H, m, CH_2OH), 4.09 (2H, m, CH_2), 3.93 (2H, m, CH_2), 2.04 (1H, t, ^3J = 6.2 Hz, O*H*); ESI-LRMS: found *m/z* = 350.12, calculated 350.10 for [M + Na]$^+$.

Synthesis of calix[4]arene bis-phthalimide 7[3]

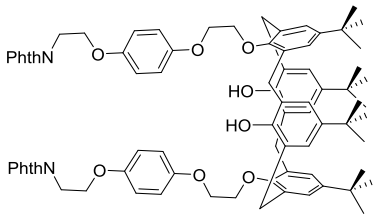

p-tert-butylcalix[4]arene (0.5 g, 0.70 mmol) and K_2CO_3 (0.075 g, 1.5 mmol) were suspended in dry acetonitrile (40 mL) and stirred at ambient temperature under an N_2 atmosphere for 1 hour. Compound **4** (0.71 g, 1.75 mmol) was added and the reaction was heated at reflux for 5 days. The reaction was cooled to ambient temperature and the solvent removed *in vacuo*. 1 M $HCl_{(aq)}$ (50 mL) was added, extracted with CH_2Cl_2 (3 × 50 ML), washed with H_2O (2 × 50 ML), dried over $MgSO_4$, and filtered. The solvent was removed *in vacuo* and the crude material purified by column chromatography (silica; EtOAc/hexane 1:1) to give the compound as a white solid (0.53 g, 60%). ^{1}H NMR (300 MHz, $CDCl_3$) δ_H 7.83 (2H, m, Ar*H*), 7.66 (2H, m , Ar*H*), 7.20 (2H, s, O*H*), 7.04 (4H, s, Ar*H*), 6.86 (4H, s, Ar*H*), 6.82 (8H, s, Ar*H*), 4.40 (4H, d, ^2J = 12.9 Hz, C*H*H), 4.27 (4H, m, CH_2), 4.20 (8H, m, OCH_2), 4.09 (4H, m,

OC*H*$_2$), 3.30 (4H, d, ^2J = 12.9 Hz, C*H*H), 1.28 (18H, s, ^{t}*Bu*), 1.01 (18H, s, ^{t}*Bu*); ESI-LRMS: found m/z = 1289.72, calculated 1289.61 for $[M + Na]^+$.

Synthesis of calix[4]arene bis-amine 8

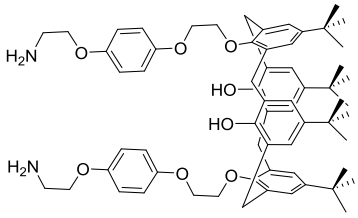

Calix[4]arene bis-phthalimide (0.8 g, 0.65 mmol) and hydrazine monohydrate (1.5 mL, 30.9 mmol) were dissolved in absolute ethanol (15 mL) and heated under microwave irradiation at 100 °C for 20 minutes. The reaction was extracted with EtOAc (3 × 50 mL), the organic phase was washed with brine (2 × 50 mL), dried over anhydrous $MgSO_4$ and filtered. The solvent was removed *in vacuo* to give the compound as a white solid (0.60 g, 92%). ^{1}H NMR (300 MHz, $CDCl_3$) δ_H 7.51 (2H, s, O*H*), 7.02 (4H, s, Ar*H*), 6.92-6.81 (12H, m, Ar*H*), 4.39 (4H, d, ^2J = 12.9 Hz, C*H*H), 4.30-4.25 (12H, m, OC*H*$_2$), 3.93 (4H, m, OC*H*$_2$), 3.29 (4H, d, ^2J = 12.9 Hz, C*H*H), 2.95 (4H, br. s, N*H*$_2$), 1.26 (18H, s, ^{t}*Bu*), 1.00 (18H, s, ^{t}*Bu*); ESI-LRMS: found m/z = 504.35, calculated 504.31 for $[M + 2H]^{2+}$.

Synthesis of calix[4]arene pyridine macrocycle 9

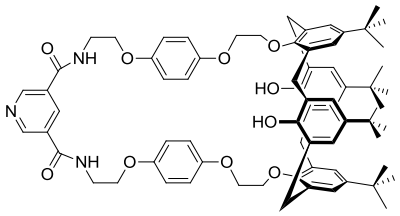

Calix[4]arene bis-amine **8** (530 mg, 0.526 mmol) was dissolved in dry CH_2Cl_2 (20 mL). Pyridine-3,5-dicarbonyl dichloride (0.631 mmol) was dissolved in dry CH_2Cl_2 (20 mL). The

solutions were added dropwise *via* syringe pump to a solution of Et_3N (0.293 mL, 2.11 mmol) in dry CH_2Cl_2 (200 mL) over 3 hours under an N_2 atmosphere. The reaction was stirred for a further 18 hours after which the solvent was washed with 1 M citric $acid_{(aq)}$ (100 mL), sat. $NaHCO_{3(aq)}$ (100 mL) and brine (100 mL) and dried over $MgSO_4$. The crude material was purified by column chromatography (silica; CH_2Cl_2/MeOH; 98:2) to give the compound as a white solid (563 mg, 94%). ^{1}H NMR (300 MHz, $CDCl_3$) δ_H 9.18 (2H, s, Ar*H*), 8.36 (1H, s, Ar*H*), 7.42 (2H, s, O*H*), 7.18 (2H, br. s, N*H*), 7.06 (4H, s, Ar*H*), 6.91-6.76 (12H, m, Ar*H*), 4.40 (4H, d, $^2J = 12.9$ Hz, C*H*), 4.36-4.23 (8H, m, , CH_2), 4.11 (4H, br. s, CH_2), 3.84 (4H, br. s, CH_2), 3.33 (4H, d, $^2J = 13.5$ Hz), 1.28 (18H, s, ^{t}*Bu*), 1.00 (18H, s, ^{t}*Bu*); ^{13}C NMR (75 MHz, $CDCl_3$) δ_C 165.1, 153.3, 152.7, 151.5, 150.5, 150.0, 147.1, 141.6, 132.7, 129.3, 127.9, 125.7, 125.2, 116.2, 115.7, 74.2, 67.4, 67.3, 39.8, 34.0, 33.8, 31.7, 31.0; ESI-HRMS: found m/z = 1160.5966, calculated 1160.5971 for $[M + Na]^+$.

Synthesis of calix[4]diquinone pyridine macrocycle 1

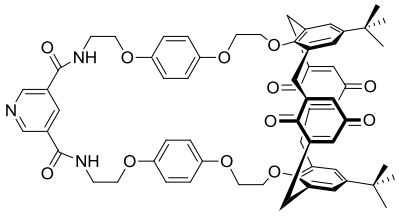

Thallium (III) trifluoroacetate (2.69 g, 4.95 mmol) was suspended in dry CH_2Cl_2 (20 mL) at 0°C under N_2 in the absence of light. A solution of calix[4]arene macrocycle **9** (563 mg, 0.495 mmol) in CH_2Cl_2 (20 mL) and trifluoroacetic acid (5 mL) was added simultaneously and the reaction was stirred at 0 °C for 35 minutes. The reaction was quenched with H_2O (10 mL) and stirred vigorously for 10 minutes. This was repeated twice and the organic layer dried over anhydrous $MgSO_4$. Purification by column chromatography

(silica; acetone/hexane 75:25→100:0) and preparative TLC (silica; CH_2Cl_2/MeOH 95:5) afforded **2** as a bright orange solid (219 mg, 42%). ^{1}H NMR (300 MHz, $CDCl_3$) δ_H 9.17 (2H, s, Ar*H*), 8.54 (1H, s, Ar*H*), 6.93-6.76 (12H, m , Ar*H*), 6.70 (4H, s, C*H*), 4.17-4.04 (8H, m, C*H,* CH_2), 3.98-3.80 (12H, m, CH_2), 3.30 (4H, d, ^2J = 12.9 Hz, C*H*), 1.14 (18H, s, ^{t}*Bu*); ^{13}C NMR (75 MHz, $CDCl_3$) δ_C 186.7, 185.6, 165.3, 153.9, 152.7, 150.9, 147.1, 146.5, 133.1, 129.8, 129.4, 126.9, 115.4, 72.6, 67.2, 67.0, 39.8, 34.1, 32.7, 31.4; ESI-HRMS: found m/z = 1076.4323, calculated 1076.4304 for [M + Na]$^+$.

Synthesis of pyridine bis-propylbromide 11[4]

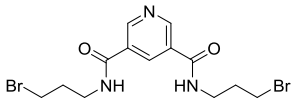

3-bromopropylamine hydrobromide (0.875 g, 6.0 mmol) and Et_3N (1.25 mL, 9.0 mmol) were suspended in dry CH_2Cl_2 (25 mL) under N_2 and cooled to 0 °C. Pyridine dicarbonyl chloride (0.613 g, 3.0 mmol) was dissolved in CH_2Cl_2 (25 mL) and added dropwise to the solution. The reaction was allowed to warm to ambient temperature and stirred under N_2 for 18 hours. The reaction was washed with 10% $HCl_{(aq)}$ (2 × 25 mL) and the organic layer discarded. Neutralisation of the aqueous phase with sat. $NaHCO_{3(aq)}$ gave a precipitate. The mixture was filtered, washed with H_2O (2 × 25 mL) and dried to give the compound as a white solid (0.781 g, 32%). ^{1}H NMR (300 MHz, DMSO-*d*$_6$) δ_H 9.10 (2H, d, ^4J = 1.9 Hz, Ar*H*), 8.95 (2H, br. s, N*H*), 8.59 (1H, t, ^4J = 1.9 Hz, Ar*H*), 3.60 (4H, t, ^3J = 6.7 Hz, CH_2), 3.48-3.32 (4H, m, CH_2), 2.17-2.01 (4H, m, CH_2); ESI-LRMS: found m/z = 407.93, calculated 407.97 for [M + H]$^+$.

Synthesis of pyridine bis-propylazide 12[4]

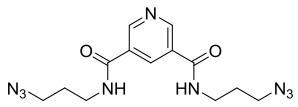

Pyridine bis-propylbromide **11** (0.5 g, 1.23 mmol) and NaN_3 (0.24 g, 3.68 mmol) were dissolved in dry DMF (30 mL) and stirred overnight under N_2 at 85 °C. The reaction was cooled to ambient temperature and the solvent removed *in vacuo*. The residue was dissolved in CH_2Cl_2 (50 mL) and washed with H_2O (3 × 50 mL), brine (3 × 50 mL), dried over $MgSO_4$ and filtered. Removal of the solvent *in vacuo* gave the product as an off-white solid (408 mg, 86%). ^{1}H NMR (300 MHz, $CDCl_3$) δ_H 9.10 (2H, s, Ar*H*), 8.50 (1H, t, ^4J = 2.0 Hz, Ar*H*), 7.55 (2H, t, ^3J = 5.6 Hz, N*H*), 3.64–3.53 (4H, m, C*H*$_2$), 3.47 (4H, t, ^3J = 6.4 Hz, C*H*$_2$), 1.99–1.88 (4H, m, C*H*$_2$); ESI-LRMS: found m/z = 332.21, calculated 332.16 for $[M + H]^+$.

Pyridine *N*-oxide axle precursor 13

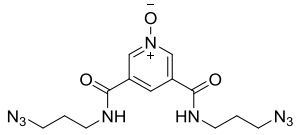

Pyridine bis-azide **12** (0.1 g, 0.301 mmol) and $NaHCO_3$ (0.858 g, 9.03 mmol) were dissolved in biphasic H_2O/ 2-butanone 1:1 (50 mL). Oxone (0.556 g, 1.81 mmol) in H_2O (10 mL) was added dropwise and the reaction was stirred at ambient temperature for 3 hours. NaCl (*ca.* 2.5 g) was added and the product was extracted with $CHCl_3$ (3 × 20 mL). The organic phase was dried over anhydrous $MgSO_4$, filtered and the solvent removed to give the product as a white solid (0.077 g, 74%). ^{1}H NMR (300 MHz, $CDCl_3$) δ_H 8.87 (2H, s, Ar*H*), 8.19 (1H, s, *Ar*H), 7.80 (2H, br s, N*H*$_2$), 3.51 (4H, t, ^3J = 6.5 Hz, C*H*$_2$), 3.39 (4H, t, ^3J = 6.5 Hz, C*H*$_2$), 1.88 (4H, m, C*H*$_2$); ESI-LRMS: found m/z = 370.16, calculated 370.13 for $[M + Na]^+$.

Synthesis of triphenyl stopper 14[5]

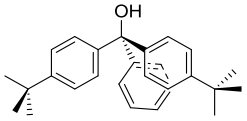

A solution of 1-bromo-4-(tert-butyl)benzene (14 mL, 80.80 mmol) dissolved in dry THF (50 mL) was added dropwise, under nitrogen, to a suspension of magnesium turnings (2.1 g, 86.38 mmol) in dry THF (150 mL) and $I_{2(cat.)}$. The mixture was heated to 60 °C during the addition until the reaction had started before being left to stir at rt for 2 hours. A solution of methyl benzoate (4.8 mL, 38.43 mmol), dissolved in dry THF (30 mL), was then added dropwise over 20 minutes and the reaction heated at reflux for 18 hours. After cooling to ambient temperature, the solution was neutralised with 10% $HCl_{(aq)}$ and H_2O was added (100 mL). The organic layer was extracted with hexane (2 × 50 mL), washed with brine (3 × 50 mL) and dried over anhydrous $MgSO_4$. After filtration, the solvent was removed *in vacuo* and the crude product recrystallised twice from MeOH to give the product as white needles (9.45 g, 66%). ^{1}H NMR (300 MHz, $CDCl_3$) δ_H 7.49-7.27 (13H, m, Ar*H*), 3.23 (1H, s, O*H*), 1.31 (18H, s, ^{t}*Bu*); ESI-LRMS: found m/z = 355.27, calculated 355.24for [M - OH]$^+$.

Synthesis of alcohol terphenyl stopper 15[5]

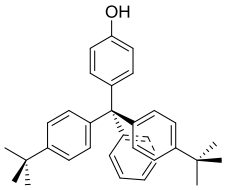

A solution of **14** (4.0 g, 10.7 mmol) dissolved in phenol (15.4 g, 163 mmol), containing 37% $HCl_{(aq)}$ (1 mL) was heated at 110 °C, under nitrogen for 48 hours. The reaction was cooled to ambient temperature, extracted with toluene (3 × 150 mL) and the combined organic phases

washed with 1M $NaOH_{(aq)}$ (3 × 50 mL) and water (3 × 50 mL) before drying over anhydrous $MgSO_4$. After filtration, the solvent was removed *in vacuo* and the crude product recrystallised from toluene/hexane to give the product as a white solid (2.15 g, 45%). ^{1}H NMR (300 MHz, $CDCl_3$) δ_H (7.35-7.26 (9H, m, Ar*H*), 7.21-7.09 (6H, m, Ar*H*), 6.77 (2H, d, ^3J = 13.3 Hz, Ar*H*), 4.23 (1H, s, O*H*), 1.37 (18H, s, ^{t}*Bu*).

Synthesis of alkyne terphenyl stopper 16[5]

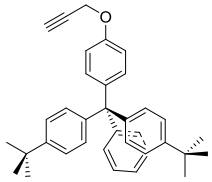

A solution of propargyl benzene sulphonate (0.60 mL, 3.83 mmol), K_2CO_3 (0.7 g, 5.06 mmol) and alcohol terphenyl stopper **15** (1.1 g, 2.34 mmol), in dry acetonitrile (15 mL), was heated in the microwave reactor for 2 hours at 160 °C. The reaction was cooled to ambient temperature and the solvent was removed *in vacuo*. The resultant solid product redissolved in 1M $HCl_{(aq)}$/CH_2Cl_2 1:1 solution (40 mL), washed with brine (2 x 20 mL), dried over anhydrous $MgSO_4$ and filtered. Purification by column chromatography (silica; hexane/CH_2Cl_2 7:3) gave the product as a white solid (0.89 g, 78%). ^{1}H NMR (300 MHz, $CDCl_3$) δ_H 7.27-7.18 (9H, m, Ar*H*), 7.14-7.08 (6H, m, Ar*H*), 6.74 (2H, d, ^3J = 13.8 Hz, Ar*H*), 4.67 (2H, d, ^4J = 2.3 Hz, CH_2), 2.52 (1H, t, ^4J = 2.3 Hz, CC*H*), 1.10 (18H, s, ^{t}*Bu*).

Synthesis of pyridine *N*-oxide axle 17[4]

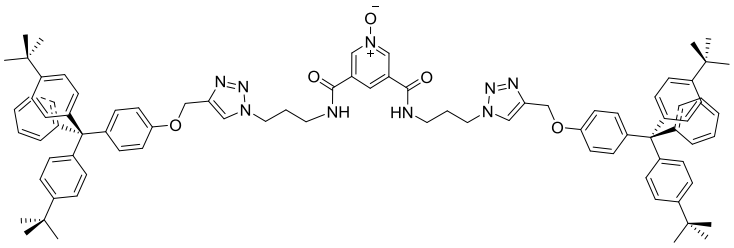

$Cu^{I}(MeCN)_4PF_6$ (5.21 mg, 0.014 mmol) was added to a solution of alkyne stopper **16** (154 mg, 0.32 mmol), TBTA (7.42 mg, 0.014 mmol), DIPEA (0.05 mL) and pyridine *N*-oxide bis-azide **13** (50 mg, 0.14 mmol) in $CHCl_3$ (20 mL). The reaction was stirred at ambient temperature under N_2 for 48 hours. The solvent was removed *in vacuo* and purified by column chromatography (silica; CH_2Cl_2/MeOH 97:3) to give the compound as a white solid (120 mg, 65%). ^{1}H NMR (300 MHz, $CDCl_3$) δ_H 9.04 (2H, s, Ar*H*), 8.54 (2H, br. s, N*H*), 8.32 (1H, s, Ar*H*), 7.62 (2H, s, Ar*H*), 7.26-7.04 (30H, m, Ar*H*), 6.76 (4H, d, ^{3}J = 14.7 Hz, Ar*H*), 5.04 (4H, s, OCH_2), 4.27 (2H, m, OCH_2), 3.50 (2H, m, OCH_2), 2.26 (2H, m, OCH_2), 1.28 (36H, s, ^{t}*Bu*); ESI-LRMS: found m/z = 1320.89, calculated 1320.73 for $[M + H]^+$.

Synthesis of calix[4]diquinone [2]rotaxane 18

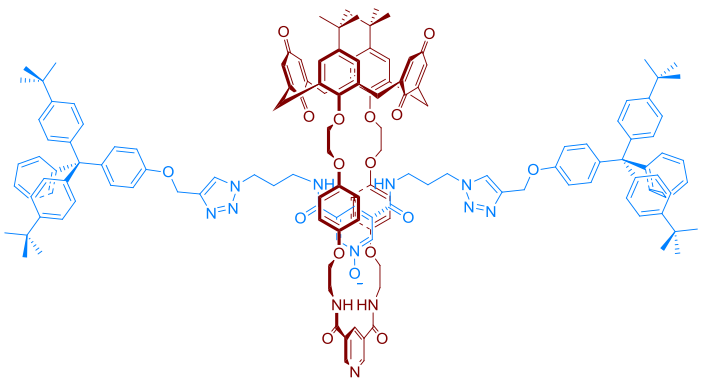

Calix[4]diquinone macrocycle **1** (30.0 mg, 0.0283 mmol) and sodium perchlorate (3.84 mg, 0.0313 mmol) were dissolved in $CHCl_3$ (10 mL) and stirred under N_2 for 16 hours. Stopper

alkyne **16** (30.39 mg, 0.0625 mmol), $Cu^{I}(MeCN)_4PF_6$ (2.08 mg, 0.00554 mmol), TBTA (2.22 mg, 0.0042 mmol) and diisopropylamine (DIPEA) (0.01 mL) were added and the reaction was stirred at ambient temperature for 36 hours under N_2. The reaction was subsequently washed with 0.25 M $EDTA_{(aq)}$ (3 × 10 mL) and the solvent removed *in vacuo*. Purification by size exclusion chromatography (SX-3; $CHCl_3$) and preparative thin layer chromatography (silica; CH_2Cl_2/MeOH; 99:1→97:3) afforded the compound as yellow solid (41.5 mg, 62 %). ^{1}H NMR (500 MHz, $CDCl_3$) δ_H 9.32 (2H, d, ^4J = 2.2 Hz, pyridine isophthalamide Ar*H*), 9.08 (1H, t, ^4J = 2.0 Hz, pyridine isophthalamide Ar*H*), 8.59 (2H, s, pyridine N-oxide isophthalamide Ar*H*), 8.35 (2H, br.s, N*H*), 7.91 (2H, br.s, N*H*), 7.75 (2H, s, triazole Ar*H*), 7.46 (1H, s, pyridine N-oxide isophthalamide Ar*H*), 7.25-7.04 (30H, m, stopper Ar*H*), 6.90-6.80 (12H, m, stopper, calix Ar*H*, quinine C*H*), 6.58 (4H, d, ^3J = 8.9 Hz, hydroquinone Ar*H*), 6.31 (4H, d, ^3J = 8.9 Hz, hydroquinone Ar*H*), 5.16 (4H, br.s, calix C*H*, CH_2), 4.38 (4H, t, ^3J = 7.0 Hz, CH_2), 4.09 (4H, s, CH_2), 3.96 (4H, s, CH_2), 3.88-3.80 (8H, m, CH_2), 3.41 (4H, s, CH_2), 3.29 (4H, d, ^2J = 11.3 Hz, calix C*H*), 2.22 (4H, s, CH_2), 2.15 (4H, br.s, CH_2), 1.30 (36H, s, ^{t}*Bu*), 1.11 (18H, s, ^{t}*Bu*); ^{13}C NMR (500 MHz, $CDCl_3$) δ_C 185.9, 166.3, 162.2, 156.4, 152.9, 152.5, 148.7, 147.9, 147.5, 147.4, 144.6, 144.1, 140.5, 140.3, 133.2, 132.8, 131.4, 130.9, 129.4, 129.0, 127.5, 126.0, 124.4, 123.5, 115.5, 114.4, 113.5, 67.6, 67.2, 63.7, 62.1, 48.3, 40.7, 37.7, 34.5, 34.4, 31.6, 31.6; remaining quaternaries undetected; ESI-HRMS: found *m/z* = 1210.0753, calculated 1210.0764 for $[M + 2Na]^{2+}$.

Synthesis of calix[4]arene isophthalamide macrocycle 19[2]

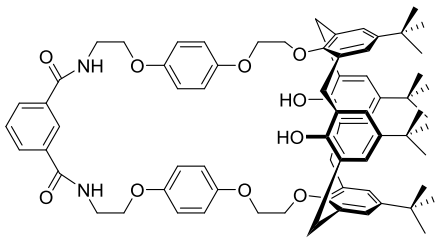

Calix[4]arene bis-amine **8** (530 mg, 0.526 mmol) was dissolved in dry CH_2Cl_2 (20 mL). Pyridine-3,5-dicarbonyl dichloride (0.631 mmol) was dissolved in CH_2Cl_2 (20 mL). The solutions were added dropwise *via* syringe pump to a solution of Et_3N (0.293 mL, 2.11 mmol) in dry CH_2Cl_2 (200 mL) over 3 hours under an N_2 atmosphere. The reaction was stirred for a further 18 hours after which the solvent was washed with 1 M citric $acid_{(aq)}$ (100 mL), sat. $NaHCO_{3(aq)}$ (100 mL) and brine (100 mL) and dried over $MgSO_4$. The crude material was purified by column chromatography (silica; CH_2Cl_2/MeOH 98:2) to give the compound as a white solid (485 mg, 81%). ^{1}H NMR (300 MHz, $CDCl_3$) δ_H 8.06 (2H, d, ^3J = 7.6 Hz, Ar*H*), 7.90 (1H, s, Ar*H*), 7.75 (2H, s, O*H*), 7.55 (1H, t, ^3J = 7.6 Hz, Ar*H*), 7.04 (4H, s, C*H*), 6.90-6.74 (12H, m, Ar*H*), 4.39 (4H, d, ^2J = 12.9 Hz, C*H*H), 4.34-4.27 (8H, m, OCH_2), 4.12 (4H, t, ^3J = 4.7 Hz, OCH_2), 3.88-3.85 (4H, m, OCH_2), 3.29 (4H, d, ^2J = 12.9 Hz, *C*H*H*), 1.26 (18H, s, ^{t}*Bu*), 1.01 (18H, s, ^{t}*Bu*); ESI-LRMS: found *m/z* = 1159.56, calculated 1159.60 for $[M + Na]^+$.

Synthesis of calix[4]diquinone isophthalamide macrocycle 20[2]

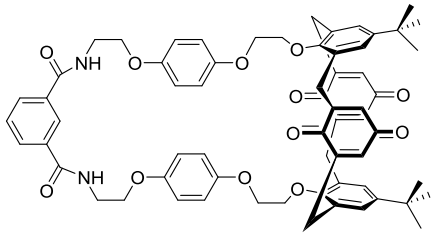

Thallium (III) trifluoroacetate (2.69 g, 4.95 mmol) was suspended in dry CH_2Cl_2 (20 mL) at 0°C under N_2 in the absence of light. A solution of calix[4]arene macrocycle **19** (563 mg,

0.495 mmol) in CH_2Cl_2 (20 mL) and trifluoroacetic acid (5 mL) was added simultaneously and the reaction was stirred at 0 °C for 35 minutes. The reaction was quenched with H_2O (10 mL) and stirred vigorously for 10 minutes. This was repeated twice and the organic layer dried over anhydrous $MgSO_4$. Purification by column chromatography (silica; acetone/hexane; 75:25) afforded **20** as a bright orange solid (198 mg, 38%). ^{1}H NMR (300 MHz, $CDCl_3$) δ_H 8.10 (2H, s, Ar*H*), 7.92 (1H, d, J = 8.5 Hz, Ar*H*), 7.45 (1H, t, ^{3}J = 7.6 Hz, Ar*H*), 6.87-6.71 (12H, m , Ar*H*), 6.61 (4H, s, C*H*), 4.12-3.74 (20H, m, CH_2), 3.23 (4H, d, ^2J = 13.5 Hz, C*H*), 1.09 (18H, s, ^{t}*Bu*); ESI-LRMS: found m/z = 1075.57, calculated 1075.44 for $[M + Na]^+$.

Synthesis of tetraethylene glycol bis-mesylate 21

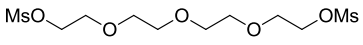

Mesyl chloride (5.98 mL, 77.0 mmol) was added dropwise to a solution of tetraethylene glycol (4.44 mL, 25.0 mmol) and triethylamine (12.0 mL, 88.0 mmol) in dry CH_2Cl_2 (100 mL) at 0 °C. The reaction mixture was stirred at RT overnight. The resulting solution was washed with 1 M $HCl_{(aq)}$ (2 × 50mL), sat. $NaHCO_3$ (50mL) and brine (50mL). The combined organic layers were dried over anhydrous $MgSO_4$ and the solvent removed *in vacuo* to give a brown oil (5.95 g, 66 %). ^{1}H NMR (300 MHz, $CDCl_3$) δ_H 4.38 (4H, m, CH_2), 3.77 (4H, m, CH_2), 3.66 (8H, m, CH_2), 3.08 (6H, s, CH_3); ESI-LRMS found m/z = 373.02, calculated 373.06 for $[M+Na]^+$.

Synthesis of tetraethylene glycol bis-azide 22

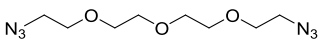

Tetraethylene bis-mesylate **21** (1.0 g, 2.85 mmol) and NaN_3 (1.11g, 17.1 mmol) were dissolved in DMSO (30 mL) and stirred at ambient temperature for 48 hours. The product was precipitated by the addition of H_2O (150 mL) and the product was extracted with diethyl ether (4 × 50 mL). The organic phase was dried with anhydrous $MgSO_4$, filtered and the solvent removed *in vacuo* to give the compound as a colourless oil (0.57 g, 82%). ^{1}H NMR (300 MHz, $CDCl_3$) δ_H 3.68 (12H, m, OC*H*$_2$), 3.40 (4H, t, ^3J = 5.3 Hz, OC*H*$_2$); ^{13}C NMR (75 MHz, $CDCl_3$) δ_C 70.7, 70.0, 50.7; ESI-LRMS found m/z = 267.09, calculated 267.12 for $[M+Na]^+$.

Synthesis of tetraethylene glycol amine-azide 23

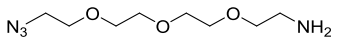

Tetraethylene glycol bis-azide (0.5 g, 2.05 mmol) was dissolved in EtOAc/Et_2O 1:1 (20 mL), 5% $HCl_{(aq)}$ (20 mL) was added and the solution was cooled to 0 °C. Triphenylphosphine (0.53 g, 2.05 mmol) in EtOAc/Et_2O 1:1 (10 mL) was added dropwise and the solution was allowed to stir at ambient temperature for 18 hours. The organic phase was discarded and the aqueous phase washed with CH_2Cl_2 (3 × 30 mL) which was also discarded. The aqueous phase was basified with 10% $NaOH_{(aq)}$ and the product extracted with CH_2Cl_2 (3 × 30 mL). The organic phase was dried over anhydrous $MgSO_4$, filtered and the solvent removed *in vacuo* to give the compound as a yellow oil (0.36g, 81%). ^{1}H NMR (300 MHz, $CDCl_3$) δ_H 3.72-3.63 (12H, m, OC*H*$_2$), 3.51 (2H, t, ^3J = 5.3 Hz, OC*H*$_2$), 3.40 (2H, t, ^3J = 5.3 Hz, OC*H*$_2$), 2.87 (2H, t, ^3J = 5.3 Hz, N*H*$_2$); ESI-LRMS found m/z = 219.13, calculated 219.15 for $[M+H]^+$.

Synthesis of pyridine bis-TEGazide 24

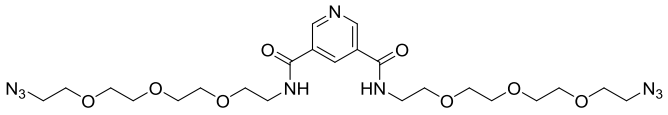

Pyridine dicarbonyl chloride (204 mg, 1.0 mmol) in dry CH_2Cl_2 (20 mL) was added dropwise to a solution of pyridine bis-TEGazide **23** (480 mg, 2.2 mmol) and Et_3N (0.42 mL, 3.0 mmol) in dry CH_2Cl_2 (30 mL) and the reaction stirred at ambient temperature for 3 hours. The reaction was washed with 10% citric $acid_{(aq)}$ (2 × 50 mL) and brine (2 × 50 mL), dried over anhydrous $MgSO_4$, filtered and the solvent removed *in vacuo*. The crude material was purified by column chromatography (silica; DCM/MeOH 95:5) to give the compound as a colourless oil (403 mg, 71%). ^{1}H NMR (300 MHz, $CDCl_3$) δ_H 9.16 (2H, d, ^4J = 2.3 Hz, Ar*H*), 8.52 (1H, t, ^4J = 2.1 Hz, Ar*H*), 7.03 (2H, br. s, N*H*), 3.73-3.59 (28H, m, OCH_2), 3.34 (4H, t, ^3J = 5.0 Hz, OCH_2); ESI-HRMS found m/z = 590.2659, calculated 590.2657 for $[M + Na]^+$.

Synthesis of pyridine *N*-oxide bis-TEGazide 25

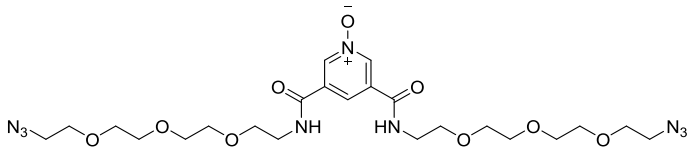

Pyridine bis-TEGazide **24** (0.17 g, 0.3 mmol) and $NaHCO_3$ (0.85 g, 9.0 mmol) were dissolved in biphasic H_2O/ 2-butanone 1:1 (50 mL). Oxone (0.55 g, 1.80 mmol) in H_2O (10 mL) was added dropwise and the reaction was stirred at ambient temperature for 3 hours. NaCl (*ca.* 2.5 g) was added and the product was extracted with $CHCl_3$ (3 × 20 mL). The organic phase was dried over anhydrous $MgSO_4$, filtered and the solvent removed to give the product as a white solid (0.108 g, 62%). ^{1}H NMR (300 MHz, $CDCl_3$) δ_H 8.84 (2H, s, Ar*H*), 8.21 (1H, s, Ar*H*), 7.91 (2H, br. s, N*H*), 3.71-3.58 (28H, m, OCH_2), 3.34 (4H, t, ^3J = 5.0 Hz, OCH_2); ^{13}C

NMR (75 MHz, $CDCl_3$) 162.4, 140.3, 133.7, 123.8, 70.6, 70.4, 70.2, 69.9, 50.6, 40.3; ESI-HRMS found $m/z = 606.2613$, calculated 606.2606 for $[M + Na]^+$.

Synthesis of TEG [2]rotaxane 26

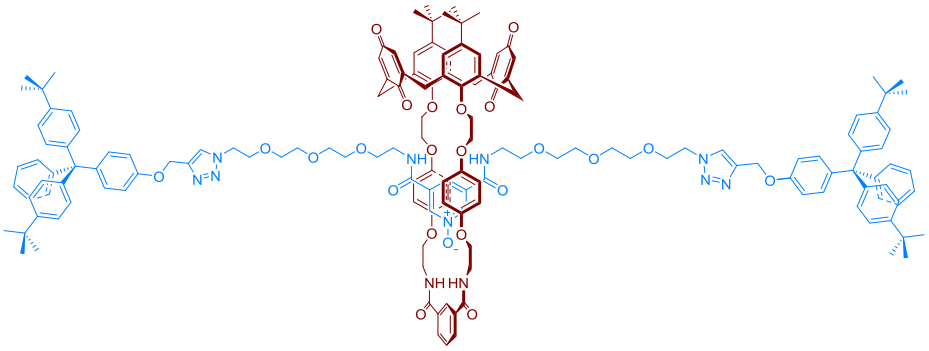

Calix[4]diquinone macrocycle **1** (30.0 mg, 0.0283 mmol) and sodium perchlorate (3.84 mg, 0.0313 mmol) and pyridine *N*-oxide bis-TEGazide **25** (16.5 mg, 0.0283 mmol) were dissolved in CH_2Cl_2 (10 mL) and stirred under N_2 for 16 hours. Stopper alkyne **16** (30.39 mg, 0.0625 mmol), $Cu^I(MeCN)_4PF_6$ (2.08 mg, 0.00554 mmol), TBTA (2.22 mg, 0.0042 mmol) and diisopropylamine (DIPEA) (0.01 mL) were added and the reaction was stirred at ambient temperature for 48 hours under N_2. The reaction was subsequently washed with 0.25 M $EDTA_{(aq)}$ (3 × 10 mL) and the solvent removed *in vacuo*. Purification by preparative TLC (silica; CH_3CN/CH_2Cl_2; 1:1) followed by (silica; CH_2Cl_2/MeOH 99:1→97:3) afforded the compound as yellow solid (3.0 mg, *ca.* 4%, 95% purity). ^{1}H NMR (300 MHz, $CDCl_3$, only peaks corresponding to product are reported) δ_H 8.72 (1H, s, Ar*H*), 8.55 (3H, s, Ar*H*), 8.45 (2H, br.s, N*H*), 8.20 (2H, d, $^3J = 7.6$ Hz, Ar*H*), 7.81 (2H, br. s, N*H*), 7.73 (2H, s, Ar*H*), 7.57 (1H, t, $^3J = 7.6$ Hz), 7.29-7.03 (30H, m, Ar*H*), 6.87-6.79 (8H, m, Ar*H*, C*H*), 6.55 (4H, d, $^3J = 8.8$ Hz, Ar*H*), 6.29 (4H, d, $^3J = 7.6$ Hz, Ar*H*), 5.13 (4H, s, OCH_2), 4.47 (4H, m, OCH_2), 4.12-3.50 (48H, m, OCH_2), 3.27 (4H, d, $^2J = 13.5$ Hz, CH*H*), 1.29 (36H, s, ^{t}*Bu*), 1.10 (18H, s, ^{t}*Bu*); ESI-HRMS found $m/z = 2632.2830$, calculated 2632.2944 for $[M + Na]^+$.

Synthesis of bromopropyl terphenyl stopper 28[5]

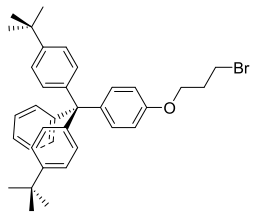

Phenol stopper **15** (3.00g, 6.14 mmol) and 1,3-dibromopropane (1.87 mL , 18.4 mmol) were dissolved in dry acetonitrile (100 mL) and heated at reflux under N_2 for 48 hours. The solvent was removed *in vacuo*, redissolved in CH_2Cl_2 (100 mL) and washed with 1M $HCl_{(aq)}$ (2 × 50 mL) and H_2O (50 mL). The residue was purified by column chromatography (silica; DCM/hexane 2:1) to afford the compound as a white solid (2.2 g, 63%). ^{1}H NMR (300 MHz, $CDCl_3$) δ_H 7.32-7.05 (15H, m, Ar*H*), 6.78 (4H, d, ^3J = 8.8 Hz, Ar*H*), 4.08 (2H, m, OCH_2), 3.61 (2H, m, OCH_2), 2.31 (2H, m, OCH_2), 1.31 (18H, s, ^{t}*Bu*).

Synthesis of azidopropyl terphenyl stopper 29[5]

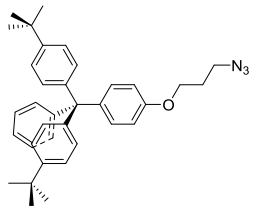

Bromopropyl terphenyl stopper **28** (2.00g, 3.51 mmol) and NaN_3 were dissolved in dry DMF (50 mL) and heated at 80 °C for 18 hours. The reaction was cooled and the solvent removed *in vacuo*. The compound was dissolved in CH_2Cl_2 (50 mL) and washed with H_2O (5 × 50 mL) to afford the compound as a white solid (1.62 g, 87%). ^{1}H NMR (300 MHz, $CDCl_3$) δ_H 7.28-7.04 (15H, m, Ar*H*), 6.77 (4H, d, ^3J = 8.8 Hz), 4.02 (2H, m, OCH_2), 3.52 (2H, m, OCH_2), 2.05 (2H, m, OCH_2), 1.31 (18H, s, ^{t}*Bu*); ESI-LRMS found m/z = 554.33, calculated 554.31 for $[M + Na]^+$.

Synthesis of aminopropyl terphenyl stopper 30[6]

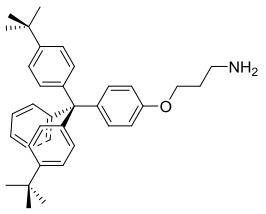

Azidopropyl terphenyl stopper **30** (300 mg, 0.56 mmol) and Pd/C 10% loading (30 mg) was suspended in EtOAc/MeOH 1:1 (25 mL) under an 5 atmospheres of $H_{2(g)}$ for 18 hours. The reaction was filtered hot through Celite and the solvent removed *in vacuo*. The crude material was purified by column chromatography (silica; DCM/MeOH 85:15) to afford the compound as a white solid (157 mg, 55%). ^{1}H NMR (300 MHz, $CDCl_3$) δ_H 7.26-7.04 (15H, m, Ar*H*), 6.77 (4H, d, ^3J = 8.8 Hz, Ar*H*), 4.02 (2H, m, OCH_2), 3.00 (2H, m, OCH_2), 2.05-1.86 (4H, m, OCH_2, NH_2), 1.28 (18H, s, ^{t}*Bu*); ESI-LRMS found m/z = 507.32, calculated 507.34 for $[M + H]^+$.

Synthesis of 3,5-pyridine-*N*-oxide dicarboxylic acid 31

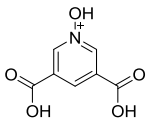

Pyridine-3-5-dicarboxylic acid (1.00g, 5.98 mmol) was dissolved in 1M $NaOH_{(aq)}$ (50 mL). Oxone (5.52 g, 17.9 mmol) was added and the reaction stirred at ambient temperature for 5 hours. The solution was acidified with conc. $HCl_{(aq)}$, filtered and washed with H_2O (3 × 100 mL) to give the compound as a white solid (0.7 g, 64%). ^{1}H NMR (300 MHz, DMSO-d_6) δ_H 8.63 (2H, s, Ar*H*), 8.06 (1H, s, Ar*H*); ESI-LRMS found m/z = 184.10, calculated 184.02 for $[M + H]^+$.

Synthesis of 3,5-pyridine-*N*-oxide dipentafluorophenyl ester 32

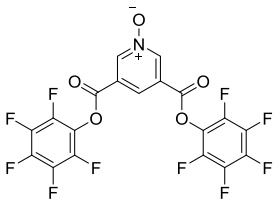

3,5-pyridine-*N*-oxide dicarboxylic acid **31** (50 mg, 0.27 mmol) was dissolved in dry DMF (5 mL). 1-Ethyl-3-(3-dimethylaminopropyl)carbodiimide (92.8 mg, 0.60 mmol) and pentafluorophenol (110 mg, 0.60 mmol) were added and the reaction stirred at ambient temperature for 18 hours. The reaction was poured onto H_2O (50 mL) and filtered immediately. This compound was used immediately without characterisation due to its high reactivity.

Synthesis of calix[4]diquinone pyridinium macrocycle 34 · $Na[BAr^F{}_4]_2$

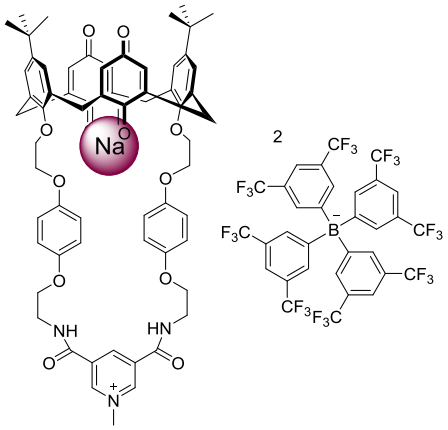

Calix[4]diquinone pyridine macrocycle **1** (100 mg, 0.095 mmol) was dissolved in $CHCl_3$ (10 mL). MeI (2 mL) was added and the solution was stirred at ambient temperature for 3 days after which time a precipitate had formed. The solvent was removed *in vacuo* and suspended in $CHCl_3$ (30 mL). Sodium tetrakis[(3,5-trifluoromethyl)phenyl]borate ($Na[BAr^F{}_4]$) (210 mg, 0.238 mmol) was added and the reaction stirred at ambient temperature for 30 minutes. The

solution was washed with H_2O (3 × 30 mL), dried over anhydrous $MgSO_4$, filtered and the solvent removed *in vacuo* to give the compound as an orange solid (264 mg, 99%). ^{1}H NMR (500 MHz, $CDCl_3$) δ_H 9.34 (2H, s, Ar*H*), 9.32 (1H, s, Ar*H*), 9.07 (2H, br. s. N*H*), 7.56 (16H, s, Ar*H*), 7.43 (8H, s, Ar*H*), 6.88-6.74 (8H, m, Ar*H*), 6.70 (4H, s, C*H*), 4.47 (3H, s, CH_3), 4.12-4.04 (4H, m, OCH_2), 4.10.4.06 (8H, m, OCH_2), 3.89 (4H, s, OCH_2), 3.84-3.76 (8H, m, OCH_2), 1.07 (18H, s, CH_3); ^{13}C NMR (75 MHz, $CDCl_3$) δ_C 189.0, 185.9, 162.1, 161.8, 161.7, 161.3, 160.9, 153.1, 153.0, 147.6, 147.1, 146.2, 140.1, 134.4, 134.3, 129.4, 129.2, 128.9, 128.7, 127.6, 125.5, 123.3, 121.2, 117.1, 115.2, 115.1, 72.3, 67.4, 66.3, 40.1, 33.6, 32.2, 30.5; ESI-HRMS: found m/z = 1068.4612, calculated 1068.4641 for $[M - 2[Bar^F{}_4]]^+$

Synthesis of 2-(4-hydroxyphenoxy)acetonitrile 35[7]

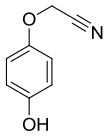

Bromoacetonitrile (3.81 mL, 55.0 mmol) was dissolved in degassed dioxane (50 mL) and added to hydroquinone (6.00 g, 54.4 mmol) and NaOH (4.36 g, 109 mmol) dissolved in degassed 1:1 dioxane/water (300 mL). The reaction mixture was stirred at ambient temperature for 1 hour under N_2. The resulting solution was then acidified with 1 M $HCl_{(aq)}$, extracted with CH_2Cl_2 (3 × 20 mL) and dried over anhydrous $MgSO_4$. Purification via column chromatography (silica; CH_2Cl_2/MeOH 98:2) gave the title compound as yellow solid (5.01 g, 62 %). ^{1}H NMR (300 MHz, $CDCl_3$) δ_H 6.88 (2H, d, ^3J = 9.4 Hz, Ar*H*), 6.78 (2H, d, ^3J = 9.4 Hz, Ar*H*), 4.70 (2H, s, CH_2); ESI-LRMS found m/z = 148.03, calculated 148.04 for $[M - H]^-$.

Synthesis of bis-nitrile macrocycle precursor 36[7]

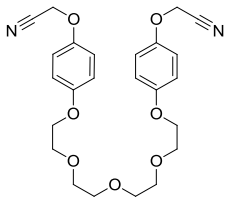

K_2CO_3 (1.39 g, 10.1 mmol) was added to a solution of the tetraethyleneglycol bis-mesylate **21** (1.76 g, 5.03 mmol) and 2-(4-hydroxyphenoxy)acetonitrile **35** (1.50 g, 10.1 mmol) dissolved in dry acetonitrile (100 mL) and heated to reflux for 48 hours. The reaction was then cooled to ambient temperature and the solution filtered to remove K_2CO_3. The solvent was removed *in vacuo* to give a white oily solid (1.71 g, 37 %). ^{1}H NMR (300 MHz, $CDCl_3$) δ_H 7.05-6.80 (8H, m, Ar*H*), 4.70 (4H, s, C*H*$_2$CN), 4.09 (4H, t, ^3J = 5.3 Hz, OC*H*$_2$), 3.84 (4H, t, ^3J = 4.7 Hz, OC*H*$_2$), 3.77-3.64 (8H, m, OC*H*$_2$); ESI-LRMS found m/z = 479.17, calculated 479.18 for $[M + Na]^+$.

Synthesis of bis-amine macrocycle precursor 37[7]

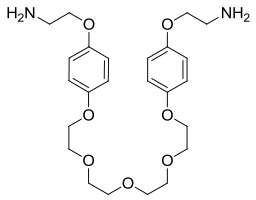

Bis-nitrile **36** (1.71 g, 3.92 mmol) was dissolved in dry THF (100 mL) and added dropwise to 1 M BH_3.THF (27.4 mL, 28.6 mmol) which had been preheated to 70 °C. The reaction mixture was heated to reflux for 4 hours under N_2. The resulting solution was cooled to ambient temperature and MeOH was added to quench the reducing agent until bubbling ceased. The solvent was reduced to 50 mL *in vacuo* and $HCl_{(g)}$ bubbled through the solution for 30 minutes. The precipitate was collected via filtration, washed with cold MeOH (50 mL)

and hexane (2 × 50 mL) and dried under high vacuum. The resulting white solid was suspended in CH_2Cl_2 (50 mL). 10 % w/w $NaOH_{(aq)}$ (50 mL) was added and the biphasic mixture stirred vigorously for 30 minutes. The organic layer was separated and the aqueous layer extracted with CH_2Cl_2 (2 × 50 mL). The organic layers were combined and dried over anhydrous $MgSO_4$ and the solvent removed *in vacuo* to give a white solid (1.34 g, 77 %). ^{1}H NMR (300 MHz, $CDCl_3$) δ_H 6.90-6.77 (8H, m, Ar*H*), 4.11-4.03 (4H, m, C*H*$_2$), 3.93 (4H, t, ^3J = 5.3 Hz, C*H*$_2$), 3.83 (4H, t, ^3J = 4.7 Hz, C*H*$_2$), 3.77-3.55 (8H, m, C*H*$_2$), 3.12-3.00 (4H, m, C*H*$_2$); ESI-LRMS found m/z = 465.26, calculated 465.26 for $[M + H]^+$.

Synthesis of pyridine bis-hexylamide 38[8]

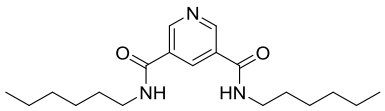

Pyridine dicarbonyl chloride (408 mg, 2.0 mmol) in dry CH_2Cl_2 (30 mL) was added dropwise to a solution of hexylamine (0.4 mL, 2.2mmol) and Et_3N (0.6 mL, 3.0 mmol) in dry CH_2Cl_2 (300 mL) and the reaction stirred under N_2 at ambient temperature for 3 hours. The reaction was washed with 10% citric $acid_{(aq)}$ (2 × 50 mL) and H_2O (50 mL). The orgnic phase was dried over anhydrous $MgSO_4$, filtered and the solvent removed *in vacuo* to give the compound as an off-white solid (573 mg, 86%). ^{1}H NMR (300 MHz, $CDCl_3$) δ_H 9.08 (2H, s, Ar*H*), 8.51 (1H, s, Ar*H*), 7.56 (2H, br. s, N*H*), 3.50-3.38 (4H, m, C*H*$_2$), 1.70-1.55 (4H, m, C*H*$_2$), 1.42-1.23 (12H, m, C*H*$_2$), 0.89 (6H, t, ^3J = 6.8 Hz, C*H*$_3$); ESI-LRMS: found *m/z* = 368.17, calculated 368.21 for $[M + Cl]^-$.

Synthesis of pyridinium bis-hexylamide 39 · Cl[8]

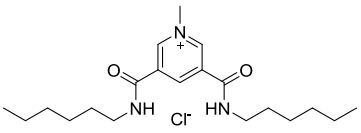

Pyridine bis-hexylamide **38** (573 mg, 1.72 mmol) was dissolved in $CHCl_3$ (20 mL). MeI (5 mL) was added and the reaction heated to reflux for 72 hours. The reaction was cooled to ambient temperature and the solvent removed *in vacuo* to give the iodide salt. This was anion exchanged with aqueous NH_4PF_6 to give the compound as an orange solid (654 mg, 99%). ^{1}H NMR (300 MHz, $CDCl_3$) δ_H 10.42 (1H, s, Ar*H*), 9.49 (2H, s, Ar*H*), 9.21 (2H, br. s, N*H*), 4.59 (3H, s, CH_3), 3.50-3.40 (4H, m, CH_2), 1.79-1.66 (4H, m, CH_2), 1.45-1.20 (12H, m, CH_2), 0.87 (6H, t, ^3J = 6.4 Hz, CH_3); ESI-LRMS: found m/z = 348.23, calculated 348.26 for [M - Cl]$^+$.

Synthesis of pyridine *N*-oxide macrocycle 40

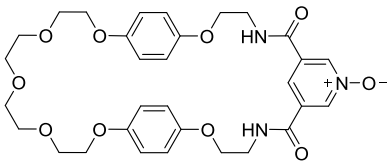

Pyridine *N*-oxide bis-ester **32** (100 mg, 0.19 mmol), pyridinium bis-hexylamide **39** · Cl (74 mg, 0.19 mmol) and Et_3N (0.081 mL, 0.58 mmol) was dissolved in dry CH_2Cl_2 (10 mL). Bis-amine **37** (90 mg , 0.19 mmol) in dry CH_2Cl_2 (10 mL) was added dropwise over 1 hour. The solvent was removed *in vacuo* and the product purified by column chromatography (silica, DCM/MeOH 97:3) to afford the compound as a white solid (27 mg, 21%). ^{1}H NMR (500 MHz, $CDCl_3$/CD_3OD 1:1) δ_H 8.73 (2H, br. s, N*H*), 8.66 (2H, s, Ar*H*), 8.16 (1H, s, Ar*H*), 6.72 (8H, s, Ar*H*), 4.05-3.92 (8H, m, OCH_2), 3.78-3.67 (8H, m, OCH_2), 3.63-3.57 (8H, m, OCH_2); ^{13}C NMR (75 MHz, $CDCl_3$/CD_3OD 1:1) δ_C 166.9, 157.1, 156.7, 144.2, 137.9, 119.4, 119.1,

74.4, 73.5, 71.9, 70.5, 43.9; ESI-HRMS: found $m/z = 634.2370$, calculated 634.2371 for $[M + Na]^+$.

Synthesis of calix[4]diquinone pyridinium [2]catenane 41 · Na[Bar$^F{}_4$]$_2$

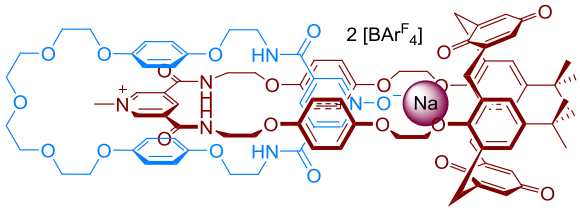

Calix[4]diquinone pyridinium macrocycle **34** · Na[Bar$^F{}_4$]$_2$ (100 mg, 0.0355 mmol) and pyridine *N*-oxide bis-ester **32** (18.3 mg, 0.0355 mmol) were dissolved in dry CH_2Cl_2 (5 mL). Bis-amine **37** (16.5 mg, 0.0355 mmol) was added dropwise *via* a syringe pump and the reaction stirred at ambient temperature for 18 hours. The solvent was removed *in vacuo* and the crude material purified by size-exclusion chromatography (Bio-Beads SX-1/ $CHCl_3$) and preparative TLC (silica; gradient elution DCM/MeOH 100:0→95:5) to afford the compound as a yellow solid (6.2 mg, 20%, *ca.* 95% purity). ^{1}H NMR (500 MHz, $CDCl_3/CD_3OD$ 1:1, only peaks corresponding to product are reported) δ_H 9.91 (1H, s, Ar*H*), 8.77 (2H, s, Ar*H*), 8.59 (1H, s, Ar*H*), 8.54 (2H, s, Ar*H*), 7.57 (16H, s, Ar*H*), 7.43 (8H, s, Ar*H*), 6.82-6.63 (16H, m, Ar*H*), 6.47 (4H, d, ^3J = 8.6 Hz, Ar*H*), 8.21 (4H, d, ^3J = 8.6 Hz, Ar*H*), 4.08 (3H, s, CH_3), 3.98-3.62 (36H, m , OCH_2), 3.24 (4H, m , OCH_2), 1.17 (18H, s, CH_3); ^{13}C NMR (126 MHz, $CDCl_3/CD_3OD$ 1:1) δ_C 162.7, 162.1, 161.8, 161.4, 161.0, 153.2, 152.8, 152.2, 145.6, 140.4, 134.6, 133.0, 129.3, 129.0, 128.8, 127.7, 125.5, 123.4, 121.2, 117.2, 115.5, 115.4, 115.2, 114.8, 70.6, 70.0, 69.5, 68.2, 67.0, 65.7, 54.6, 40.7, 33.9, 31.8, 31.4, 31.0, 29.5, 28.6; ESI-HRMS: found $m/z = 1701.6918$, calculated 1701.6939 for $[M + Na]^+$

Synthesis of *N*-propargyl-2-methylimidazole 42

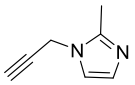

2-methylimidazole (1g, 12.2 mmol) in dry THF (25 mL) was added dropwise to a suspension of NaH (60% dispersion in mineral oil) (492 mg, 12.3 mmol) in dry THF (25 mL) and stirred at 0 °C under N_2 for 10 minutes. Propargyl bromide (80% solution in toluene) (1.37 mL, 12.3 mmol) was added dropwise and stirred for 18 hours. The reaction was quenched with H_2O (1 mL) and the solvent removed *in vacuo*. The residue was redissolved in $CHCl_3$ (50 mL), washed with H_2O (3 × 50 ml) and dried over anhydrous $MgSO_4$. The solution was filtered and the solvent removed *in vacuo* to obtain the compound as a colourless oil (1.30 g, 89%). ^{1}H NMR (300 MHz, $CDCl_3$) δ_H 6.95 (1H, s, Ar*H*), 6.92 (1H, s, Ar*H*), 4.60 (2H, s, C*H*$_2$), 2.43 (1H, s, CC*H*); ESI-LRMS: found m/z = 121.06, calculated 121.16 for $[M + H]^+$

Synthesis of *N,N'*-dipropargyl-2-methylimidazolium bromide 43 · Br

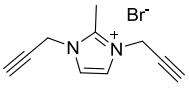

Propargyl imidazole (0.2 g, 1.66 mmol) and propargyl bromide (80% solution in toluene) (0.27 g, 1.81 mmol) was dissolved in acetone (5 mL) and heated under microwave irradiation at 150 °C for 20 minutes. The solvent was removed *in vacuo* and the residue recrystallised from CH_2Cl_2/hexane to afford the compound as a brown oil (314 mg, 79%). ^{1}H NMR (300 MHz, CD_3OD) δ_H 7.69 (2H, s, Ar*H*), 5.13 (4H, s, C*H*$_2$), 2.76 (1H, s, CC*H*); ^{13}C NMR (75 MHz, D_2O); ESI-LRMS: found m/z = 159.08, calculated 159.09 for $[M - Br]^+$

Synthesis of imidazolepropyl terphenyl stopper 45[9]

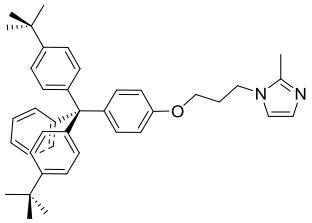

Sodium hydride (60% dispersion in mineral oil) (0.28 g, 7.0 mmol) was suspended in dry THF (50 mL) under N_2 and cooled to 0 °C. 2-methylimidazole (0.72 g, 8.8 mmol) dissolved in dry THF (20 mL) was added dropwise to the solution at 0 °C and stirred for 10 minutes. Bromopropyl stopper **28** (1.0 g, 1.76 mmol) dissolved in dry THF (30 mL) was added dropwise to the solution and the reaction stirred for 48 hours. The reaction was quenched with H_2O, the solvent removed *in vacuo.* The compound was redissolved in $CHCl_3$ (50 mL), washed with H_2O (3 × 50 mL), dried over anhydrous $MgSO_4$, filtered and the solvent removed *in* vacuo. Purification by column chromatography (silica; DCM/MeOH 97:3) afforded the target compound as a white solid (0.37 g, 37%). ^{1}H NMR (300 MHz, $CDCl_3$) δ_H 7.27-7.05 (15H, m, Ar*H*), 6.92 (1H, s, Ar*H*), 6.82 (1H, s, Ar*H*), 6.74 (4H, d, ^3J = 8.8 Hz, Ar*H*), 4.07 (2H, t, ^3J = 6.7 Hz, Ar*H*), 3.88 (2H, ^3J = 5.7 Hz, Ar*H*), 2.36 (3H, s, C*H*$_3$), 2.15 (2H, m, C*H*$_3$), 1.30 (18H, s, C*H*$_3$); ESI-LRMS: found m/z = 571.39, calculated 571.37 for $[M + H]^+$

Synthesis of imidazolium biphenyl 46 · Cl[9]

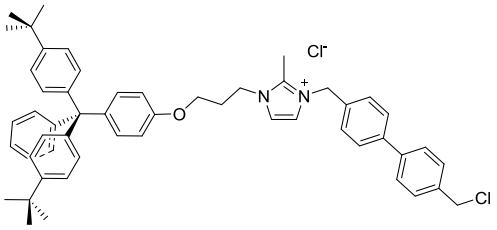

Imidazole stopper **45** (0.4 g, 0.68 mmol) and 4,4'-bis(chloromethyl)-1,1'-biphenyl (0.87 g, 3.48 mmol) were dissolved in acetone (10 mL) and heated in a sealed container under microwave irradiation at 150°C for 75 minutes. The solvent was removed *in vacuo* and the crude residue purified by column chromatography (silica; gradient elution DCM/MeOH 100:0→90:10) to afford the compound as a yellow solid (0.47 g, 81%). ^{1}H NMR (300 MHz, $CDCl_3$) δ_H 7.60 (2H, s, Ar*H*), 7.48-6.97 (22H, m, Ar*H*), 6.56 (4H, d, ^{3}J = 8.8 Hz, Ar*H*), 5.48 (2H, s, CH_2), 4.51 (2H, s, CH_2), 4.39 (2H, t, ^{3}J = 6.5 Hz, Ar*H*), 3.89 (2H, t, ^{3}J = 5.0 Hz, Ar*H*), 2.68 (3H, s, CH_3), 2.26 (2H, t, ^{3}J = 5.6 Hz, Ar*H*), 1.22 (18H, s, CH_3); ^{13}C NMR (75 MHz, $CDCl_3$) δ_C 155.8, 148.4, 147.2, 144.0, 143.8, 141.1, 140.1, 139.9, 136.9, 132.3, 131.0, 130.6, 129.2, 128.7, 127.9, 127.3, 127.2, 125.7, 124.2, 122.2, 121.8, 112.9, 63.8, 63.4, 51.9, 50.0, 45.9, 34.2, 31.3, 29.2, 10.5; ESI-LRMS: found m/z = 785.44, calculated 785.42 for [M - Cl]$^{+}$

Synthesis of imidazolium biphenyl azide 47 · Cl[9]

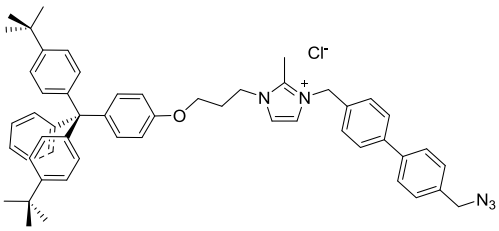

Imidazolium biphenyl **46** · Cl (0.47 g, 0.57 mmol) and NaN_3 (0.11 g, 1.72 mmol) were dissolved in dry DMF (15 mL) and heated at 80°C under N_2 for 18 hours. The solvent was removed *in vacuo*, dissolved in CH_2Cl_2 (50 mL) and washed with H_2O (4 × 100 mL). The

crude material was purified by column chromatography (silica; DCM/MeOH 85:15) to afford the compound as a white solid (0.38 g, 80%). ^{1}H NMR (300 MHz, $CDCl_3$) δ_H 7.56 (2H, s, Ar*H*), 7.42-6.88 (25H, m, Ar*H*), 6.49 (2H, d, ^{3}J = 8.8 Hz, Ar*H*), 5.43 (2H, s, CH_2), 4.32 (2H, t, ^{3}J = 6.5 Hz, CH_2), 3.82 (2H, s, CH_2), 3.25 (3H, s, CH_3), 2.26 (2H, s, CH_2), 2.19 (2H, s, CH_2), 1.14 (18H, s, CH_3); ^{13}C NMR (75 MHz, $CDCl_3$) δ_C 155.6, 148.2, 147.0, 143.7, 143.6, 140.9, 139.9, 139.6, 134.6, 132.1, 130.8, 130.4, 126.6, 126.5, 127.2, 127.0, 125.5, 124.0, 122.1, 121.6, 112.7, 63.6, 63.2, 54.1, 51.7, 49.9, 45.6, 34.0, 31.1, 29.0, 10.4; ESI-LRMS: found m/z = 792.46, calculated 792.46 for [M - Cl]$^{+}$

Synthesis of imidazolium axle 48 · Cl[9]

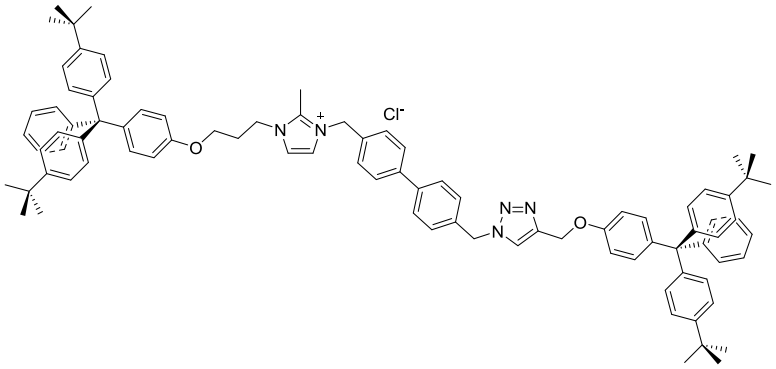

Imidazole biphenyl **47** · Cl (30 mg, 0.0378 mmol), alkyne stopper **16** (22 mg, 0.0454 mmol), TBTA (4.0 mg, 0.0076 mmol) and DIPEA (0.01 mL) were dissolved in dry CH_2Cl_2 (3 mL) under N_2. $Cu^{I}(MeCN)_4PF_6$ (2.8 mg, 0.0076 mmol) and the reaction stirred at ambient temperature for 18 hours. The solvent was removed *in vacuo* and the residue purified by column chromatography (silica; DCM/MeOH 95:5) to afford the compound as an off-white solid (26 mg, 54%). ^{1}H NMR (300 MHz, $CDCl_3$) δ_H 7.61-7.47 (8H, m, Ar*H*), 7.43-7.03 (33H, m, Ar*H*), 6.83 (2H, d, ^{3}J = 8.8 Hz), 6.67 (2H, d, ^{3}J = 8.8 Hz), 5.54-5.48 (4H, m, CH_2), 5.16

(2H, s, CH_2), 4.48 (2H, s, CH_2), 4.01 (2H, s, CH_2), 2.81 (3H, s, CH_3), 2.37 (2H, s, CH_2), 1.30 (36H, s, CH_3); ESI-LRMS: found m/z = 1279.89 calculated 1279.75 for [M - Cl]$^+$.

Synthesis of calix[4]diquinone imidazolium [2]rotaxane 49 · Cl

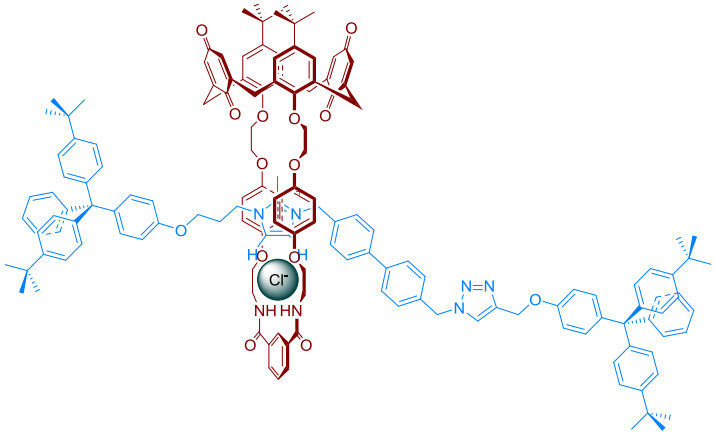

Calix[4]diquinone macrocycle **1** (30 mg, 0.0284 mmol), stopper alkyne **16** (13.9 mg, 0.0284 mmol), imidazole biphenyl **48** · Cl (22.6 mg, 0.0284 mmol), TBTA (3.0 mg, 0.0057 mmol) and DIPEA (0.01 mL) were dissolved in dry CH_2Cl_2 (5 mL) under N_2. $Cu^I(MeCN)_4PF_6$ (2.1 mg, 0.0057 mmol) was added and the reaction stirred at ambient temperature for 36 hours. The solvent was removed *in vacuo* and purified by preparative TLC (silica; DCM/MeOH 95:5) followed by (silica; DCM/MeCN 1:1) followed by (silica; gradient elution DCM/MeOH 99:1→95:5) to afford the compound as an orange solid (0.61 mg, 1%). ^{1}H NMR (500 MHz, $CDCl_3$) δ_H 8.33 (1H, s, ArH), 7.99 (2H, d, ^3J = 7.4 Hz), 7.51 (2H, d, ^3J = 6.4 Hz), 7.47 (4H, br. s, ArH, NH), 7.37-7.02 (34H, m, ArH), 6.97 (1H, s, ArH), 6.75-6.64 (12H, m, ArH, CH), 6.51 (4H, d, ^3J = 8.8 Hz), 6.31 (4H, d, ^3J = 8.3 Hz), 5.20 (2H, s, CH_2), 5.17 (2H, s, CH_2), 4.54 (2H, s, CH_2), 4.39-3.50 (22H, m, CH_2), 3.06 (4H, m, CHH), 2.57 (3H, s, CH_3), 2.33 (2H, t, ^3J = 7.6 Hz, CH_2), 2.19 (2H, s, CH_2), 1.26 (36H, s, CH_3), 1.22 (18H, s, CH_3); ESI-LRMS: found m/z = 2331.67 calculated 2332.20 for [M - Cl]$^+$.

Chapter 3 Syntheses

Synthesis of amine terphenyl stopper 50[10]

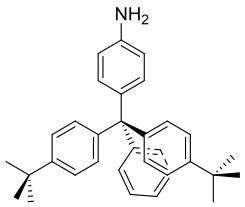

Triphenyl stopper **14** (5.00 g, 13.4 mmol) was dissolved in acetyl chloride (25 mL) and heated at reflux for 18 hours. The acetyl chloride was removed *in vacuo* and the crude material redissolved in aniline (25 mL) and heated at 105°C for 48 hours. The reaction was cooled to ambient temperature, poured onto 10% $HCl_{(aq)}$ (250 mL) and stirred vigorously for 30 minutes. The precipitate was filtered and washed with sat $K_2CO_{3(aq)}$ (2 × 50 mL) and H_2O (50 mL). Dissolution in CH_2Cl_2 (150 mL) was followed by drying with anhydrous $MgSO_4$ and the solvent concentrated *in vacuo*. The solution was then passed through a silica plug and the solvent removed *in vacuo*. Recrystallisation from toluene/hexane gave the compound as a white solid (2.6 g, 43%). ^{1}H NMR (300 MHz, $CDCl_3$) δ_H 7.30 (9H, m, Ar*H*), 7.14 (4H, d, ^3J = 8.8 Hz, Ar*H*), 7.01 (2H, d, ^3J = 8.8 Hz, Ar*H*), 6.60 (2H, d, ^3J = 8.8 Hz, Ar*H*), 3.55 (2H, br. s, NH_2), 1.34 (18H, s, CH_3); ESI-LRMS found m/z = 447.28, calculated 447.29 for [M + H]$^+$.

Synthesis of pyridine axle 51[10]

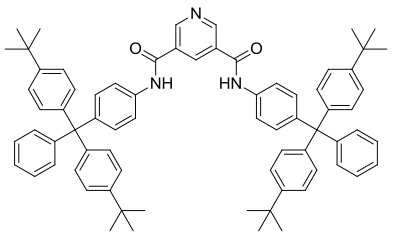

Oxalyl chloride (0.770 mL, 8.96 mmol) was added dropwise to a solution of pyridine-3,5-dicarboxylic acid (0.456 g, 0.124 mmol) in dry CH_2Cl_2 (250 mL) and dry degassed catalytic DMF (1 drop). The reaction mixture was stirred under N_2 at 40 °C for 18 hours. The solvent was removed *in vacuo* and dried under high vacuum. The resulting acid chloride intermediate was used without further purification. Aniline stopper **50** (2.00 g, 4.46 mmol) and Et_3N (2.00 mL, 14.3 mmol) were dissolved in dry CH_2Cl_2 (100 mL) and stirred until homogenous. The acid chloride was dissolved in dry CH_2Cl_2 (250 mL) and added dropwise at 0 °C, and the reaction mixture stirred for 4 hours under N_2 at ambient temperature. The solvent was removed *in vacuo*, and EtOH (100 mL) added to the resulting yellow residue. The mixture was heated at reflux for 1 hour, and then filtered to give a pale yellow solid (2.80 g, 60 %). ^{1}H NMR (300 MHz, $CDCl_3$) δ_H 9.23 (2H, br. s, Ar*H*), 8.72 (1H, br. s, Ar*H*), 8.40 (2H, br. s, N*H*), 7.57 (4H, d, ^3J = 8.3 Hz, Ar*H*), 7.26-7.10 (30H,m, Ar*H*), 1.27 (36H, m, ^{t}*Bu*); ESI-LRMS found m/z = 1060.54, calculated 1060.55 for $[M + Cl]^-$.

Synthesis of methyl pyridinium axle 52 · Cl[10]

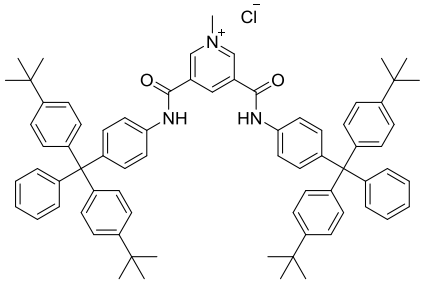

MeI (30 mL) was added to pyridine axle **51** (2.65 g, 2.58 mmol) suspended in acetone (50 mL). The reaction mixture was stirred at reflux under N_2 for 72 hours and the solvent was removed *in vacuo* to give a yellow solid (2.49 g, 93 %). ^{1}H NMR (300 MHz, $CDCl_3$) δ_H

10.71(2H, br. s, CONH), 10.26 (1H, br. s, ArH), 8.95 (2H, br. s, ArH), 7.81 (4H, d, ^3J = 8.8 Hz, ArH), 7.24-7.12 (30H, m, ArH), 4.20 (3H, s, CH_3), 1.28 (36H, m, ^tBu); ESI-LRMS found m/z = 1040.62, calculated 1040.61 for [M - I]$^+$.

Pyridinium axle **52** · I (1.00 g, 8.60 mmol) anion exchanged with $NH_4Cl_{(aq)}$ (0.912 g, 99 %). ^{1}H NMR (300 MHz, $CDCl_3$) δ_H 10.90 (2H, br. s, NH), 10.70 (1H, br. s, ArH), 8.76 (2H, br. s, PyrH), 7.80 (4H, d, ^3J = 8.8 Hz, ArH), 7.30-7.10 (30H, m, ArH), 3.83 (3H, s, CH_3), 1.29 (36H, m, ^tBu); ESI-LRMS found m/z = 1040.58, calculated 1040.61 for [M - Cl]$^+$.

Synthesis of 5-azido [2]rotaxane 54 · Cl[7]

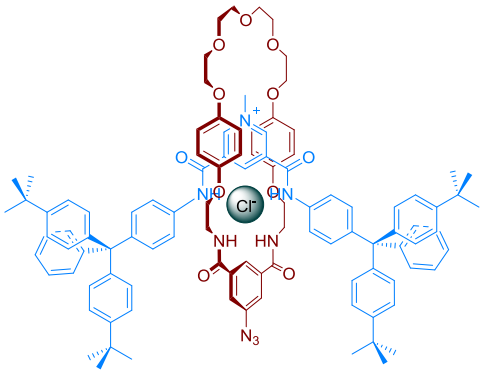

Axle **52** · Cl (248 mg, 0.23 mmol) and bis-amine **37** (107 mg, 0.23 mmol) were dissolved in dry DCM (50 mL) and stirred for 5 minutes under a nitrogen atmosphere. Triethylamine (74 µL, 0.58 mmol) and 5-azidoisophthaloyl dichloride (58 mg, 0.023 mmol) in anhydrous CH_2Cl_2 (20 mL) were then added. The reaction was stirred at room temperature for 2 hours after which the solvent was removed *in vacuo*. The crude mixture was purified by column chromatography (silica; gradient elution DCM/MeOH 99:1→95:5) followed by preparative TLC (silica; DCM/MeOH 95:5) to give **54** · Cl as a yellow solid (187 mg, 48%). ^{1}H NMR (500MHz, $CDCl_3$) δ_H 10.38 (2H, s, NH), 10.11 (1H, s, ArH), 9.01 (2H, s, ArH), 8.77 (1H, s,

Ar*H*), 8.54 (2H, s, N*H*), 7.87 (4H, d, ^{3}J = 9.0Hz, Ar*H*), 7.75 (2H, s, N*H*), 7.27-7.04 (34H, m, Ar*H*) 6.47 (4H, d, ^{3}J = 8.5Hz, Ar*H*), 6.17 (4H, d, ^{3}J = 8.5Hz, Ar*H*), 4.68 (3H, s, CH_3), 4.11 (4H, t, ^{3}J = 5.0Hz, OCH_2), 3.79-3.66 (20H, m, OCH_2), 1.29 (36H, s, ^{t}Bu); ^{13}C NMR (75.5 MHz, $CDCl_3$) δ_C 166.1, 159.0, 153.3, 151.9, 149.0, 147.0, 146.5, 143.6, 141.9, 136.2, 134.7, 132.4, 131.3, 130.9, 127.7, 126.2, 124.6, 122.5, 120.0, 116.3, 115.0, 70.9, 70.7, 70.4, 67.7, 67.3, 64.1, 49.6, 40.0, 34.6, 31.6; ESI-HRMS: found m/z = 1675.8666, calculated 1675.8680 for [M + H]$^{+}$.

Synthesis of europium [2]rotaxane 56 · PF_6

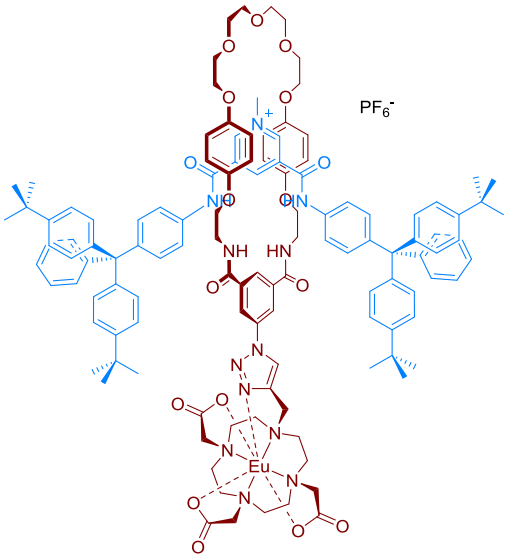

To a solution of azide rotaxane **54** · Cl (30 mg 17.5 μmol) in CH_2Cl_2/MeOH (4:1, 5 mL) was added the europium complex **55** (28 mg, 52.5 μmol). The solution was stirred for 5 minutes before $Cu^{I}(MeCN)_4PF_6$ (0.1 molar eq.) and tris[(1-benzyl-1H-1,2,3-triazol-4-yl)methyl]amine (0.15 molar eq.) were added. The solution was stirred for 48 hours at room temperature in a nitrogen atmosphere after which the solvent was removed *in vacuo*. The crude solid was dissolved in DCM (10 mL) and the organic phase was washed with an $NH_4PF_{6(aq)}$ solution. After removal of the organic solvent in vacuo the crude solid was redissolved in toluene and

filtered. Purification by size-exclusion chromatography (Bio-Beads SX-3/ toluene) gave the compound **56** · PF_6 as a yellow solid (25.6 mg, 62%). ^{1}H NMR (500 MHz, CD_3OD/CD_2Cl_2 1:1) δ_H 34.25, 30.13, 29.97, 27.92, -3.99, -4.73, -5.54, -6.14, -7.46, -8.06, -8.65, -11.77, -12.33, -16.16, -16.44, -17.18, -17.74, -19.70, -21.14; ESI-HRMS: found m/z = 1116.9801, calculated 1116.9766 for [M - PF_6 + Na]$^{2+}$; Lifetimes: DCM: 0.85 ms.

Synthesis of 4,6-dibromo-*m*-xylene 57

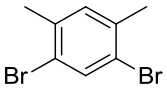

Bromine (27.9 mL, 272 mmol) was added dropwise to stirring *m*-xylene (30.0 mL, 122 mmol) over 5 minutes. Catalytic iodine (0.50 g, 1.97 mmol) was added over 30 minutes. The reaction mixture was stirred for 3 hours at RT. The solution was then neutralised with 10 % w/w NaOH(aq) (100 mL). The resulting neutralised solution was filtered and recrystallised from EtOH to give a white microcrystalline solid (25.8 g, 40%). ^{1}H NMR (300 MHz, $CDCl_3$) δ_H 7.67 (1H, s, ArH), 7.10 (1H, s, ArH), 2.31 (6H, s, C*H*$_3$); FI-HRMS found m/z = 263.8947, calculated 263.8972 for [M]$^+$.

Synthesis of 2-(tributylstannyl)pyridine 58[11]

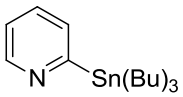

1.60 M *n*-BuLi in hexanes (15.0 mL, 24.0 mmol) was added dropwise to 2-bromopyridine (6.00 mL, 22.9 mmol) in dry THF (120 mL) at -78 °C under N_2. After 15 minutes, Bu_3SnCl (16.8 mL, 0.273 mmol) was added dropwise and the reaction mixture was stirred for 1 hour. The resulting solution was then warmed to RT and sat. $NH_4Cl_{(aq)}$ (100 mL) was added. The

aqueous layer was extracted with Et_2O (3 × 100 mL), washed with brine (50 mL) and dried over anhydrous $MgSO_4$. Purification via alumina column chromatography (hexane/EtOAc 20:1) gave a brown oil (20.2 g, 87%). ^{1}H NMR (300 MHz, $CDCl_3$) δ_H 8.73 (1H, m, Ar*H*), 7.52-7.36 (2H, m, Ar*H*), 7.14 (1H, m, Ar*H*), 1.70-0.73 (27H, m, ^tBu); ESI-LRMS found m/z = 370.12, calculated 270.16 for [M + H[$^+$.

Synthesis of 4,6-di(pyridin-2-yl)-*m*-xylene 59

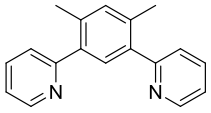

4,6-dibromo-*m*-xylene **57** (0.2 g, 0.7 mmol), 2-(tributylstannyl)pyridine **58** (0.7 mL, 2.1 mmol), $Pd(PPh_3)_2Cl_2$ (0.075 g, 0.1 mmol) and LiCl (0.65 g, 15 mmol) were dissolved in dry toluene (15 mL), degassed via 5 cycles of freeze-pump-thaw. The reaction mixture was then heated under reflux for 48 hours under N_2. The resulting solution was cooled, sat. $KF_{(aq)}$ (10 mL) was added and the solution stirred for 30 minutes. The solution was filtered through Celite, washed with water (50 mL) and toluene (50 mL) and extracted with CH_2Cl_2 after adding sat. $NaHCO_{3(aq)}$ (10 mL). Purification by column chromatography (silica; hexane/Et_2O, gradient elution from 100:0→10:90) gave the product as an off white solid (0.1 g, 51%). ^{1}H NMR (300 MHz, $CDCl_3$) δ_H 8.65 (2H, d, ^3J = 4.7 Hz, Ar*H*), 7.67 (2H, t, ^3J = 7.6 Hz, Ar*H*), 7.48 (1H, s, Ar*H*), 7.40 (2H, d, ^3J = 7.0 Hz, Ar*H*), 7.20-7.14 (3H, m, Ar*H*), 2.39 (6H, s, CH_3); ESI-LRMS found m/z = 261.15, calculated 261.14 for [M + H]$^+$.

Synthesis of 4,6-dibromoisophthalic acid 60[12]

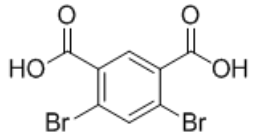

KOH (3.20 g, 58.1 mmol) was added to a solution of 1,5-dibromo-2,4-dimethylbenzene **57** (15.0 g, 56.8 mmol) in water (300 mL). The resulting solution was diluted with pyridine (150 mL) and heated to 70 °C. 5.00 g portions of $KMnO_4$ were added in 12 hour intervals until no further decolourisation of the solution was observed upon its addition (ca. 2 weeks). The resulting solution was filtered through Celite and the solution concentrated to 150 mL *in vacuo.* This solution was acidified to pH 5 with conc. $HCl_{(aq)}$. The precipitate was collected via filtration, washed with water and hexane and dried under high vacuum to give a white solid (16.5 g, 89%). ^{1}H NMR (300 MHz, CD_3OD) δ_H 8.27 (1H, s, Ar*H*), 8.09 (1H, s, Ar*H*); ^{13}C NMR (75.5 MHz, MeOD) δ_C 166.2, 139.1, 133.2, 131.9, 124.5; ESI-HRMS found m/z = 322.8376, calculated 322.8384 for $[M - H]^-$.

Synthesis of dimethyl 4,6-dibromoisophthalate 61

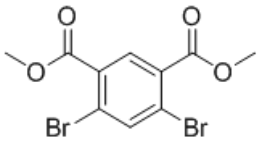

5 drops conc. $H_2SO_{4(aq)}$ were added to a solution of 4,6-dibromoisophthalic acid **60** (1.00 g, 3.11 mmol) in MeOH (15 mL) in a 20 mL microwave vial. The reaction mixture was subjected to microwave irradiation at 100 °C for 20 minutes. This was repeated 4 times and the reaction mixtures combined upon completion. The resulting solution was poured onto ice water, basified with 25 % $NH_4OH_{(aq)}$ and extracted with Et_2O (3 × 100 mL). The combined

organic layers were dried over anhydrous $MgSO_4$ and the solvent removed *in vacuo* to give a white solid (3.86 g, 89%). ^{1}H NMR (300 MHz, $CDCl_3$) δ_H 8.29 (1H, s, Ar*H*), 8.02 (1H, s, Ar*H*), 3.93 (6H, s, C*H*$_3$); ^{13}C NMR (75.5 MHz, $CDCl_3$) δ_C 164.8, 139.9, 134.1, 130.7, 125.9, 52.8; FI-HRMS found m/z = 351.8769, calculated 351.8768 for $[M]^+$.

Synthesis of dimethyl 4,6-di(pyridin-2-yl)isophthalate 62

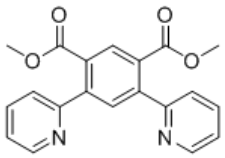

Dimethyl 4,6-dibromoisophthalate **61** (2.10 g, 5.96 mmol), 2-(tributylstannyl)pyridine **58** (6.00 mL, 18.0 mmol), $Pd(PPh_3)_2Cl_2$ (0.20 g, 0.285 mmol) and LiCl (2.00 g, 47.2mmol) were dissolved in dry toluene (100 mL), degassed via 5 cycles of freeze-pump-thaw. The reaction mixture was then heated under reflux for 48 hours under N_2. The resulting solution was cooled, sat. $KF_{(aq)}$ (10 mL) was added and the solution stirred for 30 minutes. The solution was filtered through Celite, washed with water (50 mL) and toluene (50 mL) and extracted with CH_2Cl_2 after adding sat. $NaHCO_{3(aq)}$ (10 mL). Purification by column chromatography (silica; gradient elution hexane/Et_2O 100:0→10:90) gave the product as an off white solid (1.21 g, 58%). ^{1}H NMR (300 MHz, $CDCl_3$) δ_H 8.66 (2H, d, ^3J = 5.3 Hz, Ar*H*), 8.32 (1H, s, Ar*H*), 7.78-7.68 (3H, m, Ar*H*), 7.49 (2H, d, ^3J = 7.6 Hz, Ar*H*), 7.26 (2H, app. t, ^3J = 6.5 Hz, Ar*H*), 3.74 (6H, s, C*H*$_3$); ^{13}C NMR (75.5 MHz, $CDCl_3$) δ_C 168.0, 157.2, 149.3, 143.5, 136.3, 131.5, 131.1, 123.0, 122.7, 52.3, remaining quaternary undetected; ESI-HRMS found m/z = 371.1006, calculated 371.1002 for $[M + Na]^+$.

Synthesis of platinum (II) bis-ester 63[13]

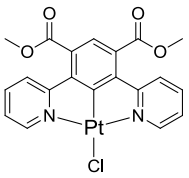

K_2PtCl_4 (50 mg, 0.1200 mmol) dissolved in water (10 mL) was added to dimethyl 4,6-di(pyridin-2-yl)isophthalate **62** (42 mg, 0.120 mmol) in acetonitrile (30 mL). The reaction mixture was heated under vigorous reflux for 3 days. The resulting solution was cooled, filtered and washed with water (10 mL), EtOH (10 mL), acetonitrile (10 mL) and Et_2O (10 mL). Solvent was removed *in vacuo* and subsequent drying under high vacuum gave a yellow solid (45 mg, 64 %). ^{1}H NMR (500 MHz, $CDCl_3$) δ_H 9.62 (2H, d, ^3J = 4.7 Hz, $^3J(^{195}Pt)$ = 18.9 Hz, Ar*H*), 8.04 (2H, d, ^3J = 7.3 Hz, Ar*H*), 7.99 (2H, app. t, ^3J = 6.8 Hz, Ar*H*), 7.80 (1H, s, Ar*H*), 7.41 (2H, app. t, ^3J = 6.6 Hz, Ar*H*), 4.03 (6H, s, CH_3); ^{13}C NMR (126 MHz, d^6-DMSO) δ_C 167.1, 163.3, 151.7, 140.6, 139.0, 129.5, 125.7, 124.4, 123.8, 54.9, 53.3; FI-HRMS found m/z = 542.0695, calculated 542.0680 for $[M - Cl]^+$.

Synthesis of platinum (II) bis-acid 64[14]

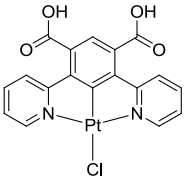

Platinum bis-ester **63** (0.200 g, 0.344 mmol) was suspended in a solution of KOH (1.93 g, 34.0 mmol) dissolved in MeOH (5 mL). The reaction mixture was stirred at 40 °C overnight. Water (2 mL) was added and the MeOH was removed *in vacuo*. The resulting solution was neutralised with conc. $HCl_{(aq)}$, filtered and washed with water (5 mL) and MeOH (5 mL).

The yellow precipitate was dried under high vacuum to give a yellow solid, the platinum bis-acid intermediate. This was used without characterisation due to low solubility.

Synthesis of platinum (II) acyclic receptor 65

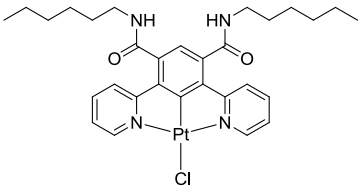

Oxalyl chloride (0.110 mL, 1.37 mmol) was added dropwise to a suspension of the platinum bis-acid **64** (0.189 g, 0.343 mmol) in dry CH_2Cl_2 (100 mL) and dry degassed catalytic DMF (1 drop). The reaction mixture was stirred under N_2 at RT until homogenous. The solvent was removed *in vacuo* and dried under high vacuum. The resulting acid chloride intermediate was used without further purification. Dry, distilled Et_3N (0.384 mL, 2.75 mmol) and hexylamine (0.270 mL, 2.06 mmol) were added to the acid chloride intermediate dissolved in CH_2Cl_2 (100 mL) at 0 °C. The reaction mixture was stirred for 2 hours at RT. The resulting solution was washed with sat. $NaHCO_{3(aq)}$ (50 mL), 10 % w/w citric acid (50 mL) and sat. brine (50 mL) and dried over anhydrous $MgSO_4$. The solvent was then removed *in vacuo*. Purification by preparative TLC (90:10 CH_2Cl_2/MeOH) gave a yellow solid (0.0152 g, 6.00 %). ^{1}H NMR (500 MHz, DMSO-d_6) δ_H 9.30 (2H, d, ^3J = 5.9 Hz, $^3J(^{195}Pt)$ = 19.0 Hz, Ar*H*), 8.88 (2H, t, ^3J = 5.4 Hz, N*H*), 8.23 (2H, app. t, ^3J = 9.8 Hz, Ar*H*), 7.85 (2H, d, ^3J = 8.3 Hz, Ar*H*), 7.62 (2H, app. t, ^3J = 6.8 Hz, Ar*H*), 7.02 (1H, s, Ar*H*), 1.53 (4H, m, CH_2), 1.29 (16H, m, CH_2), 0.84 (6H, m, CH_3); ^{13}C NMR (75.5 MHz, $CDCl_3$) δ_C 168.5, 164.2, 151.2, 137.6, 136.7, 134.1, 123.5, 121.9, 40.0, 31.6, 29.5, 26.9, 22.7, 14.1, remaining quaternaries undetected; EI-HRMS found *m/z* = 680.2791, calculated 680.2564 for $[M - Cl]^+$; UV-Vis

$\lambda_{max}(CH_2Cl_2)$/nm: 251 (ε/dm^3 mol^{-1} cm^{-1} 27,000) 295 (16,000) 318 (8,000) 362 (3,000) 379 (5,000) 416 (5,000).

Synthesis of 4-tolylterpyridine 66[15]

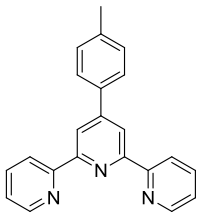

2-acetylpyridine (4.63 mL, 41.3 mmol) was added to crushed NaOH (1.70 g, 41.3 mmol) in PEG-400 (50 mL) and stirred for 10 minutes. 4-tolylaldehyde (2.43 mL, 20.7 mmol) was added and the reaction mixture stirred for 2 hours at 0 °C. 25 % $NH_4OH_{(aq)}$ (50 mL) was added and the solution was stirred at 100 °C for a further 2 hours. The resulting solution was filtered and recrystallized from EtOH to give an off-white microcrystalline solid (2.87 g, 20 %); ^{1}H NMR (300 MHz, $CDCl_3$) δ_H 8.73 (4H, s, Ar*H*), 8.67 (2H, d, ^3J = 7.6 Hz, Ar*H*) 7.80-7.91 (4H, m, Ar*H*), 7.30-7.37 (4H, m, Ar*H*), 2.43 (3H, s, C*H*$_3$); ESI-LRMS found m/z = 324.13; calculated 324.15 for [M + H]$^+$.

Synthesis of $RuCl_3$(ttpy) 67[16]

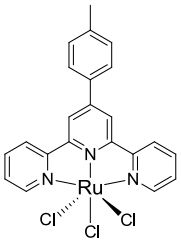

$RuCl_3.3H_2O$ (0.405 g, 1.55 mmol) was heated under reflux in EtOH (35 mL). 4-tolylterpyridine (0.500 g, 1.54 mmol) was added as a solid and rinsed with EtOH (10 mL). The reaction mixture was left under reflux for 2 hours then filtered hot. The precipitate was

subsequently washed with water, EtOH and Et_2O to give the product as a brown-black solid (0.670 g, 82 %); The compound was used without further purification.

Synthesis of ruthenium (II) bis-ester 68 · PF_6

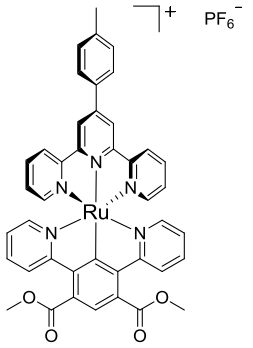

$RuCl_3$(ttpy) **67** (0.200 g, 0.377 mmol) was added to a solution of $AgBF_4$ (0.265 g, 1.36 mmol) in acetone (40 mL) in the dark. The reaction mixture was heated under reflux for 2 hours. The resulting solution was cooled and filtered through Celite. The solvent was removed *in vacuo* and the solid dissolved in n-butanol (40 mL). Dimethyl 4,6-di(pyridin-2-yl)isophthalate **5** (0.210 g, 0.602 mmol) was added and the resulting solution was heated to reflux overnight under N_2. The solution was cooled and concentrated to 10 mL *in vacuo.* Sat. $NH_4PF_{6(aq)}$ (2 mL) was added and the solution filtered. The resulting solid was purified by column chromatography (silica; 98:2 CH_2Cl_2/MeOH) to give the product as a purple solid (0.220 g, 76.0 %). ^{1}H NMR (300 MHz, $CDCl_3$) δ_H 8.81 (2H, s, Ar*H*), 8.45 (2H, d, ^3J = 7.6 Hz, Ar*H*), 8.05 (2H, d, ^3J = 8.2 Hz, Ar*H*), 7.99 (2H, d, ^3J = 8.2 Hz, Ar*H*), 7.76 (1H, s, Ar*H*), 7.64 (2H, app. t, ^3J = 7.9 Hz, Ar*H*), 7.48 (2H, d, ^3J = 7.0 Hz, Ar*H*), 7.44 (2H, d, ^3J = 8.2 Hz, Ar*H*) 7.16 (2H, app. t, ^3J = 4.1 Hz Ar*H*), 6.94 (2H, d, ^3J = 5.9 Hz, Ar*H*), 6.83 (2H, app. t, ^3J = 6.7 Hz Ar*H*), 6.73 (2H, app. t, ^3J = 6.5 Hz, Ar*H*), 4.08 (6H, s, C*H*$_3$), 2.43 (3H, s, C*H*$_3$); ^{13}C NMR (75.5 MHz, $(CD_3)_2CO$) δ_C 169.9, 166.1, 159.2, 154.6, 153.2, 151.6, 140.0, 135.6, 135.1,

130.1, 129.1, 127.4, 126.8, 124.0, 123.4, 122.8, 120.1, 52.4, 20.5, remaining quaternaries not detected; ^{19}F NMR (283 MHz, $CDCl_3$) δ_F -73.0 (d, ^1J = 713 Hz, PF_6); ^{31}P NMR (121 MHz, $CDCl_3$) δ_P -144.32 (sept., ^1J = 714 Hz, PF$_6$) ; ESI-HRMS found m/z = 772.1502, calculated 772.1504 for $[M - PF_6]^+$.

Synthesis of ruthenium bis-acid 69 · PF_6

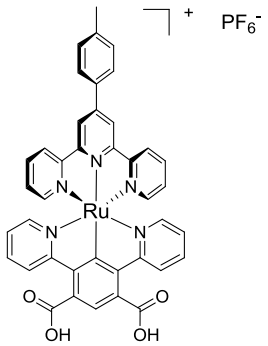

10 % w/w $NaOH_{(aq)}$ (0.9 mL) was added to a solution of ruthenium bis-ester (0.0100 g, 0.0120 mmol) dissolved in dioxane (6.7 mL) and MeOH (2.4 mL). The reaction mixture was stirred at RT overnight. Water (0.5 mL) was added and MeOH and dioxane were removed *in vacuo*. The resulting solution was then neutralised with conc. $HCl_{(aq)}$, cooled for 30 minutes at 4 °C and filtered. The solvent was removed *in vacuo* and subsequent drying under high vacuum gave a purple solid, the ruthenium bis-acid intermediate (0.00505 g, 52.1 %). This was used without further purification. ^{1}H NMR (500 MHz, CD_3CN) δ_H 8.99 (2H, s, Ar*H*), 8.57 (2H, d, ^3J = 7.0 Hz, Ar*H*), 8.31 (2H, d, ^3J = 7.8 Hz, Ar*H*), 8.11 (2H, d, ^3J = 7.8 Hz, Ar*H*), 7.76 (1H, s, Ar*H*), 7.73 (2H, app. t, ^3J = 7.8 Hz, Ar*H*), 7.64 (2H, app. t, ^3J = 7.3 Hz, Ar*H*), 7.56 (2H, d, ^3J = 6.7 Hz, Ar*H*) 7.28 (2H, d, ^3J = 4.9 Hz, Ar*H*), 7.04 (2H, d, ^3J = 6.1 Hz, Ar*H*), 6.97 (2H, app. t, ^3J = 5.8Hz, Ar*H*), 6.77 (2H, app. t, ^3J = 5.8 Hz, Ar*H*), 2.53 (3H, s, C*H*$_3$).

Synthesis of ruthenium (II) acyclic receptor 70 · PF_6

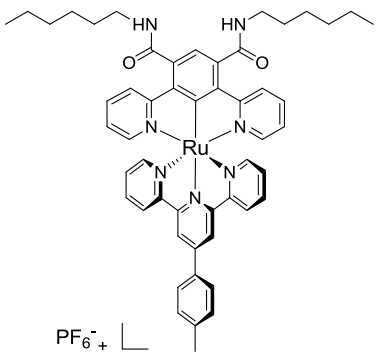

Oxalyl chloride (0.00400 mL, 0.0520 mmol) was added dropwise to a solution of ruthenium bis-acid (0.00964 g, 0.0130 mmol) in dry CH_2Cl_2 (50 mL) and dry degassed catalytic DMF (1 drop). The reaction mixture was stirred under N_2 at RT until homogenous. The solvent was removed *in vacuo* and dried under high vacuum. The resulting acid chloride intermediate was used without further purification. Dry, distilled Et_3N (0.0140 mL, 0.104 mmol) and hexylamine (0.0100 mL, 0.0780 mmol) were added to the acid chloride intermediate dissolved in CH_2Cl_2 (50 mL) at 0 °C. The reaction mixture was stirred for 2 hours at RT. The solvent was then removed *in vacuo*. The resulting solid was dissolved in CH_2Cl_2 (15 mL) and washed with 0.1 M $NH_4PF_{6(aq)}$ (10 × 10 mL) and H_2O (2 × 10 mL). The organic layer was dried over $MgSO_4$, and the solvent removed *in vacuo*. Purification by preparative TLC (silica; DCM/MeOH 90:10) gave a purple solid (0.00924 g, 81.0 %). ^{1}H NMR (500 MHz, CD_2Cl_2) δ_H 8.81 (1H, s, Ar*H*), 8.39 (2H, d, ^3J = 7.9 Hz, Ar*H*), 8.32 (2H, d, ^3J = 7.9 Hz, Ar*H*), 8.02 (2H, d, ^3J = 8.2 Hz, Ar*H*), 7.65 (2H, app. t, ^3J = 7.6 Hz, Ar*H*), 7.54 (2H, d, ^3J = 8.8 Hz, Ar*H*), 7.50 (2H, d, ^3J = 7.8 Hz, Ar*H*), 7.29 (1H, s, Ar*H*), 7.26 (2H, d, ^3J = 5.6 Hz, Ar*H*), 7.06 (2H, d, ^3J = 5.8 Hz, Ar*H*), 6.98 (2H, app. t, ^3J = 6.8 Hz, Ar*H*), 6.83 (2H, t, ^3J = 6.0 Hz, N*H*), 6.63 (2H, app. t, ^3J = 6.5 Hz, Ar*H*), 3.59 (4H, m, CH_2), 2.53 (3H, s, ArCH_3), 1.72 (4H, m,

C*H*$_2$), 1.47 (4H, m, C*H*$_2$), 1.37 (8H, m, C*H*$_2$), 0.90 (6H, m, C*H*$_3$); ^{13}C NMR (126 MHz, $CDCl_3$) δ_C 171.4, 167.4, 157.7, 156.4, 153.0, 150.0, 136.6, 135.1, 134.4, 130.5, 127.0, 123.4, 122.9, 121.4, 119.0, 65.8, 53.4, 45.9, 40.3, 31.5, 29.7, 29.2, 26.7, 22.6, 21.4, 15.3, 14.0, 8.6, remaining quaternary undetected; ^{19}F NMR (283 MHz, $CDCl_3$) δ_F -72.5 (d, ^1J = 713 Hz, P*F*$_6$) ; ^{31}P NMR (121 MHz, $CDCl_3$) δ_P -144.53 (sept., ^1J = 713 Hz, *P*F$_6$); ESI-HRMS found *m/z* = 910.3390, calculated 910.3391 for $[M - PF_6]^+$; UV-Vis $\lambda_{max}(CH_2Cl_2)$/nm: 240 (ε/dm^3 mol^{-1} cm^{-1} 21,000) 289 (34,000) 314 (19,000) 372 (5,000) 409 (4,000) 516 (7,000) 549 (7,000).

Synthesis of platinum (II) macrocyclic receptor 71

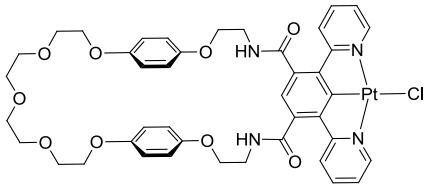

Oxalyl chloride (0.0110 mL, 0.138 mmol) was added dropwise to a solution of platinum diacid **64** (0.0190 g, 0.0346 mmol) in dry CH_2Cl_2 (100 mL) and dry degassed catalytic DMF (1 drop). The reaction mixture was stirred under N_2 at RT until homogenous. The solvent was removed *in vacuo* and dried under high vacuum. The resulting acid chloride intermediate was used without further purification. Bis-amine (0.0160 g, 0.0346 mmol), pyridinium thread **39** · Cl (0.0130 g, 0.0346 mmol) and Et_3N (0.0120 mL, 0.0865 mmol) were dissolved in dry CH_2Cl_2 (100 mL) and stirred until homogenous. The acid chloride in dry CH_2Cl_2 (100 mL) was added dropwise, and the reaction mixture stirred for 3 hours at RT under N_2. The solvent was removed *in vacuo*. The resulting solid was purified by preparative TLC (98:2 CH_2Cl_2/MeOH) to give a yellow solid (0.00810 g, 24%). ^{1}H NMR (500 MHz, DMSO-*d*$_6$) δ_H 9.32 (2H, d, ^3J = 5.4 Hz, Ar*H*), 9.14 (2H, t, ^3J = 5.9 Hz, N*H*), 8.25 (2H, app. t, ^3J = 7.8 Hz,

Ar*H*), 7.92 (2H, d, ^3J = 7.8 Hz, Ar*H*), 7.64 (2H, app. t, ^3J = 7.3 Hz, Ar*H*), 7.08 (1H, s, Ar*H*), 6.87 (4H, d, ^3J = 9.2 Hz, Ar*H*), 6.81 (4H, d, ^3J = 9.3 Hz, Ar*H*), 4.08 (4H, t, ^3J = 5.4 Hz, CH_2), 3.94 (4H, m, CH_2), 3.69 (8H, m, CH_2), 3.54 (8H, m, CH_2); ^{13}C NMR (126 MHz, DMSO-d_6) δ_C 167.8, 164.4, 152.8, 152.4, 140.5, 136.7, 135.2, 115.6, 115.3, 69.9, 69.0, 67.6, 66.5, 30.7, remaining peaks undetected; MALDI-TOF MS found m/z = 942.02, calculated 942.27 for $[M - Cl]^+$; UV-Vis $\lambda_{max}(CH_2Cl_2)$/nm: 418 (ε/dm^3 mol^{-1} cm^{-1} 1,000) 379 (1,000) 360 (1,000) 320 (3,000) 294 (7,000) 250 (8,000) 232 (9,000).

Synthesis of ruthenium (II) macrocyclic receptor 72 · PF_6

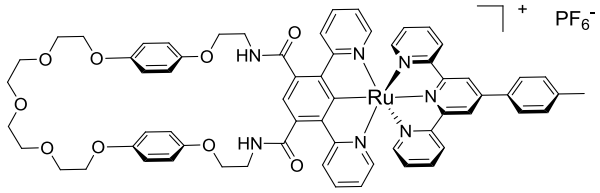

Oxalyl chloride (0.0400 mL, 0.450 mmol) was added dropwise to a solution of ruthenium bis-acid **69** · PF_6 (0.100 g, 0.112 mmol) in dry CH_2Cl_2 (100 mL) and dry degassed catalytic DMF (1 drop). The reaction mixture was stirred under N_2 at RT until homogenous. The solvent was removed *in vacuo* and dried under high vacuum. The resulting acid chloride intermediate was used without further purification. Bis-amine **37** (0.0521 g, 0.112 mmol), pyridinium thread **39** · Cl (0.0430 g, 0.112 mmol) and Et_3N (0.0400 mL, 0.281 mmol) were dissolved in dry CH_2Cl_2 (100 mL) and stirred until homogenous. The acid chloride in dry CH_2Cl_2 (100 mL) was added dropwise, and the reaction mixture stirred for 3 hours at RT under N_2. The solvent was removed *in vacuo*. The resulting solid was dissolved in CH_2Cl_2 (15 mL) and washed with 0.1 M $NH_4PF_{6(aq)}$ (10 × 10 mL) and H_2O (2 × 10 mL). The organic layer was dried over $MgSO_4$, and the solvent removed *in vacuo*. The resulting solid was purified by

column chromatography (silica; DCM/MeOH 96:4) and preparative TLC (silica; CH_2Cl_2/MeOH 98:2) to give a purple solid (0.0715 g, 48%). ^{1}H NMR (500 MHz, DMSO-*d6*) δ_H 9.46 (2H, s, Ar*H*), 9.15 (2H, t, ^3J = 5.4 Hz, Ar*H*), 9.03 (2H, d, ^3J = 8.3 Hz, Ar*H*), 8.36 (2H, d, ^3J = 8.3 Hz, Ar*H*), 8.09 (2H, d, ^3J = 8.3 Hz, Ar*H*), 7.87 (2H, app. t, ^3J = 8.8 Hz, Ar*H*), 7.70 (2H, app. t, ^3J = 8.8 Hz, Ar*H*), 7.56 (2H, d, ^3J = 7.9 Hz, Ar*H*), 7.20 (2H, d, ^3J = 4.9 Hz, Ar*H*), 7.16 (1H, s, Ar*H*), 7.12 (2H, app. t, ^3J = 7.3 Hz, Ar*H*), 7.01 (2H, d, ^3J = 4.9 Hz, Ar*H*), 6.94 (4H, d, ^3J = 9.2 Hz, Ar*H*), 6.86 (4H, d, ^3J = 9.3 Hz, Ar*H*), 6.82 (2H, app. t, ^3J = 5.9 Hz, Ar*H*), 4.17 (4H, m, C*H*$_2$), 3.98 (4H, m, C*H*$_2$), 3.74 (8H, m, C*H*$_2$), 3.57 (8H, m, C*H*$_2$), 1.19 (3H, s, C*H*$_3$); ^{19}F NMR (283 MHz, d^6-DMSO) δ_F -71.96 (d, ^1J = 713 Hz, P*F*$_6$); ^{31}P NMR not obtained due to insolubility; ESI-HRMS found *m/z* =1172.3528, calculated 1172.3508 for $[M - PF_6]^+$; UV-Vis $\lambda_{max}(CH_2Cl_2)$/nm: 233 (ε/dm^3 mol^{-1} cm^{-1} 42,000) 288 (65,000) 314 (10,000) 371 (35,000) 413 (7,000) 519 (13,000) 543 (13,000).

Synthesis of platinum (II) [2]rotaxane 73 · Cl

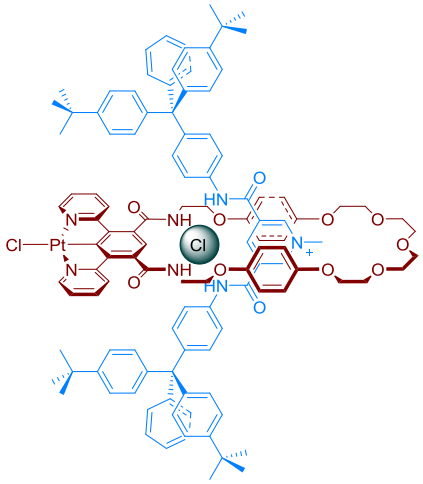

Oxalyl chloride (0.0400 mL, 0.496 mmol) was added dropwise to a solution of platinum bis-acid **64** (0.0682 g, 0.124 mmol) in dry CH_2Cl_2 (100 mL) and dry degassed catalytic DMF (1

drop). The reaction mixture was stirred under N_2 at 40 °C until homogenous. The solvent was removed *in vacuo* and dried under high vacuum. The resulting acid chloride intermediate was used without further purification. Bis-amine **37** (0.0576 g, 0.124 mmol), pyridinium axle **52** · Cl (0.133 g, 0.124 mmol) and Et_3N (0.043 mL, 0.310 mmol) were dissolved in dry CH_2Cl_2 (100 mL) and stirred until homogenous. The acid chloride in dry CH_2Cl_2 (100 mL) was added dropwise, and the reaction mixture stirred for 3 hours at RT under N_2. The solvent was removed *in vacuo*. Purification by column chromatography (silica; gradient elution DCM/MeOH 99:1→95:5), preparative TLC (silica; gradient elution DCM/MeOH 99:1→95:5) and size-exclusion chromatography (Bio-Beads S-X1/ $CHCl_3$) gave the compound as a yellow solid (7.6 mg, 3 %). ^{1}H NMR (500 MHz, $CDCl_3/CD_3OD$ 9:1) δ_H 9.31 (2H, s, Ar*H*), 9.17 (1H, s, Ar*H*), 8.76 (2H, s, Ar*H*), 7.81 (2H, d, ^3J = 8.0 Hz, Ar*H*), 7.71-7.65 (6H, m, Ar*H*), 7.41 (1H, s, Ar*H*), 7.26-7.05 (32H, m, Ar*H*), 6.67 (2H, d, ^3J = 8.2 Hz, Ar*H*), 6.31 (2H, d, ^{3}J = 8.5Hz, Ar*H*), 4.12 (3H, s, CH_3), 3.97-3.30 (24H, m , OCH_2), 1.25 (18H, s, CH_3); ^{13}C NMR (126 MHz, $CDCl_3/CD_3OD$ 9:1) δ_c 168.2, 167.1, 157.8, 151.9, 150.9, 147.7, 146.0, 143.9, 142.6, 138.4, 137.0, 134.0, 133.0, 132.7, 131.0, 130.1, 129.7, 127.9, 126.5, 125.0, 123.4, 122.6, 122.2, 118.7, 114.5, 114.0, 69.7, 69.6, 69.2, 67.3, 66.6, 65.3, 62.9, 56.9, 39.2, 37.8, 33.4, 29.4, 28.7, 28.0, 22.8, 22.0, 17.0, 13.0, 10.0; MALDI-TOF MS found m/z = 2018.89, calculated 2018.32 for $[M - Cl]^+$.

Synthesis of ruthenium (II) [2]rotaxane 74 · Cl_2

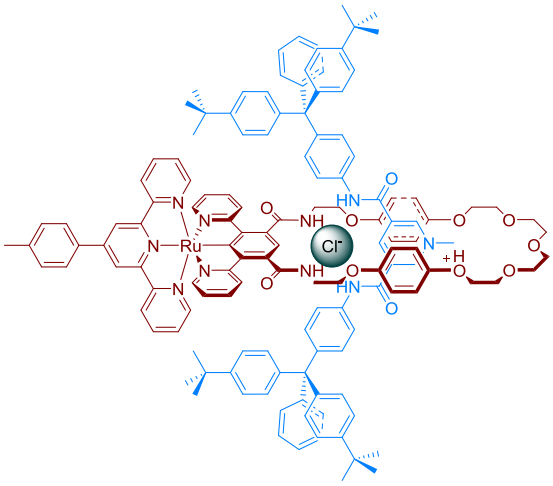

Oxalyl chloride (0.08 mL, 0.1 mmol) was added dropwise to a solution of ruthenium bis-acid **68** · PF_6 (0.023 g, 0.025 mmol) in dry CH_2Cl_2 (10 mL) and dry degassed catalytic DMF (1 drop). The reaction mixture was stirred under N_2 at 40°C until homogenous. The solvent was removed *in vacuo* and dried under high vacuum. The resulting acid chloride intermediate was used without further purification. Bis-amine **37** (0.012 g, 0.025 mmol), pyridinium axle **52** · Cl (0.027 g, 0.025 mmol) and Et_3N (0.008 mL, 0.0625 mmol) were dissolved in dry CH_2Cl_2 (10 mL) and stirred until homogenous. The acid chloride in dry CH_2Cl_2 (10 mL) was added dropwise, and the reaction mixture stirred for 3 hours at RT under N_2. The solvent was removed *in vacuo*. Purification by column chromatography (silica; DCM/MeOH 95:5) and by preparative TLC (silica; gradient elution EtOAc/MeOH 100:0→98:2) gave the compound as a purple solid (4.6 mg, 8%). ^{1}H NMR (500 MHz, CD_2Cl_2) δ_H 9.55 (1H, s, Ar*H*), 9.49 (2H, s, Ar*H*), 8.81 (2H, s, Ar*H*), 8.45 (2H, br. s, Ar*H*), 8.37 (2H, d, ^3J = 7.9 Hz, Ar*H*), 8.27 (2H, br. s, Ar*H*), 8.02 (2H, d, ^3J = 8.2 Hz, Ar*H*), 7.76 (2H, br. s, Ar*H*), 7.70 (2H, br. s, Ar*H*), 7.61-7.55 (4H, m, Ar*H*), 7.43 (4H, d, ^3J = 8.8 Hz, Ar*H*), 7.39 (1H, br. s, Ar*H*), 7.38-7.22 (28H, m, Ar*H*), 7.12 (2H, d, ^3J = 5.4 Hz, Ar*H*), 7.07 (2H, br. s, Ar*H*), 6.84 (4H, d, ^3J =

8.2 Hz, Ar*H*), 6.67 (2H, app. t, ^{3}J = 6.3 Hz, Ar*H*), 6.40 (4H, d, ^{3}J = 8.5 Hz, Ar*H*), 4.20 (3H, s, C*H*$_3$), 4.05-4.00 (4H, m, C*H*$_2$), 3.81-3.69 (16H, m, OC*H*$_2$), 3.55 (4H, br. s, OC*H*$_2$), 2.59(3H, s, C*H*$_3$), 1.41-1.27(36H, m, ^{t}*Bu*); ^{13}C NMR (126 MHz, CD_2Cl_2) δ_C 153.4, 149.2, 146.1, 144.2, 140.7, 135.3, 132.2, 131.3, 130.9, 128.0, 127.5, 126.3, 124.9, 122.1, 119.9, 116.3, 115.2, 71.0, 67.8, 64.4, 40.3, 40.1, 39.1, 34.6, 31.5, 30.1, 21.5, 1.2, remaining quaternaries undetected; ^{19}F NMR (283 MHz, $CDCl_3$) δ_F -72.2 (d, ^{1}J = 713 Hz, P*F*$_6$) ; ^{31}P NMR (121 MHz, $CDCl_3$) δ_P -144.48 (sept., ^{1}J = 712 Hz, *P*F$_6$); ESI-HRMS found m/z = 1106.4795, calculated 1106. 4795 for $[M\text{-}ClPF_6]^{2+}$.

Synthesis of ruthenium (II) [2]rotaxane 74 · $(PF_6)_2$

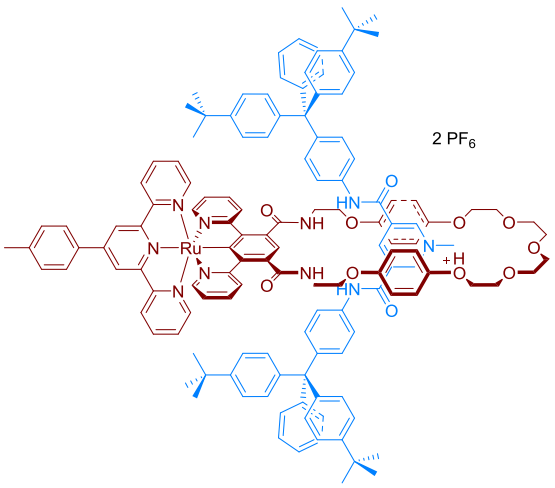

Ruthenium rotaxane **74** · Cl_2 was dissolved in CH_2Cl_2 (15 mL) and washed with 0.1 M $NH_4PF_{6(aq)}$ (10 × 10 mL) and H_2O (2 × 10 mL). The organic layer was dried over $MgSO_4$, and the solvent removed *in vacuo* to give the compound as a purple solid (0.0494 g, 95%); ^{1}H NMR (500 MHz, CD_2Cl_2) δ_H 9.56 (1H, s, Ar*H*), 9.48 (2H, s, Ar*H*), 8.42 (2H, s, Ar*H*), 8.28 (2H, d, ^{3}J = 7.3 Hz, Ar*H*), 8.02 (2H, d, ^{3}J = 8.3 Hz, Ar*H*), 7.81-7.71 (8H, m, Ar*H*), 7.59 (2H, d, ^{3}J = 8.3 Hz Ar*H*), 7.48 (2H, app. t, ^{3}J = 7.8 Hz, Ar*H*), 7.41 (6H, d, ^{3}J = 8.8 Hz Ar*H*),

7.36-7.18 (31H, m, Ar*H*), 6.88-6.73 (6H, m, Ar*H*), 6.39 (4H, d, $^{3}J = 8.8$ Hz, Ar*H*), 4.16 (3H, s, CH_3), 4.02-3.95 (4H, br. s, CH_2), 3.77-3.65 (16H, m, CH_2), 3.50 (4H, br. s, CH_2), 2.57 (3H, s, CH_3), 1.36-1.22 (36H, m, ^{t}Bu); ^{19}F NMR (472 MHz, CD_2Cl_2) δ_F -70.9 (d, $^{1}J = 742$ Hz, PF_6); ESI-HRMS found $m/z = 1106.4795$, calculated 1106.4793 for $[M - 2PF_6]^{2+}$.

Chapter 4 Syntheses

Synthesis of dimethyl-5-bromoisophthalate 75[17]

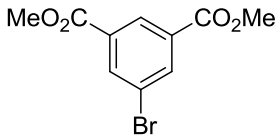

5-bromoisopthalic acid (1.00 g, 4.08 mmol) was dissolved in MeOH (6 mL) in a microwave vial. Conc. H_2SO_4 (6 mL) was added dropwise to the solution and the reaction was heated in the microwave at 120 °C for 20 minutes. The reaction mixture was poured onto ice and basified to pH 9 with 25% $NH_4OH_{(aq)}$. The aqueous mixture was extracted with Et_2O (3 × 30 mL), dried over anhydrous $MgSO_4$ and the solvent removed *in vacuo* to give the compound as a white solid (992 mg, 89 %). ^{1}H NMR (300 MHz, $CDCl_3$) δ_H 8.61 (1H, s, Ar*H*), 8.36 (2H, s, Ar*H*), 3.96 (6H, s, CH_3); ESI-LRMS: found $m/z = 272.96$, calculated 271.98 for $[M + H]^+$.

Synthesis of dimethyl-5-MEBYNOL-isophthalate 76[17]

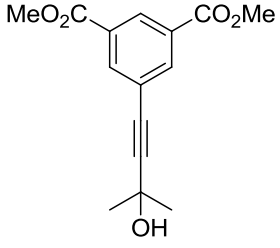

A mixture of dimethyl-5-bromoisophthalate (500 mg, 1.83 mmol), $Pd(PPh_3)_2Cl_2$ (64 mg, 0.09 mmol), CuI (17.4 mg, 0.09 mmol), and 2-methylbut-3-yn-2-ol (185 mg, 2.20 mmol) was dissolved in pyridine (5 mL) and Et_3N (10 mL) which had been purged with N_2 gas. The reaction was heated at 90 °C for 18 hours under N_2. The reaction was allowed to cool to ambient temperature, filtered through celite and washed with Et_2O (10 mL). The reaction solution was acidified to pH 4 with 10% $HCl_{(aq)}$, extracted with Et_2O (3 × 20 mL), dried over anhydrous $MgSO_4$ and the solvent removed *in vacuo*. The compound was dissolved in toluene and precipitated with *n*-hexane (*ca.* 1:1, v/v) to afford the compound as a white solid (409 mg, 81 %). ^{1}H NMR (300 MHz, $CDCl_3$) δ_H 8.61 (1H, t, $^4J = 1.5$ Hz, Ar*H*), 8.26 (2H, d, $^4J = 1.5$ Hz, Ar*H*), 3.96 (6H, s, C*H*$_3$), 2.73 (1H, s, O*H*), 1.64 (6H, s, C*H*$_3$); ESI-LRMS: found m/z = 277.09, calculated 277.11 for $[M + H]^+$.

Synthesis of dimethyl-5-ethynylisophthalate 77[17]

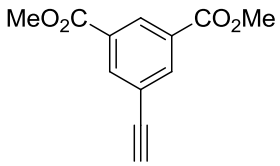

Compound **76** (300 mg, 1.09 mmol) was dissolved in dry toluene (30 mL). Sodium hydride (60 % in mineral oil, 78 mg, 1.95 mmol) was added and the reaction heated to 75°C under N_2 for 1 hour. The reaction was cooled to ambient temperature and quenched with H_2O (*ca.* 10 mL). The organic layer was separated and further washed with H_2O (2 ×20 mL). Drying over anhydrous $MgSO_4$, filtration and removal of the solvent *in vacuo* afforded the compound as an off-white solid (186 mg, 80 %). ^{1}H NMR (300 MHz, $CDCl_3$) δ_H 8.61 (1H, t, $^3J = 1.5$ Hz,

Ar*H*), 8.26 (2H, t, ^3J = 1.5 Hz, Ar*H*), 3.96 (6H, s, CH_3), 2.05 (1H, s, CC*H*); ESI-LRMS: found m/z = 219.03, calculated 219.07 for $[M + H]^+$.

Synthesis of 5-ethynylisophthalic acid 78[17]

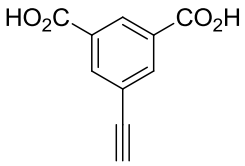

To a solution of dimethyl-5-ethynylisophthalate (250 mg, 1.15 mmol) in *n*-butanol (20 mL) was added potassium hydroxide (645 mg, 11.5 mmol). The reaction was heated under reflux under N_2 for 30 minutes. The reaction was cooled to ambient temperature, filtered and washed with EtOH (10 mL). The precipitate was dissolved in H_2O (5 mL) and acidified to with 10% $HCl_{(aq)}$. The compound was filtered and dried *in vacuo* to give the compound as a white solid (131 mg, 60 %). ^{1}H NMR (300 MHz, DMSO-d_6) δ_H 12.95 (2H, O*H*), 8.48 (1H, s, Ar*H*) 8.19 (2H, s, Ar*H*), 4.44 (1H, s, CC*H*); ESI-LRMS: found m/z = 189.05, calculated 189.01 for $[M - H]^-$.

Synthesis of 5-alkynyl [2]rotaxane 79 · Cl[18]

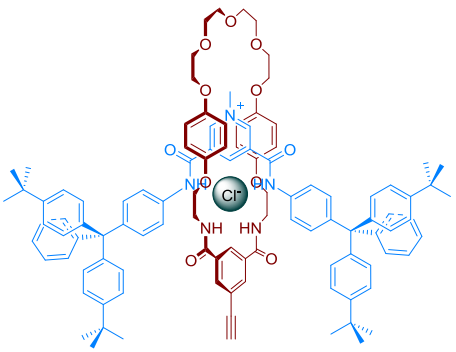

Axle **52** · Cl (496 mg, 0.46 mmol) and bis-amine **37** (214 mg, 0.46 mmol) were dissolved in dry DCM (100 mL) and stirred for 5 minutes under a nitrogen atmosphere. Triethylamine

(148 µL, 1.36 mmol) and 5-ethynylisophthaloyl dichloride (116 mg, 0.46 mmol) in anhydrous CH_2Cl_2 (20 mL) were then added. The reaction was stirred at room temperature for 2 hours after which the solvent was removed *in vacuo*. The crude mixture was purified by column chromatography (silica; gradient elution DCM/MeOH 98:2→95:5) followed by preparative TLC (silica; gradient elution DCM/MeOH 99:1→97:3) to give **79** · Cl as a yellow solid (280 mg, 36%). ^{1}H NMR (500MHz, $CDCl_3$) δ_H 9.30 (2H, s, N*H*), 9.24 (1H, s, Ar*H*), 8.79 (2H, s, Ar*H*), 8.61 (2H, s, N*H*), 8.17 (1H, ,s Ar*H*), 7.52 (4H, d, ^3J = 9.0 Hz, Ar*H*), 7.29-7.07 (34H, m, Ar*H*) 6.57 (4H, d, ^3J = 8.6 Hz, Ar*H*), 6.30 (4H, d, ^3J = 8.6 Hz, Ar*H*), 4.06 (3H, s, CH_3), 3.99-3.50 (24H, m, OCH_2), 3.07 (1H, s, CC*H*), 1.28 (36H, s, ^{t}*Bu*); ESI-HRMS: found m/z = 1659.8701, calculated 1659.8666 for [M - Cl]$^+$.

Synthesis of triazole [3]rotaxane 80 · Cl_2

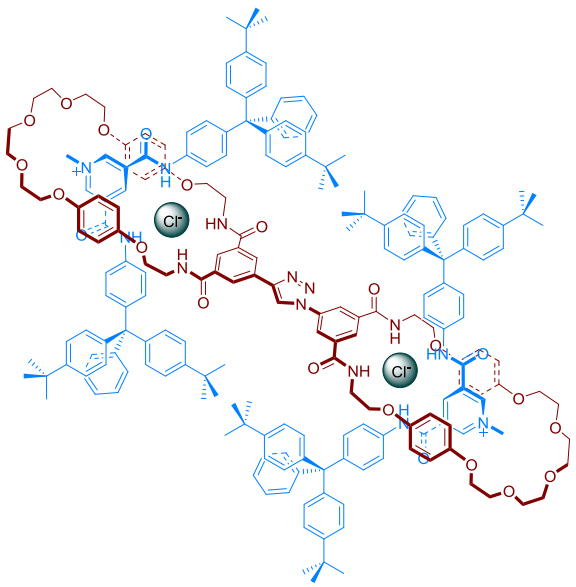

Alkyne [2]rotaxane **79** · Cl (32 mg, 18.9 µmol) and azide [2]rotaxane (34 mg, 19.8 µmol) were dissolved in dry CH_2Cl_2 (8 mL) and stirred at ambient temperature for 48 hours. The solvent was removed *in vacuo* and the crude material purified by size exclusion chromatography

(Bio-Beads SX-1/ $CHCl_3$) followed by preparative thin layer chromatography (silica; gradient elution DCM/MeOH 99:1→97:3) to obtain the compound as a yellow solid (53 mg, 83%). ^{1}H NMR (500MHz, $CDCl_3/CD_3OD$ 9:1) δ_H 9.34 (1H, s, Ar*H*), 9.16 (1H, s, Ar*H*), 8.96 (2H, s, Ar*H*), 8.93 (2H, s, Ar*H*), 8.83 (1H, s, Ar*H*), 8.55 (2H, s, Ar*H*), 8.52 (1H, s, Ar*H*), 8.48 (2H, s, Ar*H*), 8.33 (2H, br. s, N*H*), 8.08 (2H, br. s, N*H*), 7.70 (4H, d, ^3J = 8.5 Hz , Ar*H*), 7.64 (4H, d, ^3J = 8.5 Hz , Ar*H*), 7.19-6.95 (61H, m, Ar*H*), 6.49-6.43 (8H, m, Ar*H*), 6.25-6.16 (8H, m, Ar*H*), 4.44 (3H, s, C*H*$_3$), 4.35 (3H, s, C*H*$_3$), 4.00 (4H, s, OC*H*$_2$) 3.71-3.57 (24H, s, OC*H*$_2$), 1.21 (72H, s, C*H*$_3$); ESI-HRMS: found m/z = 1667.3657, calculated 1659.3706 for $[M - 2Cl]^{2+}$.

Synthesis of triazolium [3]rotaxane 81 · Cl_3

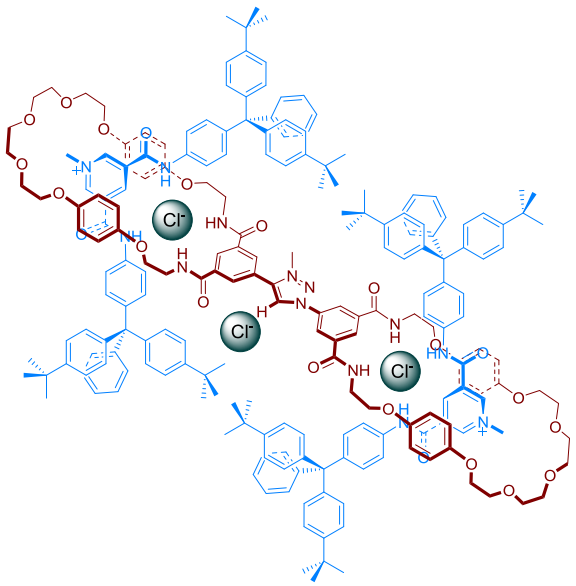

Triazole [3]rotaxane **80** · Cl_2 (50 mg, 14.67 μmol) was dissolved in dry CH_2Cl_2 (5 mL) and added dropwise to a suspension of $[Me_3O][BF_4]$ (3.25 mg, 22.00 μmol) in dry CH_2Cl_2 (5 mL) under a nitrogen atmosphere. The reaction was stirred at ambient temperature for 72 hours after which the reaction was quenched with MeOH (2 mL) and the solvent removed *in vacuo*. The crude material was anion exchanged with NH_4Cl and purified by preparative thin layer

chromatography (silica; gradient elution DCM/MeOH 96:4→93:7) to obtain the compound as a yellow solid (36 mg, 72%). ^{1}H NMR (500MHz, $CDCl_3/CD_3OD$ 9:1) δ_H 9.68 (1H, s, Ar*H*), 9.63 (1H, s, Ar*H*), 9.35 (1H, s, Ar*H*), 9.28 (1H, s, Ar*H*), 9.04 (2H, d, ^{4}J = 1.2 Hz), 9.03 (2H, d, ^{4}J = 1.2 Hz), 8.96 (1H, s, Ar*H*), 8.51 (2H, s, Ar*H*), 8.26 (2H, s, Ar*H*), 7.80 (4H, d, ^{3}J = 2.8 Hz), 7.78 (4H, d, ^{3}J = 2.8 Hz), 7.20-6.93 (60H, m, Ar*H*), 6.43 (8H, m, Ar*H*), 6.16 (8H, m, Ar*H*); ^{13}C NMR (126MHz, $CDCl_3/CD_3OD$ 9:1) δ_C 164.2, 164.1, 163.5, 163.4, 157.4, 157.4, 152.3, 151.2, 147.7, 146.1, 145.0, 143.6, 143.5, 142.6, 142.5, 137.0, 135.6, 134.5, 133.9, 133.7, 132.4, 130.9, 130.1, 129.6, 128.3, 128.0, 126.4, 126.4, 126.0, 124.9, 124.8, 123.4, 123.3, 122.8, 120.6, 119.6, 119.4, 113.9, 69.8, 69.6, 67.3, 64.5, 64.4, 62.8, 40.0, 38.2, 33.3, 30.3, 26.7, 21.7, 13.08; ESI-HRMS: found m/z = 1117.2499, calculated 1117.2547 for $[M - 3Cl]^{3+}$.

Chapter 5 Syntheses

Synthesis of dansyl-imidazole 85

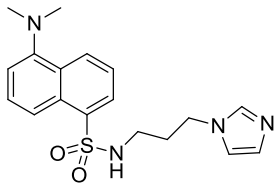

3-(1H-imidazol-1-yl)propan-1-amine (0.32 g, 2.55 mmol) and Et_3N (0.77 g, 7.60 mmol) were dissolved in dry CH_2Cl_2 (50 mL) at 0°C and stirred prior to the dropwise addition of dansyl chloride (0.75 g, 2.80 mmol) in 75 mL dry CH_2Cl_2. The reaction was allowed to warm to ambient temperature, and was further stirred for one hour. Water (30 mL) was added, the organic layer separated, dried over $MgSO_4$ and the solvent removed *in vacuo.* Purification by column chromatography (silica; MeCN/ Et_2O, 3:1) gave **85** as a yellow oil (0.70 g, 77%). ^{1}H NMR (300 MHz, $CDCl_3$) δ_H 8.57 (2H, m, Ar*H*), 8.25 (2H, m, Ar*H*), 7.57 (2H, m, Ar*H*), 7.27

(1H, s, Ar*H*), 7.20 (1H, m, Ar*H*), 6.98 (1H, s, Ar*H*), 3.91 (2H, t, ^{3}J = 6.7 Hz, CH_2), 2.90-2.83 (10H, m, CH_3, CH_2); ^{13}C NMR (75.5 MHz, $CDCl_3$) δ_C 151.9, 148.7, 136.7, 134.0, 129.4, 128.4, 128.1, 123.0, 118.3, 118.2, 115.1, 115.0, 45.7, 45.1, 39.5, 29.4; ESI-HRMS: found *m/z* = 359.1552, calculated 359.1542 for $[M + H]^+$.

Synthesis of BOC-protected ethylene diamine 86

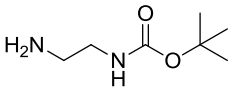

Ethylene diamine (16.70 g, 280 mmol) was dissolved in dry CH_2Cl_2 (200 mL). Di-*tert*-butyl dicarbonate (6.10 g, 28 mmol) was dissolved in dry CH_2Cl_2 (400 mL) and added dropwise over 5 hours. The reaction was stirred at ambient temperature for 36 hours after which the solvent was concentrated to *ca.* 100 mL and washed with sat. $NaHCO_{3(aq)}$ and dried over $MgSO_4$ to give the compound as a colourless oil (3.00 g, 67%). ^{1}H NMR (300 MHz, $CDCl_3$) δ_H 4.84 (1H, br. s, N*H*), 3.11 (2H, m, CH_2), 2.27 (2H, t, ^{3}J = 6.0 Hz, CH_2), 1.40 (9H, s, ^{t}*Bu*), 1.05 (2H, br. s, NH_2); ESI-LRMS: found *m/z* = 161.13, calculated 161.12 for $[M + H]^+$.

Synthesis of BOC-protected Dansyl-amine 87

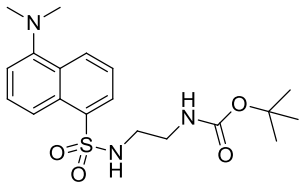

N-BOC-ethylenediamine (1.07 g, 6.69 mmol) and Et_3N (1.13 g, 11.1 mmol) were dissolved in dry CH_2Cl_2 (100 mL) at 0°C and stirred prior to the dropwise addition of dansyl chloride (1.50 g, 5.57 mmol) in 75 mL dry CH_2Cl_2. The reaction was allowed to warm to ambient temperature, and was further stirred for one hour. Water (30 mL) was added, the organic

layer separated, dried over $MgSO_4$ and the solvent removed *in vacuo.* Purification by column chromatography (silica; CH_2Cl_2/ MeOH; 98:2) gave **87** as a yellow oil (1.50 g, 66%). ^{1}H NMR (300 MHz, $CDCl_3$) δ_H 8.55 (1H, d, $^3J = 8.7$ Hz, Ar*H*), 8.29-8.21 (2H, m, Ar*H*), 7.61-7.48 (2H, m, Ar*H*), 7.19 (1H, d, $^3J = 6.6$ Hz, Ar*H*), 5.21 (1H, br. s, N*H*), 4.73 (1H, br. s, N*H*), 3.19-3.11 (2H, m, N*H*), 3.04-2.96 (2H, m, N*H*), 2.89 (6H, s, NCH_3), 1.39 (9H, s, ^{t}*Bu*); ^{13}C NMR (75 MHz, $CDCl_3$) δ_C 156.4, 151.8, 134.7, 130.3, 129.8, 129.5, 128.4, 123.1, 118.8, 115.1, 79.3, 45.3, 43.4, 40.2, 28.3; ESI-HRMS: found m/z = 416.1609, calculated 416.1614 for $[M + Na]^+$.

Synthesis of dansyl-amine 88

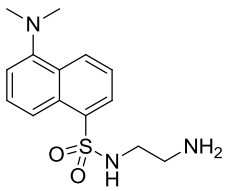

Compound **87** (1.37 g, 3.49 mmol) was dissolved in CH_2Cl_2 (20 mL). Trifluoroacetic acid (5 mL) was added dropwise and stirred at ambient temperature for 18 hours. The reaction was basified with sat. $NaHCO_{3(aq)}$, extracted with CH_2Cl_2 (3 × 20 mL) and dried over $MgSO_4$. Purification by column chromatography (silica; MeOH/ 25% $NH_4OH_{(aq)}$; 9:1) gave a brown solid (0.84 g, 81%). ^{1}H NMR (300 MHz, $CDCl_3$) δ_H 8.53 (1H, d, $^3J = 9.0$ Hz, Ar*H*), 8.32-8.21 (2H, m, Ar*H*), 7.60-7.48 (2H, m, Ar*H*), 7.18 (1H, d, $^3J = 7.8$ Hz, Ar*H*), 2.96-2.89 (4H, m, NHCH_2, NH_2), 2.88 (6H, s, NCH_3), 2.74 (2H, t, $^3J = 5.7$ Hz, CH_2); ^{13}C NMR (75 MHz, $CDCl_3$) δ_C 152.0, 134.7, 130.4, 129.6, 128.4, 123.2, 118.7, 115.2, 45.4, 40.9; ESI-HRMS: found m/z = 294.1259, calculated 294.1271 for $[M + H]^+$.

Synthesis of bromo-naphthalimide-imidazole 89

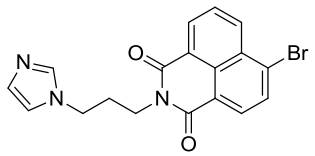

1,8-napththalic anhydride (2.00 g, 7.22 mmol) and 3-(1H-imidazol-1-yl)propan-1-amine (1.08 g, 8.66 mmol) was dissolved in dioxane (40 mL) and heated to reflux for 16 hours under N_2. The reaction was cooled to ambient temperature and precipitated with H_2O (100 mL). The precipitate was filtered and further washed with H_2O (2 × 20 mL) to give the compound **89** as a cream solid (2.25 g, 80%). ^{1}H NMR (300 MHz, $CDCl_3$) δ_H 8.58 (1H, m, Ar*H*), 8.53 (1H, m, Ar*H*), 8.33 (1H, m, Ar*H*), 7.98 (1H, m, Ar*H*), 7.79 (1H, m, Ar*H*), 7.52 (1H, s, Ar*H*), 6.99 (2H, s, Ar*H*), 4.16 (2H, t, $^3J = 7.1$ Hz, CH_2), 4.03 (2H, t, $^3J = 7.6$ Hz, CH_2), 2.21 (2H, m, CH_2) ^{13}C (75 MHz, $CDCl_3$) δ_C 163.7, 137.1, 133.6, 132.3, 131.4, 131.2, 130.7, 129.4, 128.9, 128.1, 122.7, 121.8, 118.7, 109.8, 45.0, 37.8, 29.5; ESI-HRMS: found $m/z = 384.0340$, calculated 384.0342 for $[M + H]^+$.

Synthesis of naphthalimide-imidazole 90

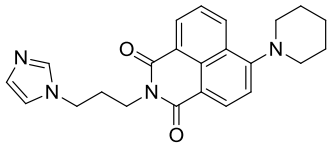

Compound **89** (400 mg, 1.04 mmol) was dissolved in *N,N*-dimethylformamide (10 mL). Piperidine (0.2 mL, 2.08 mmol) was added and the reaction was heated under N_2 and heated at 110 °C for 16 hours. The reaction was cooled to ambient temperature, H_2O (50 mL) was added and the product was extracted with EtOAc (3 × 20 mL) and dried over $MgSO_4$. Purification by column chromatography (silica; DCM/MeOH; 95:5) afforded the compound as a bright orange solid (372 mg, 92%). ^{1}H NMR (300 MHz, $CDCl_3$) δ_H 8.50 (1H, d,

^{3}J = 7.5 Hz, Ar*H*), 8.43 (1H, d, ^{3}J = 8.1 Hz, Ar*H*), 8.33 (1H, d, ^{3}J = 8.1 Hz, Ar*H*), 7.62 (1H, dd, ^{3}J = 8.4 Hz, ^{3}J = 7.5 Hz, Ar*H*), 7.49 (1H, br. s, Ar*H*), 7.12 (1H, d, ^{3}J = 8.1 Hz, Ar*H*), 7.96 (2H, m, Ar*H*), 4.17 (2H, t, ^{3}J = 8.4 Hz, CH_2), 4.00 (2H, t, ^{3}J = 7.5 Hz, CH_2), 3.18 (4H, t, ^{3}J = 5.1 Hz, CH_2), 2.19 (2H, m, CH_2), 3.96 (4H, m, CH_2), 1.66 (2H, m, CH_2); ^{13}C (75 MHz, $CDCl_3$) δ_C 164.6, 164.0, 157.5, 137.2, 132.9, 131.1, 130.9, 129.9, 129.4, 126.1, 125.3, 122.7, 118.7, 115.3, 114.7, 54.5, 45.0, 37.4, 29.8, 26.1, 24.3; ESI-HRMS: found *m/z* = 389.1974, calculated 389.1972 for $[M + H]^+$.

Synthesis of bromo-naphthalimide-BOC-amine 91

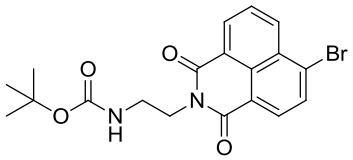

1,8-napththalic anhydride (2.11 g, 7.61 mmol) and *N*-BOC-ethylene diamine **86** (1.46 g, 9.14 mmol) was dissolved in dioxane (40 mL) and heated to reflux for 16 hours under N_2. The reaction was cooled to ambient temperature and precipitated with H_2O (100 mL). The precipitate was filtered and further washed with H_2O (2 × 20 mL) to give the compound as a cream solid (2.71 g, 85%). ^{1}H NMR (300 MHz, $CDCl_3$) δ_H 8.58 (1H, d, ^{3}J = 7.2 Hz, Ar*H*), 8.46 (1H, d, ^{3}J = 8.1 Hz, Ar*H*), 8.33 (1H, d, ^{3}J = 8.4 Hz, Ar*H*), 7.96 (1H, d, ^{3}J = 7.5 Hz, Ar*H*), 7.77 (1H, dd, ^{3}J = 8.1Hz, ^{3}J = 7.5 Hz, Ar*H*), 5.02 (1H, br. s, N*H*), 4.31 (2H, t, J = ^{3}5.7 Hz, CH_2), 3.51 (2H, m, CH_2), 1.26 (9H, s, ^{t}*Bu*); ^{13}C (75 MHz, $CDCl_3$) δ_C 163.8, 156.0, 133.2, 132.1, 131.3, 131.0, 130.4, 130.3, 128.9, 128.0, 122.8, 121.9, 79.1, 40.0, 39.4, 28.2; ESI-HRMS: found *m/z* = 441.0418, calculated 441.0426 for $[M + Na]^+$.

Synthesis of naphthalimide-BOC-piperidine 92

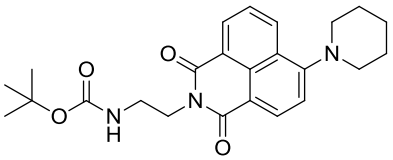

Compound **91** (2.77 g, 6.60 mmol) was dissolved in *N,N*-dimethylformamide (30 mL). Piperidine (1.3 mL, 13.2 mmol) was added and the reaction was heated under N_2 and heated at 110 °C for 16 hours. The reaction was cooled to ambient temperature, H_2O (150 mL) was added and the product was extracted with EtOAc (3 × 60 mL) and dried over $MgSO_4$. Purification by column chromatography (silica; DCM/MeOH; 95:5) afforded the compound as a bright orange solid (2.48 g, 88%). ^{1}H NMR (300 MHz, $CDCl_3$) δ_H 8.57 (1H, d, ^3J = 6.9 Hz, Ar*H*), 8.50 (1H, d, ^3J = 8.1 Hz, Ar*H*), 8.41 (1H, d, ^3J = 7.8 Hz, Ar*H*), 7.68 (1H, dd, ^3J = 8.1 Hz, ^3J = 7.8 Hz, Ar*H*), 7.19 (1H, d, ^3J = 8.1 Hz, Ar*H*), 5.03 (1H, br. s, N*H*), 4.35 (2H, t, ^3J = 5.4 Hz, CH_2), 3.51 (2H, m, CH_2), 3.24 (4H, t, ^3J = 5.4 Hz, CH_2), 1.90 (4H, m, CH_2), 1.73 (2H, m, CH_2), 1.31 (9H, s, ^{t}*Bu*); ^{13}C (75 MHz, $CDCl_3$) δ_C 164.9, 164.4, 157.4, 156.0, 132.8, 131.2, 130.7, 130.0, 126.1, 125.3, 122.8, 115.6, 114.6, 78.9, 54.5, 40.0, 40.0, 28.2, 26.2, 24.3; ESI-HRMS: found *m/z* = 446.2049, calculated 446.2050 for $[M + Na]^+$.

Synthesis of naphthalimide-amine 93

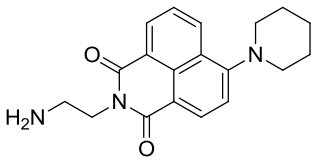

Compound **82** (120 mg, 0.28 mmol) was dissolved in CH_2Cl_2 and cooled to 0°C. Trifluoracetic acid (1 mL) was added dropwise and the reaction was stirred at ambient temperature for 16 hours. The reaction was neutralised slowly by dropwise addition of sat.

$NaHCO_{3(aq)}$. The organic layer was washed further with sat. $NaHCO_{3(aq)}$ (2 × 5 mL) and dried over $MgSO_4$ to give the title compound as an orange oil (86 mg, 94%). ^{1}H NMR (300 MHz, $CDCl_3$) δ_H 8.49 (1H, d, ^3J = 7.8 Hz, Ar*H*), 8.41 (1H, d, ^3J = 8.1 Hz, Ar*H*), 8.31 (1H, d, ^3J = 8.7 Hz Ar*H*), 7.59 (1H, t, ^3J = 8.4 Hz, Ar*H*), 7.09 (1H, d, ^3J = 8.4 Hz, Ar*H*), 4.22 (2H, t, ^3J = 6.3 Hz, CH_2), 3.16 (4H, t, ^3J = 5.7 Hz, CH_2), 3.03 (2H, t, ^3J = 6.6 Hz, CH_2), 1.98 (2H, br. s, NH_2), 1.82 (4H, m, CH_2), 1.66 (2H, m, CH_2); ^{13}C (75.5 MHz, CD_3OD) δ_C 164.6, 164.2, 157.4, 132.3, 130.6, 130.5, 129.4, 125.7, 124.9, 122.2, 114.7, 114.3, 54.2, 53.4, 39.9, 39.1, 25.9, 24.0; ESI-HRMS: found m/z = 324.1706, calculated 324.1707 for $[M + H]^+$.

Synthesis of butyl-naphthalimide-imidazole 94

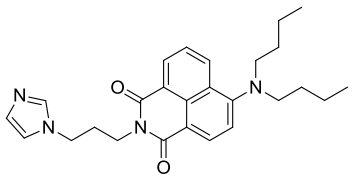

Compound **89** (400 mg, 1.04 mmol) was dissolved in *N,*N-dimethylformamide (10 mL). Dibutylamine (0.48 mL, 2.08 mmol) was added and the reaction was heated under N_2 and heated at 110 °C for 16 hours. The reaction was cooled to ambient temperature, H_2O (50 mL) was added and the product was extracted with EtOAc (3 × 20 mL) and dried over $MgSO_4$. Purification by column chromatography (silica; CH_2Cl_2/MeOH; 97:3) afforded the compound as an orange oil (452 mg, 89 %). ^{1}H NMR (300 MHz, $CDCl_3$) δ_H 8.57 (1H, d, ^3J = 6.9 Hz, Ar*H*), 8.46 (2H, m, Ar*H*), 7.66 (1H, dd, ^3J = 8.7 Hz, ^3J = 6.9 Hz, Ar*H*), 7.55 (1H, br. s, Ar*H*), 7.20 (1H, d, ^3J = 8.1 Hz, Ar*H*), 7.04 (1H, s, Ar*H*), 7.01 (1H, s, Ar*H*), 4.23 (2H, t, ^3J = 7.2 Hz, CH_2), 4.06 (2H, t, ^3J = 7.5 Hz, CH_2), 3.37 (4H, t, ^3J = 6.9 Hz, CH_2), 2.25 (2H, m, CH_2), 1.59 (4H, m, CH_2), 1.28 (2H, m , CH_2), 0.86 (6H, t, ^3J = 6.9 Hz, CH_3); ^{13}C

(75 MHz, $CDCl_3$) δ_C 164.7, 164.1, 156.0, 137.1, 132.3, 131.2, 130.3, 129.4, 127.0, 125.1, 122.8, 118.7, 116.6, 114.8, 53.4, 45.0, 37.4, 29.8, 29.2, 20.3, 13.9; ESI-HRMS: found m/z = 433.2603, calculated 433.2598 for $[M + H]^+$.

General Procedure for Synthesis of Gold Nanoparticles[19]

$H[AuCl_4]$ (100 mg, 0.29 mmol) was dissolved in H_2O (20 mL). Aliquat336 (130 mg) was dissolved in toluene (20 mL). The two solutions were combined and stirred vigorously for 10 minutes. The aqueous layer was discarded and the organic phase transferred cooled to 0°C. The dansyl ligand (3 eq.) was dissolved in CH_2Cl_2 (20 mL) and added to the cooled toluene solution. $NaBH_4$ (60 mg, 1.47 mmol) was dissolved in H_2O (5 mL) and added dropwise at 0°C. The reaction mixture was stirred for two hours at ambient temperature after which the CH_2Cl_2 was removed *in vacuo* and the remaining solution washed with H_2O (3 × 50 mL). The solvent volume was concentrated *in vacuo* and MeOH (100 mL) was added. Filtration and washing with copious MeOH afforded the nanoparticles as a dark solid.

Synthesis of Au · 85

CHNS Analysis Found C, 10.5 ; H, 1.2 ; N, 2.3; S, 1.4; UV-vis ($CHCl_3$) 348, 529; TEM mean diameter 3.1 nm (± 0.7, n = 104)

Synthesis of Au · 88

CHNS Analysis Found C, 7.9; H, 0.9; N, 1.8; S, 1.5; UV-vis ($CHCl_3$) 342, 524; TEM mean diameter 3.2 nm (±0.7, n = 104)

6.3 References

1. C. D. Gutsche and M. Iqbal, *Org. Synth*, 1990, **68**, 234-237.
2. A. V. Leontiev, C. A. Jemmett and P. D. Beer, *Chem.–Eur. J.*, 2011, **17**, 816-825.
3. M. D. Lankshear, N. H. Evans, S. R. Bayly and P. D. Beer, *Chem.–Eur. J.*, 2007, **13**, 3861-3870.
4. F. Zapata, O. A. Blackburn, M. J. Langton, S. Faulkner and P. D. Beer, *Chem. Commun.*, 2013, **49**, 8157-8159.
5. V. Aucagne, K. D. Hanni, D. A. Leigh, P. J. Lusby and D. B. Walker, *J. Am. Chem. Soc.*, 2006, **128**, 2186-2187.
6. H. Y. Zheng, W. D. Zhou, J. Lv, X. D. Yin, Y. J. Li, H. B. Liu and Y. L. Li, *Chem.-Eur. J.*, 2009, **15**, 13253-13262.
7. L. M. Hancock and P. D. Beer, *Chem.-Eur. J.*, 2009, **15**, 42-44.
8. J. A. Wisner, P. D. Beer and M. G. B. Drew, *Angew. Chem.-Int. Edit.*, 2001, **40**, 3606-+.
9. G. T. Spence, N. G. White and P. D. Beer, *Org. Biomol. Chem.*, 2012, **10**, 7282-7291.
10. J. A. Wisner, P. D. Beer, M. G. B. Drew and M. R. Sambrook, *J. Am. Chem. Soc.*, 2002, **124**, 12469-12476.
11. H. Nierengarten, J. Rojo, E. Leize, J.-M. Lehn and A. Van Dorsselaer, *Eur. J. Inorg. Chem.*, 2002, **2002**, 573-579.
12. L. Chardonnens, P. Sunderplassmann and T. Stauner, *Helv. Chim. Acta*, 1979, **62**, 657-666.
13. J. A. G. Williams, A. Beeby, E. S. Davies, J. A. Weinstein and C. Wilson, *Inorg. Chem.*, 2003, **42**, 8609-8611.
14. B. Wieczorek, B. Lemcke, H. P. Dijkstra, M. R. Egmond, R. J. M. Klein Gebbink and G. van Koten, *Eur. J. Inorg. Chem.*, 2010, **2010**, 1929-1938.
15. A. Winter, A. M. J. van den Berg, R. Hoogenboom, G. Kickelbick and U. S. Schubert, *Synthesis*, 2007, 642-642.
16. Y. Halpin, D. Dini, H. M. Y. Ahmed, L. Cassidy, W. R. Browne and J. G. Vos, *Inorg. Chem.*, 2010, **49**, 2799-2807.
17. I. M. Hauptvogel, W. Seichter and E. Weber, *Supramolecular Chem.*, 2011, **23**, 398-406.
18. L. M. Hancock, E. Marchi, P. Ceroni and P. D. Beer, *Chem.-Eur. J.*, 2012, **18**, 11277-11283.
19. M. Brust, M. Walker, D. Bethell, D. J. Schiffrin and R. Whyman, *J. Chem. Soc.-Chem. Commun.*, 1994, 801-802.

Chapter 7: Summary of Conclusions

Chapter 2

Heteroditopic rotaxane and catenane host structures incorporating calix[4]diquinone based macrocyclic components were synthesised using both cation and anion templation strategies. In concert with a pyridine *N*-oxide containing axle the rotaxane host structure exhibited a strong preference for alkali metal halides which were bound in an unprecedented 'axle separated' ion pair configuration. Chloride and bromide binding was enhanced by over an order of magnitude in the presence of sodium cations, with significant cooperativity also seen for potassium. The binding mode was elucidated by X-ray crystallography of the related catenane which contained a bound separated sodium chloride ion-pair within the catenanes heteroditopic cavity.

Chapter 3

The use of anion templation to construct *d*- and *f*-metal containing interlocked sensing hosts was explored. The synthesis of a lanthanide appended rotaxane was achieved *via* a CuAAC post-synthetic rotaxane modification strategy. Anion sensing studies, monitoring the lanthanide luminescent probe, demonstrated that signalling of the binding event occurred for chloride and the oxoanions acetate and dihydrogenphosphate. Importantly the host displayed a selective response for chloride due to binding at both the peripheral lanthanide centre and within the rotaxane cavity. The incorporation of luminescent ruthenium (II) and platinum (II) dipyridylbenzene complexes into macrocyclic and interlocked rotaxane structures was

successful. Luminescence studies showed that the platinum derivatives are effective sensors which display a range of responses to anions. In contrast the ruthenium complexes did not exhibit luminescent discrimination between anions. However, the ruthenium rotaxane host displayed a high affinity for chloride in competitive aqueous solvent media.

Chapter 4

A rotaxane post-synthetic modification strategy using a CuAAC reaction to couple alkyne- and azide-functionalised [2]rotaxanes produced a novel higher ordered [3]rotaxane. The synthesis of a 'rotaxane stoppered' [4]rotaxane was also attempted but was unsuccessful. However, the method of interlocked molecular post-synthetic modification has potential as a facile route to otherwise inaccessible higher order interlocked architectures.

Chapter 5

Novel fluorophore ligand functionalised gold nanoparticle conjugates were shown to act as effective sensors for sulphur mustard (HD) and its derivatives. Exploiting the hierarchy of binding energies of different ligands with gold nanoparticle surfaces, a displacement assay method was developed that switches on fluorescence, where weakly bound nanoparticle ligands are rapidly displaced by strongly ligating sulphide analytes. These preliminary studies act as a proof of concept and with refinement these ligand nanoparticle conjugates have potential use as new sensory materials for detecting CWAs.

Appendices

A.1 Crystal Structure Information

A.1.1 General Information

All structures within this thesis were grown and solved by the author, R. C. Knighton. Data was collected at 150(2) K using either graphite monochromated Mo Kα radiation (λ = 0.71073 Å) on a Nonius KappaCCD diffractometer in the case of dipyridylbenzene ligand **62**. dansyl-amine ligand **88** and naphthalimide-imidazole ligand **90**. For the other structures, calix[4]diquinone macrocycle **1**, calix[4]diquinone pyridinium macrocycle **34** · Cl, [2]catenane **41** · NaCl[BAr^F_4], azide [2]rotaxane **54** · Cl, ruthenium (II) acyclic receptor **70** · Cl, ruthenium (II) macrocyclic receptor structures of **72** · PF_6 and alkyne [2]rotaxane **79** · Cl were collected using silicon double crystal monochromated synchrotron radiation (λ = 0.66890 Å) at Diamond Light Source, Beamline I19 on a custom built Rigaku diffractometer at 100 K.

When using the Nonius machine, a series of ω-scans were typically performed in such a way as to collect every independent reflection to a maximum resolution of 0.77 Å, aiming for 99.5% completeness. Cell parameters and intensity data (including inter-frame scaling) were processed using the DENZO-SMN package.[1] When using synchrotron radiation, ω-scans were performed such that a half-sphere of data was collected to a maximum resolution of 0.77 Å. Cell refinement, data reduction and scaling were performed using the CrystalClear package.[2]

The structures were solved by direct methods using the SIR92 software[3] or by charge flipping using Superflip.[4] Structures were refined using full-matrix least-squares on F^2 within the CRYSTALS suite.[5] All non-hydrogen atoms were refined with anisotropic displacement parameters unless specified otherwise. Disordered portions were modelled using refined partial occupancies. Geometric and vibrational restraints were applied where appropriate to ensure physically reasonable models.

In some cases, the molecular structure within solvent voids could not be resolved in the difference map and PLATON SQUEEZE[6] was therefore used to account for the residual electron density in the refinement.

After the construction of a stable, physically reasonable and complete model, the weights were optimised,[7] analogous reflections were omitted and absent high-angle data (in the case of poorly diffracting samples) were pruned using the Wilson plot. This generally led to convergence of the refinement, giving the final structure. For the more challenging structures, in which the refinement did not converge immediately, initially half-shifts, then restraints and finally rigid body refinement were used to overcome the problem. IUCr CheckCIF/PLATON[8] was used to validate the structures and warnings were dealt with as appropriate or justified using validation reply forms.

The .cif files and their corresponding Crystals files have been included in the digital appendix.

A.1.2 Crystal structure of calix[4]diquinone macrocycle 1

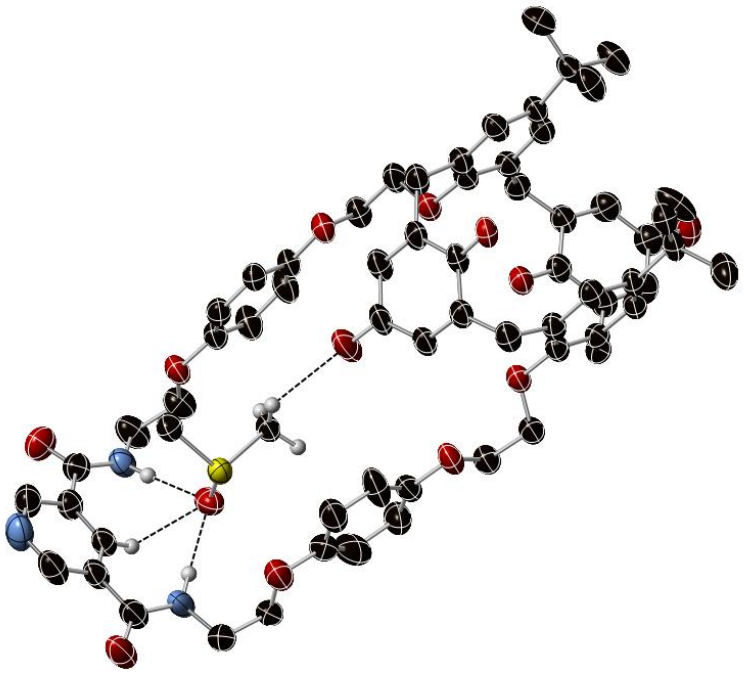

Figure A.1: Single crystal X-ray structure of calix[4]diquinone macrocycle **1** (Ellipsoid plotted at 50% probability, non-hydrogen bonding hydrogen atoms omitted for clarity)

Compound reference	**Calix[4]diquinone macrocycle 1**
Chemical formula	$C_{63}H_{63}N_3O_{12} \bullet C_2H_6OS$
Formula Mass	1132.34
Crystal system	Triclinic
a/Å	12.6430(12)
b/Å	14.2835(16)
c/Å	16.9650(12)
α/°	80.423(8)
β/°	87.747(7)
γ/°	74.632(9)
Unit cell volume/Å^3	2912.9(5)
Temperature/K	100
Space group	$P\bar{1}$
No. of formula units per unit cell, Z	2
No. of reflections measured	27664
No. of independent reflections	13925
R_{int}	0.103
Final R_1 values ($I > 2\sigma(I)$)	0.0979
Final $wR(F^2)$ values ($I > 2\sigma(I)$)	0.2492
Final R_1 values (all data)	0.1191
Final $wR(F^2)$ values (all data)	0.3129

Table A.2: Crystal structure data for calix[4]diquinone macrocycle **1**

A.1.3 Crystal structure of calix[4]diquinone pyridinium macrocycle 35 · Cl

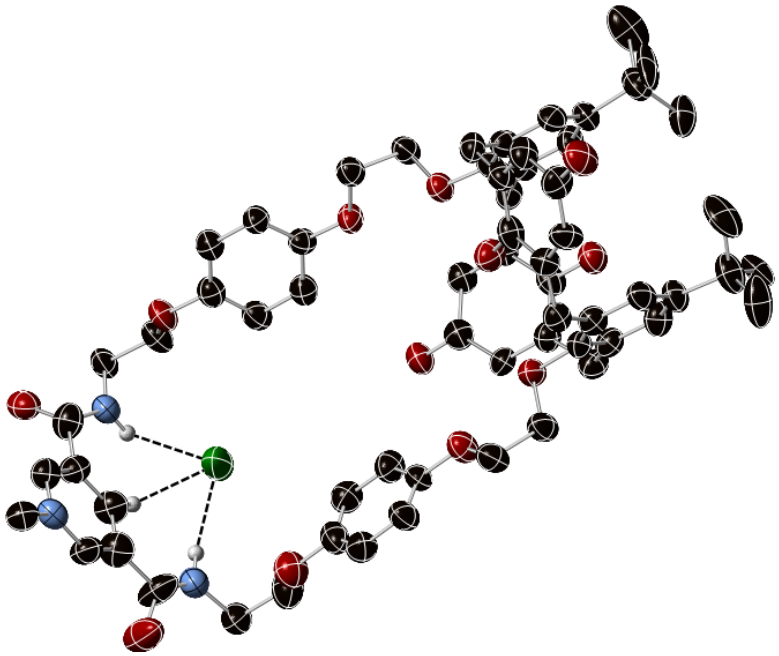

Figure A.3: Single crystal X-ray structure of calix[4]diquinone pyridinium macrocycle **35** · Cl (Ellipsoid plotted at 50% probability, non-hydrogen bonding hydrogen atoms omitted for clarity)

Compound reference	**Calix[4]diquinone pyridinium macrocycle 35 · Cl**
Chemical formula	$C_{63.60}H_{64.80}N_3O_{12} \bullet Cl \bullet {}_{0.}404(CH_3)$
Formula Mass	1104.69
Crystal system	Orthorhombic
a/Å	11.2073(7)
b/Å	20.3291(15)
c/Å	25.6084(16)
α/°	90
β/°	90
γ/°	90
Unit cell volume/Å^3	5834.5(7)
Temperature/K	100
Space group	$P212121$
No. of formula units per unit cell, Z	4
No. of reflections measured	5144
No. of independent reflections	5059
R_{int}	0.135
Final R_1 values ($I > 2\sigma(I)$)	0.0635
Final $wR(F^2)$ values ($I > 2\sigma(I)$)	0.0758
Final R_1 values (all data)	0.1071
Final $wR(F^2)$ values (all data)	0.0947

Table A.4: Crystal structure data for calix[4]diquinone pyridinium macrocycle **35** · Cl

A.1.4 Crystal structure of [2]catenane 41 · NaCl[BAr^F_4]

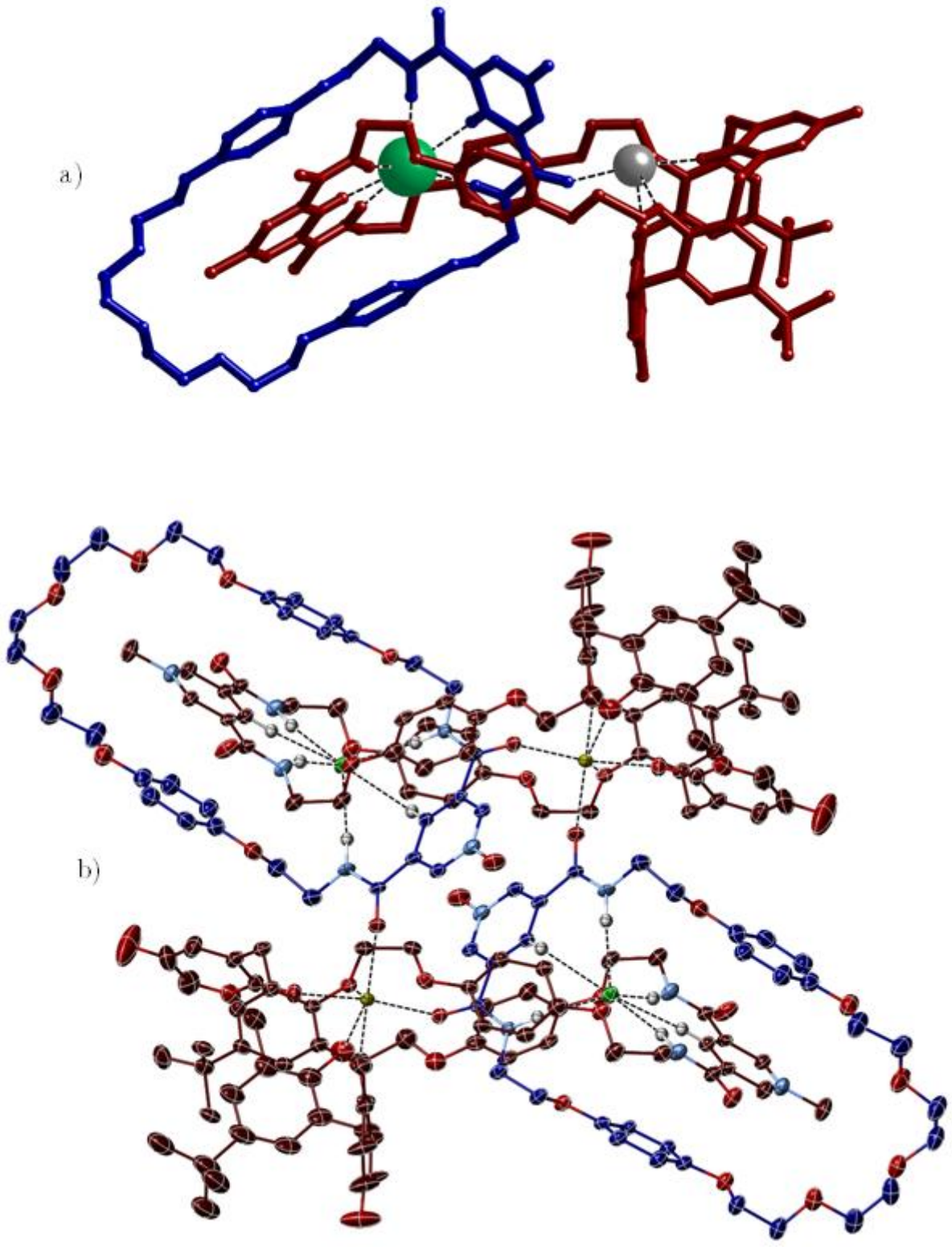

Figure A.5: Single crystal X-ray structure of [2]catenane **41** · NaCl[BAr^F_4] a) stick representation b) ellipsoid plot (Ellipsoid plotted at 30% probability, non-hydrogen bonding hydrogen atoms and BAr^F_4 counteranion omitted for clarity)

Compound reference	**[2]catenane 41 · NaCl[BAr$^{F}_{4}$]**
Chemical formula	$C_{190.02}H_{204.98}N_{12}Na_{1.66}O_{44} \bullet 2(C_{32}H_{12}BF_{24}) \bullet 2(Cl)$
Formula Mass	2598.17
Crystal system	Triclinic
a/Å	13.0829(10)
b/Å	24.11(2)
c/Å	24.51(2)
α/°	109.487(15)
β/°	90.816(17)
γ/°	90.235(9)
Unit cell volume/Å^3	7287(9)
Temperature/K	293
Space group	$P\bar{1}$
No. of formula units per unit cell, Z	2
No. of reflections measured	52582
No. of independent reflections	52584
R_{int}	0.000
Final R_1 values ($I > 2\sigma(I)$)	0.1260
Final $wR(F^2)$ values ($I > 2\sigma(I)$)	0.3149
Final R_1 values (all data)	0.1431
Final $wR(F^2)$ values (all data)	0.3454

Table A.6: Crystal structure data for [2]catenane **41** · NaCl[BAr$^{F}_{4}$]

A.1.5 Crystal structure of azide [2]rotaxane 54 · Cl

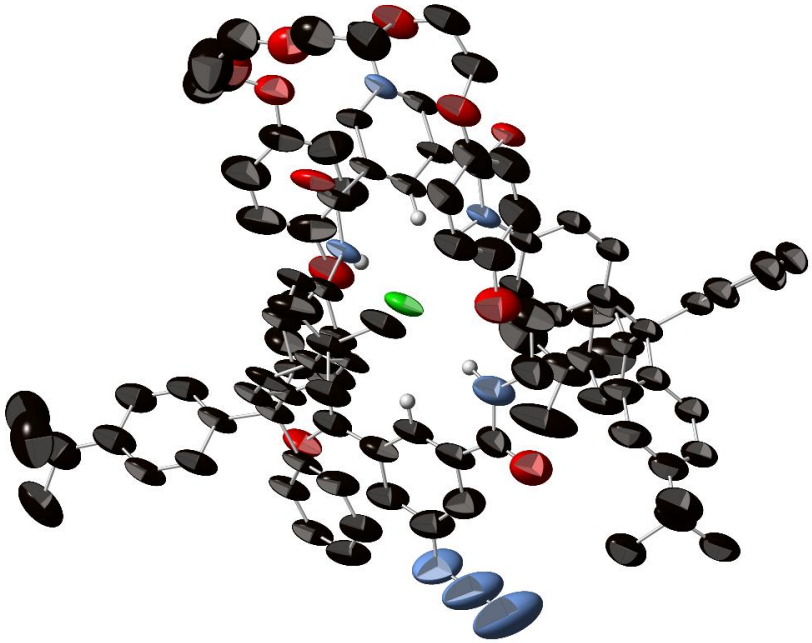

Figure A.7: Single crystal X-ray structure of azide [2]rotaxane **54** · Cl (Ellipsoid plotted at 50% probability, non-hydrogen bonding hydrogen atoms omitted for clarity)

Compound reference	**azide [2]rotaxane 54 · Cl**
Chemical formula	$C_{106}H_{115}Cl_1N_8O_{11}$
Formula Mass	1712.58
Crystal system	Triclinic
a/Å	13.2580(9)
b/Å	20.3837(18)
c/Å	26.4826(17)
α/°	85.599(6)
β/°	81.344(5)
γ/°	81.232(6)
Unit cell volume/Å^3	6982.0(9)
Temperature/K	100
Space group	$P\bar{1}$
No. of formula units per unit cell, Z	2
No. of reflections measured	49935
No. of independent reflections	25858
R_{int}	0.136
Final R_1 values ($I > 2\sigma(I)$)	0.1315
Final $wR(F^2)$ values ($I > 2\sigma(I)$)	0.2476
Final R_1 values (all data)	0.1605
Final $wR(F^2)$ values (all data)	0.3002

Table A.8: Crystal structure data for azide [2]rotaxane **54** · Cl

A.1.6 Crystal structure of dipyridylbenzene ligand 62

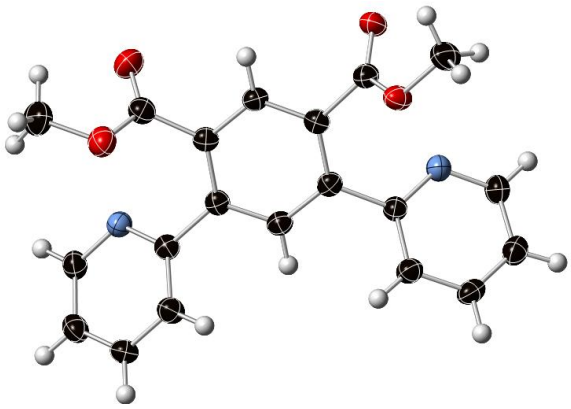

Figure A.9: Single crystal X-ray structure of dipyridylbenzene ligand **62** (Ellipsoid plotted at 50% probability, hydrogen atoms shown as spheres of arbitrary radius)

Compound reference	**Dipyridylbenzene ligand 62**
Chemical formula	$C_{20}H_{16}N_2O_4$
Formula Mass	348.36
Crystal system	Monoclinic
a/Å	7.0471(3)
b/Å	10.9564(4)
c/Å	11.2964(5)
α/°	73.2309(16)
β/°	89.9992(15)
γ/°	90.0079(19)
Unit cell volume/Å^3	835.11(6)
Temperature/K	150
Space group	$P2111$
No. of formula units per unit cell, Z	2
No. of reflections measured	6494
No. of independent reflections	3704
R_{int}	0.027
Final R_1 values ($I > 2\sigma(I)$)	0.0670
Final $wR(F^2)$ values ($I > 2\sigma(I)$)	0.1723
Final R_1 values (all data)	0.0744
Final $wR(F^2)$ values (all data)	0.1835

Table A.10: Crystal structure data for dipyridylbenzene ligand **62**

A.1.7 Crystal structure of ruthenium (II) acyclic receptor 70 · Cl

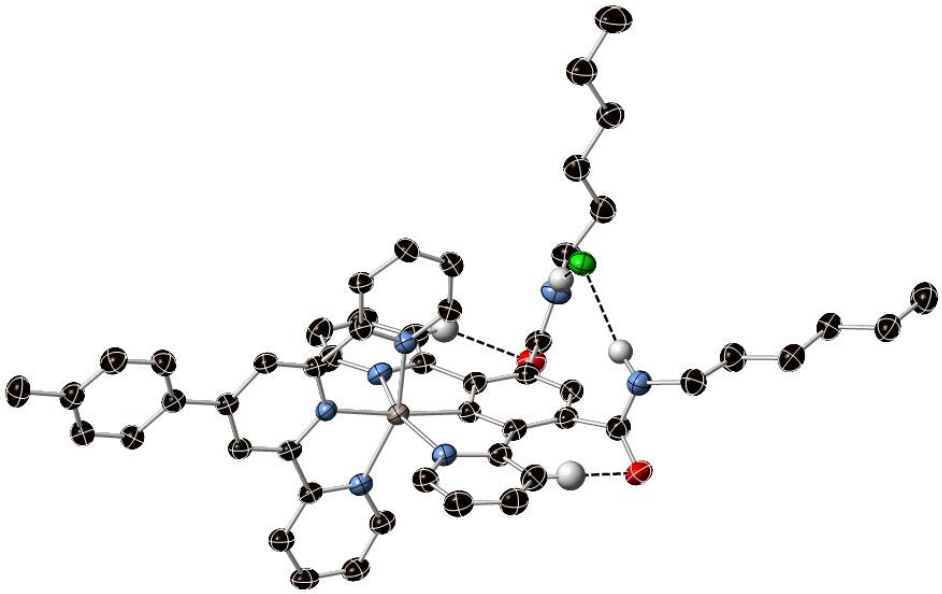

Figure A.11: Single crystal X-ray structure of ruthenium (II) acyclic receptor **70** · Cl (Ellipsoid plotted at 50% probability, non-hydrogen bonded hydrogen atoms omitted for clarity)

Compound reference	**Ruthenium (II) acyclic receptor 70 · Cl**
Chemical formula	$C_{52}H_{54}N_7O_2RuCl$
Formula Mass	945.57
Crystal system	Triclinic
a/Å	11.9614(5)
b/Å	13.3167(7)
c/Å	16.8542(6)
α/°	70.539(4)
β/°	79.249(3)
γ/°	65.151(5)
Unit cell volume/Å^3	2293.5(2)
Temperature/K	150
Space group	$P\bar{1}$
No. of formula units per unit cell, Z	2
No. of reflections measured	36392
No. of independent reflections	14727
R_{int}	0.049
Final R_1 values ($I > 2\sigma(I)$)	0.0554
Final $wR(F^2)$ values ($I > 2\sigma(I)$)	0.1293
Final R_1 values (all data)	0.0687
Final $wR(F^2)$ values (all data)	0.1469

Table A.12: Crystal structure data for ruthenium (II) acyclic receptor **70** · Cl

A.1.8 Crystal structure of *syn*-ruthenium (II) macrocyclic receptor 72 · PF_6

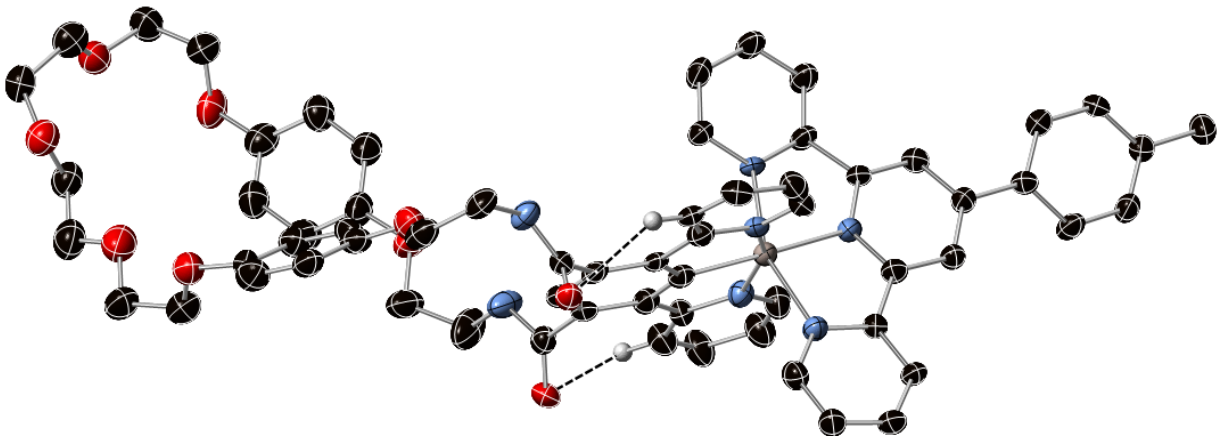

Figure A.13: Single crystal X-ray structure of *syn*-ruthenium (II) acyclic receptor **72** · PF_6 (Ellipsoid plotted at 50% probability, non-hydrogen bonded hydrogen atoms omitted for clarity)

Compound reference	**Ruthenium (II) macrocyclic receptor 72 · PF_6**
Chemical formula	$C_{64}H_{60}N_7O_9Ru \bullet F_6P \bullet CHCl_3$
Formula Mass	1436.6
Crystal system	Triclinic
a/Å	11.6196(4)
b/Å	15.1032(6)
c/Å	19.5089(9)
α/°	95.892(3)
β/°	96.002(3)
γ/°	90.684(3)
Unit cell volume/Å^3	3386.0(2)
Temperature/K	100
Space group	$P\bar{1}$
No. of formula units per unit cell, Z	2
No. of reflections measured	11024
No. of independent reflections	10271
R_{int}	0.079
Final R_1 values ($I > 2\sigma(I)$)	0.0758
Final $wR(F^2)$ values ($I > 2\sigma(I)$)	0.1902
Final R_1 values (all data)	0.0913
Final $wR(F^2)$ values (all data)	0.1859

Table A.14: Crystal structure data for *syn*-ruthenium (II) macrocyclic receptor **72** · PF_6

A.1.9 Crystal structure of *anti*-ruthenium (II) macrocyclic receptor 72 · PF_6

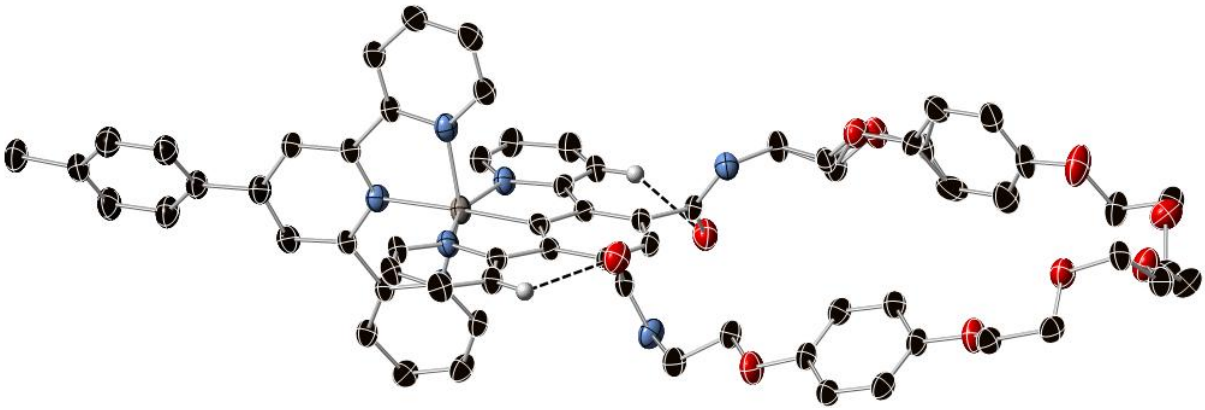

Figure A.15: Single crystal X-ray structure of *anti*-ruthenium (II) acyclic receptor **72** · PF_6 (Ellipsoid plotted at 50% probability, non-hydrogen bonded hydrogen atoms omitted for clarity)

Compound reference	**Ruthenium (II) macrocyclic receptor 72 · PF_6**
Chemical formula	$C_{64}H_{56}N_7O_9Ru \bullet F_6P \bullet C_3H_6O$
Formula Mass	1373.30
Crystal system	Triclinic
a/Å	10.4341(5)
b/Å	12.3603(5)
c/Å	24.9734(12)
α/°	80.884(4)
β/°	84.607(4)
γ/°	76.012(4)
Unit cell volume/Å^3	3080.6(3)
Temperature/K	100
Space group	$P\bar{1}$
No. of formula units per unit cell, Z	2
No. of reflections measured	25967
No. of independent reflections	17475
R_{int}	0.041
Final R_1 values ($I > 2\sigma(I)$)	0.0491
Final $wR(F^2)$ values ($I > 2\sigma(I)$)	0.0915
Final R_1 values (all data)	0.0660
Final $wR(F^2)$ values (all data)	0.1029

Table A.16: Crystal structure data for *anti*-ruthenium (II) macrocyclic receptor **72** · PF_6

A.1.10 Crystal structure of alkyne [2]rotaxane 79 · Cl

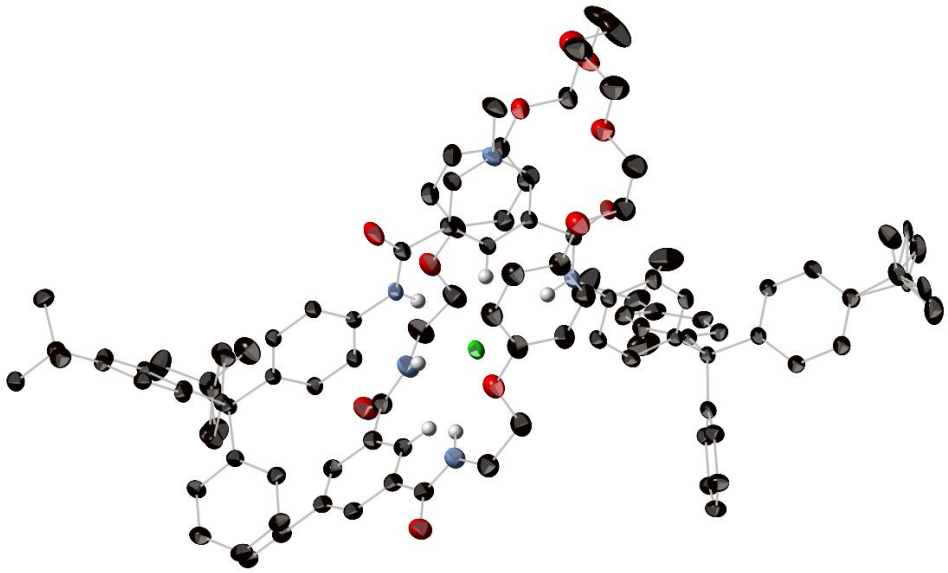

Figure A.17: Single crystal X-ray structure of alkyne [2]rotaxane **79** · Cl (Ellipsoid plotted at 30% probability, non-hydrogen bonded hydrogen atoms omitted for clarity)

Compound reference	**Alkyne [2]rotaxane 79.Cl**
Chemical formula	$C_{74}H_{78}N_3O_2 \bullet C_{34}H_{38}N_2O_9 \bullet Cl$
Formula Mass	1695.59
Crystal system	Monoclinic
a/Å	11.5457(3)
b/Å	25.4763(6)
c/Å	36.0443(7)
α/°	90
β/°	97.191(2)
γ/°	90
Unit cell volume/Å^3	10518.7(4)
Temperature/K	100
Space group	$P21/c$
No. of formula units per unit cell, Z	4
No. of reflections measured	30370
No. of independent reflections	24539
R_{int}	0.070
Final R_1 values ($I > 2\sigma(I)$)	0.0834
Final $wR(F^2)$ values ($I > 2\sigma(I)$)	0.2536
Final R_1 values (all data)	0.1027
Final $wR(F^2)$ values (all data)	0.3088

Table A.18: Crystal structure data for alkyne [2]rotaxane **79** · Cl

A.1.11 Crystal structure of dansyl-amine 88

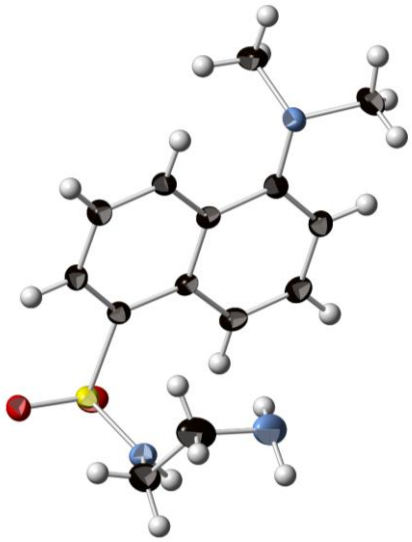

Figure A.19: Single crystal X-ray structure of dansyl-amine ligand **88** (Ellipsoid plotted at 50% probability, hydrogen atoms shown as spheres of arbitrary radius)

Compound reference	**Dansyl-amine 88**
Chemical formula	$C_{14}H_{19}N_3O_2S$
Formula Mass	293.39
Crystal system	Orthorhombic
a/Å	8.0889(2)
b/Å	11.4745(3)
c/Å	15.4252(5)
α/°	90
β/°	90
γ/°	90
Unit cell volume/Å^3	1431.71(7)
Temperature/K	150
Space group	$P21cn$
No. of formula units per unit cell, Z	4
No. of reflections measured	3108
No. of independent reflections	1842
Final R_1 values ($I > 2\sigma(I)$)	0.0366
Final $wR(F^2)$ values ($I > 2\sigma(I)$)	0.0815
Final R_1 values (all data)	0.0423
Final $wR(F^2)$ values (all data)	0.0873

Table A.20: Crystal structure data for dansyl-amine ligand **88**

A.1.12 Crystal structure of naphthalimide-imidazole ligand 90

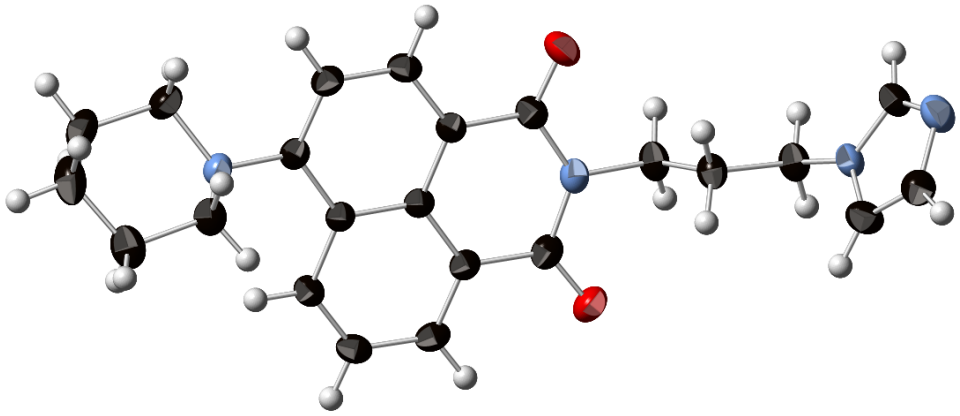

Figure A.21: Single crystal X-ray structure of naphthalimide-imidazole lignd **90** (Ellipsoid plotted at 50% probability, hydrogen atoms shown as spheres of arbitrary radius)

Compound reference	**Naphthalimide-imidazole ligand 90**
Chemical formula	$C_{23}H_{24}N_4O_2$
Formula Mass	388.47
Crystal system	Monoclinic
a/Å	12.69780(10)
b/Å	9.28910(10)
c/Å	32.6042(3)
α/°	90
β/°	95.5768(4)
γ/°	90
Unit cell volume/Å^3	3827.50(6)
Temperature/K	150
Space group	$P21/n$
No. of formula units per unit cell, Z	8
No. of reflections measured	16265
No. of independent reflections	8658
R_{int}	0.026
Final R_1 values ($I > 2\sigma(I)$)	0.0349
Final $wR(F^2)$ values ($I > 2\sigma(I)$)	0.0802
Final R_1 values (all data)	0.0518
Final $wR(F^2)$ values (all data)	0.0767

Table A.22: Crystal structure data for naphthalimide-imidazole ligand **90**

A.2 Anion Titration Protocol

Initial NMR sample volumes and concentrations were 500 μL and 2.0 mM respectively. Solutions (100 mM) of anion were added as their tetrabutylammonium salts and metals as their hexafluorophosphate, triflate or tetraphenylborate salts. In the case of the ion-pair titrations one equivalent of metal salt was dissolved in 100 μL of CD_3OD and diluted with a 400 μL $CDCl_3$ solution of the [2]rotaxane host. Spectra were recorded at 0, 0.2, 0.4, 0.6, 0.8, 1.0, 1.2, 1.4, 1.6, 1.8, 2.0, 2.5, 3.0, 4.0, 5.0, 7.0 and 10 equivalents. In all cases where association constants were calculated, bound and unbound species were found to be in fast exchange on the NMR timescale. Association constants were obtained by analysis of the resulting data using the WinEQNMR2[9] computer program. Binding stoichiometry was investigated by visual analysis of the titration data, and using approximations of Job plots. Estimates for the association constant and the limiting chemical shifts were added to the program's input file. The parameters were refined by non-linear least-squares analysis using WINEQNMR2 to achieve the best fit between observed and calculated chemical shifts. The input parameters for the final chemical shift and association constant were adjusted based on the program output until convergence was reached. Comparison of the calculated and experimental binding isotherms demonstrated that an appropriate model with an appropriate stoichiometry was being used.

Luminescence experiments were carried out on a Varian Cary-Eclipse Fluorolog 3 spectrometer for the platinum (II) receptors using an excitation wavelength of 320 nm at 293 K. To a 2.5 mL, 1 x 10^{-5} M solution of each receptor was added aliquots of the TBA salts dissolved in a stock solution made up with the receptor, such that the same concentration of

the host was maintained throughout the titration experiments. Luminescence experiments were carried out on a Horiba Fluorolog 3 spectrometer for the ruthenium (II) receptors using an excitation wavelength of 530 nm at 293 K. To a 1 mL, 1 x 10^{-4} M solution of each receptor was added aliquots of the TBA salts dissolved in a stock solution made up with the receptor, such that the same concentration of the host was maintained throughout the titration experiments.

A.3 Chapter 5 Experiments

A.3.1 Quantitative Titrations

A 2.5 mL solution of GNPs (0.04 g/mL) was used. The emission intensity at 501 nm of the GNPs was monitored for seventeen titration points (for 0, 0.2, 0.4, 0.6, 0.8, 1.0, 1.2, 1.4, 1.6, 1.8, 2.0, 2.5, 3.0, 4.0, 5.0, 7.0 and 10.0 equivalents of analyte added). A chloroform solution of the analyte was added with 2 µL corresponding to 0.2 molar equivalents of dansyl ligand. The emission intensity was allowed to stabilise for five minutes preceding the recording of the emission spectra. Association constants were calculated using the SPECFIT[10] program assuming a 1:1 binding model.

A.3.2 Qualitative Control Experiments

A solution of GNPs (0.04 mg/mL) was used. 50 µL of analyte was added to a 2.5 mL solution of the GNPs and the fluorescence spectra monitored directly after addition and at five intervals thereafter.

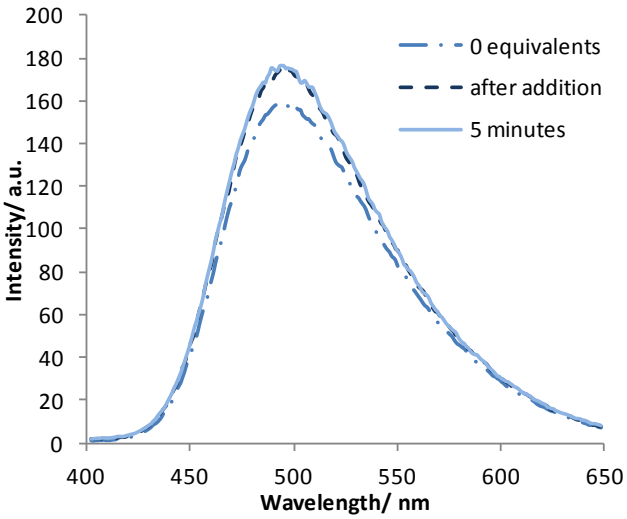

Figure A.23: Change in emission intensity of **Au · 85** upon addition of octan-1-ol (λ_{ex} = 345 nm)

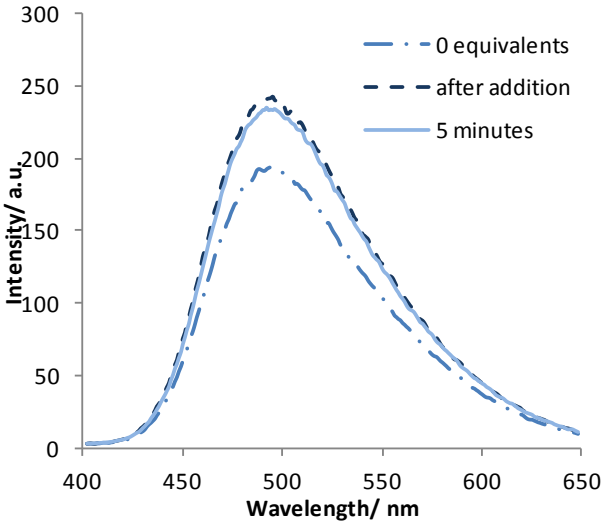

Figure A.24: Change in emission intensity of **Au · 88** upon addition of octan-1-ol (λ_{ex} = 345 nm)

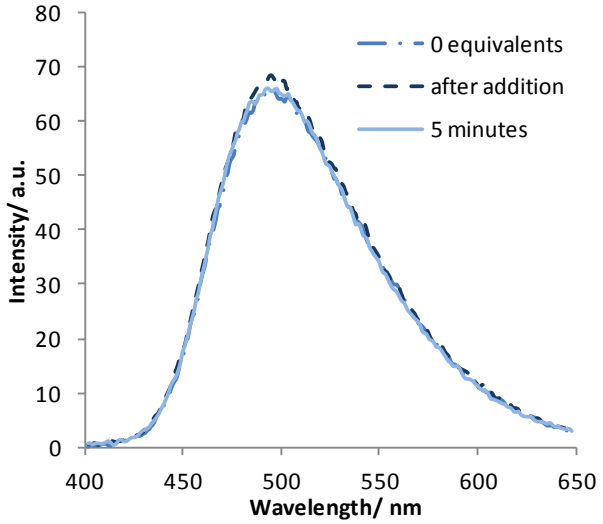

Figure A.25: Change in emission intensity of **Au · 85** upon addition of di-*n*-butylether(λ_{ex} = 345 nm)

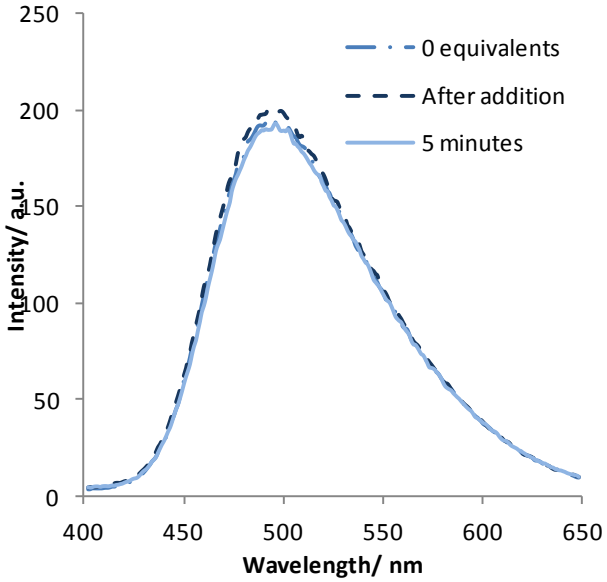

Figure A.26: Change in emission intensity of **Au · 88** upon addition of di-*n*-butylether (λ_{ex} = 345 nm)

A.3.3 ^{1}H NMR Experiments

3.5 mg of **Au · 1** was dissolved in 500 µL of $CDCl_3$ and the ^{1}H NMR spectrum recorded.

Ten equivalents of CEMS were added and the spectra recorded after 30 minutes.

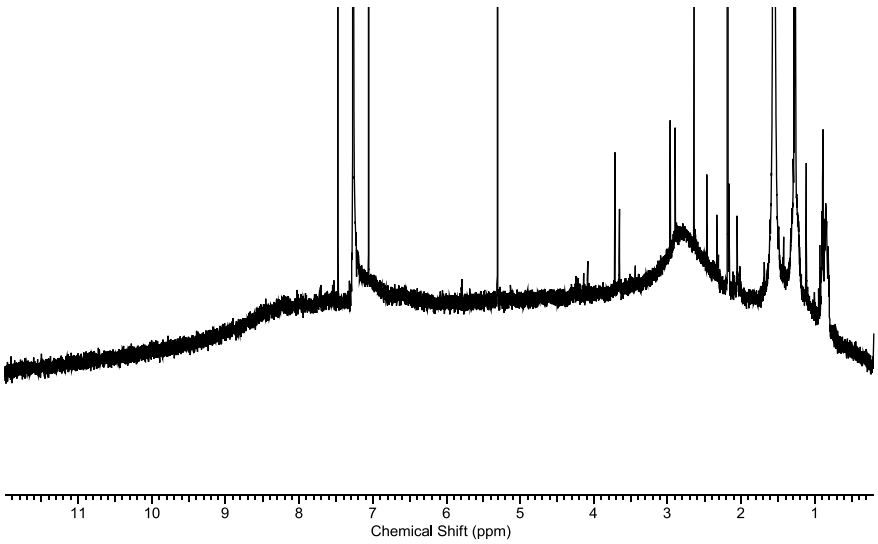

Figure A.27: ^{1}H NMR spectra of **Au · 85** ($CDCl_3$, 500 MHz, 298 K)

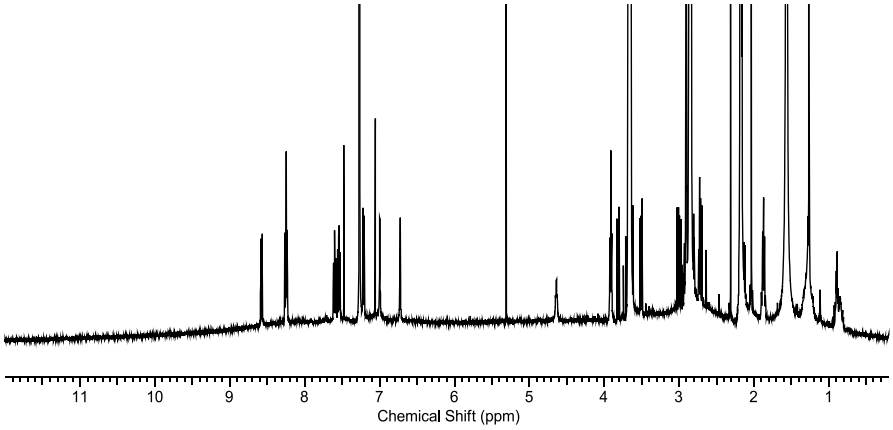

Figure A.28: ^{1}H NMR spectra of **Au · 85** (top) and 30 minutes after exposure to ten equivalents of CEMS (bottom) ($CDCl_3$, 500 MHz, 298 K)

A.4 References

1. Z. Otwinowski and W. Minor, in *Methods in Enzymology*, ed. Charles W. Carter, Jr., Academic Press, 1997, vol. Volume 276, pp. 307-326.
2. Rigaku (2007). CrystalClear. Version 1.3.5. Rigaku Inc., Tokyo, Japan.
3. A. Altomare, G. Cascarano, C. Giacovazzo and A. Guagliardi, *J. Appl. Crystallogr.*, 1994, **27**, 1045-1050.
4. L. Palatinus and G. Chapuis, *J. Appl. Crystallogr.*, 2007, **40**, 786-790.
5. P. W. Betteridge, J. R. Carruthers, R. I. Cooper, K. Prout and D. J. Watkin, *J. Appl. Crystallogr.*, 2003, **36**, 1487-1487.
6. A. L. Spek, *J. Appl. Crystallogr.*, 2003, **36**, 7-13.
7. J. R. Carruthers and D. J. Watkin, *Acta Crystallogr. Sect. A*, 1979, **35**, 698-699.
8. M. Fourmigue and P. Batail, *Chem. Rev.*, 2004, **104**, 5379-5418.
9. M. J. Hynes, *J. Chem. Soc.-Dalton Trans.*, 1993, 311-312.
10. SPECFIT, 2.02; Spectrum Software Associates Chapel Hill, NC, USA.